Lipid Membrane Engineering for Biotechnology

Ana Carolina Gomes Almeida

Doctor of Philosophy

Aston University

October 2023

Abstract

Lipid Membrane Engineering for Biotechnology

The growing scientific knowledge about microorganisms has enabled the development of improved microbial strains currently used in biotechnology. The hyper Acetone-Butanol-Ethanol producer *C. saccharoperbutylacetonicum* is an attractive cell factory for butanol production. However, the organic acids and solvents accumulation during fermentation affects the membrane fluidity and the stress of the cells, lowering the yields and productivities. Butanol, for example, is thought to permeabilise the cell, compromising not only its viability, but the entire fermentation process. The membrane lipid composition and the stress response are two potential targets to optimise cell factories not only for butanol and weak acids production, but also more generally.

With that in mind, *C. saccharoperbutylacetonicum* N1-4(HMT) was engineered by manipulating the genes involved in phospholipid synthesis, *pssA*, *pgsA* and *cls*. The *mt*1 gene, coding for an antioxidant enzyme, was also heterologous expressed in *C. saccharoperbutylacetonicum* N1-4(HMT) to combat any effects in the lipid membrane composition. Finally, the *C. saccharoperbutylacetonicum* N1-4(HMT) *BCL* strain, provided by Biocleave Ltd, is a mutant strain that displays a distinct membrane morphology, providing a butanol-producing strain with altered membrane characteristics.

The strains in which *pssA* is knocked out or overexpressed have opposite lipid composition profiles. The strains in which *pssA*, *pgsA* and *cls* is overexpressed produce more phosphatidylethanolamine than the wild type. The strain overexpressing *mt*1 has significantly more lysophosphatidylethanolamine and less phosphatidylglycerol than the wild type, similarly to the strain with the *pssA* knockout. The *BCL* strain had a very similar lipidome as the wild type. The strains overexpressing *pssA*, *pgsA*, *cls* strains and the *BCL* strain produce similar concentrations of butanol to the wild type. The strains with the *pssA* knockout and overexpressing *mt*1 accumulate organic acids and do not produce butanol. Although, the butanol toxicity still needs optimisation, these results suggest a network between membrane composition, cell stress and ABE fermentation and reveal future routes for membrane engineering. However, it must be noted that effects of modulating lipid biosynthesis genes are not always predictable nor beneficial.

Acknowledgements

My heartfelt gratitude goes to my supervisors, Dr. Alan Goddard and Professor Roslyn Bill. Their invaluable guidance, incredible support, and insights were very important in navigating the challenges of this work. Their exemplary leadership has been a constant source of inspiration.

I extend my thanks to Biocleave Ltd for the opportunity to collaborate and deepen my understanding of Clostridia.

A big thank you to my lab colleagues, especially John and Monse, for their guidance and technical expertise that enriched my work.

My appreciation also extends to the principal investigators and colleagues who were always open to discussions, addressed my queries, and played a crucial role in my development.

I'm grateful to the Memtrainees, a group of 12 fellow PhD students. I had the opportunity to get to know amazing people that I'll never forget.

I'm very thankful for having Diana, Laura, Idoia, Cristina, Divya and Bita next to me during these three years.

Lastly, a special mention to my husband, my family, and friends. Your unwavering support and encouragement during these challenging three years have been my strength. Thank you for standing by me.

List of abbreviations

ABE: Acetone-butanol-ethanol

ADP - Adenosine diphosphate

ATP - Adenosine triphosphate

bp - Base pair

CDP - Cytidine diphosphate

Cer – Ceramide

CGM – Clostridial Growth media

CL - Cardiolipin

CoA - Coenzyme A

CRISPR - Clustered regularly interspaced short palindromic repeats

DAG - Diacylglycerol

DGDG – Digalactosyldiacylglycerol

DMSO – dimethyl sulfoxide

DNA – Desoxyribonucleic acid

dNTPs – deoxynucleoside triphosphates

EPB_NS – electroporation buffer without salt

EPB_S – electroporation buffer with salt

FA – Fatty acid

HPLC: High-performance liquid chromatography

GC – gas chromatography

MS: Mass Spectrometry

MW: Molecular Weight

NAD(P)H – Nicotinamide adenine dinucleotide phosphate

NHEJ – non-homologous end-joining

OD – optical density

ORF: Open Reading Frame

p: p-value

P: Phosphate

PAM – Proto-adjacent motif

PE: Phosphatidylethanolamine

PC: Phosphatidylcholine

PG: Phosphatidylglycerol

PS: Phosphatidylserine

PCR: Polymerase Chain Reaction

RCM – Reinforce Clostridial media

RE – restriction enzyme

RNA – Ribonucelic acid

ROS: Reactive oxygen species

TLC: Thin layer chromatography

Table of Contents

List of Figures

1 Introduction

1.1 Biotechnology

The combustion of fossil fuels lead to the release of pollutants that contaminate the air, water and land (Nanda et al., 2018). The continuous use of fossil fuel also compromises the carbon budget of the planet as the accumulation of carbon dioxide in the atmosphere increases the global temperature faster than organisms can adapt to(Cherubini et al., 2009). The last decades have witnessed new advances to promote a paradigm-shift from petrochemical industries to bio-based ones, where transportation biofuels, bioenergy, biochemicals, biomaterials, food and feed are efficiently produced in an environmentally sustainable manner (Cherubini et al., 2009).

Biotechnology is a multidisciplinary field that combines the principles of biological sciences and engineering. It aims to exploit biological systems, including organisms, cells, and molecular components, to develop products and services that address some of most pressing challenges for humanity (Gavrilescu 2009; Kumar, Sharma, and Ahluwalia 2017). Technologies rooted in biotechnological principles find applications in diverse areas such as manufacturing, agriculture, food processing, medicine, environmental conservation, and energy sectors (Wittmann and Liao 2017). Moreover, the growing environmental challenges have emphasized the importance of biotechnology in pollution control and prevention and in minimizing waste generation (Figure 1.1) (Gavrilescu 2009).

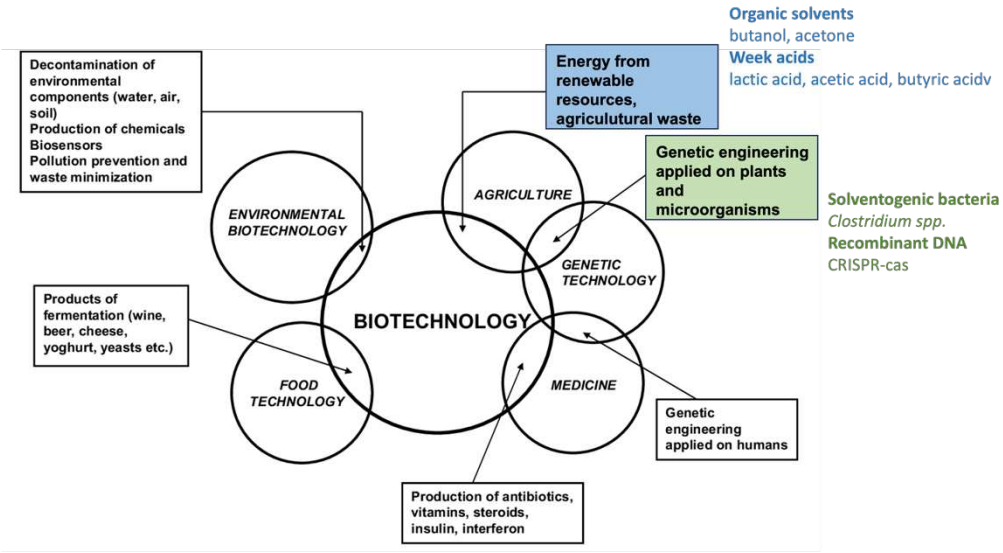

Figure 1.1. Overview of Biotechnology applications. Agriculture, food processing, medicine, environmental conservation, and energy sectors are the different areas of impact to produce high value products required for human health and for the environment. Genetic technology advances have enabled the engineering of microorganisms to efficiently produce high-value compounds, including organic acids and solvents, using renewable resources. Adapted from Gavrilescu 2009.

Additionally, modern biotechnology has exponentially increased the development of high value products important in medicine such as, vaccines, antibodies, vitamins and other drugs (Gavrilescu 2009). Developments in food technology has improved the production of yoghurts, cheese, bread, or drinks, such as wine and beer (Gavrilescu 2009). In food technology, genetic engineering of plants has optimised crops to improve nutrition levels. At the environmental level, the production of solvents, week acids, plastics from renewable resources and waste can provide novel opportunities for sustainability (Gavrilescu 2009). All of this is made possible through technological advances in fermentation, processing, DNA structure, genetics, recombinant DNA, cloning, genome and biochemistry (Rangel, Gómez Ramírez, and González Barrios 2020; Usmani et al., 2021).

Biotechnology has gained much recent attention beyond the wide range of applications due to the fact that the latter rely on non-renewable resources, are limited and are non-environmentally friendly (Rangel 2020; Usmani et al., 2021). However, the main issue affecting biotechnology is the economic viability of the processes when compared to traditional industries, such as refineries using fossil feedstocks (de Jong and Jungmeier, 2015). Although still

with lower yield than petrochemical industries, processes such as fermentation have been optimised and obtained increasing concentration of butanol, ethanol, biodiesel and lactic acid (Kell et al., 2015; Kordi et al., 2022; Kumar, Sharma, and Ahluwalia 2017).

White biotechnology is one subfield of biotechnology and is focused on using biological organisms or its by-products, for example, enzymes, as tools to make or modify products or processes. The diverse characteristics of biological organisms such as fungi, yeast and bacteria and the development of new technologies around these biology tools has increased the variety of products (Kordi et al., 2022). Included within these technological innovations are biology tools, machine learning, synthetic biology and omics (Kordi et al., 2022). Omics allow a full understanding of the genome and transcriptome of different organisms and identification of target sequences of DNA. This can be used to, for example, alter enzyme activity, improve metabolic pathways, add resistance to stress conditions and consequently increase the yield and productivity of targeted high-value chemicals (Kordi et al., 2022).The biological conversion of renewable feedstock into high value chemicals is performed in many cases by microbial cell factories (Rangel 2020; Usmani et al., 2021).

1.2 Microbial cell factories

Microbial cell factories are engineered microorganisms optimized for producing chemicals from renewable resources, offering a sustainable alternative to conventional chemical processes (Cho et al., 2022). These microorganisms eliminate the need for toxic solvents and catalysts therefore contributing to a global shift in chemical production methodologies. Various microorganisms have unique traits that allow them to be used as platforms to use renewable biomass to generate high value chemicals, such as butanol (Sauer and Mattanovich, 2012). Additionally, microbial cell factories play important roles in the production of food additives or food supplements, enzymes important to the food industry, probiotics, biotherapeutic agents, antibiotics, fuels and plastics. Some of these organisms are also important to improve agriculture, producing more environmentally friendly pesticides and fertilizers, helping the crops become more tolerant to stressful situations (Kordi et al., 2022).

Technological advances have allowed a detailed characterisation of microorganisms including their genomes, physiology and metabolism, broad and flexible substrate utilization, high tolerance to substrates, metabolic products, oxidative stress, extreme pH, pressure and temperature (Charubin et al., 2018). Data has been used to improve bacteria as cell factories and transforming biotechnology into a more economically attractive way, bearing in mind the

major global challenges such as energy, environment, food and health security (Gustavsson and Lee, 2016; Kordi et al., 2022).

In this thesis, the focus is on bacterial cell factories which are robust in the production of weak acids, such as lactic acid, acetic acid and butyric acid and solvents such as butanol and acetone. These compounds have high biotechnological interest; solvents have great potential to replace or supplement petroleum-derived liquid transportation fuels or also in the production of bioplastics (de Jong and Jungmeier, 2015; Gavrilescu, 2009; Kordi et al., 2022; Sanders et al., 2007). Organic acids such as acetic acid, lactic acid and butyric acids have great potential to replace polymers, to be used as green solvents, applied in food and in therapeutics (Sauer et al., 2008).

1.2.1 *Clostridium* organisms as microbial cell factories

Traditionally, solventogenic *Clostridium* species have shown to be strong candidates for application in industrial settings (Wang et al., 2019; Xue et al., 2017; Yu et al., 2011). Solventogenic *Clostridium* species are very attractive cell factories. These species have one of the broadest and more flexible systems for substrate utilization, being able to use complex carbohydrates, such as cellulose, xylans and other polysaccharides (Charubin et al., 2018). This is particularly attractive as around 60% of the operational costs are related to the pre-treatment of renewable biomass and its conversion into less complex substrates that will be assimilated by microorganisms (Sahoo et al., 2019). Another positive characteristic of solventogenic *Clostridium* is its powerful primary metabolism with very high carbon and electron fluxes, generating ATP in unique systems (Sauer and Mattanovich 2012). Additionally, these species have a well-developed fermentation pathway, that has been described and improved for more than 100 years for the acetone-butanol-ethanol fermentation (ABE) (Charubin et al., 2018).

Acetone-Butanol-Ethanol fermentation (ABE)

Described for the first time in 1862 by Louis Pasteur and established at an industrial level by the production of acetone and butanol in 1915 by Chaim Weizman, ABE fermentation is a biphasic process to produce solvents and bulk chemicals in a sustainable process (Karstens, Trippel, and Götz 2021). The native metabolic pathway for solvent production has been comprehensively elucidated and is mediated by coenzyme A (CoA) (Figure 1.2). A vast number of substrates such as hexoses, pentoses, and oligomers are assimilated through the phosphoenolpyruvate-dependent phosphotransferase system (PTS) and degraded to pyruvate via the pentose

phosphate pathway (PPP) and Embden–Meyerhof–Parnas (EMP) pathways along with the production of ATP and NADH (Figure 1.2) (Li et al., 2020). The intermediates acetyl-CoA and butyryl-CoA are converted into oxidized products such as acetone and acetate and/ or reduced products, such as butanol, ethanol, or butyrate.

The ABE fermentation can be divided into the acidogenic and solventogenic phases (Figure 1.2). The acidogenic phase occurs during the exponential growth of the cells generating lactic acid, acetic acid and butyric acid as the main fermentation products. Acid accumulation and the associated decrease in intracellular pH, along with surplus of ATP and NAD(P)H/NAD(P)$^+$, lead to changes in the intracellular microenvironment (Li et al., 2020). These modifications in the cells and other factors such as butyryl-phosphate and formic acid trigger the expression of solventogenic enzymes, shifting the metabolic pathway to the solventogenic phase (Figure 1.2). Lactate, acetate and butyrate are re-assimilated as co-substrates to generate CoA derivatives such as acetyl-CoA and butyryl-CoA, using the ATP and NAD(P)H/NAD(P)$^+$ from the acidogenic phase to produce acetone butanol and ethanol (Figure 1.2).

Solventogenic Clostridia, such as *Clostridium acetobutylicum*, *Clostridium beijerinckii*, *Clostridium saccharoperbutylacetonicum* and *Clostridium saccharobutylicum* are the most common and best characterized models used in the ABE fermentation producing acetone, butanol and ethanol in a molar ratio of 3:6:1 (Xue and Cheng, 2019). Many studies on these strains have been performed to optimise their solvent production, highlighting the production of butanol (Table 1).

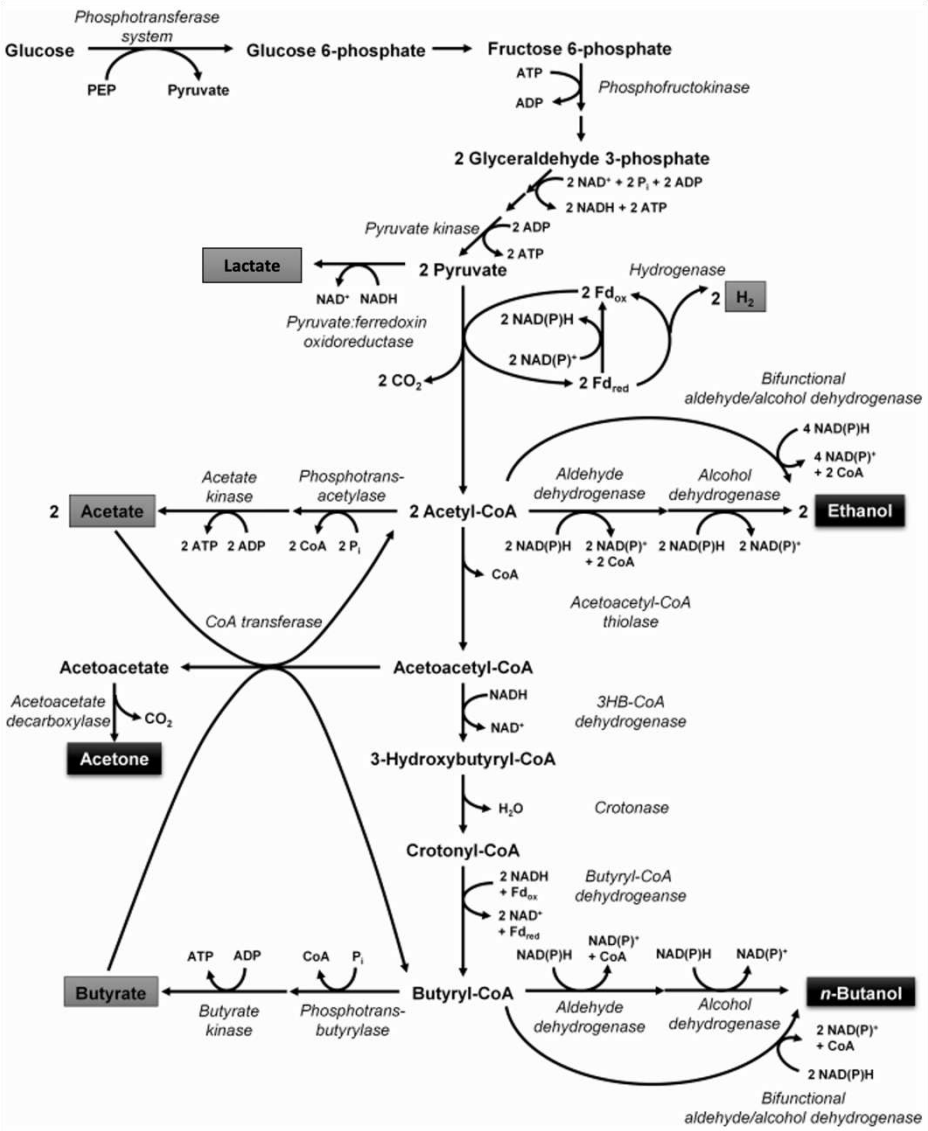

Figure 1.2. Simplified metabolism of ABE fermentation by solventogenic Clostridia. Initial substrate uptake occurs via the phosphoenolpyruvate-dependent phosphotransferase system (PTS) and/or non-PTS transport systems. Subsequent degradation through the Embden–Meyerhof–Parnas (EMP) pathway leads to the generation of Pyruvate. During exponential growth, the acidogenesis phase commences, converting pyruvate and key intermediates of acetyl-CoA and butyryl-CoA into lactate, acetate, and butyrate (highlighted in grey). The acidified environment and elevated ATP and NAD(P)H/NAD(P)$^+$ levels trigger a shift to the solventogenesis phase, where acids are re-assimilated to produce coenzyme A (CoA) derivatives (acetyl-CoA and butyryl-CoA), ultimately yielding acetone, ethanol, and butanol (highlighted in black). Adapted from (Moon et al., 2016).

Table 1. Examples of engineered and wild type *Clostridium spp.* strains on butanol production (Charubin et al., 2018; Monaghan et al., 2022).

Strain	Strategy	Control strain Butanol ($g.L^{-1}$)	Engineered strain Butanol ($g.L^{-1}$)
C. acetobutylicum BKM19	Random mutagenesis, screening cells on fluoroacetate plates	15.9	17.6
C. acetobutylicum ATCC 824	Overexpressing both *pfkA* and *pykA* genes (involved in the glycolysis pathway)	14.78	19.12
C. beijerinckii CC101	Overexpressing *adhE2* and *ctfAB* (ABE fermentation enzymes)	2.6	12.0
C. acetobutylicum EA 2018	Disrupting the acetone pathway by TargeTron technology	7.4	13.6
C. acetobutylicum ATCC 824 (pGROE1)	Overexpression of the *groESL* operon genes	~13	17.1
C. saccharoperbutylacetonicum N1-4	Wild type (cassava and batch fermentation)	16.4	-
C. saccharoperbutylacetonicum ATCC 27022	Wild type (bagasse and batch fermentation)	16.5	-
C. saccharoperbutylacetonicum N1-4 (HMT)	*GapN* deletion (ABE metabolic pathway)	~13	~13

1.2.2 Organic acid and solvent production

As previously described, during the ABE fermentation produced organic acids such as lactic acid, acetic acid and butyric acid are assimilated as substrates to produce solvents: acetone, butanol and ethanol. All the weak acids and solvents produced by solventogenic Clostridia are, thus, building blocks of high biotechnological interest (Sauer et al., 2008).

The C_3 lactic acid ($CH_3CH(OH)COOH$), for example, has been used in the food, cosmetic, pharmaceutical, leather and polymer industries (Chen and Nielsen, 2016). One of the most attractive applications of lactic acid is the synthesis of biodegradable plastic polylactide, that is used in, increasingly demanded, food containers (Chen and Nielsen 2016; Sauer et al., 2008). The C_2 acetic acid (CH_3COOH) has a wide range of applications in biotechnology. It can be used as a building block, as vinylacetate for biopolymers and ethylacetate as a green solvent (Sauer et al., 2008). Butyric acids are another type of carboxylic acid carboxylic acid ($CH_3CH_2CH_2$–COOH) with important application in the chemical, food, and pharmaceutical industries. This building block is involved in the synthesis of thermoplastics and is used to supply butter-like notes in food flavours and as additives to increase fruit fragrance. In therapeutics, derivatives from butyric acids are used in antithyroid and vasoconstrictor drugs (Sauer et al., 2008; Xu and Jiang 2011).

An additional advantage of all the organic acids is that they are used to synthesize other high-value chemicals, such as ethanol, butanol and acetone. For example, acetic acid is a promising feedstock to produce a wide range of biochemicals, replacing the use of glucose as substrate. Technologies to obtain bio-based acetic acid are less expensive than the treatments used to obtain glucose and have been created to exclude glucose and turn the process economically more attractive (Gong et al., 2022).

Acetone, butanol and ethanol are high-value chemicals produced by solventogenic *Clostridium*, that have been used in biotechnology for many years (Sauer 2016). Acetone is an C_3 organic molecule $(CH_3)_2CO$ that has been used as building block to produce a wide range of materials, including waxes, resins, rubber, paints, acrylic glass and polypropylene (Liew et al., 2022). Acetone has potential value to the fuel sector as green diesel and jet fuel substitute with the additional advantage of reducing emissions and enhancing performance (Sauer 2016).

Butanol is a C_4 alcohol (C_4H_9OH) that can have four isomeric structures, n-butanol, 2-butanol, isobutanol, and tet-butanol; n-butanol is the most produced during ABE fermentation (Xue and Cheng, 2019). It is a high-value chemical used as building block for the synthesis of polymers, plasticisers and solvents (Dahman et al., 2019; Linney et al., 2023). n-butanol is probably the solvent receiving more attention lately especially due to its potential use as a biofuel that is able to replace pure gasoline (Dahman et al., 2019; Sauer 2016). This alcohol is described as superior to ethanol, has higher energy density as result of two extra carbons, consisting of 29.2 $MJ.L^{-1}$, whereas ethanol has 19.5 $MJ.L^{-1}$ (Xue and Cheng, 2019). Additionally, it is less hygroscopic and volatile than ethanol (Li et al., 2020).The higher calorific value, increased blending capabilities, and being safer to handle are aspects that make butanol very attractive to replace gasoline (Dahman et al., 2019; Linney et al., 2023).

Despite all the very attractive characteristics of these chemicals, the production of these chemicals during ABE fermentation increases cellular toxicity (Fischer et al.,, 2008; Weber and De Bont, 1996). For example, native solventogenic *Clostridium* has been shown to produce 5 to 16 $g.L^{-1}$ of butanol (Li et al., 2020). In *C. acetobutylicum* cells, butanol concentrations of 7 to 13 $g.L^{-1}$ show a negative impact on cell growth (Linney et al., 2023). Understanding the mechanisms involved in solvent stress can serve as a potential target to modulate and create more stress tolerant strains with higher economic viability and environmentally friendly.

1.3 Solvent stress

The production of organic acids and solvents in solventogenic *Clostridium*, along with many other cell factories, increases cellular stress. During ABE fermentation, both cell growth and solvents production can be significantly impacted by various inhibitory factors, including product inhibition, substrate inhibition, nutrient deficiencies, redox imbalances, collectively termed as solvent stress (Amoah et al., 2019; Fischer, Klein-Marcuschamer, and Stephanopoulos 2008; Sauer 2016; Tran and Zhao 2022).

The synthesis of these chemicals is thought to permeabilize and cause changes in the fluidity of the cell membrane (Linney et al., 2023). Butanol is thought to incorporate into the phospholipid polar head-group and the fatty acyl chains of the phospholipid bilayer, allowing the passive flux of ATP, protons, ions, and macromolecules, such as proteins, which causes the dissipation of the proton motive force (Linney et al., 2023). A decrease in the proton gradient and electrochemical potential will lead to a decrease on the energy status of the cell (Tomas, Welker, and Papoutsakis 2003). Solvent accumulation in the membrane also inhibits active transport, the membrane-bound ATPase and glucose uptake. The cumulative effects can partially or completely abolish the membrane gradient, further compromising cell viability (Xue and Cheng, 2019).

The production of organic acids and solvents can also create an imbalance between the reactive species (oxidants) and the antioxidant mechanisms leading to oxidative damage in a variety of biomolecules, such as DNA, proteins and lipids (Costantini 2019). Lipid damage can in turn affect the membrane stability thus compromising the solvent tolerance of the cell. Although the production and accumulation of solvents, such as butanol, lead to increased levels of cytotoxicity, the mechanisms associated to this response are not fully described (Vasylkivska and Patakova, 2020; Xue and Cheng, 2019).

1.3.1 Oxidant species versus antioxidant mechanisms

Amongst a variety of oxidants, the Reactive Oxygen Species (ROS) have profound biological relevance. During normal oxidative metabolism, O_2 accepts free electrons which can lead to ROS production leading to the generation of superoxide radical ($O_2{\cdot}^-$) and hydroxyl radical (HO·), as well as the oxidant hydrogen peroxide (H_2O_2). Besides ROS, there are other important reactive

species with notable impact on redox biology such as; reactive nitrogen species (RNS) including, nitric oxide (NO), nitrogen dioxide (NO_2), and peroxynitrite ($OONO^-$); reactive sulphur species (RSS) including persulfate (RSSH); chlorine (RCS) including hypochlorous acid (HOCl) and; reactive carbonyl species (RCS) including various forms of metabolically generated aldehydes (Sies, Berndt, and Jones 2017). Other processes may lead to electron transport uncoupling, such as multiple enzyme systems including the cytochrome P450 monoxygenase system, xanthine oxidoreductase and nitric oxide synthases can enhance the production of ROS. Additionally, metabolic by-products of cellular respiration can produce superoxide ($O_2\cdot^-$), for example through nicotinamide adenine dinucleotide phosphate (NADPH) oxidases (Costantini 2019). Prokaryotes and eukaryotes have developed an array of enzymatic and non-enzymatic modules to control the reactive species formed, usually involving low molecular weight molecules (Sies, Berndt, and Jones 2017). As for the non-enzymatic defence, glutathione (GSH) and thioredoxin are two of the most characterized examples. The enzymatic modules of oxidative stress defence can include catalases, thioredoxin, glutathione peroxidases, peroxiredoxins, aquaporins and metallothioneins (Robinson, Whitehall, and Cavet 2001; Sies, Berndt, and Jones 2017). In bacteria, ROS scavenging is often accomplished by catalases and alkyl hydroperoxide reductases, which reduce H_2O_2 to H_2O and O_2. This reaction is not favourable for strict anaerobic bacteria, which is the case of Clostridia (Riebe et al., 2009).

Metallothioneins (MTs) were selected, in this work, to improve our knowledge on solvent tolerance. MTs have been described to play an important role on cell homeostasis (Shabb, Muhonen, and Mehus 2017). The term Metallothioneins incorporates a family usually described as highly conserved, heat-stable, low-molecular-weight and cysteine-rich intracellular proteins (Blindauer 2011). Although their cellular functions have not been fully described yet, these proteins are described as “molecular soldiers” capable of immobilizing the “intruder or enemy” metal(loid) blocking its toxic action. In microorganisms *mt* expression is induced by environmental factors, that is not only dependent on the presence of metals such as Zinc but also of heat and cold shocks, pH fluctuation, starvation and oxidative stress. The function(s) of MTs remain unknown despite some experimental evidence pointing to the importance in multiple and very different cellular processes (Gutiérrez et al., 2019). The heterologous expression of MTs from tilapia, humans and mouse in *Escherichia coli* cells have been shown to induce tolerance to higher levels of butanol (Chin et al., 2013, 2017).

1.3.2 Oxidative stress in anaerobic bacteria

Anaerobic bacteria control the redox balance through central metabolism. The reducing agents generated at the end of the glycolytic pathway are re-oxidized during alcohol synthesis and hydrogen production (Figure 1.3). The presence of reactive species during ABE fermentation is believed to affect the redox balance required for the butanol metabolic pathways as the presence of molecular oxygen can oxidize important enzymes, inactivating them (Zhang Lei et al., 2014).

Substrates and inhibitors present in the biomass feedstocks such as polyphenols, thiols and carbohydrates can become oxidized forming hydrogen peroxide that can diffuse into the cells and increase the redox imbalance during fermentation (Imlay 2002). Additionally, when obligate anaerobes are exposed to air, low potential flavoproteins causes the production of ROS such as superoxide and hydrogen peroxide (Imlay 2002).

The catabolism of substrates into butanol, mainly the conversion of pyruvate to acetyl-CoA mediated by the pyruvate:ferredoxin oxireductase (PFOR), is severely affected by the presence of oxygen (Imlay 2002, 2020). In normal conditions this enzyme catalyses the oxidative decarboxylation of pyruvate, transfers electrons to ferredoxin which in turn will be delivered to hydrogenase and produces H_2 (Figure 1.3). PFOR contains up to three iron-sulphur clusters to which ferredoxin binds and where electrons are transferred into but, in the presence of oxygen, these clusters are oxidized inactivating this enzyme and consequently compromising the metabolic pathway (Figure 1.3) (Imlay 2002).

It has been described that Clostridia use reducing agents such as NAD(P)H and Ferredoxin (Fd) to reduce oxidative stress, compromising their availability for the ABE metabolic pathways (Figure 1.3) (Zhang Lei et al., 2014). This increases the redox imbalance towards solvent synthesis, such as butanol. To push the metabolic pathways towards butanol production, the redox balance in some Clostridia species has been manipulated by the addition of artificial electron carriers, for example methyl viologen and, by inhibiting the hydrogen synthesis pathway (Figure 1.3) (Du et al., 2015).

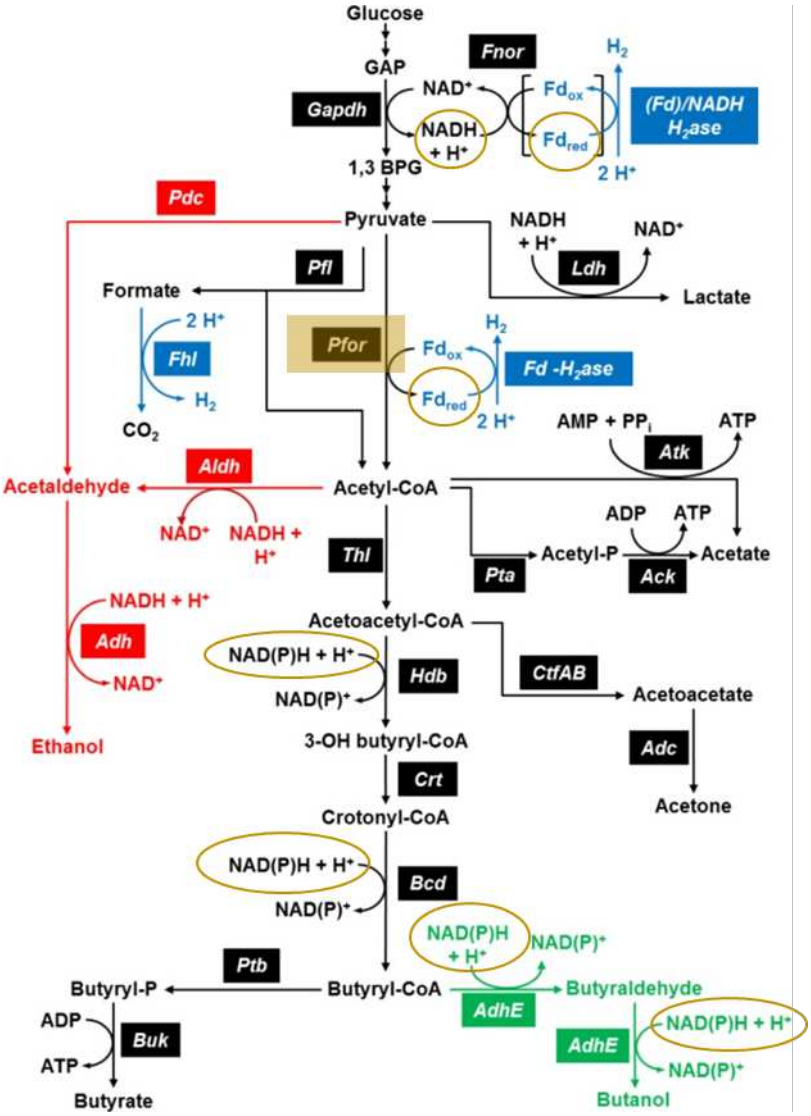

Figure 1.3. Illustration of the generic enzymatic and redox reactions of the ABE metabolic pathways in *Clostridium spp*. During acidogenesis there is an increase in reducing agents such as NAD(P)H and Ferredoxin (Fd) that will be lately used in the solventogenic phase. Using these agents when there is an increase of the oxidative stress compromise their availability for the ABE metabolic pathways.The Acetone, Butanol and Ethanol pathways are represented in black, green and red, respectively. In blue is represented the hydrogen metabolic pathway. The NAD(P)H, Fd (yellow circles) describe the redox reactions occurring during butanol fermentation. The pyruvate:ferredoxin oxireductase (Pfor) codes an enzyme that is oxidized in the presence of oxygen (yellow rectangle) (Mazzoli 2012).

These anaerobic species have developed mechanisms to survive under a limited exposure to oxygen, expressing genes encoding for detoxification systems including flavodiiron proteins, desulfoferrodoxin and rubrerythrins. Their reducing equivalents are used for scavenging of ROS

and molecular oxygen which is important to protect the metabolic enzymes that are oxygen sensitive (Zhang Lei et al., 2014).

Transcriptomic analysis in *C. beijerinckii* and *C. acetobutylicum* have shown an increase on the expression of heat-shock proteins (HSPs) during the acidogenesis and solventogenesis phases (Tomas, Welker, and Papoutsakis 2003). Usually, these proteins function as molecular chaperones and are involved in protein folding and stabilization and also influence DNA conformation (Patakova et al., 2019). Butanol production and accumulation upregulates the expression of heat shock genes, mediated by the operons *groESL* and *dnaK* (Patakova et al., 2019a). In *C. acetobutylicum* the overexpression of the *groESL* operon has improved solvent tolerance, prolonged and enhanced the growth of the cells and consequently the production of more solvent (Tomas, Welker, and Papoutsakis 2003). Other heat shock proteases, such as *grpE* and *htpG,* when overexpressed in *C. acetobutylicium*, and have shown a slight increase in butanol production (Xue and Cheng, 2019) This might be indicative that the generation of reactive species during ABE fermentation is affecting the structure of important proteins for cell homeostasis (Alsaker, Paredes, and Papoutsakis 2010). Beyond this, the free radicals or other oxidants can oxidase more biomolecules such as DNA or lipids. Lipid oxidation can affect the phospholipids composition, compromising the cell structure and signalling (Spickett, Reis, and Pitt 2011).

The heterologous expression of antioxidant enzymes, such as metallothionein in *E. coli* cells, have been shown to tolerate higher levels of butanol (Chin et al., 2013). The improvement in butanol production, expressing MTs was then sustained in an engineered *E. coli* strain with the Clostridia*l* metabolic pathway for butanol production. The overexpression of the tilapia MT resulted in an improved n-butanol productivity of 320 $mg.L^{-1}$, which is approximately a 3x increase in capacity, comparing to the control strain (95.1 $mg.L^{-1}$) (Chin et al., 2017).

Throughout evolutionary processes, microorganisms have been developing an array of strategies to bolster cellular resilience against solvent stresses, including metabolic detoxification, heat shock stress proteins and other transcriptional responses (Ezraty et al., 2017; Riebe et al., 2009. However, the butanol production in large scale still faces impediments due to toxicity towards producing cells. The efforts trying to obtain more tolerant strains fail to exhibit a corresponding enhancement in butanol production capacity. Furthermore, the molecular mechanisms underlying butanol tolerance remain incompletely understood, being a challenge for further improvement of Clostridia.

1.4 Bacterial cell envelope

The bacterial cell envelope is a complex and flexible structure that is responsible for the shape, protection and homeostasis of the cell (Dörr, Moynihan, and Mayer 2019; Silhavy, Kahne, and Walker 2010). Organic acid accumulation within bacterial cells lead to a more acidic internal environment due to deprotonation of the weak acid in the cytoplasm which affect the cell envelope stability (Guo et al., 2020). Another example is butanol, this high value chemical is believed to primarily affect phospholipid headgroups, resulting in membrane thinning and acyl chain splaying. This disruption in membrane fluidity can lead to intracellular component leakage and the breakdown of ion gradient maintenance across the cell membrane (Chang and Cronan, 1999; Fozo and Quivey, 2004; Wu et al., 2012).

The production and accumulation of solvents in bacteria, including in solventogenic *Clostridium* species, have been observed to induce alterations in the composition of the cell envelope. Modifying the lipid species in the membrane is also a very common mechanism of protection against the solvent stress. These changes in the cell envelope are manifested in the lipid species present in the membrane, such as phospholipids, glycolipids, sphingolipids, and hopanoids, as well as in the fatty acid (FA) profile of these lipids (Chang and Cronan, 1999; Fozo and Quivey, 2004; Wu et al., 2012). These modifications serve to stabilize the cell envelope, counteracting the effects of solvents on membrane fluidity, which could otherwise compromise cell survival.

Although the lipid membrane composition and its regulatory mechanisms in anaerobic Clostridia remain poorly understood, solvent accumulation has been implicated in inducing modifications or damage to the lipid membrane during ABE fermentation (Xue and Cheng, 2019). Investigating the solventogenic *Clostridium* lipidome and its regulation mechanisms can be an important key to understand the network between solvent production and toxicity, which can be the key to find better strategies to improve cell factories (Linney et al., 2023).

Clostridium spp. are Gram-positive bacteria, which means their cell wall has two main layers, corresponding to the inner or cytoplasmatic membrane and a thick peptidoglycan layer (Figure 1.4). In contrast, Gram-negative bacteria have three principal layers, the outer membrane, the peptidoglycan and the cytoplasmic or inner membrane (Silhavy, Kahne, and Walker 2010). The outer membrane has an important role in stabilizing the inner membrane in Gram-negative bacteria, however, both bacteria live in harsh environments. The thicker peptidoglycan layer of Gram-positive bacteria compensates and confers rigidity to the cell and is the key for cell shape. It is made up of repeating units alternating monosaccharide residues β-1,4-linked N-

acetylglucosamine (GlcNAc) and N-acetylmuramic acid (MurNAc), that are cross-linked via short peptide bridges attached to MurNac residues (Dörr, Moynihan, and Mayer 2019). Threading through the peptidoglycan are anionic polymers that help maintain the structure and function of the envelope (Silhavy, Kahne, and Walker 2010).

The inner membrane has a crucial role in cell homeostasis and viability, it controls the transport or diffusion of molecules between the intracellular and extracellular space, it shapes the cell, controls cell division and the electrochemical gradient(Parsons and Rock, 2013; Silhavy et al.,, 2010; Strahl and Errington, 2017). In bacteria, this membrane is composed of proteins, sugars and lipids, where the lipids form a bilayer structure (Strahl and Errington, 2017).

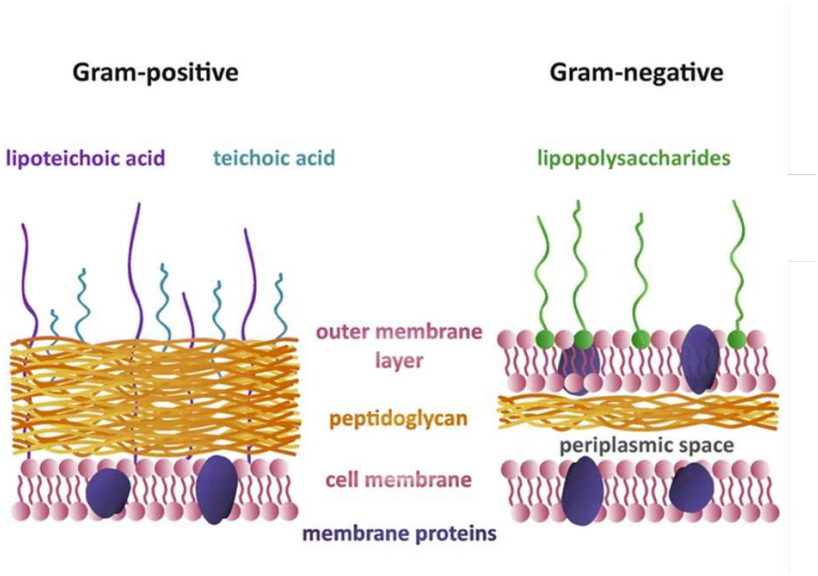

Figure 1.4. Illustration of the generic cell envelope composition of Gram-negative and Gram-positive bacteria. Gram-positive cell walls are characterised by a single lipid plasma membrane and a thick layer of peptidoglycan intertwined with teichoic and lipoteichoic acids. In contrast, Gram-negative bacteria possess both an inner and an outer cell membrane, with a thin layer of peptidoglycan located in the periplasmic space between the two membranes. Additionally, Gram-negative bacteria feature a layer of lipopolysaccharide that lines the outer membrane (Pajerski et al., 2019).

1.4.1 Role of lipids in the membrane structure and stability

Lipids are a diverse and ubiquitous group of compounds which have many key biological and structural roles in the cell membranes (Charubin et al., 2018). The lipid composition not only defines the structure of the membrane but also plays a critical role in its function (Guo et al.,

2020). Understanding how lipids assemble to form the lipid bilayer, how their composition changes during different growth stages, in response to various stress conditions, and their impact on membrane structure, stability, and fluidity are crucial aspects of membrane biology and microbiology (Guan and Goldfine, 2021; Parsons and Rock, 2013; Strahl and Errington, 2017). This knowledge is essential to understand how cells adapt and balance the organization of the membrane under hostile conditions (Sohlenkamp and Geiger, 2015).

Lipid organization in the membrane

Advances into understanding the organisation and properties of lipid bilayers led to the definition of three key parameters: lipid head groups, fatty acid moieties, and phase behaviour (Strahl and Errington, 2017). These aspects provide valuable insights into the fluidity and packing of lipid bilayers. Although the majority of studies used *E. coli*, they can serve as a model to understand general membrane biology in bacteria. This can shed light on both the common and unique adaptations that different bacterial strains have developed in response to specific environments and requirements (Parsons and Rock, 2013; Strahl and Errington, 2017).

Phospholipids are glycerolipids that contain two fatty acid chains and are the main lipids of the bacterial membrane (Zhang and Rock 2008). Their cylindrical shape allows the spontaneously formation of bilayers (Strahl and Errington, 2017). Other lipid groups, such as glycolipids and cholesterol, can also form part of the membrane structure (Strahl and Errington, 2017). Phosphatidylglycerol (PG), phosphatidylserine (PS) and di-glycosylated diacylglycerol (DGDG) are generally the most common constituents of the bilayer. Lipids such as phosphatidylethanolamine (PE), mono-glycosylated diacylglycerol (MGDG) and cardiolipin (CL) are less prone to form bilayers as their small headgroup and conical shape tend to form non-lamellar phases (Goldfine 2019). Thus, the ratio between bilayer forming lipids and non-bilayer preferring lipids is balanced to maintain the bilayer structural conformation (Goldfine 2019).

The interaction of lipids in the cell membrane results in the formation of a bilayer structure with minimal curvature, primarily due to the cylindrical shape of the lipids involved (Strahl and Errington, 2017). The FA chains of phospholipids and glycolipids are hydrophobic in nature, causing them to orient themselves towards the centre of the bilayer (Figure 1.5). In this arrangement, stable associations are established with adjacent chains through non-covalent interactions (Silhavy et al., 2010; Strahl and Errington, 2017).

The liquid crystalline phase (L_c) is the most common under physiological conditions; the polar head groups align together at the interface with water and the hydrophobic FAs align in parallel to one another away from the water (Figure 1.5). In this state, lipids have relative fluidity, they can rotate, have lateral diffusion, allow proteins to embed and have a functional conformation in the membrane (Fonseca et al., 2019; Goldfine 2019) (Figure 1.5). Modifications in the conditions of the cell, such as temperature, lead to a slightly change of the bilayer arrangement, becoming less rigid in the so-called gel phase (L_β) (Figure 1.5). As the temperature increases, the lipid bilayer transitions from a structured gel phase to a more dynamic fluid phase (L_α), where the lipids are highly disordered, with increased lateral and rotational diffusion (Fonseca et al., 2019; Startek et al., 2019).

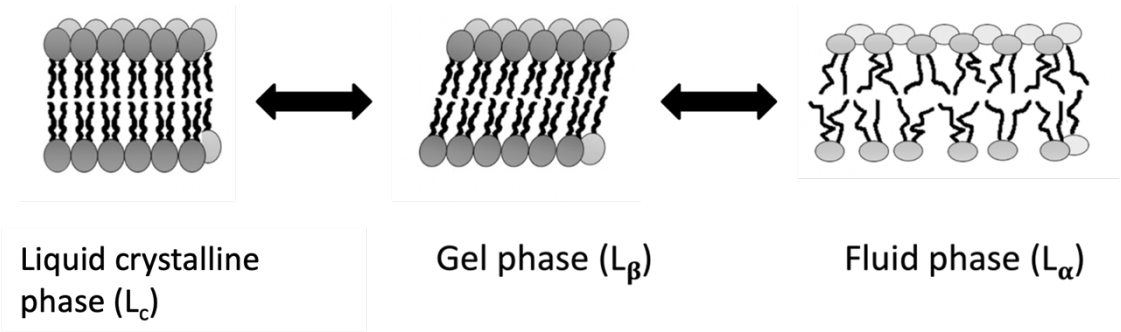

Figure 1.5. Simplified scheme of the lipid membrane phases. In the liquid crystalline phase (L_c) the lipids align in parallel to one another, having relative fluidity, showing lower rotation and lateral diffusion, allowing proteins to embed and have a functional conformation. The FA chains can be tilted with respect to the liquid crystalline phase, forming the gel phase (L_β). The membrane can transition to a more fluid phase (L_α), where the lipids highly disordered with increasing lateral and rotational diffusion (Adapted from Startek et al., 2019).

The FA chains have an important role on the degree of packing and in the temperature needed to change the lamellar phase of the membrane. In the FAs both chain length and unsaturation ratio have been described as important factors controlling bilayer packing (Fonseca et al., 2019; Kranenburg and Smit 2005). The membrane fluidity is highly related to the ratio between saturated fatty acids (SFA) and unsaturated fatty acids (UFA). The presence of more cis-unsaturation and trans-unsaturation is more prone to increase the membrane fluidity (Figure 1.6). It has been also described that cyclic fatty acids (CFA) also modulate the membrane fluidity in response to pH stress (Fonseca et al., 2019).

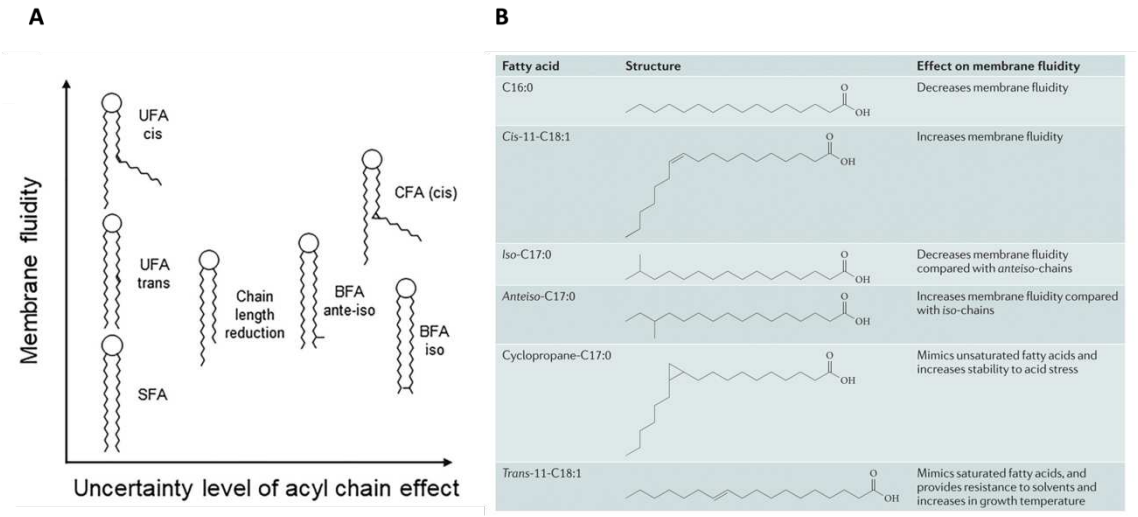

Figure 1.6. Representation of the different FA chain compositions and their possible role in the membrane fluidity.The structure and geometry of FA chains have a crucial role in determining the shape of lipids and the extent of lipid packing within the bilayer. Acyl chains conformations that hinder dense and regular packing contributes to increased membrane fluidity (Zhang and Rock 2008). For example, unsaturation in the cis conformation, shorter chain lengths, ante-iso-branched chains of fatty acids, and cyclic fatty acids (CFA) have all been documented to enhance membrane fluidity. FA: fatty acids; UFA: unsaturated FA; SFA: saturated FA; BFA: branched FA; CFA: cyclic FA (cycC19:0) (Fonseca et al., 2019).

The number of carbons in the FA also play a role in the transition between phases. Longer FA chains require higher temperatures for the transition from gel phase to fluid phase and, for that reason are thought to increase the stability of the membrane (Kranenburg and Smit, 2005). Effects on the FA chain length, unsaturation level and production and accumulation of solvents in *E. coli*, has also shown to be interconnected. In *E. coli*, an increase in the ratio of UFA/SFA in the membrane lipids can potentially increase the ethanol tolerance (Luo et al., 2009). Higher productions of *trans* unsaturated fatty acids (TUFA) in *E. coli* have shown to improve tolerance to octanoic acid (Tan et al., 2016). When toluene was added to a *Pseudomonas putida* culture, a conversion of cis-unsaturated fatty acids to the corresponding trans-fatty acids was observed (Weber, Lsken, and De Bont 1994). This was probably a mechanism to reduce the fluidity of the membrane by reshaping he lipid bilayer (Zhang and Rock 2008).

1.4.2 Lipids

Lipids are a heterogeneous collection of molecules in terms of structure and functionality (Fahy et al., 2011). According to the International Lipid Classification and Nomenclature Committee (LIPID MAPS), lipids are divided in eight categories, the fatty acids, glycerolipids, glycerophospholipids, sphingolipids, saccharolipids, polyketides, sterol lipids and prenol lipids (Fahy et al., 2011). In bacteria, the cytoplasmatic membrane is formed essentially from phospholipids. However, it can also be found phosphorous-free membrane lipids, including ornithine lipids (OLs), sulfolipids, diacylglyceryl-N,N,N trimethylhomoserine (DGTS), glycolipids (GLs), diacylglycerols (DAG) and hopanoids (HOPs) (Sohlenkamp and Geiger 2016).

Phospholipids

Almost all phospholipids derive from phosphatidic acids (PAs), molecules where the third hydroxyl is esterified to a phosphoric acid (Figure 1.7). From PA other different phospholipid classes can be synthesized, such as phosphatidylethanolamine (PE), phosphatidylcholine (PC), lipids phosphatidylserine (PS), phosphatidylinositol (PI), phosphatidylglycerol (PG) or cardiolipin (CL) (Figure 1.7).

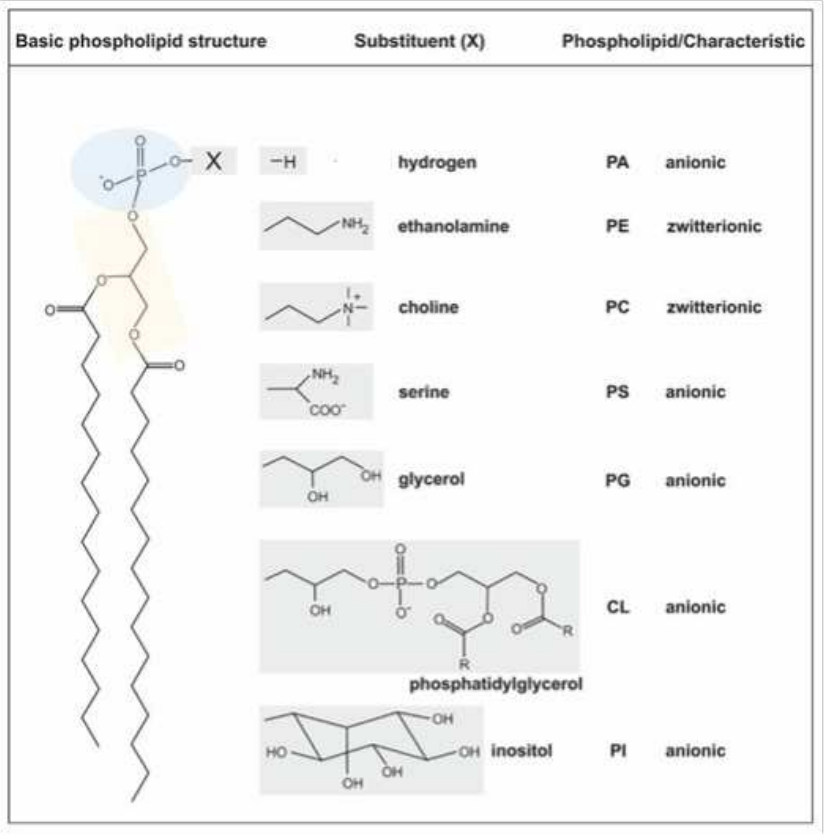

Figure 1.7. Chemical structure of general phospholipids.Structures illustrated contain the two fatty acids chains, linked to a glycerol (yellow), the phosphate group (blue) and the polar head group (grey) attached via a phosphodiester bond. The most common head groups and their charges are listed in this figure; phosphatidic acid (PA); phosphatidylethanolamine (PE); phosphatidylcholine (PC); phosphatidylserine (PS); phosphatidylglycerol P(G); cardiolipin (CL) and phosphatidylinositol (PI). Adapted from Aktas and colleagues (2014).

The most abundant phospholipids found in both Gram-negative and Gram-positive bacteria are PE, PG, and CL (Sohlenkamp and Geiger 2016). A few bacteria also accumulate the anionic lipid PS which is an intermediate in the synthesis of PE. Normally the enzyme phosphatidylserine decarboxylase (Psd) is very efficient in converting PS into PE, leaving barely detectable amounts of PS. However, studies using techniques such as TLC and gas-chromatography identified PS as a major phospholipid in *C. botulinum* (Evans et al., 1998).

Modifications to phospholipids, including PE and PG, are commonly found in many bacteria e.g. the mono- and di- methylation of PE (Sohlenkamp and Geiger, 2015). During this process, the headgroup of PE undergoes a three-fold methylation process, resulting in the intermediate phosphatidyl-N,N-dimethylethanolamine (PDME) or phosphatidyl-N-monomethylethanolamine

(PMME) (Figure 1.8) (Kleetz et al., 2021). The three methylation reactions are catalyzed by enzymes known as phospholipid N-methyltransferases (Pmts). Bacteria may possess one or multiple Pmts, which can either catalyze all three methylation reactions from PE to PMME and PDME or convert PE to PC, although the latter is less common (Kleetz et al., 2021).

Aminoacylation of PGs is a process in which the glycerol moiety is esterified with amino acids such as lysine or alanine (Figure 1.8) and it represents a mechanism in which bacterial membranes adapt to changing environmental conditions (Hebecker et al., 2015). Some bacterial species exhibit aminoacylation in cardiolipin (CL), leading to the formation of L-CL (Roy 2009). Initially, this mechanism was thought to primarily help bacteria reduce the net negative charge of their cell envelope, thereby decreasing its affinity for various antibacterial agents like cationic antimicrobial peptides (CAMPs), which are produced during host infections (Roy 2009). However, subsequent findings have demonstrated that aminoacyl-PGs (aa-PGs) also provide advantages in other challenging growth conditions, such as those encountered during osmotic or acidic stress (Hebecker et al., 2015; Roy 2009).

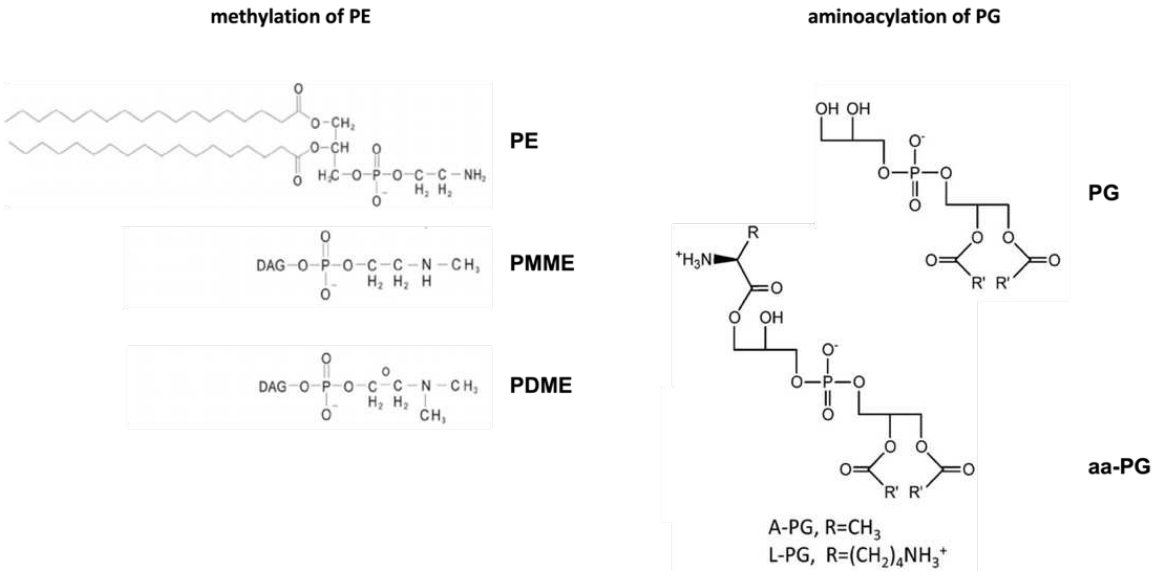

Figure 1.8. Two common modifications of PE and PG in bacteria.Methylation of PE producing PMME and/or PDME. Aminoacylation of PG producing A-PG or L-PG, depending on the R group. Figure adapted from Aktas and Narberhaus 2009; Roy 2009.

Lysophospholipids (LPLs) are a class of phospholipids characterized by having a single fatty acid chain and a polar head group. These compounds can be found in bacterial membranes, although

they typically constitute a smaller fraction. However, in stressed bacterial cells, the levels of LPLs may accumulate (Zheng et al., 2017). In Gram-negative bacteria, lysophosphatidylethanolamine (LPE) is the most encountered form of LPLs. While the precise biological role of LPLs in bacteria remains incompletely understood, several theories have been proposed. One prominent hypothesis suggests that LPLs serve as a metabolic intermediate during the turnover of phospholipids (Zheng et al., 2017). These molecules possess some degree of water solubility, enabling them to access not only the lipid membranes but also non-membranous cellular compartments like the cytoplasm (Zheng et al., 2017). Intriguingly, experiments have demonstrated that exposure increasing temperature (from 30 to 42°C) can lead to a four-fold increases in LPE levels (Zheng et al., 2017). Another hypothesis is that LPE may exhibit chaperone-like properties during protein folding and confer protection against thermal denaturation (Kern et al., 2001). Furthermore, it was observed that LPE accumulation is often accompanied by an increase in CL and, in *E. coli* a CL microdomain is localized in the septal region of dividing cells. This led to the possibility that LPE might be present at the cell division site to possibly maintain an optimal membrane curvature (Zheng et al., 2017).

Many anaerobic bacteria have plasmalogens, described as 1-O-alk-1-enyl 2-acyl glycerol phospholipids (Goldfine 2010). The difference between plasmalogens comparing to other phospholipids is that these compounds have an aldehyde linked by an ether bond in the *sn*-1 of glycerol (Figure 1.9). The fatty aldehyde easily acquires the enol form by transposition of a hydrogen and double bond change (Blanco and Blanco, 2017). The most commonly plasmalogen forms of glycerophospholipids found in bacteria derive from PE, PG, PS and CL (Goldfine 2010; Guan and Goldfine 2021). The ether linkage characteristic of plasmalogens can also occur in glyceroglycolipids (Figure 1.9 d) (Goldfine 2010).

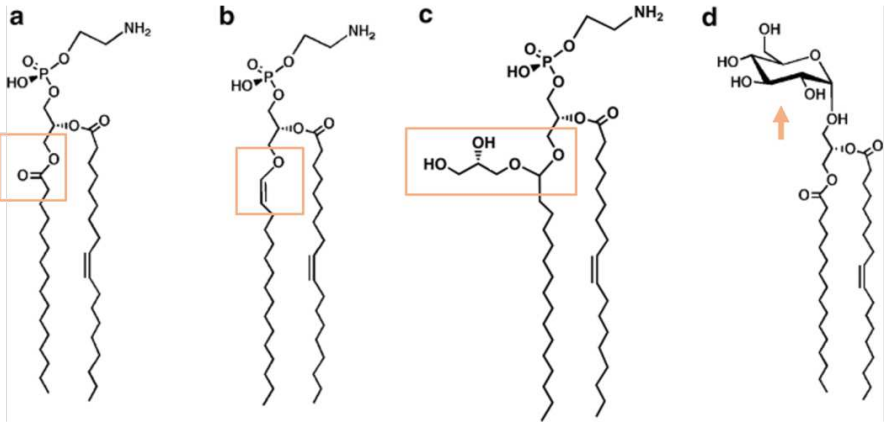

Figure 1.9. Examples of plasmalogen forms of PE and glyceroglycolipids in bacteria.(a) phosphatidylethanolamine (PE); (b) plasmalogen form of PE; (c) glycerol acetal of the plasmalogen form of PE (GAPlsE); (d) glucosyldiacylglycerol an example of a glycolipid. The orange rectangles highlight the differences between PE and its derivatives. The arrow shows the sugar moiety (Goldfine 2019).

Glycolipids

Many bacterial species contain certain glyceroglycolipids and glycolipids (Sohlenkamp and Geiger, 2015). Although not a major component, these lipids can be found in both Gram-positive and Gram-negative bacteria (Figure 1.9). Glyceroglycolipids and glycolipids are constituted by a sugar and a lipid moiety and vary greatly in the structure and in number of sugar moieties attached to the glycerol backbone (Guan and Goldfine 2021). The glycolipids structure lacks the phosphate group. Several of them contain a diacylglycerol backbone (DAG) and the presence of glycosylated DAG derivatives (GLs) has been known in Gram-positive bacteria (Goldfine 2019).

Changes in FA composition and cholesterol content, as well as variations in growth temperature conditions, have been observed to induce alterations in the ratio of mono- and di-glycosylated DAG, known as MGDG and DGDG, respectively, in *Acholeplasma laidlawii*. Specifically, higher temperatures or elevated levels of unsaturated fatty acids were found to increase the MGDG:DGDG ratio. This change in ratio may represent an adaptive mechanism employed by the cells to cope with more disordered environmental conditions (Guan and Goldfine 2021; Parsons and Rock 2013).

Hopanoids and sphingolipids

Other lipids such as hopanoids (HOPs) and sphingolipids (SLs), that do not have a DAG backbone can be found in the membrane of almost all characterized α-proteobacteria (Belin et al., 2018). It is thought that hopanoids modulate the fluidity and permeability of membranes enhancing the stability and impermeability of the bacterial membrane (Belin et al., 2018). On the other hand, SLs are found in more restricted groups of bacteria, containing sugar moieties or deriving from PE or PG (Sohlenkamp and Geiger, 2015). Ceramide phosphoethanolamine (Cer-PE) and ceramide phosphoglycerol (Cer-PG) have been detected in some anaerobic bacteria (Sohlenkamp and Geiger, 2015).

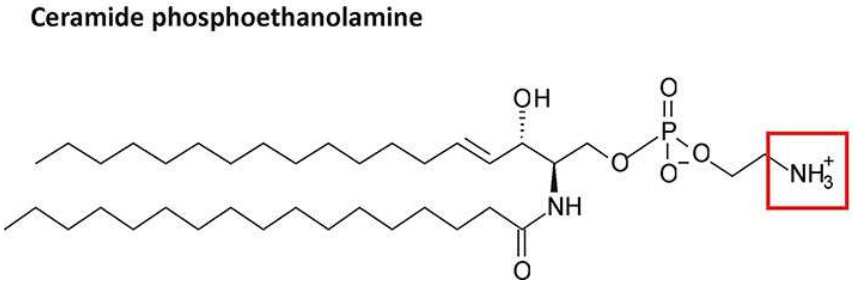

Figure 1.10. Example of a ceramide phosphoethanolamine structure in bacteria. Consists of a ceramide backbone with two hydrocarbon chains: a long-chain base linked to a fatty acid via an amide bond attached to a phosphorylethanolamine molecule (Panevska et al., 2019).

The main lipids in *Clostridium*

Clostridium comprises a genus of hundreds of different species with important roles in human health and biotechnology (Johnson 2009). The extensive genetic diversity across the genus translates into variations in the lipidome characteristics (Guan and Goldfine, 2021). *C. saccharoperbutylacetonicum* is a solventogenic bacterium and has been noted to possess PE; PG and CL, including their plasmalogen forms (Duerre, 2005). Although the full lipidome of *C. saccharoperbutylacetonicum* remains incompletely characterized and quantified, insights into its lipidome have been inferred by dividing the *Clostridium* genus into new genera based on the analysis of the 16S RNA gene sequence (Linney et al., 2023; Wiegel, Tanner, and Rainey 2006). Group I, to which *C. saccharoperbutylacetonicum* belongs, also includes species like *Clostridium butyricum*, *C. beijerinckii*, *C. saccharobutylicum*, and a group Clostridial species called *Clostridium*

botulinum, which have been characterized (Duerre 2005; Guan and Goldfine 2021). In this group, in addition to PE, PG, CL and their plasmalogen forms, some of these species have been found to contain glycerol acetal forms of plasmenylethanolamine (GAPlsE), as represented in Figure 1.9. *C. beijerinckii*, for instance, was found to have phosphatidyl-N-monomethylethanolamine (PMME) and its plasmalogen form. Meanwhile, *C. acetobutylicum*, although phylogenetically distinct from *C. beijerinckii*, shares certain lipidomic features, where main differences include higher quantities of glycosyldiradylglycerols and a phosphoethanolamine-modified monoglycosyldiradylglycerol (Figure 1.9). In *C. acetobutylicum*, as solvent production rises, there is an increase in the presence of ethanolamine-phosphate-modified lipids, including dihexosyldiradylglycerol (DihexDAG) and Etn-P-modified monogalactosyl diradylglycerol. (Tian, Guan, and Goldfine 2013).

In sum, the presence of three major phospholipids, namely PE, PG, and CL, in both their acyl and alk-1-enyl acyl (plasmalogen) forms, represents a common feature among *Clostridium* species. Additionally, glycolipids such as dihexosyldiacylglycerol (DihexDAG) and EtnP-galactosyldiradylglycerol have been described in *Clostridium*, primarily under conditions of stress (Goldfine 2010, 2017, 2019; Guan and Goldfine 2021; Tian, Guan, and Goldfine 2013). While sphingolipids and hopanoids have not been specifically identified in the Group I, which includes *C. saccharoperbutylacetonicum*, these lipids are recognized as significant regulators of membrane fluidity in numerous bacterial species (Belin et al., 2018; Duerre 2005; Otto Geiger, Sohlenkamp, and López-Lara 2019; Guan and Goldfine 2021; Sohlenkamp and Geiger 2015). Consequently, they may play a role, albeit indirect, in butanol tolerance (Belin et al., 2018). Investigating the potential presence of these lipid species in solventogenic *Clostridium* could aid in characterizing and understanding its lipidome, as well as elucidating lipid adaptations during ABE fermentation.

1.4.3 The FA metabolic pathway

Fatty acids (FAs) are integral components of phospholipids and are synthesized through a distinct metabolic pathway known as type II fatty acid synthesis (FASII) (Geiger et al., 2019; Schujman and de Mendoza, 2008). FA synthesis occurs in two phases: initiation and elongation (Figure 1.11).

The initiation begins with the carboxylation of acetyl-CoA, resulting in the formation of malonyl-coenzyme A (malonyl-CoA), a process mediated by acetyl-CoA carboxylase (ACC). The malonyl-CoA malonate group is then transferred to an acyl carrier protein (ACP) to produce malonyl-ACP, a reaction catalyzed by FabD (Figure 1.11) (Parsons and Rock, 2013).

The transition from initiation to elongation occurs when the previously generated malonyl-ACP is condensed with a short-chain acyl-CoA molecule (C2-C5) (Parsons and Rock, 2013). This leads to the production of acetoacetyl-ACP (or Ketoacyl-ACP), which is subsequently elongated by two carbon units until a long-chain acyl-ACP is formed (Figure 1.11). This elongation process is mediated by a group of Fab enzymes. FabG initiates the elongation by reducing acetoacetyl-ACP to β-hydroxyacyl-ACP (Parsons and Rock, 2013).

The second step in elongation involves converting β-hydroxyacyl-ACP to trans-2-enoyl-ACP (Figure 1.11), that in *E. coli*, is mediated by FabA and FabZ. Beyond this role, FabA and FabZ contribute during synthesis of unsaturated fatty acids in Gram-positive bacteria (Parsons and Rock, 2013; Schujman and de Mendoza, 2008). The subsequent reaction in the elongation cycle is catalysed by NAD(P)H trans-2-enoyl-ACP reductase, that can involve the FabI, FabK, or FabV enzymes depending on the microorganism. Rounds of elongation continue with the assistance of enzymes such as FabF or FabB, depending on the bacteria, until the acyl-ACP reaches a sufficient chain length to be transacylated in three steps to glycerol-3-phosphate (G3P) (Parsons and Rock, 2013; Sohlenkamp and Geiger, 2015). This step generates an intermediate in the synthesis of phospholipids known as phosphatidic acid (PA).

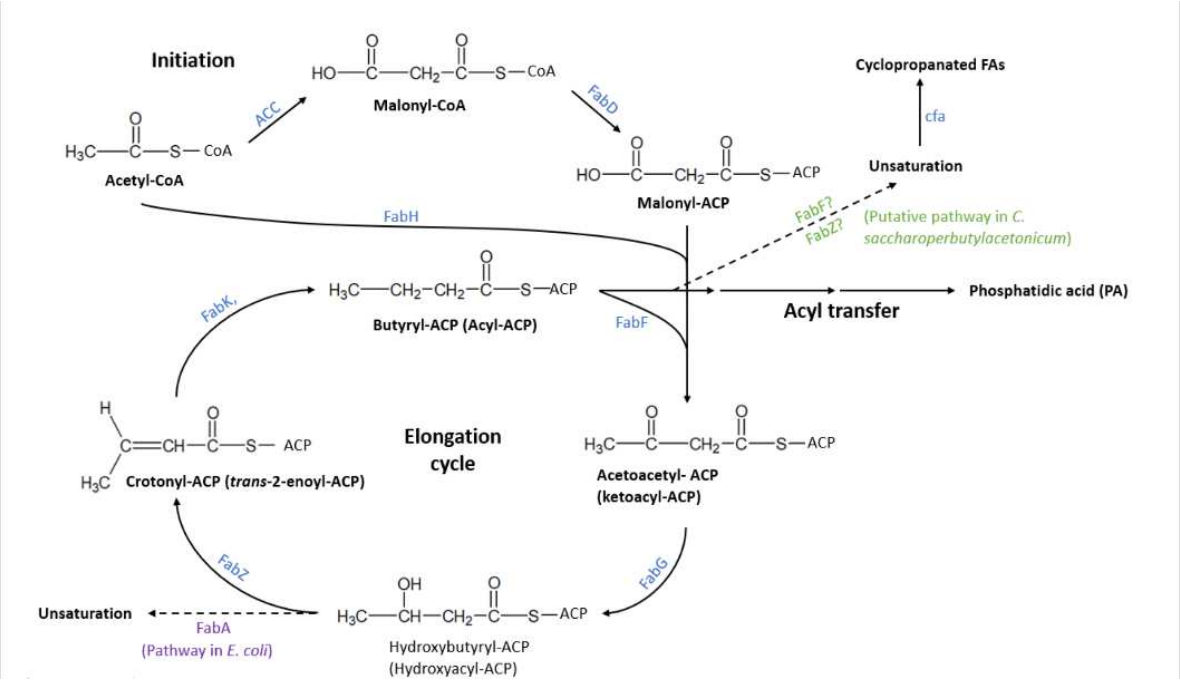

Figure 1.11. Type II fatty acid synthesis in bacteria. The initiation module usually starts with the condensation of an acyl-CoA with malonyl-ACP via FabH. Malonyl-CoA is formed by acetyl-CoA carboxylase via ACC and then converted into Malonyl-ACP via FadD. The elongation module receives the β-ketoacyl-ACP and malonyl-ACP and extend the fatty acid by two carbons, via FabG, FabZ, FabK and FabF. Unsaturations in the FA involve FabA (*E. coli*) and possibly FabZ/F (*Clostridium*). The acyl-ACP of the fatty acyl chains are transferred to the glycerol 3- phosphate (Linney, 2021; Parsons and Rock, 2013).

1.4.4 Phospholipids biosynthesis

The general phospholipid biosynthesis in bacteria starts with the acylation of a molecule of glycerol-3-phosphate (G3P) (Parsons and Rock, 2013). An acyl group from acyl-ACP is transferred to G3P in a two-step process mediated by PlsX and PlxY, to form lysophosphatidic acid (LPA). A second acylation catalysed by PlsC add another acyl chain from acyl-ACP forming the phosphatidic acid (PA) (Sohlenkamp and Geiger, 2015).

PA is the precursor for the synthesis of other phospholipids and glycolipids (Figure 1.12). Following the phospholipid biosynthesis, CDP-diacylglycerol synthase (CdsA) produces CDP-diacylglycerol (CDP-DAG) from PA and cytosine triphosphate (CTP) (Sohlenkamp and Geiger, 2015). The CDP-DAG can proceed either to the synthesis of PS and PE or synthesis of PG and CL (Goldfine 2019).

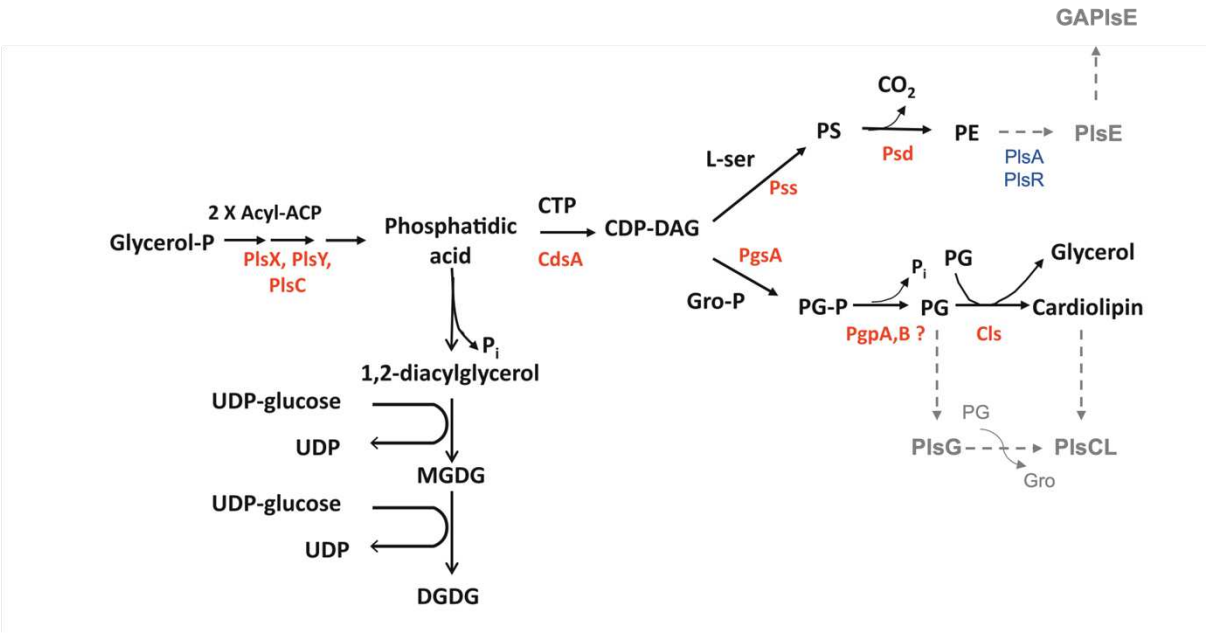

Figure 1.12. General phospholipid synthesis in bacteria. The phospholipid synthesis starts with synthesis of phosphatidic acid (PA) by the acylation of Glycerol-P mediated by the enzymes PlsX, PlsY, PlsC. Cytosine diphosphate -diacylglycerol (CDP-DAG) is a key intermediate in phospholipid synthesis and is formed by CdsA from PA and cytosine triphosphate (CTP). Phosphatidylethanolamine (PE) and Phosphatidylglycerol (PG) are produced from CDP-DAG in two steps; mediated by phosphatidylserine synthase (PssA) and phosphatidylserine decarboxylase (Psd), for PE synthesis; mediated by phosphatidylglycerol synthase (PgsA) and phosphatidylglycerol phosphate phosphatase (PgpP) for PG synthesis. Cardiolipin (CL) is synthesized through the condensation of two PG molecules by cardiolipin synthase (Cls). Glycolipids can be synthesised from PA by the reaction of a uridine diphosphate sugar with diacylglycerol. The enzymes involved are represented in red. In grey are represented the extra lipids produced in solventogenic *Clostridium* (Goldfine 2019; Guan and Goldfine 2021).

The enzyme phosphatidylserine synthase (Pss) condenses a serine molecule to the CDP-DAG, coupled with the release of cytidine monophosphate (CMP), leading to the synthesis of phosphatidylserine (PS) (Parsons and Rock, 2013). The final reaction that culminates in phosphatodylethanolamine (PE) being catalysed by phosphatidylserine decarboxylase (Psd), which decarboxylates the serine headgroup resulting in the release of CO_2 (Figure 1.12) (Parsons and Rock, 2013).

CDP-DAG also undergoes another route to produce PG and CL the other main glycerophospholipid classes found in bacteria membrane (Figure 1.12). The synthesis of PG occurs in two steps, in the first CMP is displaced from CDP-DAG in a reaction mediated by phosphatidylglycerol synthase (PgsA) generating PG-P (Figure 1.12). The second step is to

remove the extra phosphate from the molecule, in a process mediated by phosphate phosphatase (Pgp). *E. coli* has three *pgp* genes (*pgpA, pgpB* and *pgpC*) in its genome, it is believed that not all are involved in this process (Parsons and Rock, 2013). PG can be converted into cardiolipin (CL), this latter glycerophospholipid is formed by the fusion of two molecules of PG with the release of a glycerol in a process mediated by cardiolipin synthase (Cls) (Parsons and Rock, 2013).

Phospholipid synthesis in bacteria goes beyond the synthesis of PE, PG and CL. Variations of these lipids are commonly found in wide range of bacteria species, which is the case for *Clostridium*. The solventogenic bacteria used in this work has been described to produce variations of these lipids, such as the plasmalogens or other derivatives and, it has been described to produce glycolipids (Guan and Goldfine, 2021; Sohlenkamp and Geiger, 2015) (Figure 1.12).

Synthesis of plasmalogens

Plasmalogens are vinyl ether-containing lipids that have the ether-linked chain at the glycerol sn-1 position (Kolek et al., 2015). They have been described in anaerobic and aerobic organisms (higher eukaryotes); however, their synthesis is completely different. In aerobic organisms, the vinyl ether is formed through an oxidation process that requires oxygen and is mediated by CarF and TMEM189 enzymes (Figure 1.13) (Goldfine 2022; Jackson et al., 2021).

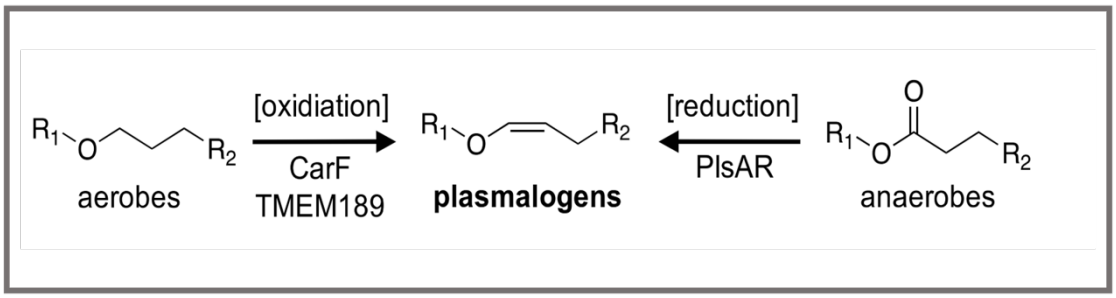

Figure 1.13. Plasmalogen biosynthesis metabolic pathway in aerobic bacteria, eukaryotic higher organisms, and anaerobic bacteria.In humans and other animals, the vinyl ether is synthesized through an oxygen-dependent oxidation process facilitated by desaturases (TMEM). In aerobic bacteria, this reaction occurs via an integral membrane enzyme called CarF. Conversely, in anaerobic bacteria, the characteristic vinyl ether is mediated by the reductases PlsA and PlsR (Jackson et al., 2021).

The biosynthesis pathway of plasmalogens in anaerobic organisms occurs through glycerophospholipids and glycolipids precursors (Goldfine 2022). The precursor lipids PA, CDP-diacylglycerol and PS have very low levels of plasmalogens whereas the end products of the metabolic pathway such as, PE, PG and CL have higher levels (Goldfine 2022). Inhibition of Psd which is responsible for the decarboxylation of PS (Figure 1.12) affects the production of plasmalogen PE (PlsE) (Figure 1.9). More recently *plsA* and *plsR*, have been found to encode reductases capable of converting acyl ester into vinyl ether (Goldfine 2022; Jackson et al., 2021). These genes have been found among the *Clostridium* genus, other Firmicutes and in facultative anaerobic bacteria (*Listeria*) (Goldfine 2022).

Synthesis of glycolipids

The membrane of gram-positive bacteria has phosphorous-free lipids such as glycosyl diacylglycerols (GLs) (Parsons and Rock, 2013). Their synthesis is predominantly diacylglycerol (DAG) dependent, that can occur through dephosphorylation of PA (Figure 1.12). Glycotransferases transfer uridine diphosphate glucose or other sugars (UDP- sugars) to a DAG molecule generating for example monoglycosyl-DAG (MGDG) or diglycosyl-DAG (DGDG) if one or two glucotransferase reaction occurs respectively (Parsons and Rock, 2013).

1.4.5 Lipid membrane homeostasis

In response to environmental changes such as temperature, osmolarity, salinity, and pH, bacteria modify their membrane composition (Zhang and Rock 2008). The phospholipid polar head groups proportion is tightly controlled to maintain the balance between the zwitterionic or neutral phospholipids such as PE and the acidic phospholipids PG and CL (Zhang and Rock 2008). This balance directly influences the biophysical properties of membranes and is controlled by enzymes controlling phospholipids biosynthesis, such as *PssA*, Psd, Cls and PgsA (Zhang and Rock 2008).

Bacteria have evolved mechanisms to control the production of new fatty acids and modify the structure of existing fatty acids, and these allow bacteria to adjust membrane viscosity to match environmental requirements (Zhang and Rock 2008). Control at the fatty acid biosynthesis level is crucial for membrane homeostasis, because the biophysical properties of membranes are

determined in large part by the composition of the fatty acids. Although the biophysical properties of membranes can be changed by altering the ratio of the polar head groups in membrane phospholipids, bacteria seem to use biochemical and genetic mechanisms to modify the composition of the fatty acids that are produced by type II fatty acid synthesis (FASII) (Zhang and Rock 2008).

Phospholipid homeostasis

The expression of specific genes, described in the phospholipid metabolic pathway (Figure 1.12) such as *pss, psd*, *pgsA* and *cls* is responsible for the synthesis of PE, PG and CL, respectively (Parsons and Rock, 2013). Some studies, although not recent, have contributed to understand the regulation of PE and PG/CL synthesis, shedding light on membrane stability and lipid synthesis control. For instance, in *E. coli*, overexpressing *pss* or *pgsA* had limited effects on lipid metabolism. It was suggested that excess enzyme production does not control lipid metabolism in *E. coli* (Ohta et al., 1981). In a related study, PG was continuously removed from growing cells by adding arbutin. This resulted in increased levels of the PgsA enzyme but had no apparent impact on the amount of PE, suggesting that regulation of these two enzymes in *E. coli* is independent (B. J. Jackson, Gennity, and Kennedy 1986). Furthermore, the cellular co-localization of Pss in *E. coli* indicated that elevated levels of CDP-DAG or PS increased enzyme levels in the membrane, suggesting induction of enzyme production by substrate availability Figure 1.14 (Louie, Chen, and Dowhan 1986). *E. coli pssA* mutant strains shown PE depletion and divalent metal ions became essential for growth (Parsons and Rock, 2013).

E. coli pgsA mutant strains exhibited reduced acidic lipids, such as PG and CL, as well as decreased PE synthesis (Saha et al., 1996). These findings imply that *PssA* activity in *E. coli* may depend on the presence of PG in the membrane, allowing the enzyme to interact with the membrane and catalyse PS and consequently PE synthesis (Figure 1.14). However, different Pss enzymes may have distinct regulation mechanisms (Saha, Nishijima, et al., 1996). Heterologous expression of *pss* from *B. subtilis* in *E. coli pgsA* mutant strains restored PE production independently of PG/CL levels. This suggest that native *E. coli PssA* require PG to become active in the membrane, while Pss from *B. subtilis*, which is an integral membrane protein, operate independently of anionic lipids (Saha et al., 1996).

In *B. subtilis*, knockout strains of *psd* and *pss* resulted in a drastic reduction in PE and a minor decrease in PG and CL content, with increased levels of glycolipids such as mono-, di-, and tri-

glucosyldiacylglycerols in the cells (Matsumoto et al., 1998). In Gram-positive bacteria, glycolipid synthesis involves the transfer of glucose from UDP-glucose to diacylglycerol, generated by dephosphorylation from phosphatidic acid (Figure 1.12) (Sohlenkamp and Geiger, 2015). Thus, the accumulation of PA in the absence of Pss or Psd triggers DAG synthesis, leading to glycolipid synthesis (Zhang and Rock 2008). These results suggest that both Gram-positive and Gram-negative bacteria have distinct regulation mechanisms for phospholipid synthesis (Matsumoto et al., 1998).

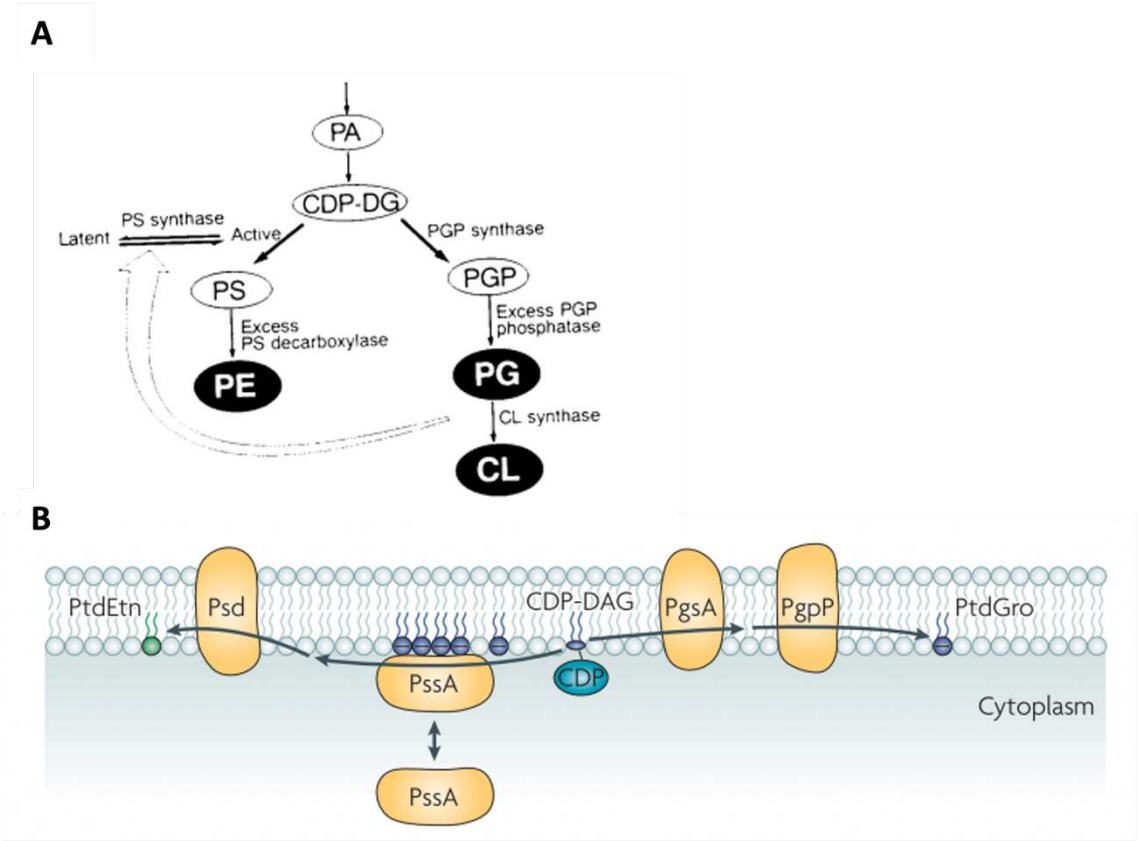

Figure 1.14. Possible mechanism responsible for the balanced synthesis of PE and PG in *E. coli*.(A) (B) The excess of acidic phospholipids, for example PG, triggers the electrostatic interaction of phosphatidylserine synthase (PssA) with the cytoplasmic membrane activating its activity. CDP-DG: CDP-diacylglycerol; PE: phosphatidylethanolamine; PG: phosphatidylglycerol (Saha, Nishijima, et al., 1996).

FA structure homeostasis

The length and degree of unsaturation in FA chains hold significant importance in maintaining the crystalline phase of the membrane bilayer (Zhang and Rock 2008). This is crucial for

preventing excessive disorganization, which could compromise cell viability (Parsons and Rock, 2013). The regulation of FabH, FabF, and FabB, and phospholipid acyltransferases is a key determinant in acyl chain length regulation (Figure 1.11) (Parsons and Rock, 2013). Condensing enzymes exhibit substrate specificity limited to acyl-ACP molecules containing a maximum of 20 to 22 carbons, while acyltransferases require a minimum of 12 to 14 carbons to add the FA to G3P (Parsons and Rock 2013).

The number of double bonds in fatty acids is also important to maintain membrane homeostasis (Fonseca et al., 2019; Startek et al., 2019). In response to temperature fluctuations, bacteria adjust the proportion of unsaturated fatty acids to modulate membrane fluidity (Fonseca et al., 2019). When temperatures drop, causing increased rigidity, bacteria tend to increase the proportion of unsaturated fatty acids. Conversely, rising temperatures, leading to greater membrane fluidity, prompt a decrease in unsaturated fatty acids. The mechanisms governing unsaturated fatty acid production can vary among bactertira (Parsons and Rock, 2013). For instance, in *E. coli*, FabA and FabB are described to introduce double bonds (Parsons and Rock, 2013). *Staphylococcus aureus* possesses only one FabZ enzyme, exclusively producing saturated fatty acids (Parsons and Rock, 2013). In contrast, *Enterococcus faecalis* has a FabZ-like enzyme capable of a reaction similar to FabA in *E. coli* (Parsons and Rock, 2013). These diverse mechanisms underscore the adaptability of bacteria in regulating their membrane composition in response to changing environmental conditions (Parsons and Rock, 2013).

Some bacteria, including some solventogenic *Clostridium* species, also produce unsaturated fatty acids (Vasylkivska and Patakova, 2020). In the case of *C. acetobutylicium*, the *fab* operon controls fatty acid biosynthesis through three putative *fabF* genes (Patakova et al., 2019). The precise mechanism governing unsaturated fatty acid synthesis in these bacteria, however, remains elusive (Patakova et al., 2019).

In *Clostridium* species, the production of cyclopropane fatty acids involves the methylenation of the double bond in specific unsaturated fatty acids (Patakova et al., 2019). This chemical transformation is catalysed by cyclopropane-fatty-acid-synthetase (cfa) (Figure 1.11). It is postulated that solventogenic bacteria produce these lipids to replace unsaturated fatty acids in the presence of butanol. This adaptation is believed to enhance resistance and better maintain membrane function under such conditions (Patakova et al., 2019).

Molecular dynamics simulations have provided insights into the role of cyclopropane fatty acids. These lipids are shown to restrict rotation around the cyclopropane moieties, thereby preserving or even enhancing membrane fluidity (Poger and Mark 2015).

1.5 Optimising cell factories

Natural microorganisms, though useful in their habitats, are usually not suitable for big-scale industry due to their low productivity and inability to endure industrial scale settings (Zeng et al., 2020). To address these challenges, various strategies have been tested, some of them involve reshaping microbial cell factories by altering their physiological functions at the genetic level and optimizing growth conditions and maximize product yield (Sandberg et al., 2019; Zeng et al., 2020). Numerous techniques have been developed, including random mutagenesis, rational engineering, physical and chemical mutagenesis, adaptive laboratory evolution (ALE) and genetic and metabolic engineering (Sandberg et al., 2019; Zeng et al., 2020).

The screening of microbial strains adaptability to various environments through beneficial genetic mutations is vital to build microorganisms resilient to harsh conditions, boost growth rates, enhance substrate use, and increase product output (Figure 1.15) (Cho et al., 2022). The cell membrane is an important target to screen; knowledge on cell membrane structure and stability is important to develop strategies to enhance the yields and productivities of these cell factories (Cho et al., 2022). Understanding how membranes adapt and develop ways to combat oxidative stress can transform chemical production by microorganisms like *C. saccharoperbutylacetonicum* and unlock the potential of many cell factories (Linney et al., 2023; Zhu and Yang, 2003).

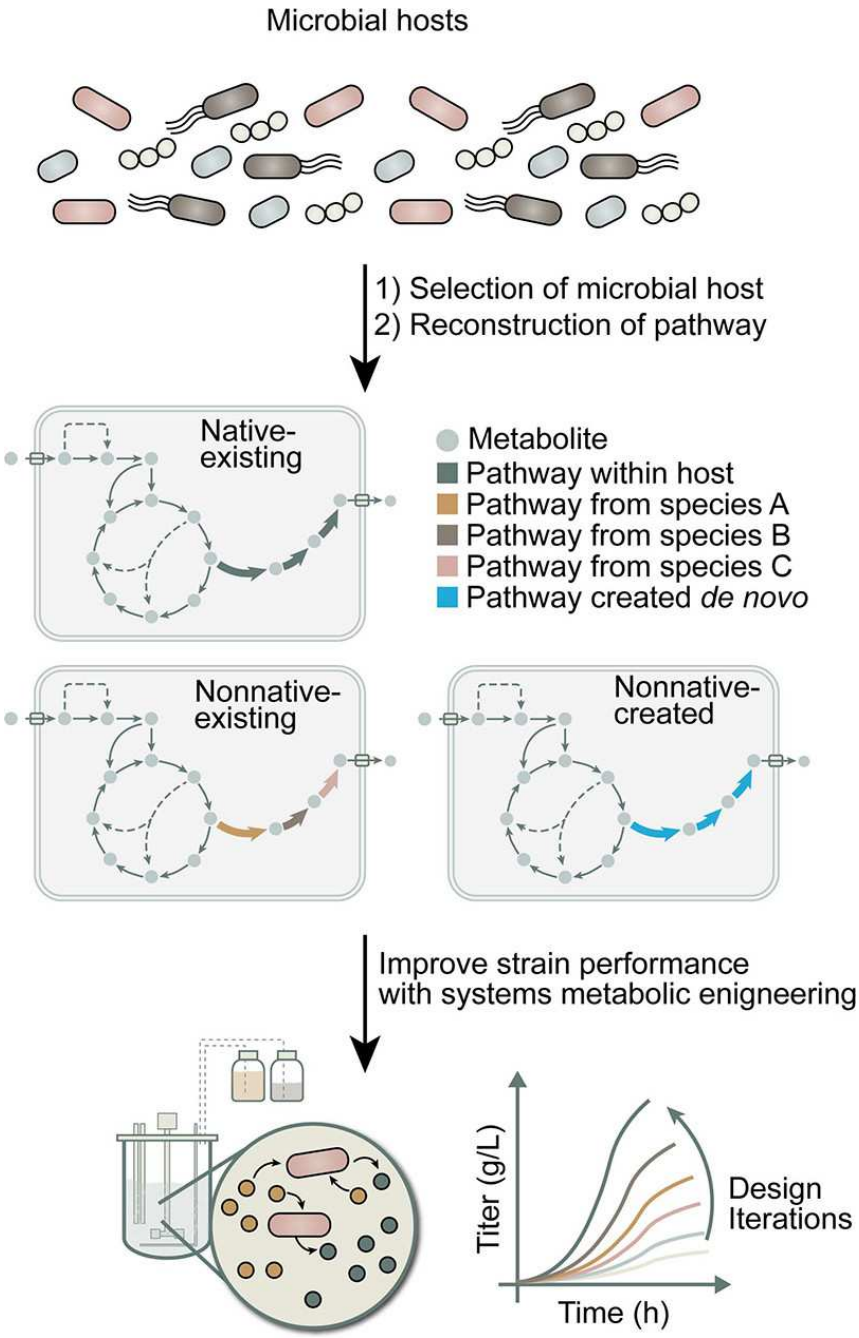

Figure 1.15. Cell factory designing process, from the selection of suitable microorganisms, to enhancing their performance. This is achieved by subjecting their biosynthetic pathways to systems metabolic engineering, always keeping the targeted high-value chemical in mind (Cho et al., 2022).

1.5.1 Metabolic engineering

One of the major challenges in optimising cell factories, particularly *Clostridium* strains, is the limited genetic engineering tools and understanding of physiology (Moon et al., 2016). Efforts have been made to genetically modify various Clostridia species, resulting in higher yield and

productivity (Li et al., 2020). In *C. acetobutylicum*, DNA integration tools have been developed and are widely applicable (Heap et al., 2012). However, these methods have limitations, including challenges in identifying insertion sites, potential residual activity, and polar effects on downstream genes (Heap et al., 2012).

The Clustered Regularly Interspaced Short Palindromic Repeats (CRISPR) and its associated Cas proteins as genome editing tools has gained popularity (Atmadjaja et al., 2019; Wang et al., 2019; Xue and Cheng 2019). CRISPR-Cas-mediated modifications allow precise changes such as single nucleotide polymorphisms (SNPs), in-frame deletions, or insertions in the genome. This technology has been successfully applied in the hyper butanol producer *C. saccharoperbutylacetonicum* N1-4(HMT) to generate deletions (SNPs) and integrate new DNA, demonstrating promising advances in improving and developing new pathways for various Clostridia strains (Atmadjaja et al., 2019).

Various analytical techniques can be employed to evaluate engineered strains functioning as improved cell factories. Chromatography techniques, such as high-performance liquid chromatography (HPLC), are instrumental in assessing substrate utilization and chemical production in *C. saccharoperbutylacetonicum* (Gu et al., 2018; Linney et al., 2023). However, for a comprehensive understanding in context of discovery, it becomes essential to characterise these biological systems. This encompasses clonal interference, regulatory rewiring, and responses to genetic perturbations or suboptimal growth conditions (Sandberg et al., 2019; Zeng et al., 2020).

Exploring fundamental aspects of biology includes investigating how regulatory gene networks respond to external stressors or adapt to new environments. It also involves understanding the impact of genome shuffling and recombination techniques on the development of industrially relevant strains (Figure 1.15) (Sandberg et al., 2019).

Omics technologies have revolutionized these aspects, providing valuable insights into the genomes of various cell factories, stress mechanisms under different fermentation conditions and the production of high-value chemicals (Kolek et al., 2015; Patakova et al., 2013). Furthermore, omics approaches enable more comprehensive characterization and quantification of the lipidome in different strains.

In lipidomics, mass spectrometry serves as a valuable complement to techniques like thin-layer chromatography (TLC). While TLC is a simple and cost-effective method for lipid separation based on hydrophobicity and detection, mass spectrometry offers greater robustness. It separates lipids based on mass-to-charge ratio, providing not only identification and

quantification of lipid classes but also information on the length of carbon chains and the degree of unsaturation within fatty acid components (Cajka and Fiehn, 2017; Tuzimski and Sherma, 2016).

Numerous studies have focused on optimizing solventogenic *Clostridium* as cell factories, aiming to enhance growth rates, increase tolerance, improve substrate utilization, and deepen knowledge of cell factory functions, evolutionary traits, and network dynamics. This research has also led to the development of optimised techniques for these cell factories, but increasing product yields and productivities are still needed (Liao et al., 2015; Linney et al., 2023; Xue and Cheng 2019; Yu et al., 2011). These processes remain challenging, particularly from an economic standpoint. Low solvent concentrations require larger feedstock quantities, more fermentation cycles, and increased purification steps, all contributing to higher costs (Gong et al., 2022; Sauer 2016; Vasylkivska and Patakova 2020):

2 Aims and Objectives

Microbial cell factories are important in Biotechnology, especially for producing high-valuable compounds, such as butanol. Yet, their limited yield and productivity challenge the economic feasibility of the process. *C. saccharoperbutylacetonicum* stands out as a promising cell factory, given its high butanol production capabilities and its versatility in substrate utilization, surpassing other species. However, its effectiveness is undermined by increased stress and diminished membrane stability during chemical production and accumulation. Therefore, the main aim of this study was to modify the cell membrane of *C. saccharoperbutylacetonicum* to increase butanol tolerance. To achieve this, this project adopted the following strategies:

- To modify the phospholipid metabolic pathways in *C. saccharoperbutylacetonicum* N 1-4 HMT. This involved creating knockout and overexpressing strains of the genes *pgsA* and *cls*, which are integral to the synthesis of PG and CL, respectively.
- To express Metallothionein1 in *C. saccharoperbutylacetonicum* N 1-4 HMT. This was aimed at producing a strain that expresses an antioxidant enzyme, thereby assisting in mitigating solvent and acid-induced stress in the membrane.
- To characterize the mutants that were generated, as well as the pre-existing knockout *pssA* (Δ*pss*A), and overexpressing *pssA* (*pss*A^{+}) strains, which are involved in the synthesis of PE and another mutant strain (*BCL*) provided by the industrial partner Biocleave Ltd. This characterisation was focused on assessing their lipid membrane composition and the chemicals they produce during ABE fermentation.

3 Methods

3.1 Biological material

The bacterial strains, plasmids for overexpression, plasmids for CLEAVE™ and primers used in this work are listed in Table 2, Table 3, Table 4 and Table 5, respectively.

Table 2. List of the bacterial strains used and generated in this work.

Bacterial Strains	Description	Reference
Clostridium saccharoperbutylacetonicum N1-4(HMT)	Strain provided by the company partner	Biocleave, UK
Δ*pssA*	*C. saccharoperbutylacetonicum* N1-4(HMT) Δ*pssA* strain (*pssA* knockout)	(John Andrew Linney 2021)
pssA$^+$	*C. saccharoperbutylacetonicum* N1-4(HMT) Δ*pssA* strain + (pBT-*pssA*) (*pssA* overexpression)	(John Andrew Linney 2021)
Δ*pgsA*	*C. saccharoperbutylacetonicum* N1-4(HMT) Δ*pgsA* strain (Δ*pgsA* knockout)	This work
pgsA$^+$	*C. saccharoperbutylacetonicum* N1-4(HMT) strain + (pBT-*pgsA*) (*pgsA* overexpression)	This work
Δ*cls*	*C. saccharoperbutylacetonicum* N1-4(HMT) Δ*cls* strain (Δ*cls* knockout)	This work
cls$^+$	*C. saccharoperbutylacetonicum* N1-4(HMT) strain + (pBT-*cls*) (*cls* overexpression)	This work
mt1$^+$	*C. saccharoperbutylacetonicum* N1-4(HMT) strain + (pBT-*mt1*) (*mt1* overexpression)	This work
hmt1$^+$	*C. saccharoperbutylacetonicum* N1-4(HMT) strain + (pBT-*hmt1*) (*mt1* overexpression with a 6xHistag)	This work
BCL	Mutated *C. saccharoperbutylacetonicum* N1-4(HMT) strain	Biocleave, UK
Escherichia coli DH5-α	Genotype: F$^-$ Φ80lacZΔM15 Δ(lacZYA-argF) U169 recA1 endA1 hsdR17(r_k^-, m_k^+) phoA supE44 thi-1 gyrA96 relA1 λ$^-$	ThermoFisher Scientific, UK
Escherichia coli DH10b	F– *mcrA* Δ(*mrr-hsdRMS-mcrBC*) ϕ80*lacZ*ΔM15 Δ*lacX74 recA1 endA1 araD139* Δ (*ara-leu*)7697 *galU galK* λ– *rpsL*(Str^R) *nupG*	Biocleave Ltd, UK

Table 3. List of the vectors used in this work for gene overexpression.

Plasmids for overexpression	Description	Reference
pBT	backbone vector containing the Psec promoter	Biocleave, UK
pBT-Cpa1	pBT containing the *cpa*1 cDNA	Biocleave, UK
pPgsA	pBT containing the *pgsA* cDNA	This work
pHPgsA	pBT containing the *pgsA* cDNA in fusion with an 8xHistag at the N-terminus	This work
pCls	pBT containing the *cls* cDNA	This work
pHCls	pBT containing the *cls* cDNA in fusion with an 8xHistag at the N-terminus	This work
pMAL-c2x-MT1	Bacterial expression plasmid with the *mt*1 from *Mus musculus* (NM 013602.3, NCBI)	(Mercogliano and DeRosier 2007)
pMt1	pBT containing the *mt*1 cDNA	This work
pHMt1	pBT containing the *mt*1 cDNA in fusion with an 6xHistag at the N-terminus	This work

Table 4. List of the vectors used in this work for gene deletion using CLEAVE^{TM} technology.

Plasmids for CLEAVE^{TM}	Description	Reference
pBT	Backbone vector for step 1 CLEAVE^{TM}	Biocleave, UK
Killing vector	Backbone vector for step 2 CLEAVE^{TM}	Biocleave, UK
pUC57_step1_Δcls	Vector with the DNA sequence containing the *cls* mutation	GenScript, UK
pBT_step1_Δcls	Vector for the step 1 CLEAVE^{TM} to generate the *cls* knockout	This work
pET-K^{+}__step1_ΔpgsA	Vector with the DNA sequence containing the *pgsA* mutation	GenScript, UK
pBT_step1_ΔpgsA	Vector for the step 1 CLEAVE^{TM} to generate the *pgsA* knockout	This work
pUC57_step2_Δcls	Vector with the spacer sequence from *cls*	GenScript, UK
Killing vector_Δcls	Vector with the spacer to target the strains that do not have the correct *cls* knockout	This work
pBT_step2_ΔpgsA	Vector with the spacer sequence from *pgsA*	GenScript, UK
Killing vector_ΔpgsA	Vector with the spacer to target the strains that do not have the correct *pgsA* knockout	This work

Table 5. List of primers used to clone the vectors for gene overexpression and deletion (CLEAVE™).

Primers for CLEAVE™	Description (5' – 3')	Reference
PF_Mt1_Histag	ATGCATCACCATCACCATCACGACCCCAACTGCTCCTGCTC	Amplifies the *mt*1 and adds a 6xHistag at the 5' end
PR_Mt1_mcs	CCTCGAGATCTCCATGGACGCGTGACGCTAGGCACAGCACG TGCA C	Amplifies the *mt*1 and add the homologous region of the plasmid at the 3' end
PF_Psec_Histag_Mt1	CATAATTTACAGAGGGGGATTAAGATGCATCACCATCACCAT CAC	Amplifies the 6xHistag with the *mt*1 gene and add the homologous region of the plasmid at the 5' end
PF_Psec_Mt1	CATAATTTACAGAGGGGGATTAAGATGGACCCCAACTGCTCC TGCTCCAC	Amplifies the *mt*1 and add the homologous region of the plasmid at the 5' end
M13 F	GTAAAACGACGACGGCCAGT	Amplifies homologous region for *pgsA and cls* knockout Sequencing primer
M13R	CAGGAAACAGCTATGAC	Amplifies homologous region for *pgsA and cls* knockout Sequencing primer
Primer 1: FP_clsKO_seq	GGC CTT ATT CGT TTT GAA G	Binds to the outer region of the homologous region1 -Δ*cls* - homologous region2
Primer 2: RP_clsKO_seq	GAA CAA GTA AGC TCA TAG GC	Binds to the homologous region 2 of the Δ*cls*
Primer 3: RP_clsKO_seq2	CCCAGGAATTTTGCCTC	Binds to the region of *cls* that doesn't exist in the Δ*cls genome*
FP_pssAKO_seq	ATTGGTGCACTTGTCTTCTCG	Binds to the outer region of the homologous region1 - Δ*pssA* - homologous region2
RP_pssAKO_seq1(CA)	AGCACTTCCCTGTACTAAGC	Binds to the homologous region 2 of the Δ*pssA*
RP_pssAKO_seq2(CA)	GCCGGTGCAACTCCAAAGG	Binds to the region of *pssA* that doesn't exist in the Δ*pssA genome*

3.2 Culture Conditions

Clostridial cells were grown in anaerobic conditions using three different culture media, Reinforced Clostridial Media (RCM), Clostridial Growth Media (CGM) and TYIR. Complete RCM media was obtained from Oxoid, CGM consisted of 2.5 $g.L^{-1}$ yeast extract, 0.375 $g.L^{-1}$ K_2HPO_4, 0.375 $g.L^{-1}$ KH_2PO_4, 0.2 $g.L^{-1}$ $MgSO_4$, 0.005 $g.L^{-1}$ $FeSO_4$, 0.005 $g.L^{-1}$ $MnSO_4$, 0.5 $g.L^{-1}$ NaCl, 1 $g.L^{-1}$ $(NH_4)_2SO_4$, 1 $g.L^{-1}$ L- asparagine and 5% (w/v) glucose, the pH of the final media was adjusted to between 6.6 and 6.8. TYIR media consisted of 2.5 $g.L^{-1}$ yeast extract, 2.5 $g.L^{-1}$ tryptone, 0.025 $g.L^{-1}$ $FeSO_4$, 0.5 $g.L^{-1}$ $(NH_4)_2SO_4$, 10 mM MES and 5% (w/v) glucose. Cultured cells were incubated in anaerobic conditions at 37 °C overnight and 32 °C for solvent screening purposes without agitation.

E. coli DH5-α and DH10b cells were grown in Luria–Bertani (LB) medium containing 10 $g.L^{-1}$ tryptone, 5 $g.L^{-1}$ yeast extract, 10 $g.L^{-1}$ NaCl, at 37 °C and 250 rpm. Recombinant *E. coli* DH5α and *C. saccharoperbutylacetonicum* N1-4(HMT) cells were selected in via addition of antibiotics (Table 6). For RCM, CGM, TYIR and LB solid media 15 $g.L^{-1}$ agar was added.

Table 6. List of antibiotics and respective work concentrations used in this work.

Antibiotic	*E. coli* ($\mu g.ml^{-1}$)	*C. saccharoperbutylacetonicum* ($\mu g.ml^{-1}$)
Ampicillin	100	-
Chloramphenicol	25	25
Thiamphenicol	-	75
Kanamycin	30	-
Erythromycin	500	100 liquid / 40 solid

3.3 Cloning strategy

3.3.1 Restriction enzyme digestion

Restriction reactions were performed using the enzymes *BstB*I, *BamH*I, *Nco*I, *Sma*I, *Kpn*I, *Hind*III, *Stu*I, *Zra*I and *Xho*I (New England Biolabs, UK) according to the manufacturer's instructions. DNA fragments were run on an 1 % (w/v) agarose gel electrophoresis gel (section 3.3.5).

3.3.2 DNA gel extraction

DNA fragments were extracted from the agarose gel using the Monarch® DNA Gel extraction Kit (New England Biolabs, UK) according to the manufacturer's instructions. DNA concentration was determined using the NanoDrop 1000 Spectrophotometer (ThermoFisher Scientific, UK).

3.3.3 PCR amplification

DNA amplification for cloning and sequencing purposes was performed using Q5® High-Fidelity DNA Polymerase (New England Biolabs, UK) and Phusion High-Fidelity DNA Polymerase (New England Biolabs, UK). DNA amplification for colony PCR purposes was performed using OneTaq DNA Polymerase (New England Biolabs, UK). The PCR conditions are described in Table 7. The PCR was performed in the MultiGene OptiMax Thermal Cycler (Labnet, UK).

Table 7. Table with the PCR conditions used in this work. (A) PCR reaction mix. (B) Thermocycling conditions for the PCR.cc – concentration.

A

	Q5® High-Fidelity DNA Polymerase	Phusion High-Fidelity DNA Polymerase	OneTaq DNA Polymerase
Reaction buffer	1x cc	1x cc	1x cc
dNTPs	200 µM	200 µM	200 µM
Primer 1	0.5 µM	0.5 µM	0.2 µM
Primer 2	0.5 µM	0.5 µM	0.2 µM
DNA Polymerase	0.02 U/µl	1.0 U/50 µl	0.025 U/µL
DNA template	<1000ng	< 250 ng	< 1000 ng

B

Step	Q5® and Phusion High-Fidelity DNA Polymerase		OneTaq DNA Polymerase	
Initial Denaturation	98˚C	30 sec	94˚C	30 sec
Denaturation	98˚C	10 sec	94˚C	10 sec
Annealing	Primer dependent	30 sec	Primer dependent	30 sec
Extension	72˚C	30 sec per kb	68˚C	1min per kb
Nº of cycles	30		30	
Final Extension	72˚C	2 min	68˚C	5 min
Hold	10˚C	∞	10˚C	∞

3.3.4 Colony PCR

For colony PCR of *Clostridium* cells, colonies were mixed with 25 µl TE buffer and 200 U of proteinaseK at 55 °C for 15 min. To inactivate the enzyme, the mixture was subjected to a heat treatment at 80 °C for 15 minutes. For the PCR reaction, 1 µl of the final product from the above steps was used as a template. Colony PCR in *E. coli* consisted of increasing the initial denaturarion of the PCR to 5 min at 98 °C.

3.3.5 Agarose Gel Electrophoresis

DNA products were separated and visualized by agarose gel electrophoresis. DNA products were mixed with 1 x concentrated Gel Loading Dye Purple (New England Biolabs, UK) and loaded in an 1% (w/v) agarose dissolved in 1 X TAE buffer (40 mM Tris Acetate, 2 mM EDTA, pH 8.5) and stained with GelRed Nucleic Acid 1x (EMD Milipore Corp., UK). DNA size bands were compared to the molecular weight ladders GeneRuler 1 kb DNA Ladder (ThermoFisher Scientific, UK) and 1kb plus GeneRuler 1kb Plus DNA Ladder (ThermoFisher Scientific, UK).

3.3.6 DNA ligation

DNA ligation was conducted utilizing T4 DNA Ligase (New England Biolabs, UK) as per the manufacturer's instructions. Various ratios of insert to vector were tested, specifically at mass-to-mass ratios of 1:1, 1:2, 1:3, 1:5, 1:7, 2:1, and 3:1. Different quantities of vector were tested, including 10 ng, 20 ng, and 50 ng. The volume of the insert used for the ligation reaction was determined using the following formula: (ng of vector x kb of insert / kb of vector) x the specified ratio.

3.3.7 Plasmids extraction

Plasmids were extracted using the Monarch® Plasmid Miniprep Kit (New England Biolabs, UK) according to the manufacturer’s instructions. DNA concentration was determined on the Nanodrop 1000 Spectrophotometer (ThermoFisher Scientific, UK).

3.3.8 DNA Sequencing

The correct insertion of the fragment into the vector and the correct genome deletion was confirmed using Sanger DNA sequencing by Source Bioscience, UK and Eurofins, UK.

3.3.9 Gap Repair

The construction of plasmids pMT1 and pHMT1 was carried out using the gap repair procedure as outlined by Jacobus and Gross (2015). The inserts consisted of the cDNA sequence flanked by

homologous regions in the vector. The sequences Homologous Region 1 - *mt*1- Homologous Region 2 and Homologous Region 1 - 6x Histag - *mt*1- Homologous Region 2 were amplified by PCR. The vector (pBT-Cpa1) was linearized by enzymatic digestion with *BstB*I and *BamH*I.

For amplification of the mt1 gene, PCR was performed using the pMAL-c2x-Mt1 plasmid as a template, containing the *mt*1 gene from *Mus musculus* (NM 013602.3, NCBI). The insert HR1-6xHistag-*mt*1-HR2 was amplified using the primers (PF_Mt1_Histag and PR_Mt1_mcs) described in Table 5.

The PCR product obtained from this amplification was purified through gel extraction and subsequently used as a new template for a second PCR. The second PCR amplified the final sequence of Homologous Region 1 - 6x Histag-*mt*1- Homologous Region 2 and the insert Homologous Region 1-*mt*1- Homologous Region 2 using the primers (PF_*Psec*_Histag_Mt1 and PR_Mt1_mcs) described in Table 5

For the gap repair transformation to generate pMT1 and pHMT1, the linearized vector (pBT-Cpa1), along with the amplified DNA containing homologous region 1-mt1-homologous region 2 or homologous region 1-6x Histag_mt1-homologous region 2, were used to transform in *E. coli* DH5-α competent cells. The transformation followed the protocols outlined by Jacobus and colleagues in 2015, utilizing 150 ng of linearized vector and 300 ng of insert. See protocol in section 3.3.10.

3.3.10 *E. coli* transformation

DH5-α competent cells were previously prepared using the rubidium chloride method, as outlined in Green and Sambrook (2012). DH10b competent cells were obtained from Biocleave, UK. DNA transformation into these cells was carried out by pipetting around 100 ng of DNA into an aliquot of competent cells. The mixture was incubated for 20 minutes on ice. Subsequently, the mixture was subjected to a 1-minute heat shock in a water bath at 42 °C. Immediately after the heat shock, the tubes were placed on ice for 5 minutes. To the tube 240 µl of LB media was added, and the cells were allowed to recover in a shaking incubator at 37 °C for 45 minutes. Finally, 200 µl of the transformed cells were plated onto LB Agar media containing the appropriate antibiotic, and the plates were incubated at 37 °C overnight.

3.3.11 *C. saccharoperbutylacetonicum* N1-4(HMT) transformation

C. saccharoperbutylacetonicum N1-4(HMT) cells were transformed by electroporation using a protocol described by Atmadjaja and colleagues (2019). Clostridia cells were inoculated in 30 mL of RCM media and grew overnight in the anaerobic cabinet at 32 °C. Following this, cells were transferred to new CGM containing 5% glucose culture media to obtain a final OD_{600} of 0.2 in a final volume of 60 ml. Cells were grown in anaerobic conditions at 32 °C to mid-exponential phase and then pelleted at 4000 x g for 10 min at 4 °C. Competent Clostridia cells were prepared by washing the pellet with an EPB_S buffer solution (300 mM sucrose, 0.6 mM Na_2HPO_4, 4.4 mM NaH_2PO_4, 10 mM $MgCl_2$), centrifuged again under the same conditions followed by the addition of 2 ml of EPB_NS buffer solution (300 mM sucrose, 0.6 mM Na_2HPO_4, 4.4 mM NaH_2PO_4. 200 µl of competent cells were transferred to electroporation cuvettes (Cell Projects) together with 500-100 ng of DNA and incubated on ice for 5 min. After pulsing at 1.5 KV (BioRad), 800 µl of CGM containing 5% glucose culture media. Cells were plated on respective CGM containing 5% glucose culture media with the required antibiotic and incubated in the anaerobic cabinet at 32 °C for 2 to 7 days. All the steps except the centrifugation were carried in anaerobic cabinets (Don Whitley).

3.3.12 CLEAVE™ technology

C. saccharoperbutylacetonicum N1-4 (HMT) knockouts were obtained using CLEAVE technology (Atmadjaja et al., 2019). The cDNA sequences of the genes of interest from *C. saccharoperbutylacetonicum* N1-4 (HMT) were obtained using BLAST on NCBI (Table 8). These genes were then synthesized by GeneScript and cloned in pUC57 and pET vectors. The DNA inserts required for CLEAVE™ were cloned into the homologous recombination vectors (pBT) and killing vectors. The CLEAVE™ standard operating procedure was conducted at the Biocleave laboratories in Milton Park, Oxford.

Table 8. List of the target genes for CLEAVE™ used in this work. The *pssA* gene had been deleted and overexpressed in a prior study. For all the chosen genes, the objective was to create knockout strains (Δ) and overexpression strains (+).

Gene name	NCBI code	Encoded protein function	Modification type	Reference
pssA	-	Biossynthesis of PE	Δ / +	(John Andrew Linney 2021)
pgsA	AGF55125.1	Biossynthesis of PG	Δ / +	This work
cls	AGF59059.1	Biossynthesis of CL	Δ / +	This work

In essence, CLEAVE™ comprised two steps, as depicted in Figure 4.7. The first step involved homologous recombination of the target deletion genes (*pgsA* and *cls*) into the genome of *C. saccharoperbutylacetonicum* N1-4 (HMT). This sequence included only the initial and final 45 bp of the original gene, flanked on both ends by 1800 bp sequences upstream and downstream of the original gene (referred to as homology regions or HR). The step1 vector (Table 4) was inserted in *C. saccharoperbutylacetonicum* N1-4 (HMT) by electroporation. Transformed cells underwent homologous recombination resulted in a truncated gene.

The second step involved the cloning of the targeting vector (killing vector) for the native CRISPR-Cas system. This plasmid contained a spacer sequence of approximately 36 nucleotides and a leader sequence that matched a sequence in the middle of the original gene sequence, without overlapping with the truncated recombinant sequence. The killing vector (Table 4) was transformed in *C. saccharoperbutylacetonicum* N1-4 (HMT) by electroporation. Bacteria with the wild type gene sequence were targeted by this vector, leading to cleavage, and as a result, the cells did not survive. This led to the creation of a population of knockout strains at the genome level, as those bacteria that underwent homologous recombination in the first stage of CLEAVE™ remained viable.

3.4 Small-scale bottle screening

C. saccharoperbutylacetonicum N1-4HMT cells were grown anaerobically overnight in 30 mL of RCM at 37 ˚C to an OD_{600} > 2.0 and pH >5.0. Overnight cultures with the expected $OD_{600,}$ pH and showing motility under the microscope were transferred (6mL) to a new culture media TYIR containing 50 $g.L^{-1}$ glucose and 30 mM MES (54 mL). Overexpressing strains were supplemented with Chloramphenicol 25 $\mu g.mL^{-1}$. The bottles were incubated anaerobically at 32 ˚C for 48 h and

sampled at 0, 6, 24 and 48 h. At each time point, 4 mL of each bottle was collected to measure the OD_{600} and pH. Collected samples were centrifuged at 4 000 x g for 15 min, supernatant was filtered through a 0.2 μm cellulose filter and diluted 4 times for HPLC analysis. Filtered and diluted samples and the remaining cell pellet were kept at -20 ˚C.

3.5 Lipid Extraction

The lipids were extracted from *Clostridium* cells using two distinct methods, a modified Bligh and Dyer procedure and, a modified Methyl- tert -Butyl Ether Extraction protocol (Bligh and Dyer, 1959; Eggers and Schwudke, 2016).

Modified Bligh and Dyer procedure

Overnight grown cells were centrifuged for 15 minutes at 14,000 x g and to 0.5 mg of pelleted cells, 0.5 mL of pre-heated methanol (50°C) was added. Resuspended cells were incubated in a sonicating bath for 15 min. An equal volume of chloroform was then added, and the sonication procedure was repeated. 0.5 mL of KCl 0.88% (w/v) was added, tubes were vortexed and centrifuged at 1,000 *g* for 2 min. The organic bottom layer, containing the lipids, was transferred to a new tube, dried under a stream of nitrogen and stored and -20 °C.

Modified Methyl- tert -Butyl Ether procedure

Due to the challenges of breaking the cell wall of *Clostridium*, before proceeding to the MTBE lipid extraction protocol, cells were sonicated. The cell pellet collected at 0, 6, 24 and 48 h of incubation in TYIR was resuspended in lysis buffer (1 M Tris, 5 M NaCl, pH 8.0) and sonicated (Sonic Dismembrator, Fisherbrand) at 70 % intensity with periods of 30 sec on and 30 sec of for 20 min. Sonicated samples were centrifuged in the ultracentrifuge (Beckman Coulter Optima XPN-100 Ultracentrifuge, TYPE 25 rotor), for 30 min at 100 000 x *g*. The supernatant was discarded and the pellet containing lipids and cell debris was resuspended in 500μL of molecular biology grade H_2O. To the 500 μL of resuspended lipids and cell debris was added 2.5 mL of a MTBE:methanol (10:3 v/v) solution containing 0.05 $mg.mL^{-1}$ of butylated hydroxytoluene (Eggers and Schwudke, 2016). The mixture was placed on shaker for 45 min and vortexed every 15 min. To the reaction tube molecular biology H_2O was added and a final volumetric ratio of 10:3:2.5 (v/v/v) of MTBE:methanol: dH_2O was obtained. Samples were vortexed and centrifuged for 10

min at 1000 x *g*. The upper phase, or lipid containing phase was transferred to a collection vial dried down and stored at -20 °C (Eggers and Schwudke, 2016).

3.6 Lipid Quantification

Total phospholipids quantification was determined by a modified colorimetric ammonium ferrothiocyanate assay (Charles and Stewart, 1980). The dried down lipids from the lipid extraction were resuspended in 100 µL of chloroform and, 5 µL were transferred to a new tube followed by addition of 2 mL of chloroform and 1 mL of ammonium ferrothiocyanate (0.1 M $FeCl_3.6H_20$, 0.4 M ammonium thiocyanate). The tube was thoroughly mixed and centrifuged at 14500 x *g* for 5 min. The organic (coloured) layer was transferred to new glass tubes and their absorbance was measured at an OD_{488} in a glass cuvette.

Phospholipids quantification was calculated by comparison to the standard lipid solutions, which consisted of a 1 $mg.mL^{-1}$ solution of 1-palmitoyl-2-oleoyl-sn-glycero-3-phosphoethanolamine (PE), 1-palmitoyl-2-oleoyl-glycero-3-phosphocholine (PC) and 1-palmitoyl-2-oleoyl-sn-glycero-3-phospho-(1'-rac-glycerol) (PG) and 1',3'-bis[1-palmitoyl-2-oleoyl-sn-glycero-3-phospho]-glycerol (CL) all of them obtained from Avanti Polar lipids. The following standard solutions were tested: PG:PC:PE (ratio of 1:1:1), PE:PG:CL (ratio of 1:1:1) and PE:PG:CL (ratio of 2:1:1). Mass ratios and molar ratios were tested.

3.7 Thin Layer Chromatography (TLC)

TLC was performed using distinct solvent systems: i consisted of chloroform:methanol:water (65:25:4, v/v/v); solvent system ii consisted of chloroform:methanol:ammonium hydroxide (65:25:4, v/v/v), solvent system iii consisted of chloroform:hexane:methanol:acetic acid (50:30:10:5, v/v/v/v) and solvent iv which consisted of toluene:pyridine:water (60:60:10) (Annex 1).

A filter paper was added into the glass tank together with the selected solvent system. TLC Silica gel 60 F_{254} (Merck, UK) plates were used as a stationary phase, to which 20 µg of extracted lipids from the *C. saccharoperbutylacetonicum* N 1-4 HMT WT and mutant cell cultures, and 20 µg of standards were added. The selected standards were 1-palmitoyl-2-oleoyl-sn-glycero-3-

phosphoethanolamine, 1-palmitoyl-2-oleoyl-glycero-3-phosphocholine, 1-palmitoyl-2-oleoyl-sn-glycero-3-phospho-(1'-rac-glycerol), 1-palmitoyl-2-oleoyl-sn-glycero-3-phospho-L-serine and, 1',3'-bis[1-palmitoyl-2-oleoyl-sn-glycero-3-phospho]-glycerol (Avanti Polar lipids). Considering that the standard phospholipids selected vary essential on their head group, in this report they are described as phosphatidylcholine (PC), phosphatidylethanolamine (PE), phosphatidylserine (PS), phosphatidylglycerol (PG) and cardiolipin (CL).

After adding all the samples, the silica plate was placed into the glass tank, the lid was closed, and the mobile phase allowed to move up towards the top of the stationary phase. Before reaching the top, the plate was removed and, with a pencil, a line was draw at the front of the solvent before its evaporation. For each solvent system two TLC Silica gel plates were used, the first was sprayed with molibdenum blue which has developed a colour. The second plate was stained with ninhydrin and after heating it at 100 °C for 5-15 min the amino-containing lipids appeared as pink spots.

3.8 Mass Spectrometry

Mass spectrometry was used to analyse the Phospholipids and DGDGs. Lipids were extracted using the following procedure described by the company (Creative Proteomics).

Sample preparation

Lipids were extracted using tubes with Teflon-lined screw caps. To 0.8 parts of cells/tissue (homogenized) in aqueous solution was added a solution of chloroform and methanol. (ratio1:2). After mixing, another solution of chloroform and water was added (ratio 1:1). Samples were centrifuged (1000 x *g*) for 5-10 min. The lower containing the chloroform with lipids was retained.

Lipid samples were analysed by Mass Spectrometry following the instrument and sample analysis parameters described in Table 9; the internal standards described in Table 10 and; the settings to identify the targeted lipids described in Table 11.

Table 9. Instrument and sample analysis parameters used by Creative Proteomics.

Mass Spectrometry conditions	
Instrument	Waters Xevo TQS
Cycle time (secs)	Automatic
Source Temperature (°C)	150
Desolvation Temperature (°C)	250
Cone Gas Flow (L/Hr)	150
Desolvation Gas Flow (L/Hr)	650
Flow (mL/min)	0.14
Nebuliser Gas Flow (Bar)	7

Table 10. Internal standards used in the lipidomic analysis by Creative Proteomics.

Compound Name	Compound Formula	Alternative Name	Mass of Ion	Used to Quantify	Scan Mode	Adduct Detected	nmol/sample
C21H44O7PN	lysoPC(13:0)		454.3	LysoPC	+Prec184	[M+H]+	0.12
C27H56O7PN	lysoPC(19:0)		538.3	LysoPC	+Prec184	[M+H]+	0.12
C32H64O8PN	PC(12:0/12:0)		622.4	PC	+Prec184	[M+H]+	0.12
C56H108O8PN	PC(24:1/24:1)		954.9	PC	+Prec184	[M+H]+	0.12
C19H40O7PN	lysoPE(14:0)		426.3	LysoPE	+NL141	[M+H]+	0.06
C23H48O7PN	lysoPE(18:0)		482.3	LysoPE	+NL141	[M+H]+	0.06
C29H58O8PN	PE(12:0/12:0)		580.5	PE	+NL141	[M+H]+	0.06
C45H90O8PN	PE(20:0/20:0)	diphytanoyl PE	804.7	PE	+NL141	[M+H]+	0.06
C34H67O10P	PG(14:0/14:0)		684.5	PG	+NL189	[M + NH4]+	0.06
C46H91O10P	PG(20:0/20:0)	diphytanoyl PG	852.7	PG	+NL189	[M + NH4]+	0.06
C34H66O10PN	PS(14:0/14:0)		680.6	PS	+NL185	[M+H]+	0.04
C46H90O10PN	PS(20:0/20:0)	diphytanoyl PS	848.8	PS	+NL185	[M+H]+	0.04
C31H61O8P	PA(14:0/14:0)		610.5	PA	+NL115	[M + NH4]+	0.06
C43H85O8P	PA(20:0/20:0)	diphytanoyl PA	778.7	PA	+NL115	[M + NH4]+	0.06
C43H83O13P	PI(16:0/18:0)		856.7	PI	+NL277	[M + NH4]+	0.06
C49H92O15	DGDG(18:0/16:0)		938.6	DGDG	+NL341	[M + NH4]+	0.265
C51H96O15	DGDG(18:0/18:0)		966.6	DGDG	+NL341	[M + NH4]+	0.785

Table 11. Settings used by Creative Proteomics to identify the targeted lipids (compounds).

Compound	Function	m/z range	Start/end time (min)	Scan duration (s)	Ionization mode	Cone voltage (V)	Collision energy (V)
PA	Neutral Loss of 115.00	606 to 784	4.0 to 10.0	0.9	ES+	40	5
PG	Neutral Loss of 189.04	680 to 858	2.0 to 15.0	0.9	ES+	40	8
LysoPE, PE	Neutral Loss of 141.02	422 to 894	2.0 to 20.0	2.36	ES+	40	12
LysoPMME, PMME	Neutral Loss of 155.02	422 to 910	2.0 to 20.0	2.44	ES+	40	12
LysoPDME, PDME	Neutral Loss of 169.02	436 to 925	2.0 to 20.0	2.44	ES+	40	12
DihexDG	Neutral Loss 31.11	875 to 1000	2.0 to 20.0	0.625	ES+	40	16
PS	Neutral Loss of 185.00	675 to 1000	4.0 to 15.0	1.7	ES+	40	13
LysylPG	parent of 145.1	780 to 1000	20.1 to 30.0	1.1	ES-	40	-35

3.9 High-performance liquid chromatography (HPLC)

Samples from the extracellular component from the solvent screening cultures were run in the HPLC using the Bio-Rad Aminex HPX-87H column (Bio-Rad, USA). The conditions used to analysed the acids, solvents and sugar by HPLC are described in Table 12.

Table 12. HPLC Conditions for Quantifying Acids, Solvents, and Sugars in *Clostridium* cell cultures.

HPLC conditions	Setting
Flow rate	0.6mL/min
Oven temperature	35 ˚C
Run time	50 min
Injection volume	20 µL
Mobile phase	5 mM H_2SO_4
Detector type	Refractive Index at 35 ˚C
Injector wash	HPLC grade water

3.10 Statistical Analysis

For data analysis, GraphPad Prism v.8. was used. Statistical test used was the non-parametric Kruskall-Wallis and the uncorrected Dunn's test was used for multiple comparisons and to calculate the *p-values*.

4 Engineering *C. saccharoperbutylacetonicum* N1-4(HMT) results

This chapter aimed to generate new *C. saccharoperbutylacetonicum* N1-4(HMT) strains to investigate two pivotal aspects affecting the efficacy of this cell factory in biotechnology: oxidative stress, and alterations in membrane fluidity during fermentation and solvent production (Charubin et al., 2018). The accumulation of solvents is known to escalate cellular toxicity, hinder growth, and obstruct the production of high-value compounds (Linney et al., 2023; Patakova et al., 2013; Xue and Cheng 2019). Genetically engineering strains by incorporating a well-characterized antioxidant protein could demonstrate the importance of these components in reducing oxidative stress and, subsequently, influencing the production of high-value compounds (Chin et al., 2013). Moreover, manipulating the lipid metabolic pathway in *Clostridium*, specifically targeting the lipid species and composition related to the production of high-value products, represented an innovative approach to enhancing these cell factories for various applications (Sauer 2016; Sauer et al., 2008).

Engineering *Clostridium* strains has traditionally received less attention compared to other bacterial species like *E. coli* or yeast strains such as *S. cerevisiae* (Mattanovich, Sauer, and Gasser 2014; Sauer 2001). Nevertheless, recent advances in genetic engineering enabled successful modifications and optimization of solventogenic *Clostridium* (Atmadjaja et al., 2019).

This chapter highlights the efforts undertaken to generate mutant strains of *C. saccharoperbutylacetonicum* N1-4(HMT) to characterize the impact of a ROS scavenger and the expression of different enzymes involved in phospholipid biosynthesis on the lipid plasma membrane composition and, consequently, solvent production. This section provides a detailed account of various cloning strategies to:

• Overexpress *mt*1 gene, coding for the ROS scavenger Metallothionein 1

• Overexpress the genes *pgsA* and *cls*, involved in the synthesis of PG and CL, respectively.

• Silence the *cls* gene in the genome of *C. saccharoperbutylacetonicum* N1-4(HMT) using the CRISPR-Cas based CLEAVE™ technology, developed by Biocleave Ltd.

4.1 Cloning *metallothionein* 1 in *C. saccharoperbutylacetonicum* N1-4(HMT)

To study the expression of Metalothionein 1 from *Mus musculus* in *C. saccharoperbutylacetonicum* N1-4(HMT), the corresponding gene was cloned in the constitutive plasmid pBT by gap-repair (Bessa et al., 2012; Chino, Watanabe, and Moriya 2010). This fast and efficient procedure consisted of *in vivo* cloning of the *mt*1 fragment in the vector pBT, providing short stretches of homology with the vector (Figure 4.1). The amplified insert and the gapped vector were co-transformed in *E. coli* DH5α cells (Figure 4.1A, B), where the recombination occurred within the two pairs of flanking stretches of homologous sequences between vector and insert (Figure 4.1C). A circularised vector containing the *mt*1 gene was obtained (Figure 4.1D).

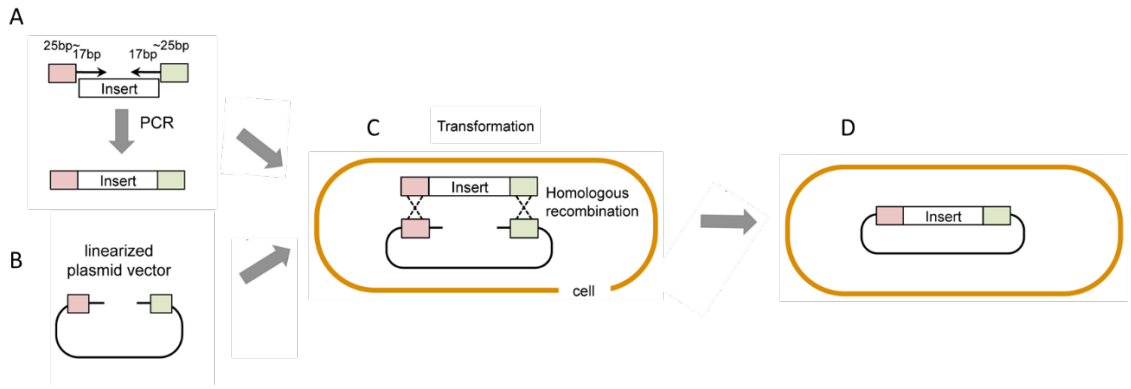

Figure 4.1. Illustration of the gap-repair cloning procedure. The amplified insert (A) with short stretches homologous to the linearized vector (B) was transformed in *E. coli* DH5α cells where the homologous recombination occurred (C) and a circularised vector containing the insert of interest is obtained (D). Adapted from Chino, Watanabe, and Moriya 2010.

To clone the *mt*1 gene in the backbone vector pBT-cpa1, the DNA sequence of the *cpa*1 had to be removed (Figure 4.2). Figure 4.2 shows that the *Psec* promoter, the ribosome binding site (RBS) and the *cpa*1 coding sequence are in frame without any other nucleotides bridging the sequences, thus preventing a traditional restriction enzyme cloning strategy. Considering this, a gap-repair cloning strategy was designed to swap the *cpa*1 sequence in the pBT-cpa1 plasmid for the *mt*1 *open reading frame* (ORF).

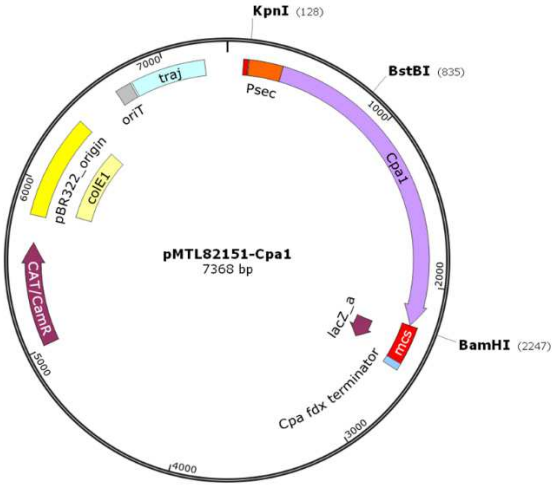

Figure 4.2. Structure of the pBT-cpa1 vector. The promoter *Psec* and the gene *cpa*1 are represented by the orange, purple fragments, respectively.

The objective was to insert the *mt*1 coding sequence in fusion with an encoded 6xHistag at the 5' end, generating the vector pHMt1. Using the same strategy, the *mt*1 coding sequence was also cloned in the same destination vector, without the 6xHistag, generating the vector pMt1. For the generation of the pMt1, *mt*1 was amplified by PCR using a forward and reverse primer (Figure 4.3A) that added the overlapping sequences to perform the gap-repair. To create pHMt1, corresponding to the *mt*1 coding sequence in fusion with an encoded 6xHistag at the 5' end, two PCRs were needed: the first one using a forward primer that added the 6xHistag sequence; using the first PCR product as template the second PCR was performed to include gap-repair overlapping sequences (Figure 4.3B).

Figure 4.3. Schematic describing the amplified (A) *mt*1 and (B) 6xHistag-*mt*1, containing the overlapping nucleotides (orange and red fragments) required for the homologous recombination.

The vector pBT-cpa1 was linearized with the restriction enzymes *BstB*I and *BamH*I (Figure 4.2), resulting in a partial excision of the *cpa*1 gene. The linearized plasmid and the amplified inserts were co-transformed in *E. coli* DH5-α competent cells, to obtain re-circularized plasmids containing the gene of interest (Figure 4.4).

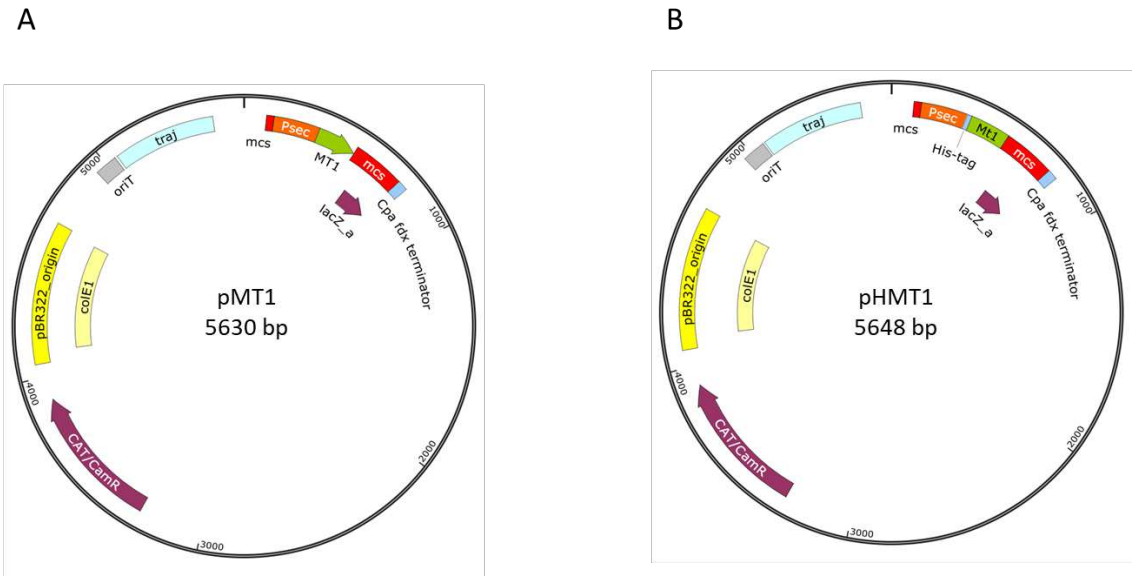

Figure 4.4 Structure of the plasmids designed to clone *mt*1 gene in pBT.pMt1 vector structure with the *mt*1 gene. (B) pHMt1 vector structure containing a 6xHistag in frame with the *mt*1. The promoter *Psec*, the gene *mt*1 and the 6xHistag are represented by the orange, green and blue fragments, respectively.

The gap-repair transformation had resulted in 5 and 3 colonies for the pHMt1 and pMt1, respectively. All colonies were screened for the insert using colony PCR, and all the PCR products exhibited the expected length (Figure 4.4). However, following plasmid extraction and restriction confirmation with the enzymes *Kpn*I and *Hind*III, only the colony designated as number 6 exhibited the anticipated restriction fragments (446 bp and 4527 bp for the pMt1; 428 bp and 4527 bp for the pHMt1) (Figure 4.5D). The correct insertion of the *mt*1 gene in colony number 6 was confirmed by Sanger sequencing.

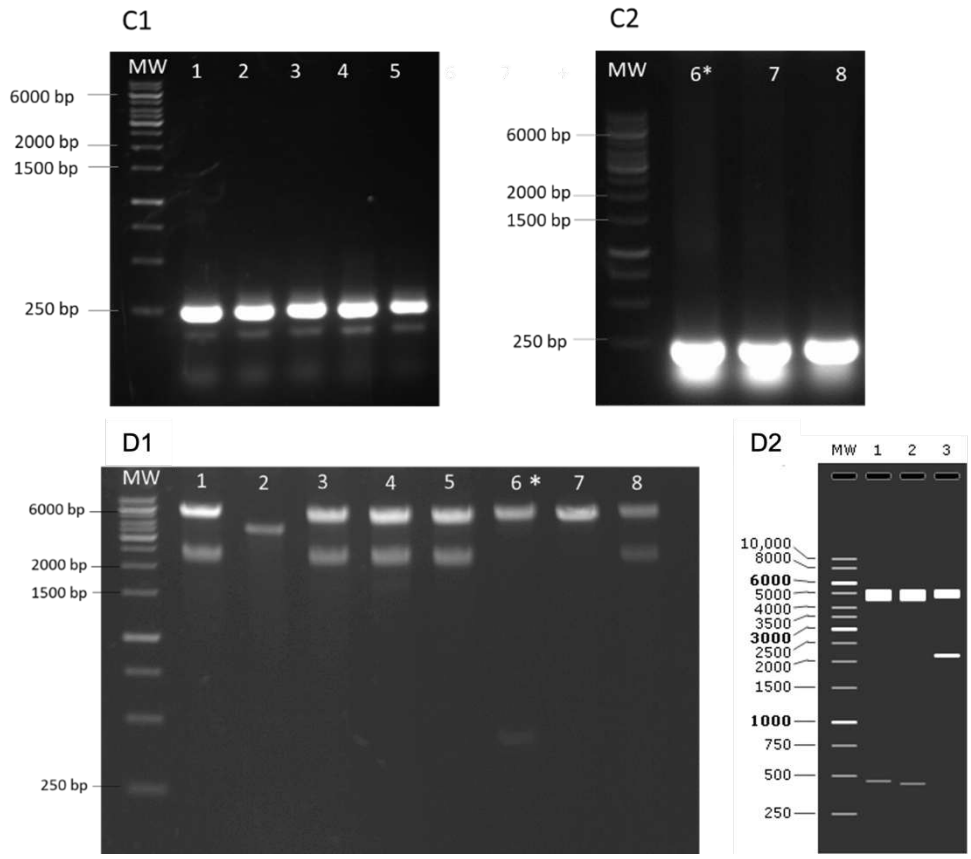

Figure 4.5. Agarose gel electrophoresis of the colony PCR products (C1 and C2), digested fragments with *Kpn*I and *Hind*III from the obtained clones (D1) and a simulation of the fragments after digesting pMt1, pHMt1 and pBT-Cpa1 vectors with *Kpn*I and *Hind*III (D2).Numbers 1 to 5 from C1, C2 and D1 correspond to *E. coli* DH5α cells containing the pHMt1 vector and numbers 6 to 8 correspond to *E. coli* DH5α cells containing the pMt1 vector. Numbers 1 to 3 from D2 correspond a simulation of the DNA fragments after digesting pMt1, pHMt1 and pBT-cpa1 vectors with *Kpn*I and *Hind*III, respectively. Colony represented in lane 6* has the correct vector. MW: GeneRuler 1Kb DNA ladder (ThermoFisher Scientific, UK).

4.2 Cloning *cls* and *pgsA* in *C. saccharoperbutylacetonicum* N1-4(HMT)

The overexpression of *cls* and *pgsA* genes involved in the synthesis of CL and PG, respectively (Figure 1.12), was tested by cloning these genes from *C. saccharoperbutylacetonicum* N1-4 HMT, in the constitutive plasmid pBT. The cDNA sequence of *pgsA* (AGF55125) and *cls* (AGF59059) was designed to be cloned in this vector with and without an additional 8xHistag sequence at the 3' end of each of these genes (Figure 4.6).

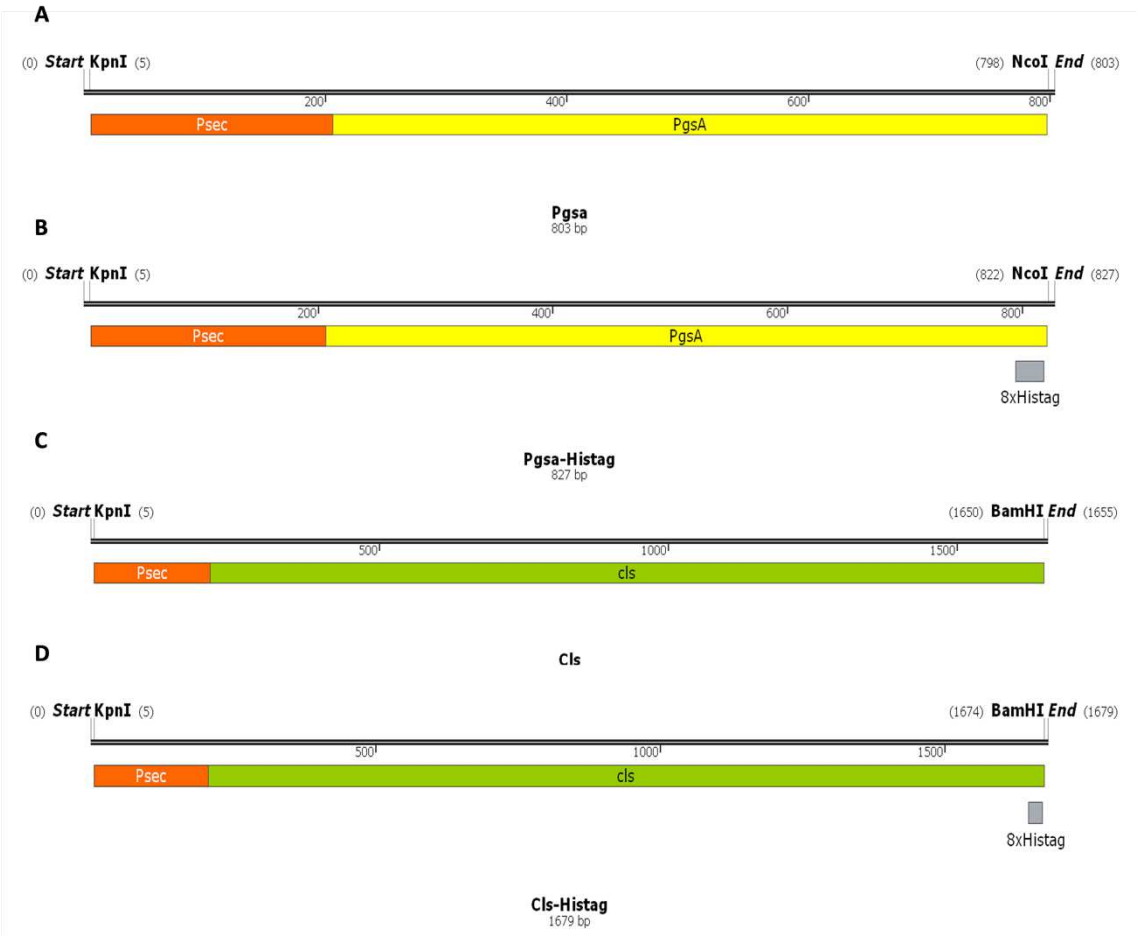

Figure 4.6. Illustration of DNA sequences inserted into pBT. (A) The *Psec* promoter with *pgsA*. (B) The *Psec* promoter with *pgsA*, with an 8xHistag sequence at its 3' end. (C) The *Psec* promoter aligned with *cls*. (D) The *Psec* promoter paired with *cls* and an 8xHistag sequence at the 3' end.

The inserts *pgsA*, *pgsA*-8xHistag, *cls* and *cls*-8xHistag were synthesised and cloned in the pBT vector by GenScript, generating the vectors; *pPgsA*, *pHPgsA*, *pCls* and *pHCls*; that were transformed in *C. saccharoperbutylacetonicum* N1-4 HMT, generating strains *pgsA*$^{+}$, *HpgsA*$^{+}$, *cls*$^{+}$ and *Hcls*$^{+}$, respectively. The transformation resulted in numerous colonies, with a positive control (pBT) and negative control (tris 10mM) of thousands of colonies and 0 colonies, respectively (data not shown). In this work only strains *pgsA*$^{+}$ and *cls*$^{+}$ were used for an initial characterisation of their effect in the lipid membrane composition and ABE fermentation.

4.3 Generation of the knockout strains by CLEAVE™ Technology

The genetic engineering of *Clostridium* genus genomes is technically challenging (Wang et al., 2019). However, recent advances have led to the development of tools specifically designed for genetic manipulation in *Clostridium* species, such as CLEAVE™ technology (Atmadjaja et al., 2019). This innovative approach utilizes the CRISPR-Cas based system and has been devised to effectively target and eliminate specific DNA sequences through the screening of homologous recombination events in *Clostridium* (Atmadjaja et al., 2019). As a result, this technology has proven successful in achieving the deletion of desired genetic elements.

In this work, the goal was to modify *C. saccharoperbutylacetonicum* N1-4 (HMT) to create two knockout strains: Δ*pgsA* and Δ*cls*, by silencing the *pgsA* and *cls* genes respectively. Both genes encode critical enzymes in phospholipid biosynthesis. Specifically, *pgsA* encodes for phosphatidylglycerol synthase, which is involved in synthesizing PG, while *cls* encodes cardiolipin synthase, playing a role in synthesizing CL (Parsons and Rock, 2013).

The creation of knockout strains in *C. saccharoperbutylacetonicum* N1-4 (HMT) via CLEAVE™ required two vectors (Figure 4.7). The first vector was designed to facilitate homologous recombination, containing homology regions (HR) that correspond to the desired mutation site on the genome, with the mutation itself placed between these HR regions. This facilitated a recombination event between the bacterial chromosome and the HR regions. Subsequently, a second vector, often referred to as the targeting or killing vector, was introduced into the bacterial cells. Its role was to selectively identify and eliminate cells that failed to undergo recombination while maintaining those with the correct mutation intact.

This section will detail the results from each necessary step and every vector cloned with the aim to silence these genes in *C. saccharoperbutylacetonicum* N1-4 (HMT). Unfortunately, despite numerous attempts, the step1 vector intended for the Δ*pgsA* strain could not be cloned. Consequently, the creation of this knockout was put on hold, and the CLEAVE™ procedure was applied only to the generation of the Δ*cls* strain. The following results show the cloning procedures to obtain the step1 vector for the *cls* knockout, the killing vector utilized to select the *cls* mutants, and screenings to validate the accurate knockouts, respectively.

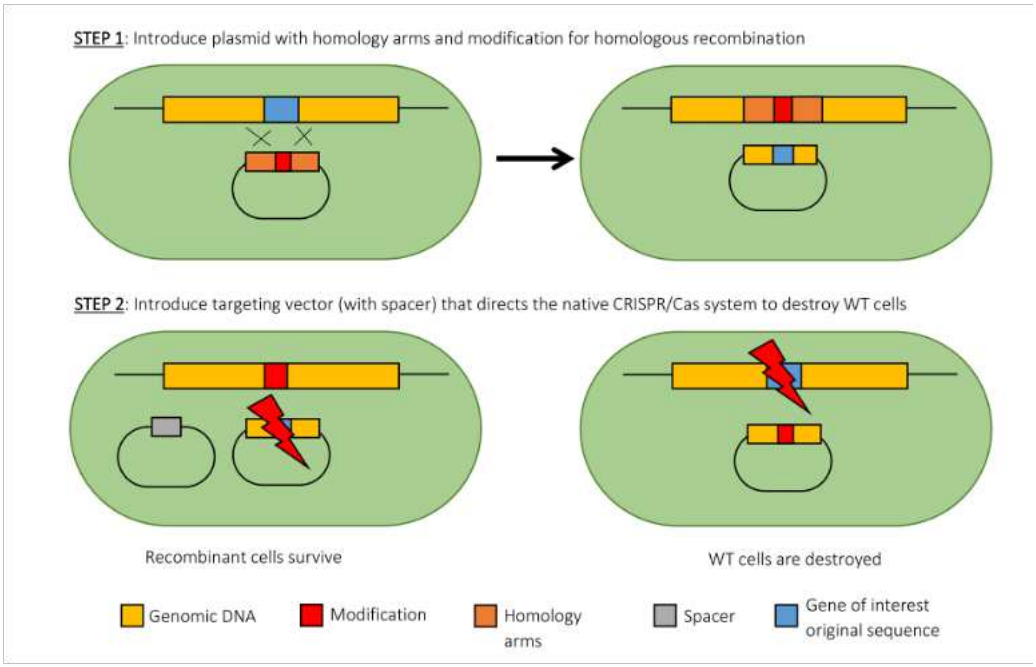

Figure 4.7. Scheme of the CLEAVE^{TM} technology to edit the genome of *C. saccharoperbutylacetonicum* N1-4 HMT. Step1: a plasmid, containing the sequence meant for deletion, is transformed into *C. saccharoperbutylacetonicum* N1-4 (HMT) cells, allowing the homologous recombination, given by two homology arms. Step2: Targeting vector is transformed into the previously cloned cells. This vector carries a spacer sequence guiding the inherent CRISPR-Cas system to a cleavage site. Hence, the spacer's sequence should align with a locus in the gene of interest within the original sequence. WT sequences that contain the spacer will be targeted and cleaved by the CRISPR-Cas system, while recombinant cells, lacking these sequences due to the truncated deletions, will not be targeted (Linney 2021).

4.3.1 *C. saccharoperbutylacetonicum* N1-4 (HMT) *cls* knockout strain

Construction of the step1 vector

For the construction of the homologous recombination vector aimed at generating the knockout of the *cls* gene, specific regions were cloned based on the genomic sequence CP004121.1 (GenBank accession number). The 800 nucleotides upstream and downstream of the region 5893228-5894670 in the genome were synthesised flanking the mutation sequence, which consisted of the 45bp segment from the 5' end and the 45bp segment from the 3' end from the *cls* gene (region 5893228-5894670 in the genome). This arrangement resulted in the formation of the sequence HR1 - Δ*cls* - HR2, as illustrated in Figure 4.8, this DNA sequence was synthesized

and subsequently cloned into the pUC57 vector by Genscript, resulting in the creation of the vector pUC57_step1_Δ*cls*.

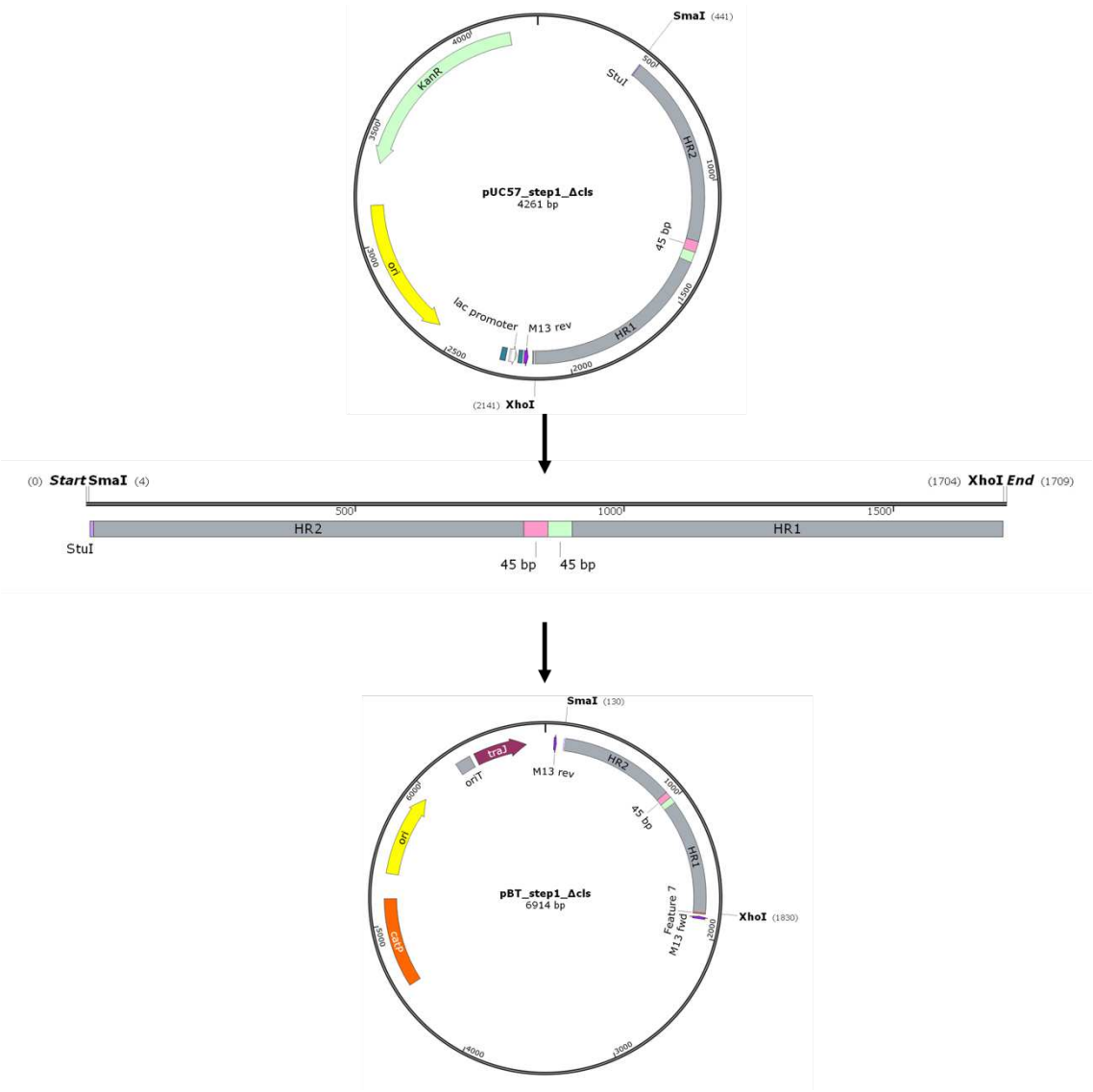

Figure 4.8. Diagram from Snapgene illustrating the cloning process to create the pBT_step1_Δ*cls* vector. The HR1- Δ*cls* -HR2 DNA fragment was extracted from pUC57_step1_Δ*cls* and inserted into the pBT vector.

The DNA fragment corresponding to the HR1 – Δ*cls* – HR2 sequence was digested from the vector pUC57_step1_Δ*cls* with the restriction enzymes *Sma*I and *Xho*I resulting in two fragments; one with 1700 bp, corresponding to the insert (HR1 – Δ*cls* – HR2) and a second fragment with 2561 bp that is the remaining sequence of the pUC57 vector (Figure 4.9A). The plasmid pBT was digested with the same restriction enzymes resulting in two fragments, one

with 40 bp (not visible in the agarose gel) and another fragment with 5214 bp, corresponding to the linearized vector (Figure 4.9A).

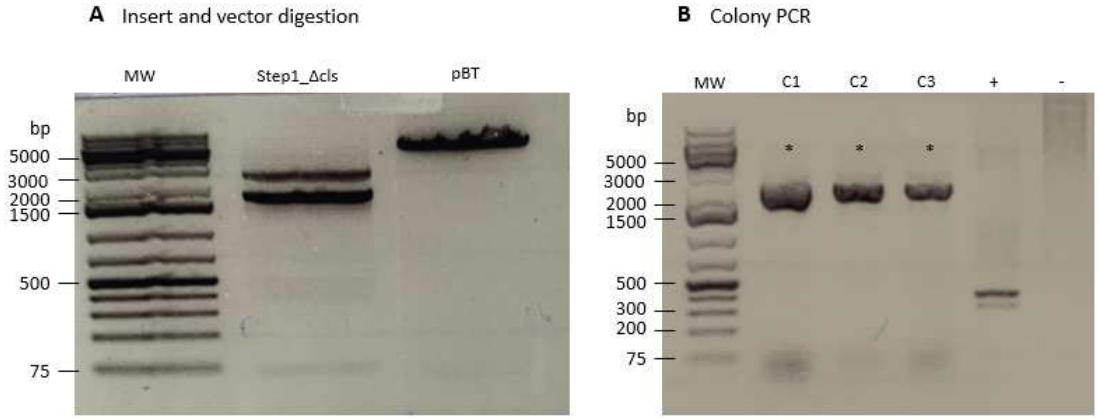

Figure 4.9. Agarose Gel Electrophoresis and Colony PCR Results for step1_Δ*cls* Insert and pBT Vector. (A) Gel electrophoresis of the digestion products aimed to obtain the step1_Δcls insert and linearized pBT. (B) Colony PCR to verify the cloning of pBT_step1_cls. MW is the molecular weight ladder (GeneRuler 1kb Plus DNA Ladder, ThermoFisher). C1-C3 indicate the three colonies acquired post-cloning. (+) and (-) denote the positive and negative controls of the colony PCR, corresponding to the backbone vector pBT and 10mM Tris, respectively.

The 1700 bp DNA fragment, corresponding to the HR1 - Δ*cls* - HR2 insert, was ligated with the linearized pBT vector (Figure 4.8) and subsequently transformed into *E. coli* Dh10b competent cells. Following the transformation, three colonies were obtained, along with a positive control containing numerous colonies and a negative control without any colonies. To confirm the presence of the pBT_step1_Δcls vector in the three colonies, a colony PCR was conducted. The colony PCR yielded a final product of approximately 2000 bp, which aligned with the expected size of 1953 bp (Figure 4.9B). Plasmids from colonies C1 and C3 (Figure 4.9B) were subjected to sequencing, and the results confirmed the presence of the correct pBT_step1_Δcls sequence.

Construction of the killing vector

To selectively target and eliminate cells lacking the *cls* deletion, a killing vector was created. This killing vector comprised a cassette designed for genome editing using the endogenous CRISPR-Cas system. It was constructed by cloning a leader sequence and direct repeats derived from the

CRISPR-Cas machinery of *C. saccharoperbutylacetonicum* N1-4 (HMT). It's important to note that these specific sequences are the intellectual property of Biocleave Ltd (Atmadjaja et al., 2019). A spacer sequence was inserted between the direct repeats, resulting in the sequence depicted in Figure 4.10A.

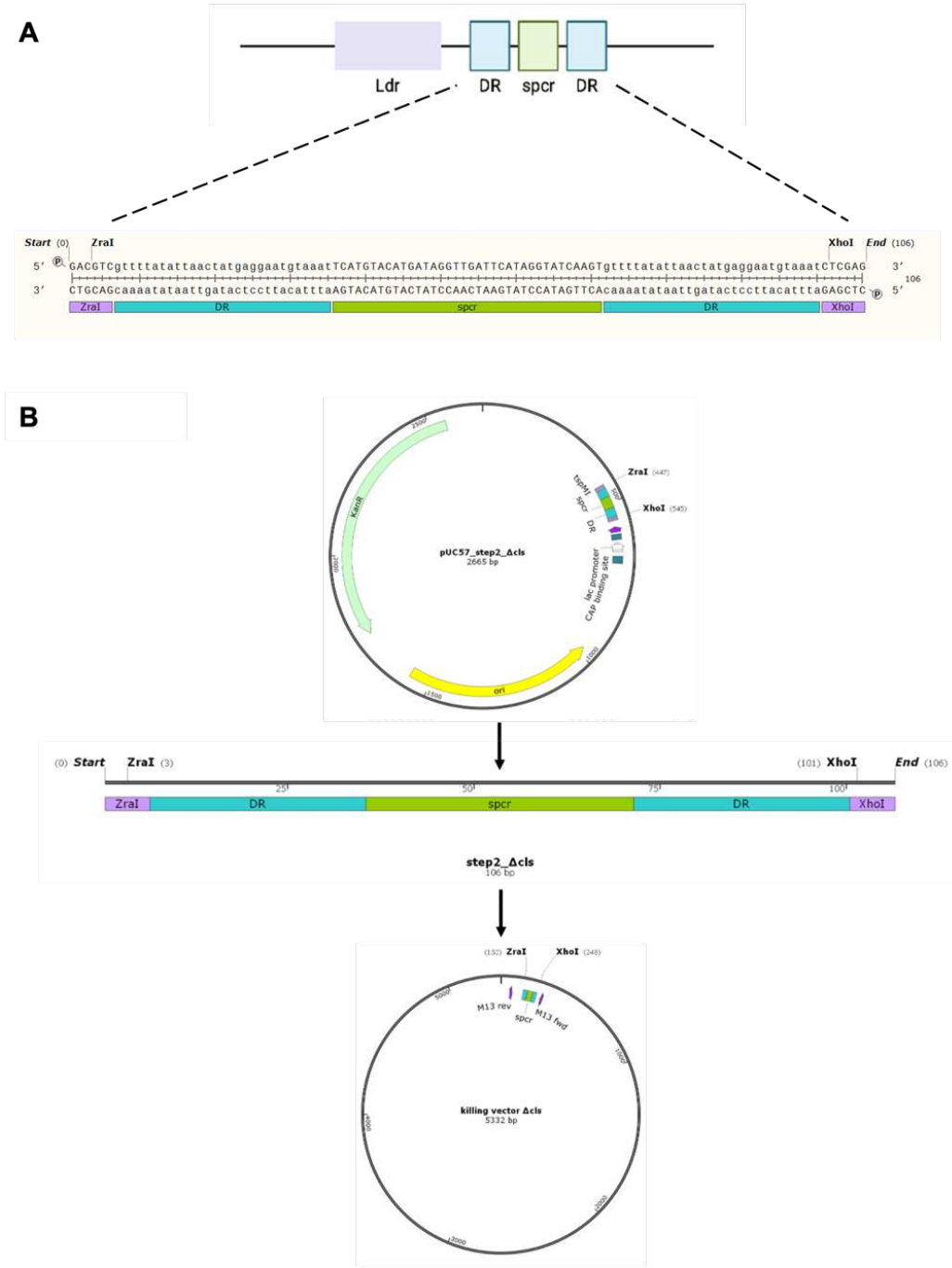

Figure 4.10. Killing vector construction.(A) The spacer (spcr) to target *cls* gene flanked by the direct repeats (DR), downstream the leader sequence (Ldr). (B) The DR-spcr-DR to target the gene flanked by the restriction enzymes *Zra*I and *Xho*I was cloned first in vector pUC57 and; (C) subsequently was cloned in the killing vector (backbone), generating the killing vector ∆*cls*.

To determine the spacer sequence for the killing vector, a selection process was carried out. Approximately 30 nucleotides adjacent to a Protospacer Adjacent Motif (PAM) motif, identified as CCN, where N can be any other nucleotide, were chosen. Utilizing a proprietary software developed by Biocleave Ltd, five potential spacer sequences were evaluated, and the most efficient sequence was selected based on its ability to identify, target, and cleave the double-stranded DNA. To prevent the killing vector itself from being targeted by the CRISPR-Cas system, the Direct Repeat sequence was intentionally designed without the PAM sequence. This selection ensured that the killing vector would specifically target the WT strain (Atmadjaja et al., 2019). The chosen spacer sequence was synthesised between the direct repeats, flanked by *Zra*I and *Xho*I restriction sites and cloned in the pUC57 by Genscript (UK) (Figure 4.10B).

To obtain the insert containing the DR-spcr-DR sequence (referred to as step2_Δcls), the vector pUC57_step2_Δcls was digested with *Zra*I and *Xho*I restriction enzymes. This digestion resulted in two distinct fragments: one fragment measuring approximately 5000 bp and a second fragment of 98 bp (Figure 4.11A). The latter fragment corresponds to the desired insert, step2_Δcls.

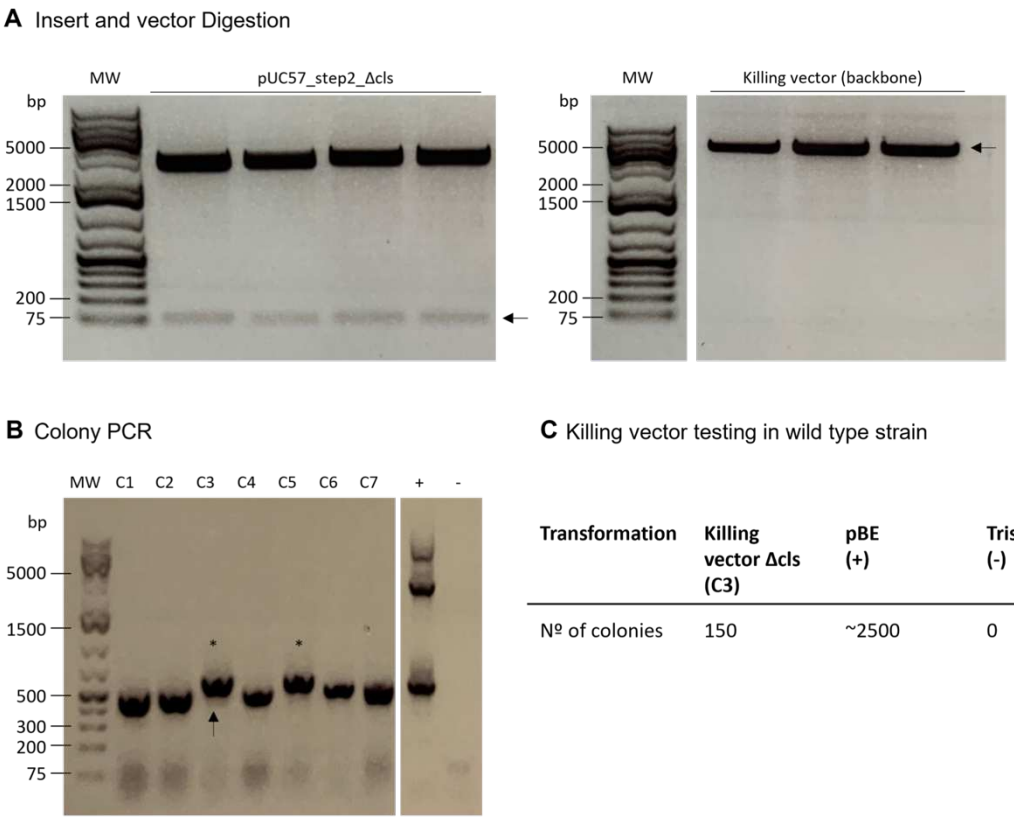

Transformation	Killing vector Δcls (C3)	pBE (+)	Tris 10mM (-)
Nº of colonies	150	~2500	0

Figure 4.11. Results of the cloning procedure to generate and test the killing vector Δ*cls*.(A) Agarose gel electrophoresis image depicting the products obtained after digesting pUC57_step2_Δcls and killing vectors (backbone). The arrow highlights the bands corresponding to the insert and linearized vector. (B) Colony PCR results showing the analysis of 7 colonies selected to confirm the presence of the correct plasmid sequence. (C) Quantitative data displaying the number of colonies obtained following the transformation of the killing vector Δcls and pBE into *C. saccharoperbutylacetonicum* N1-4 (HMT). MW is the generuler 1kb plus DNA ladder (ThermoFisher, UK). (+) and (-) represent the positive and negative controls. C1 to C7 are the tested colonies. (*) denotes the positive colonies with the desired plasmid sequence.

The backbone vector, also known as the killing vector, was prepared for cloning by linearizing it through digestion with the same restriction enzymes. The resulting digestion product appeared as a DNA fragment of approximately 5000 bp, as shown in (Figure 4.11A). It is worth noting that the agarose gel image displays a white band separating the DNA ladder (MW) from the digestion products, this shows a cut on the gel image, to remove data not relevant for this experiment. The two bands highlighted by arrows in Figure 4.11A, one measuring 98 bp and the other approximately 5000 bp, were excised, purified, and subsequently ligated. The ligated product was then transformed into Dh10b competent cells and plated on LBA plates supplemented with

the antibiotic and the plates were incubated overnight at 37 °C. Subsequently, all seven obtained colonies were subjected to colony PCR analysis (Figure 4.11B). The PCR product from colonies C3 and C5 have a DNA band size higher than that of the positive control, pBE as depicted in Figure 4.11B. The plasmid isolated from colony C3 was further tested in *C. saccharoperbutylacetonicum* N1-4 (HMT) cells. The transformation of this plasmid resulted in the growth of approximately 150 colonies for the killing vector Δ*cls* (C3), around 2500 colonies for pBE (positive control), and no colonies for the 10 mM Tris (negative control) (Figure 4.11C). The significant reduction, over 16-fold, in colony formation between the killing vector Δ*cls* and the positive control indicates that the selected spacer had indeed activated the CRISPR-Cas system, leading to the cleavage of the DNA strand in the WT strain and reducing its viability. The plasmids extracted from colony C3 were selected to proceed with the CLEAVE™ technology.

cls knockout procedure

The deletion of the cardiolipin synthase gene (*cls*) was achieved using the CRISPR-Cas technology CLEAVE™ involving the transformation of the vectors pBT_step1_Δcls and the killing vector Δcls in *C. saccharoperbutylacetonicum* N1-4 (HMT) cells. First it was the transformation of pBT_step1_Δcls vector into *C. saccharoperbutylacetonicum* N 1-4 (HMT) that resulted in the emergence of hundreds of colonies, while the positive control (pBT) yielded thousands of colonies and the negative control (10 mM tris) produced zero colonies. 6 of the transformants obtained with the pBT_step1_Δcls vector were subsequently subcultured eight times in RCM media supplemented with antibiotic. This step is important to enhance the chances of double recombination occurring between the step1 vector and the genomic DNA, thereby increasing the likelihood of obtaining a deletion of the *cls* gene. The efficiency of recombination in bacteria is strongly influenced by cell division (Atmadjaja et al., 2019). Additionally, bacteria in exponential growth typically possess up to 8 copies of their chromosome, which can further reduce recombination efficiency (Fels, Gevaert, and Van Damme 2020).

After subculturing a subset of the initial colonies, the cells were transformed with the killing vector Δ*cls*. This transformation allowed the cells to create a CRISPR RNA (crRNA) and build an effector complex. This complex could identify the target PAM site in the gene by pairing bases with the complementary strand (Atmadjaja et al., 2019). As a result, the DNA of these cells lacking the deletion was cleaved, selectively favouring the mutated ones (Δ*cls*). The transformation of the cells with the killing vector Δ*cls*, along with the positive control pBE, and the negative control tris 10mM, yielded 18 colonies, approximately 2500 colonies, and no

colonies, respectively. The significant reduction, over 55-fold, in the number of colonies obtained between the transformation with the killing vector Δ*cls* and the positive control suggests that the crRNA system effectively targeted the chromosomal DNA of *C. saccharoperbutylacetonicum* N1-4 (HMT), leading to DNA cleavage.

In the screening process for positive deleted strains, a subset of the 18 colonies obtained was subjected to colony PCR using two different strategies, as described below, and shown in Figure 4.12:

Strategy 1

In this approach, chromosomal DNA from the obtained colonies was amplified using Primer 1 as a forward primer, which initiates the amplification before the homologous region 1 (HR1), and Primer 2 as a reverse primer, which starts the amplification within homologous region 2 (HR2).

Strategy 2

In this strategy, the chromosomal DNA from the obtained colonies was amplified using Primer 1 as a forward primer, which initiates the amplification before homologous region 1 (HR1), and Primer 3 as a reverse primer, which starts the amplification in the middle of the gene. This gene sequence is absent in cells with the correct mutation, allowing for the detection of WT cells.

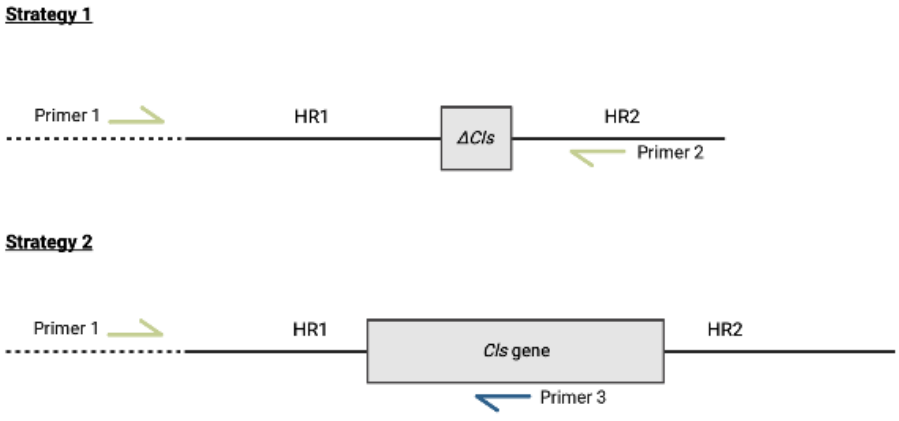

Figure 4.12. Diagram outlining colony PCR strategies to confirm the knockout *cls* strains. HR- homologous region; Δ*cls* – *cls* knockout.

The results from the colony PCR testing the Δ*cls* strains using strategy 1 and strategy 2 is highlighted in Figure 4.13. Strategy 1 was designed to be able to amplify the DNA from both

mutated and WT strains, generating different DNA size bands. In an agarose gel (1% w/v), the mutated strain was expected to yield a PCR product with a band size of 1291 bp (Figure 4.13A, lane 1), whereas the WT strain was anticipated to produce a fragment of 2644 bp (Figure 4.13A, lane 2). In contrast, Strategy 2 was specifically designed to selectively amplify DNA from the wild-type strain. Primer 3 (Figure 4.12) was specifically designed to bind to a *cls* sequence unique to the WT strain. As a result, this strategy was intended to generate PCR products only in the presence of the WT strain genomic DNA, while yielding an amplification with the mutated strain (Figure 4.13C).

Both strategies were applied to test the obtained Δ*cls* colonies. In Strategy 1 (Figure 4.13B), colonies C3, C11, and C15 were the only ones to yield a PCR product with a fragment size ranging between 1000-1500 bp, suggesting a strong possibility of a successful knockout. Conversely, the other colonies exhibited two bands: one in the 1000-1500 bp range and another at approximately 2000 bp, like the positive control (2644 bp) (Figure 4.13A, B). A colony PCR utilizing the primers from Strategy 2 was performed on the same colonies, resulting in the generation of DNA fragments of the same size as the positive control (Figure 4.13D). These results indicate that the selected colonies possibly correspond to the WT strain.

The conflicting results between Strategy 1 and Strategy 2 prompted further investigation to understand this discrepancy. A primer blast search was conducted on NCBI to explore all possible binding sites of Primer 1-2 and Primer 1-3 within the genome of *C. saccharoperbutylacetonicum* N 1-4 (HMT) (Figure 4.14). The primer blast analysis revealed that Primer 1 and Primer 2 are specific to the DNA regions chosen for testing the knockout strain, i.e., upstream of HR1 and within HR2 (Figure 4.12). However, these primers also possess specificity to bind to other regions of the genome, resulting in the amplification of a PCR product measuring 1671 bp (Figure 4.14). This finding may explain the presence of two bands observed in colonies C1, C5, C7, C9, and C17 (Figure 4.13B).

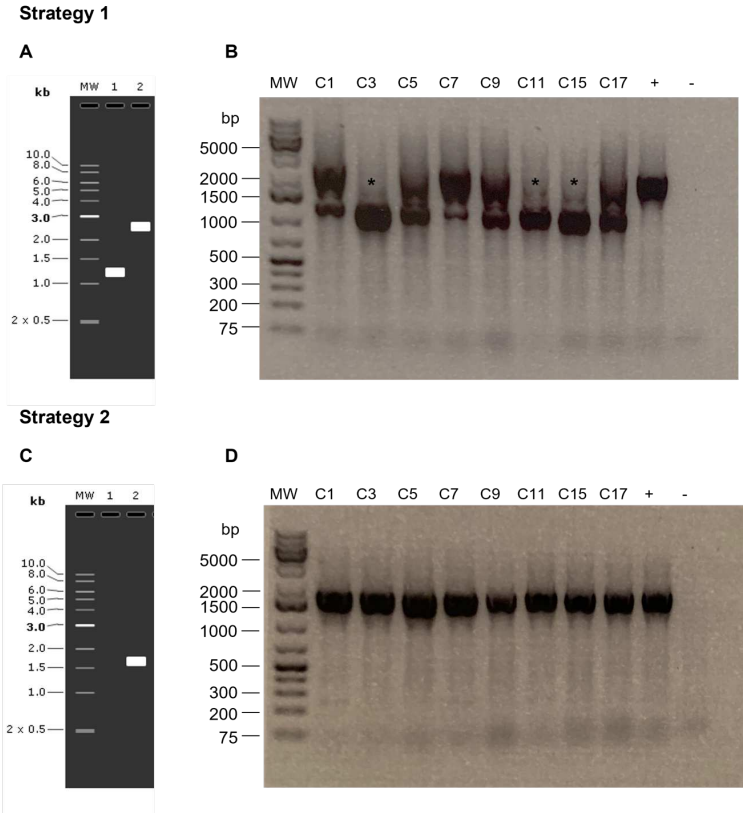

Figure 4.13. Agarose gel electrophoresis of the colony PCR results to confirm the Δ*cls*. Strategy 1 (A) simulation of the DNA migration in the 1%(w/v) agarose gel in case of a correct deletion (1291 bp, lane 1) and in case of no mutation (2644 bp, lane 2); (B) Colony PCR results showing the analysis of 8 colonies using strategy 1. Strategy 2 (C) simulation of the DNA migration in a 1%(w/v) agarose gel in case of a correct deletion (no band, lane 1) and in case of no mutation (1766 bp, lane 2); (D) Colony PCR results showing the analysis of 8 colonies, using strategy 2. C1, C3, C5, C7, C9, C11, C15 and C17 correspond to the tested colonies, (+), (-) correspond to the positive and negative controls, respectively. MW is the generuler 1kb plus DNA ladder, ThermoFisher, UK. In strategy 1, C3, C11 and C15 (*) are the only colonies with a PCR product of around 1291 bp.

Strategy 1

Primer pair 1

	Sequence (5'->3')
Forward primer	GGCCTTATTCGTTTTGAAG
Reverse primer	GAACAAGTAAGCTCATAGGC

Products on target templates

>NC_020291.1 Clostridium saccharoperbutylacetonicum N1-4(HMT), complete sequence

```
product length = 2644
Forward primer  1        GGCCTTATTCGTTTTGAAG  19
Template        5892294  ...................  5892312

Reverse primer  1        GAACAAGTAAGCTCATAGGC  20
Template        5894937  ....................  5894918


product length = 1671
Forward primer  1        GGCCTTATTCGTTTTGAAG  19
Template        3380810  .TAAC....G.........  3380828

Forward primer  1        GGCCTTATTCGTTTTGAAG  19
Template        3382480  TC.......TT.......A  3382462
```

Strategy 2

Primer pair 1

	Sequence (5'->3')
Forward primer	GGCCTTATTCGTTTTGAAG
Reverse primer	CCCAGGAATTTTGCCTC

Products on target templates

>NC_020291.1 Clostridium saccharoperbutylacetonicum N1-4(HMT), complete sequence

```
product length = 1766
Forward primer  1        GGCCTTATTCGTTTTGAAG  19
Template        5892294  ...................  5892312

Reverse primer  1        CCCAGGAATTTTGCCTC  17
Template        5894059  .................  5894043


product length = 1143
Forward primer  1        GGCCTTATTCGTTTTGAAG  19
Template        1728064  ..G...C..TT........  1728046

Reverse primer  1        CCCAGGAATTTTGCCTC  17
Template        1726922  T.G.A..C.......A.  1726938


product length = 1671
Forward primer  1        GGCCTTATTCGTTTTGAAG  19
Template        3380810  .TAAC....G.........  3380828

Forward primer  1        GGCCTTATTCGTTTTGAAG  19
Template        3382480  TC.......TT.......A  3382462
```

Figure 4.14. Primer Pair Specificity Analysis for Strategy 1 and Strategy 2 primers in *C. saccharoperbutyacetoncium* N 1-4 (HMT) genome (NC_020291.1). The analysis highlights the potential PCR products and the corresponding binding sites of the primers in the wild type genome. Strategy 1 can result in two PCR products with 2644 bp and 1671 bp. Strategy 2 can result in three PCR products with 1766 bp, 1671 bp and 1143 bp. This simulation was obtained using Primer Blast from NCBI.

Investigation into the primer pairing specificity between forward primer 1 and reverse primer 3, in *C. saccharoperbutylacetonicum* N 1-4 (HMT), revealed three potential PCR products (Figure 4.14). One product with 1766 bp, corresponding to the amplification of DNA spanning from the upstream region to HR1 and the middle of the *cls* gene (Figure 4.12). The other two potential PCR products were estimated to be 1143 bp and 1671 bp, amplifying regions of the genome and a mega plasmid from *C. saccharoperbutylacetonicum* N 1-4 (HMT), respectively (Figure 4.14) (Gu et al., 2018). These findings can provide an explanation for the band obtained (1500 – 2000 bp) for all the colonies using Strategy 2 in the colony PCR analysis.

To obtain sufficient DNA for sequencing and confirm the presence of the desired knockout in colonies 3 and 11 (C3 and C11), a new colony PCR using Strategy 1 primers was performed. However, the results indicated a negative outcome for the Δ*cls* strain in both colonies. (Figure 4.15). Further attempts were made to identify a positive Δ*cls* strain (Figure 4.15). Colony 3, along with new colonies (C2, C4, C6, and C12), were subjected to colony PCR analysis. The agarose gel image in Figure 4.15 displayed a DNA fragment ranging between 1200-1500 bp, closely resembling the expected size (1291 bp), in colonies 6 and 12 (C6, C12). Colonies 2 and 4 exhibited multiple fragments, including one around 1291 bp and another around 3000 bp, similar to the positive control. Notably, the colony 3 result differed significantly from the previous colony PCR analysis shown in Figure 4.13B.

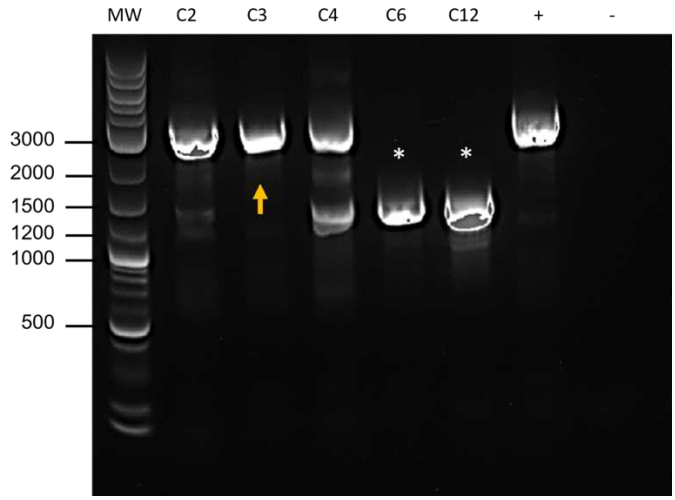

Figure 4.15. Agarose gel electrophoresis of the colony PCR result to confirm the Δ*cls*, using strategy 1 primers. C2, C3, C4, C6 and C12 correspond to the tested colonies, (+), (-) correspond to the positive and negative controls, WT cells and 10 mM tris, respectively. MW is the 1kb plus DNA ladder NEB, UK. (*)

highlight the colonies with a PCR product of around 1291 bp; the yellow arrow highlights the fragment obtained for colony 3 (C3).

The knockout of essential genes can present challenges, as cells may become non-viable or can undergo reversion by swapping the mutation, in this situation with the HR-Δ*cls*-HR region transferred to the step1 vector during homologous recombination (Tan et al., 2017). Although the killing vector is designed to effectively cleave the DNA after recombination, its efficiency is not guaranteed to be 100%, as observed in the results.

Cloning summary

This cloning section resulted in the generation of the following strains:

- *mt*1^{+}: strain overexpressing *mt*1 that codes for the antioxidant enzyme Metallothionein 1
- *pgsA*$^{+}$: strain overexpressing *pgsA*, that codes for the enzyme PgsA involved in the synthesis of the lipid PG.
- *HpgsA*$^{+}$: strain overexpressing *PgsA* in fusion with an 8xhistag, that codes for the enzyme PgsA involved in the synthesis of the lipid PG.
- *cls*$^{+}$: strain overexpressing *cls*, that codes for the enzyme Cls involved in the synthesis of the lipid CL.
- *Hcls*$^{+}$: strain overexpressing *cls* in fusion with an 8xhistag, that codes for the enzyme Cls involved in the synthesis of the lipid CL.

The strains *mt*1^{+}, *pgsA*$^{+}$, and *cls*$^{+}$, in addition to the previously generated strains Δ*pssA* and *pssA*$^{+}$, which were created by Dr. John Linney and Dr. Maria Monserrat Roman Lara, were selected for characterisation of their lipid content and solvent production. The Δ*pssA* and *pssA*$^{+}$, correspond to strains with the *pssA* gene deleted in *C. saccharoperbutylacetonicum* N 1-4 HMT genome and, to the same gene (*pssA*) cloned in the constitutive vector (pBT-*Psec*) and transformed in *C. saccharoperbutylacetonicum* N 1-4 HMT cells. The expression levels of the *mt*1, *pssA*, *pgsA*, and *cls* genes in the respective overexpressing strains were not measured in this study. However, it was assumed that their expression levels were higher than those in the wild type strain. Furthermore, the mutant strain *BCL*, provided by Biocleave, was also included in the analysis. The results of these characterizations are presented in the subsequent sections.

5 Lipidomic Analysis Results

The cell membrane serves as a protective barrier with a crucial function of keeping the homeostasis of the cells (Strahl and Errington, 2017). Various external factors, such as temperature, pressure, nutrients, ions, enzyme activity, growth phase, and solvent production, impact its physicochemical properties and overall performance (Chin et al., 2017; Huffer et al., 2011). In solventogenic *Clostridium,* during fermentation, the production and accumulation of weak acids and solvents affect the oxidative stress levels of the cells. This leads to changes in lipid balance, membrane stability, fluidity, and interactions between lipids and proteins (Mrozik and Łabużek, 2004).

Lipids play a significant role in the stability and robustness of the membrane, thereby influencing the capacity of the cells to become an improved cell factory (Parsons and Rock, 2013). However, while lipid synthesis is relatively well understood in some bacteria, including *E. coli*, less is known about the regulation of synthesis, particularly how different lipid classes and isoforms adapt to internal and external conditions essentially in *Clostridium* (Strahl and Errington, 2017). *C. saccharoperbutylacetonicum* is noted to have PE, PG, and CL as the main lipids but also their plasmalogen forms as well as glycosyldiradylglycerols. However, PE, PG and CL are described as the main lipids (Guan and Goldfine, 2021). The simplified metabolic pathway for their synthesis is depicted in Figure 5.1.

To enhance cell factories, most research has focused on protein expression, transmembrane transport, and modifications in protein interactions, often neglecting the importance of the cellular lipidome (Goel et al., 2012; Gustavsson and Lee, 2016; Sauer and Mattanovich, 2012). Nevertheless, recent studies have highlighted the significance of lipids in the stability and survival of the cells. For instance, manipulating the conformation and saturation of phospholipid fatty acids has been shown to improve tolerance to valuable products (Tan et al., 2017).

To gain valuable insights into desired lipid compositions for various fermentative outcomes, an analysis of the lipidome was performed on *C. saccharoperbutylacetonicum* N 1-4 (HMT) WT strain and several mutant strains related to phospholipid biosynthesis (Δ*pssA*, *pssA*$^{+}$, *pgsA*$^{+}$, *cls*$^{+}$) and oxidative stress reduction (*mt*1^{+}) and a mutant strain generated by our industrial partner Biocleave Ltd, with different membrane morphologies (*BCL*). The lipidome of these strains was investigated using two techniques: thin-layer chromatography (TLC) and mass spectrometry.

TLC is a cost-effective and convenient method that separates lipids in a mixture based on their hydrophobicity and its identification can be inferred using lipid standards. Staining with Molibdenum Blue (MB) and Ninhydrin (N) allows for the visualization of lipids with specific functional groups, such as phospholipids and lipids with amino groups, respectively. Although TLC provides initial insights into complex lipid mixtures, it has limitations in clear qualitative and quantitative identification of lipid classes (Deranieh, Joshi, and Greenberg 2013). For a more detailed analysis, mass spectrometry was chosen due to its sensitivity and selectivity (Köfeler et al., 2012). While complete detection and quantification of all individual lipids remain challenging, lipidomic analysis aims to identify and quantify as many individual lipids as possible (Guan and Goldfine, 2021; Köfeler et al., 2012).

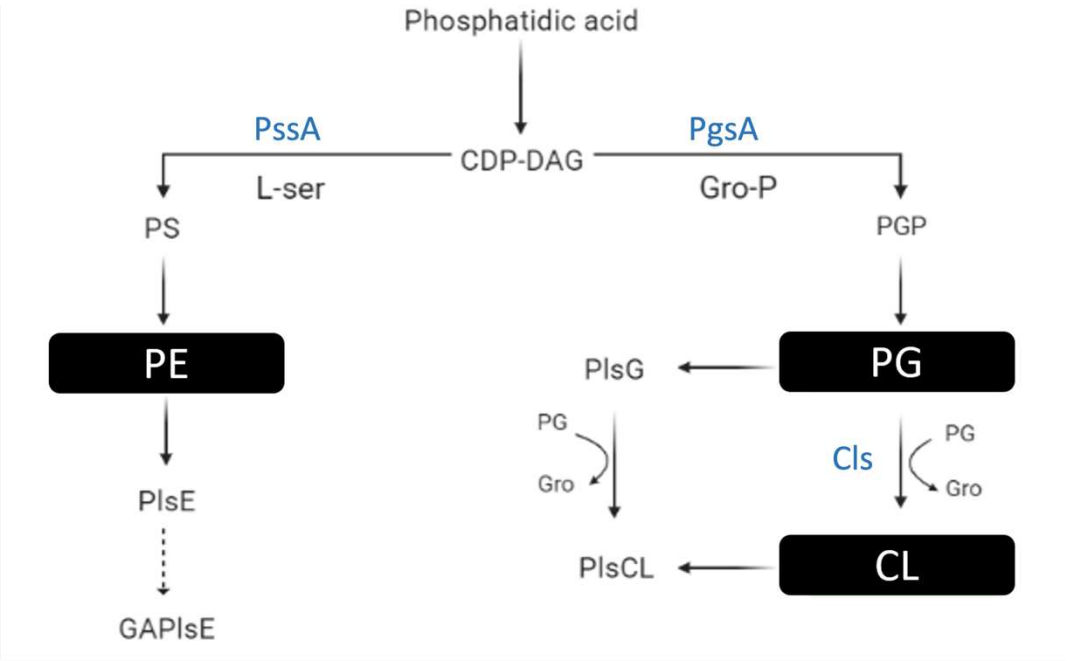

Figure 5.1. Simplified scheme of the phospholipid biosynthesis in *Clostridium*. The enzyme PssA is responsible for the conversion of CDP-DAG in PS, which will lately result in the synthesis of PE. The enzyme PgsA is responsible for the conversion of CDP-DAG in PGP, which will lately result in the synthesis of PG. The condensation of two PG molecules results on the synthesis of CL (Goldfine 2019).

5.1 Thin Layer Chromatography

To analyse the lipidomic profile of *C. saccharoperbutylacetonicum* N 1-4 (HMT) and its mutant strains (Δ*pssA*, *pssA*$^{+}$, *pgsA*$^{+}$, *cls*$^{+}$, *BCL*, and *mt*1^{+}) through TLC, lipids were extracted, quantified, and separated based on head group hydrophobicity on a TLC silica plate. In the first group of experiments, a modified Bligh and Dyer method (Bligh and Dyer, 1959) was utilized for lipid extraction from *BCL* and WT cell pellets, with corresponding lipids analysed in Figure 5.3, via TLC. Subsequent TLC assays employed the MTBE lipid extraction method (Eggers and Schwudke, 2016). One of the biggest differences between these two methods is the separation between the organic and aqueous phases. The MTBE method has the advantage of the lipid-rich organic layer to be above the aqueous phase, whereas the lipid-rich chloroform layer that is below the aqueous phase in the modified Bligh and Dyer method. With the MTBE method, contaminations of the organic sample with the aqueous phase are less common (Eggers and Schwudke 2016). For lipid quantification, the Ammonium Ferrothiocyanate Assay was utilized (Charles and Stewart, 1980), involving the creation of a standard curve with known phospholipid concentrations to estimate lipid content in the mixture, utilizing optical density readings at 488nm.

To establish the standard curves, three different mixtures of phosphatidylethanolamine (PE), phosphatidylglycerol (PG), cardiolipin (CL), and phosphatidylcholine (PC) were tested (Figure 5.2). Standard curve 1 consisted of a mixture with a mass ratio of PE:PC:PG as 2:1:2, standard curve 2 was a mixture of PE:PG:CL with a mass ratio of 2:1:2, and standard curve 3 comprised a molar ratio of PE:PG:CL as 2:1:2. While the standard mixture PE:PC:PG was typically used by the research group, the decision to replace PC with CL was based on published information concerning the main phospholipids in *C. saccharoperbutylacetonicum* N 1-4 (HMT) and their respective ratios (Duerre, 2005; Guan and Goldfine, 2021). Significant differences were observed on quantifying the lipid samples when using the standard curve 1, comparing to the standard curve 2 and 3 (Figure 5.2).

	Mass Ratio		Molar Ratio
	Standard 1 PE:PC:PG	Standard 2 PE:PG:CL	Standard 3 PE:PG:CL
Sample 1 (µg)	29.91	67.17	61.36

Figure 5.2. Representation of the results obtained for the quantification of a lipid mixture using the standard mixtures: (1) PE:PC:PG mass ratio of 1:1:1, (2) PE:PG:CL mass ratio of (2:1:2) and (3) PE:PG:CL molar ratio of 2:1:1, using the colorimetric assay Ferrothiocyanate Assay.

The results depicted in Figure 5.2 indicated variations in the detection using the assay for different phospholipids. However, no significant differences were observed when using the mass and molar ratio PE:PG:CL standard curves. These findings align with the initial challenges encountered during the TLC experiments (data not shown). Loading 20 µg of quantified lipids using standard curve 1 on the TLC silica plate resulted in detectable lipids, whereas loading the "same" amount (20 µg) of quantified lipids from standard curve 2 or 3 only showed a very faint amount of lipids. This discrepancy in detection can be attributed to the different affinity of the technique for various lipids, which is two-fold higher for Std1 compared to Std2/Std3 (Figure 5.2). This assay, commonly used for determining phospholipid concentration, faces limitations including its insensitivity to PG-based phospholipids and other bilayer molecules like cholesterol and its reliance on a calibration curve that demands precise knowledge of the lipid matrix composition (Di Prima, Librizzi, and Carrotta 2020).

The initial TLC assays shown in Figure 5.3 were conducted using lipids quantified based on the standard curve 1 method, where 20 µg of sample was consistently loaded on the TLC silica plate. However, once the issue with varying affinity for different phospholipids was addressed, standard curve 3 method was consistently adopted for quantifying all the extracted lipids from samples collected at 0h, 6h, 24h, and 48h of incubation. In this approach, a higher amount of lipids (between 35 – 40 µg) was spotted on the silica plate. This adjustment significantly improved the reliability of lipid quantification, overcoming the assay varying affinity for different phospholipids.

5.1.1 *BCL* strain lipid analysis by TLC

BCL is a *C. saccharoperbutylacetonicum* N1-4(HMT) mutant strain developed by Biocleave through random mutagenesis, and it shows different membrane morphologies compared to the WT strain (data not shown). Membrane engineering is a complex process and having strains with distinct membrane morphologies provides a valuable platform for investigating the effects of membrane composition and structure.

The analysis of the lipid composition in both the WT and *BCL* cells by TLC was initially performed on overnight grown cells, to test different mobile phases in separating the lipids on the silica plate (stationary phase). Figure 5.3 presents the results obtained from the TLC experiments in overnight grown cells with an OD_{600} between 2-3 and a pH greater than 5. In these experiments, phospholipids such as PE, PG, PS, PC and CL were used as standards.

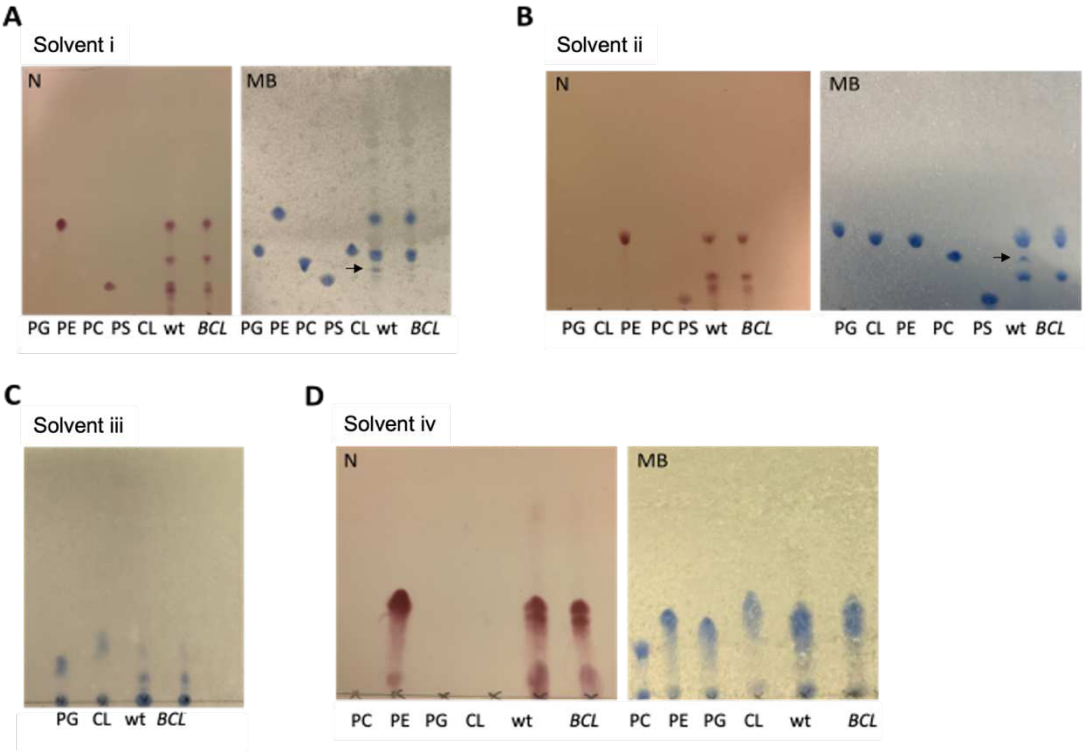

Figure 5.3. Lipid analysis by TLC from WT and *BCL* cells. Employed mobile phases included: (A) solvent i (chloroform: methanol: water 65:25:4); (B) solvent ii (chloroform: methanol: water 65:25:4); (C) solvent iii (toluene: pyridine: water 60:60:10) and (D) solvent iv (chloroform: hexane: methanol: acetic acid 50:30:10:5). The standards used were PC, PE, PG, CL and PS. The samples were stained with molybdenum blue (MB) to detect phospholipids and ninhydrin (N) for detection of amino groups. 20 µg of sample was added to each spot. The arrow indicates the most substantial lipid content discrepancy observed between the two strains.

Analysing the plates stained with molybdenum blue and ninhydrin it was possible to observe a very similar migration pattern between the WT and the mutated strains, for all the selected solvent systems (Figure 5.3). Both strains presumably contain PE within their membrane compositions, as indicated in Figure 5.3A, B and D. In solvents i, ii and iv the migration of PG and CL was very similar preventing the separation and identification of these two lipid classes individually. Solvent iii was selected because is more specific for the separation of these two phospholipids however, in the plate shown in Figure 5.3C, there lipid migration and staining were not very clear.

In the molybdenum blue stained plates represented in Figure 5.3A and B, there was a visible small spot only in the WT with a similar migration as PC. In the plates stained with ninhydrin and molybdenum blue it was possible to see spots with different migrations comparing to the selected standards, which can be indicative of other lipid classes, they can represent plasmalogen and derivatives of different phospholipids, such as PE, PG and CL, that are very common in *Clostridium* strains (Goldfine 2010; Guan and Goldfine, 2021). In Figure 5.3 it was also possible to observe that, for solvents i and ii, in the plates stained with ninhydrin there were more spots than the plates stained with molybdenum blue. These results indicated the presence of lipids that are not phospholipids in both strains. Apart from the spot highlighted in Figure 5.3A and B, that appears only in the WT strain, the TLC experiments shown a similar lipid content between WT and *BCL* strains in an overnight grown culture.

To understand the lipidome of these strains during fermentation, acidogenesis and solventogenesis phase, TLC experiments were done to separate and identify the lipids of cells at 0h, 6h, 24h and 48h of incubation (Figure 5.4). Lipids were extracted using the MTBE method and quantified. Due to the low concentration obtained for almost all the lipid samples, only mobile phase i (chloroform: methanol: water 65:25:4) was used to separate the lipids from the mixture in duplicate, where one plate was stained with molybdenum blue and the other plate with ninhydrin.

In Figure 5.4, it was possible to observe the separation of phospholipids (A) and the lipids containing amino groups (B) from WT and *BCL* cells at difference growth stages. The 0h time point results mirrored those in Figure 5.3. The same spot indicated by the arrow in Figure 5.3 was observable at 0h, which was absent in the mutated strain (Figure 5.4A, spot 3). The intensity of that spot in the WT (Figure 5.4A, spot 3) dramatically reduced at the 6h samples, marking the beginning of the acidogenesis phase, but is noticeable again at 24h. Conversely, in the mutant

strain, a spot with identical migration appears at 6h and 48h samples (Figure 5.4A, spot 3), denoting the beginning of the acidogenesis phase and the solventogenesis phase, respectively. New unidentified spots become visible after 48h of incubation in the mutant strain cells (Figure 5.4A, spot 4).

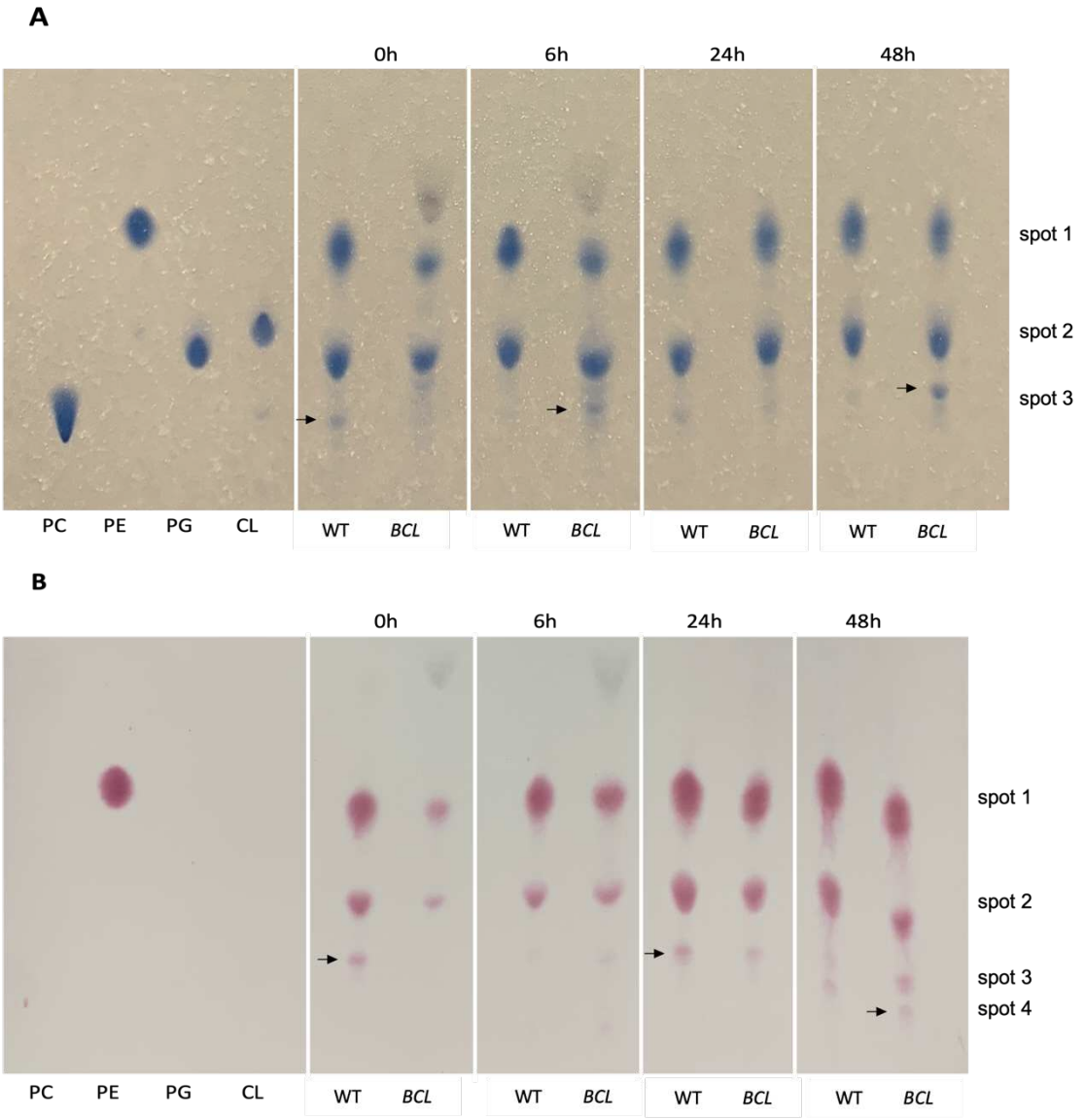

Figure 5.4. Lipid analysis by TLC from WT and *BCL* cells collected at 0h, 6h, 24h and 48h of culture growth. To each spot were loaded 20 μg of the standards PC, PE, PG, CL and PS and 35 μg of sample. Mobile phase was solvent i: Chloroform:Methanol:Water (65:25:4).(A) Phospholipid stained with molybdenum blue.(B) Lipids with amino groups stained with ninhydrin. The arrow represents the biggest difference on the lipid content observed.

In Figure 5.4A spot 2 the spots have a similar migration as the standards PG and CL, indicating the presence of one or both of these phospholipid species in both strains, which is in concordance with the literature (Goldfine 2019; Guan and Goldfine, 2021; Sohlenkamp and Geiger, 2016). However, in Figure 5.4B spot 2 the migration of the lipids, seem to have a very similar migration pattern as the ones shown in Figure 5.4A spot 2. The phospholipids PG and CL do not have on its structure amino groups, as it was possible to see on the plates stained with ninhydrin, the PG and CL standards cannot be stained. This result indicated that additional lipid classes with similar hydrophobicity are part of the lipidome of both strains and are expressed during all the 48h of incubation. According to the TLC plates from Figure 5.4A both WT and *BCL* strains are producing PE, PG and CL throughout the 48h of incubation. Variations on the lipid content between these two strains were observed and those modifications were visible at the different growth stages of the cells.

5.1.2 Δ*pssA* and *pssA*$^{+}$ strains lipid analysis by TLC

PE is one of the main phospholipid classes described in *Clostridium* membrane (Goldfine, 2019; Guan and Goldfine, 2021; Linney et al., 2023). According to the TLC data shown in the previous figures and in comparison, to the PE standards, PE is present in the cells during all periods of growth. Changing its biosynthesis can give have an important influence on the membrane structure, stability and cell function (Linney et al., 2023). The gene *pssA* codes for an enzyme involved in the synthesis of PE (Figure 1.12). Strains with a *pssA* knockout (Δ*pssA*) and overexpressing *pssA* (*pssA*$^{+}$), were generated to test the production of PE and the general lipidome of the cell during cell growth, acids and solvents production.

To understand the lipidome of these mutant strains during fermentation, cells were collected at different time points of fermentation, namely at 0h, 6h, 24h and 48h, following the same procedure described in the previous section. Figure 5.5 displays the migration and identification of phospholipids, while Figure 5.6 illustrates the migration and identification of lipids containing amino groups, from the three strains. In Figure 5.5 the mobile phase movement throughout the TLC plate was not in a straight line, reason why the spots were displayed in a rounded shape in the plate.

Both TLC plates revealed the presence of PE, a phospholipid with an amino group, which becomes evident upon staining with molybdenum blue and ninhydrin (Figure 5.5, Figure 5.6). Interestingly, PE seems to be present in every strain investigated, including the Δ*pssA* strain. At

the 0h, 6h and 24h time points, the intensity of the PE spot seemed stable across all three strains. However, by the 48h mark, the Δ*pssA* strain exhibited a notable decrease in the intensity of the PE spot (spot 1).

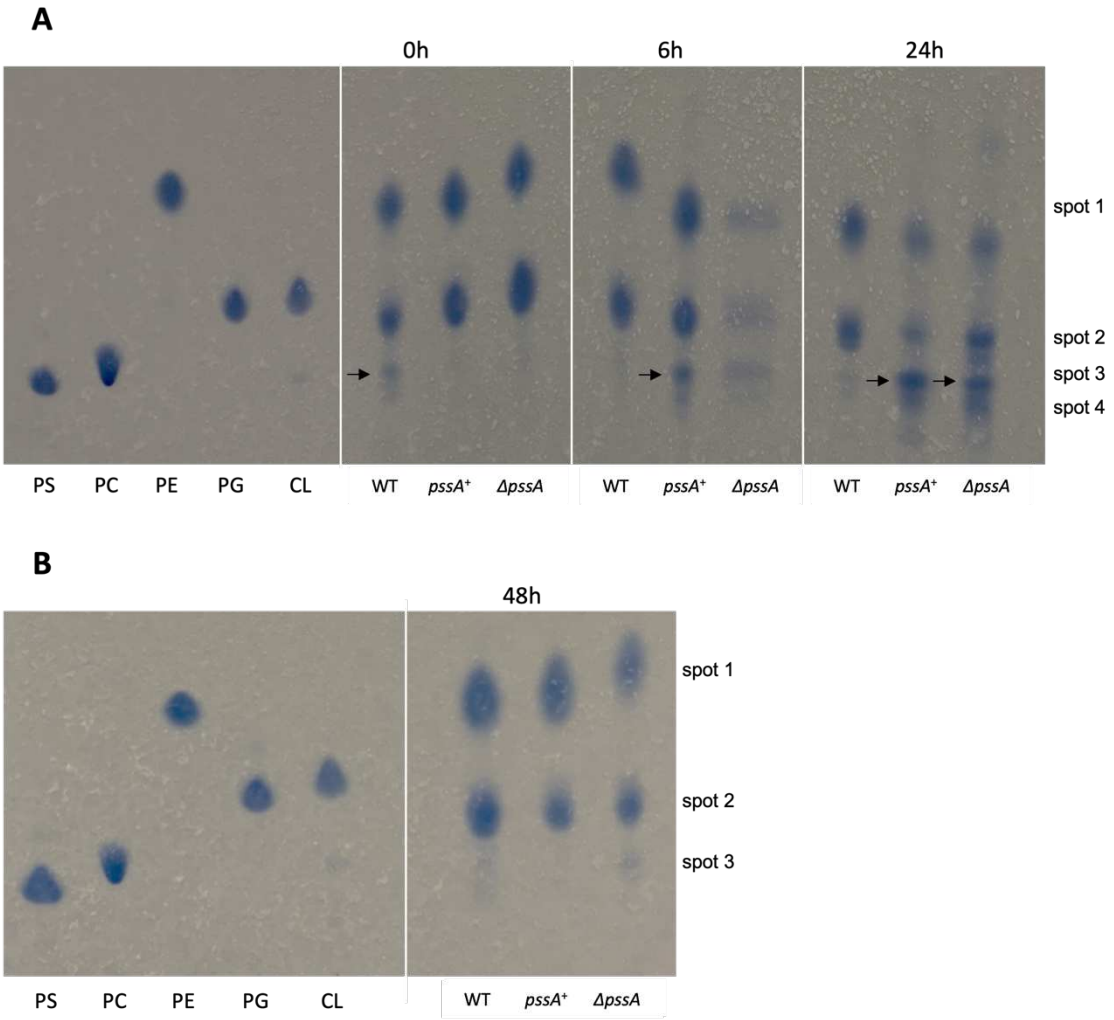

Figure 5.5. Lipid analysis by TLC from WT, Δ*pssA* and *pssA*$^{+}$ cells collected at: (A) 0h, 6h and 24h and; (B) at 48h of culture growth. Phospholipid stained with molybdenum blue. To each spot were loaded 20 μg of the standards PC, PE, PG, CL and PS and 35 μg of sample. Mobile phase was solvent i: Chloroform:Methanol:Water (65:25:4). The arrows represent the biggest difference on the lipid content observed.

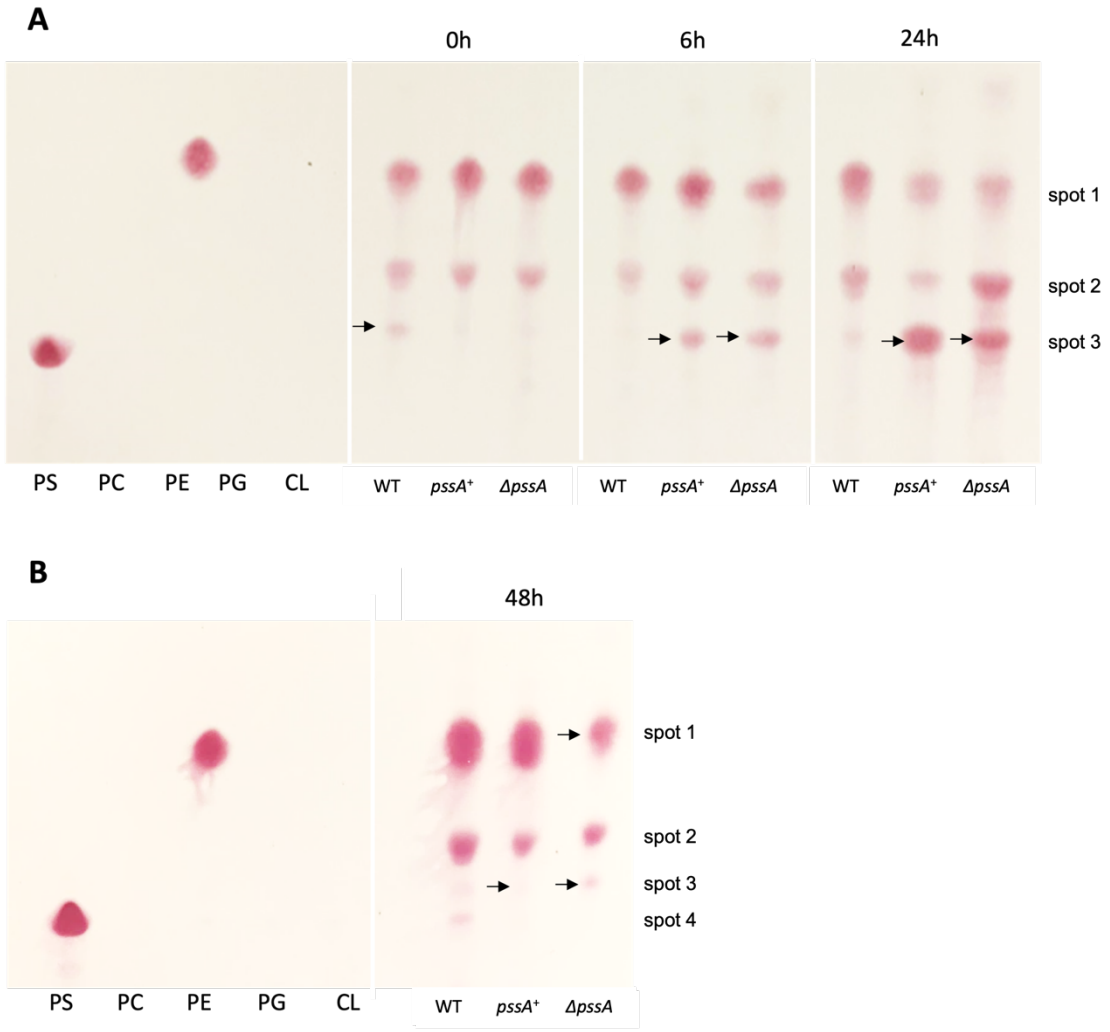

Figure 5.6. Lipid analysis by TLC from WT, Δ*pssA* and *pssA*$^{+}$ collected at: (A) 0h, 6h and 24h and (B) at 48h of culture growth. Staining with ninhydrin to detect the lipids containing amino groups. To each spot were loaded 20 μg of the standards PC, PE, PG, CL and PS and 35 μg of sample. Mobile phase was solvent i: Chloroform:Methanol:Water (65:25:4). The arrow represents the biggest difference on the lipid content observed.

PG and CL can only be identified in Figure 5.5, these two phospholipids have very similar characteristics and head group hydrophobicity, leading to a very similar interaction between the silica plate and the mobile phase, and consequently have a very similar migration, as it was possible to observe. These two lipids were observed in the three strains for all the four time points.

Major differences in the lipids from spots 3 and 4 were noticeable between the strains WT, Δ*pssA*, and *pssA*$^{+}$ in both Figure 5.5 and Figure 5.6. At 0h, WT displayed a small spot (spot 3) with

a migration similar to PS and PC, whereas spots with similar migration were observed in Δ*pssA* and *pssA*$^{+}$, but not in WT, only at 6h and 24h (Figure 5.5 and Figure 5.6,spot 3), and this lipid nearly vanished in all three strains after 48h of culture.

At 48h incubation, variations were detected in the lipidomes of the WT, Δ*pssA*, and *pssA*$^{+}$ strains, with PE spots identified across all strains and times sampled. While PG and CL were noted on the plate stained with molybdenum blue, the plate stained with ninhydrin suggested that other, unidentified lipids might exhibit similar migration to PG and CL. Spots analogous in migration to PC and PS were presumed to be PS, considering there is no recorded PC in *Clostridium* (Guan and Goldfine, 2021). They displayed various alterations potentially impacting PE synthesis due to PS acting as a metabolic pathway intermediate and the *pssA* gene encoding an enzyme crucial for PS synthesis. Notably, spot 3 (Figure 5.5 and Figure 5.6) exhibited variations across the culture timeline and between strains, showing increased intensities in the mutant strains at 6h and 24h compared to the WT.

5.1.3 *pgsA*$^{+}$ and *cls*$^{+}$ strains lipid analysis by TLC

The same TLC procedure was carried out for strains overexpressing *pgsA* (*pgsA*$^{+}$) and overexpressing *cls* (*cls*$^{+}$) that are involved in the synthesis of PG and CL, respectively (Sohlenkamp and Geiger, 2015). The analysis of lipids from WT, *cls*$^{+}$ and *pgsA*$^{+}$ at 0h, 6h, 24h, and 48h followed the identical procedure for TLC analysis outlined in previous sections, involving extraction, quantification, separation and staining of the lipids.

According to Figure 5.7, the three strains produced PE during all the culture growth. In Figure 5.7A it was possible to observe the presence of spots identified as PG/CL in all the strains, also during the 48h of culture growth (spot 2).

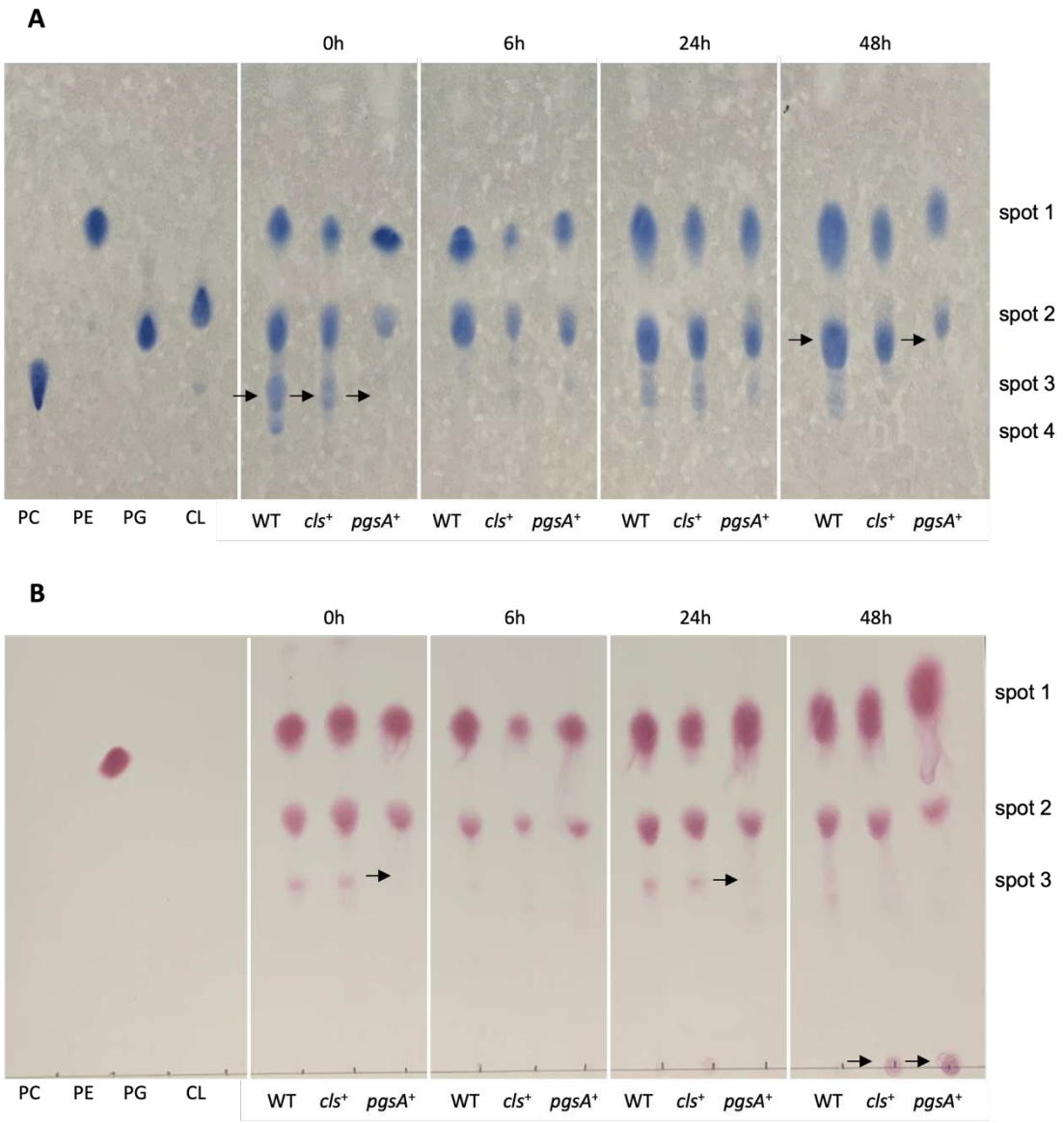

Figure 5.7. Lipid analysis by TLC from WT, *pgsA*$^+$ and *cls*$^+$ cells collected at 0h, 6h, 24h and 48h of culture growth. (A) shows the phospholipid staining with molybdenum blue. (B) shows the lipids with amino groups staining with ninhydrin. To each spot were loaded 20 μg of the standards PC, PE, PG, CL and PS and 35 μg of sample. Mobile phase was solvent i: Chloroform:Methanol:Water (65:25:4). The arrows represent the biggest difference on the lipid content observed.

Differences in the lipid composition between strains were observed, as highlighted by the arrows in Figure 5.7. At the initial time point (0h), certain lipids were exclusively detected in the WT and *cls*$^+$ strains (Figure 5.7A and B, spot 3). At the 48h incubation mark, a substantial diminution in spot intensity between WT and *pgsA*$^+$ strains was observed in the plate stained with molybdenum blue (Figure 5.7A, spot 2). Moreover, in the samples from the 48h timeframe,

a pink spot emerged at the point where the lipid mixture was spotted in both mutated strains, without moving with the mobile phase, corresponding to more unknown lipids present in the mutant cells (Figure 5.7B).

In summary, strains engineered for enhanced CL expression (*cls*$^+$) did not exhibit discernible differences in the lipid synthesis when compared to the WT. Nonetheless, for the *pgsA*$^+$ strain, notable variations in lipid composition were observed throughout the 48h incubation, particularly in lipid samples from the 0h, 24h, and 48h time points.

5.1.4 *mt*1$^+$ lipid analysis by TLC

With the intention of studying any possible correlation with the heterologous expression of a ROS scavenger with the lipid content in *C. saccharoperbutylacetonicum* N 1-4 (HMT) the same TLC procedure as previously shown was carried out for *mt*1$^+$. The lipid content of *mt*1$^+$ strain at 0h, 6h, 24h and 48h is shown in Figure 5.8, in comparison to the WT.

In Figure 5.8A and B, showing the plates stained with molybdenum blue and ninhydrin respectively, spots indicative of a similar migration pattern to PE were noticeable across both strains. Spots aligning with both PG and CL standards were also apparent for each strain throughout the culture development. At the 0h mark, an intense spot is discernible only in the *mt*1$^+$ strain (Figure 5.8A and B, spot 3). Following 6h and 24h of incubation, lipids mirroring the migration of the previously described spot were evident in the WT strain but absent in the *mt*1$^+$ strain. For samples collected at 48h, this same spot was clear in the WT strain in both plates (Figure 5.8A and B, spot 3). While this spot was visible on both plates, a spot with matching migration (spot 3) was noted on the *mt*1$^+$ plate, altough with substantially fainter intensity compared to the WT.

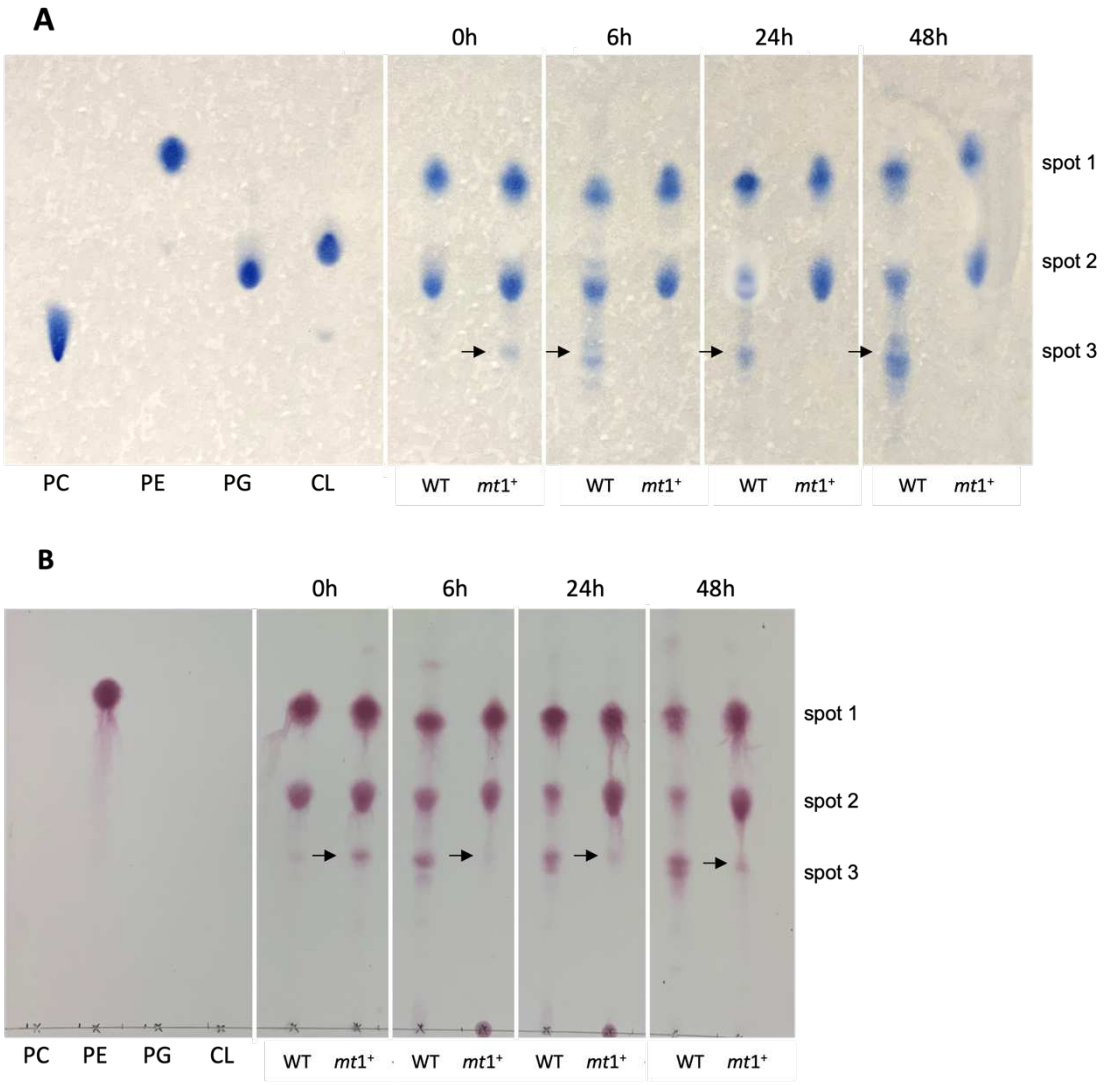

Figure 5.8. Lipid analysis by TLC from WT and *mt*1^{+} cells collected at 0h, 6h, 24h and 48h of culture growth. (A) shows the phospholipid staining with molybdenum blue. (B) shows the amino group lipids staining with ninhydrin. To each spot were loaded 20 μg of the standards PC, PE, PG, CL and PS and 35 μg of sample. Mobile phase was solvent i: Chloroform:Methanol:Water (65:25:4). The arrows represent the biggest difference on the lipid content observed.

Cloning *C. saccharoperbutylacetonicum* N 1-4 (HMT) with a vector expressing an antioxidant enzyme led to changes in the lipidome. In the WT strain, lipidome alterations were primarily observed at 6h, 24h, and 48h, time intervals that signify the acidogenesis phase, the transition to the solventogenesis phase, and the accumulation of solvents, respectively. These alterations, highlight the lipids from spot 3, were not observed in *mt*1^{+} strain cells, rendering the characterisation of acid and solvent production by these strains a point of intrigue.

TLC summary

TLC provided an accessible means for conducting a preliminary analysis and comparison of the lipidomes of WT and mutant strains due to its cost-effectiveness and capacity to simultaneously separate and visualize various lipids within a mixture. It was possible to observe that all the mutant strains and the WT appeared to have PE, PG and CL, including the Δ*pssA* strain. There were other spots visible unidentified due to lack of standards, and it was also possible to observe that the lipidome of *C. saccharoperbutylacetonicum* N 1-4 (HMT) was not just phospholipids. In general, considering the lipids observed during cell culture and making a comparative analysis with the WT:

- Observations at both 6h and 48h showed an increased number of spots in the *BCL* strain.
- Differences were noted at 6h and 24h in the lipid spots from both Δ*pssA* and *pssA*$^{+}$ strains, where more spots were observed.
- Regarding the pgsA^{+} and *cls*$^{+}$ strains, the pattern was very similar to the WT. Only a few differences were observed for the *pgsA*$^{+}$ strain.
- During all observed timeframes (0h, 6h, 24h, and 48h), the *mt*1^{+} strain exhibited variations, with fewer or less intense spots observed.

Throughout the entire culture growth, variations in the lipid spots were perceptible, potentially signifying variances in lipid production by the different strains and possibly indicative of adaptations to varied cellular environments. However, some aspects are relevant to highlight relatively to these experiments. Notably, the WT spots observed at 0h, 6h, 24h, and 48h did not exhibit identical patterns across different TLC plates. For instance, WT samples collected at 0h yielded three spots in Figure 5.3, Figure 5.4 and Figure 5.5, four visible spots in Figure 5.7A, and two in Figure 5.8A. At 6h, WT samples presented two visible spots in all TLC silica plates, except in Figure 5.8B, where five spots were identified but, three of which shown higher intensity. WT samples from 24h exhibited three visible spots on TLC plates in all figures, although with fluctuating intensities. Meanwhile, the 48h WT samples revealed three visible spots in every figure, although the signal of the final was notably weaker and demonstrated more variability among strains. It Is important to acknowledge that although the culture growth assay initiated by transferring overnight cultures to new culture media—marked as the 0h time point and signifying the commencement of the bottle screening—this time point might correspond to cells within a window of growth stage, that can correspond variations in the membrane lipidome. As the culture growth proceeded, the WT lipidome pattern tended to homogenize across all plates.

Nevertheless, achieving consistent results can be challenging due to potential variations in factors such as plate preparation, sample preparation and application and, chromatogram development conditions (Tuzimski and Sherma, 2016).

To complement the information given by the TLC experiments, the lipidome of these strains underwent more detailed characterisation via mass spectrometry. Samples collected at 24h of culture from the strains discussed in this section were analysed by targeted mass spectrometry, the details of which are shown in the next section.

5.2 Mass Spectrometry

In the previous section, differences in the lipid content were observed by TLC between WT and mutant strains, throughout the 48h of cell culture. Acknowledging the limitations of TLC and its provision of fundamental insights (Cheng, Huang, and Shiea 2011), a more comprehensive investigation on the lipid composition was undertaken. The extreme diversity of the lipid species in most biological samples is a challenge to uncover using techniques such as TLC. In TLC the lipids were separated based on the head group polarity, using standards of the main lipid classes it was possible to infer the presence of lipids such as PE, PG, CL and PS, and it was possible to observe the presence of other lipids species unknown due to the lack of standards. However, it was not possible to observe variations in the lipid species, such as the plasmalogen forms of PE (PE-O) or phosphatidyl-N-monomethylethanolamine (PMME). It was also not possible to characterise the FA chains between strains, its length, and the number of unsaturations. It was not possible to identify glycolipids. All these aspects are important to characterise the lipidome of *Clostridium*, its lipid classes, together with their variations in structure are an important key to understand the response of the bacteria to different stress conditions during fermentation (Evans et al., 1998; Guan and Goldfine, 2021; Liao et al., 2015; Tian et al., 2013).

Mass spectrometry has greatly enhanced our understanding of the biological activities of individual lipids, lipid classes and lipid subclasses (Hines and Xu, 2019; Köfeler et al., 2012). A detailed characterisation on the lipidome of *C. sacharoperbutyacetonicum* N 1-4 HMT will provide an important understanding on the adjustment of the plasma membrane throughout the organic acids and solvents production. This information will be also important to characterise the mutant strains lipidome and try to correlate it with their potential application as cell factories.

To complement the results obtained with TLC, where differences in the lipidome between strains were obvious, the samples were subjected to detailed mass spectrometry analysis conducted by Creative Proteomics. This analysis was performed in samples from four biological replicate cultures with 24h of growth in TYIR media with 50 $g.L^{-1}$ of glucose and 30 mM MES, at 32°C in anaerobic conditions from the WT strain and the mutant strains Δ*pssA*, *pssA*$^{+}$, *pgsA*$^{+}$, *cls*$^{+}$, *BCL*, and *mt*1^{+} . Ideally, the lipidome of these strains would be characterized at different growth stages but, as a first approach the 24h cultures were selected considering that at this stage of growth, there is a transition from the acidogenesis to the solventogenic phases, this

means that the acids produced in the first stage (acidogenesis) are being converted into solvents (butanol, acetone), so there is an accumulation of both inside the cell and its surroundings.

The targeted mass spectrometry analysis focused on the identification of phospholipids, cardiolipins, glycosyldiacylglycerols and sphingolipids. The phospholipids identified were phosphatidic acid (PA), that is the precursor for the other phospholipids such as: phosphatidylglycerol (PG); cardiolipin (CL); phosphatidylserine (PS); phosphatidylethanolamine (PE); phosphatidylcholine (PC) and phosphatidylinositol (PI). Some lysophospholipids, which only contain one FA chain, were also analyzed in this study, namely lysophosphatidylglycerol (LPG); lysophosphatidylethanolamine (LPE) and lysophosphatidylcholine (LPC). Variations of PE and PC were also targeted for identification and quantification, including plasmalogen forms of PE and PC (PE -O, PC -O) phosphatidyl monomethylethanolamine (PMME) and lyso phosphatidyl monomethylethanolamine (LPMME). Some sphingolipids were tested in this analysis, such as sphingomyelin (SM), dihydro sphingomyelin (DSM) and ceramide phosphatidylethanolamine (PE – Cer). The last group of lipids targeted in this study were the glycolipids digalactolysdiacylglycerol (DGDG). The detailed list of lipid species targeted in this study is described in Figure 5.9. Among the selected lipids for the targeted lipidomics, only some of them were identified, corresponding to PG, LPE, PE, PE-Cer, PA, PS, DGDG, PMME and LPMME. These identifications matched with the lipid groups described as the most abundant in the Clostridia genus (Duerre, 2005; Guan and Goldfine, 2021; Kolek et al., 2015).

The PE-Cer is a ceramide phospharylethanolamine corresponding to a sphingolipid analogue of PE and it was the only sphingolipid identified in this analysis. Very low concentrations of it were found within the strains, because of that its analysis was excluded from the lipid group comparisons, being analysed only individually and in comparison, between strains in an univariant analysis.

The results from cardiolipins were not described in this result section due to problems with the equipment needed for their analysis at Creative Proteomics. Nonetheless cardiolipins are described as one of the main lipids in within Clostridia genus, specifically the group that encompasses *C. saccharoperbutylacetonicum* (Guan and Goldfine, 2021), their identification and quantification will add an important input for this study.

Abbreviations	Common name
LPG	Lysophosphatidylglycerol
PG	Phosphatidylglycerol
LPE	Lysophosphatidylethanolamine
PE	Phosphatidylethanolamine
ePE	Ether-linked phosphatidylethanolamine
PE-cer	Ceramide phospharylethanolamine (sphingolipid analog of PE)
lysoPC	Lysophosphatidylcholine
PC	Phosphatidylcholine
ePC	Ether-linked phosphatidylcholine
SM	Sphingomyelin
DSM	Dihydro sphingomyelin
PA	Phosphatidic acid
PI	Phosphatidylinositol
PS	Phosphatidylserine
DihexDAG	Glycosyldiacylglycerol
PMME	Phosphatidyl monomethylethanolamine
LPMME	Lysophosphatidyl monomethylethanolamine

Figure 5.9. List of targeted lipids for the mass spectrometry analysis by Creative Proteomics. The lipid classes identified from *C. sacharoperbutyacetonicum* N 1-4 HMT samples, including the WT and mutant strains, are highlighted in grey.

The mass spectrometry analysis yielded a comprehensive dataset of approximately 800 to 1000 individual lipid species in total. These lipid species were quantified in nanomoles (nmol) of lipid per 10^6 cells and for further comparisons the concentrations were normalized as a percentage based on the total lipids identified in each sample. To better comprehend the data, the first analysis was on the overall lipid profiles identified across all strains, encompassing both the WT and mutant strains (Figure 5.10). Subsequent analyses focused on comparing lipid classes between strains. The comparative analysis extended to the fatty acids (FA) chain lengths and unsaturation levels between the WT and mutant strains. This aimed to verify whether mutant strains exhibited divergent chain lengths and unsaturation profiles in their composition. These factors are known to impact the membrane structure, fluidity, and stability, variations on the aspects between strains (Evans et al., 1998; Guan and Goldfine, 2021; Tian et al., 2013).

The results were divided in four sections, similarly to the TLC results, the first section was the data analysis between the WT and the mutants Δ*pssA* and *pssA*$^+$; second section was the analysis of the WT and the mutants *pgsA*$^+$ and *cls*$^+$*;* the third section was the analysis of the WT and the mutant *mt*1$^+$ and; the fourth section was the analysis of the WT and the mutant *BCL*.

For each section the total lipids were determined and compared between strains and differences on the lipid production were characterized by univariant analysis. The FA chain profiles identified and quantified for all the strains were analyzed, including, the presence of plasmalogens, the FA chain length and the unsaturation levels.

5.2.1 Mass Spectrometry data analysis in Δ*pssA*, *pssA*$^{+}$ strains

The *pssA* gene is involved in the synthesis of PE in *Clostridium* (Figure 5.1) (Guan and Goldfine, 2021). Silencing this gene or overexpressing it from *C. saccharoperbutylacetonicum* N1-4 HMT was shown, in the TLC results section, to cause a change in phenotype in terms of lipid composition by these strains when compared to the WT and between these two mutants (Figure 5.5). A detailed lipidomic characterisation by mass spectrometry resulted in the identification and quantification of lipids from 9 different lipid groups, including PA, PG, LPE, PE, LPMME, PMME, PS, Cer-PE, PMME-Cer and DihexDAG.

Lipid group analysis

The production of these lipid groups varied between the three strains and their relative abundance in the cells is shown in Figure 5.10. On average a total of 5.70, 6.01 and 6.25 nmol of lipid per 10^6 cells were identified in the WT, Δ*pssA* and *pssA*$^{+}$ strains, respectively. According to Figure 5.10, LPE, PE and LPMME were the main group of lipids produced by the three strains, corresponding to around 80-90% of all the lipids identified in this analysis. It was seen that the Δ*pssA* strain produced PE (9.76%), in lower amounts than the *pssA*$^{+}$ strain (21.44%) and the WT (14.58%). The other lipid groups, such as, PMME, PA, PG, PS and DihexDAG were identified in lower percentages.

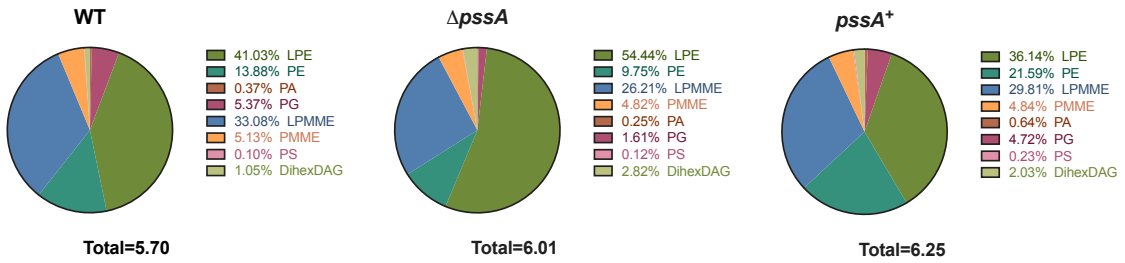

Figure 5.10. Overall lipid distribution in the WT, Δ*pssA* and *pssA*$^{+}$ strains. The charts depict the relative abundance of the lipid classes identified by mass spectrometry. Different colours distinguish different lipid classes. Data corresponds to the average of four biological replicates for each strain, expressed in percentage and the total lipids in nmol of lipid per 10^6 cells.

To better comprehend these differences observed in the lipid profiles between strains, the median of the standardized lipid percentage and the 95% confidence interval (median, 95% CI) was plotted for each lipid group (Figure 5.11) and the differences between strains were analyzed for its significance by performing a non-parametric test, Kruskall-Wallis. Significant differences found on the lipid groups were then analyzed in more detail by univariant analysis.

Figure 5.11 presents the comprehensive results for the total LPE, PE, LPMME, PMME, PG, DihexDAG, PA and PS content obtained from the three strains. Among these, the lysolipids LPE and LPMME were the main lipids identified across all strains, while PA and PS were found in lower concentrations in all strains. Significant differences were observed for the lipid classes LPE, PE, LPMME, PG, PA and PS identified between the strains (Figure 5.11).

For LPE (Figure 5.11A) significant differences were noted between the Δ*pssA* and WT and between the Δ*pssA* and *pssA*$^{+}$ strains, with a p=0.0262 and p=0.0009, respectively. The Δ*pssA* strain produced more LPE than the *pssA*$^{+}$ and WT strains, corresponding to medians of 53.38 % (95% CI, 53.77-55.21), 36.14 % (95% CI, 36.03 - 36.24) and 41.22 % (95% CI, 33.24 – 48.42), respectively.

For PE, the pattern was the opposite, the *pssA*$^{+}$ produced significantly more PE than the WT and Δ*pssA* strains, with p= 0.0083 and p=0.0001, respectively (Figure 5.11A). The median percentage of PE found in the *pssA*$^{+}$, WT and Δ*pssA* strains was 21.94 % (95% CI, 20.38 – 22.11), 13.29 % (95% CI, 11.27 – 17.67) and 9.74 % (95% CI, 8.58 – 10.93), respectively. The *pssA*$^{+}$ strain produced in median more than the double of PE than the Δ*pssA*.

For LPMME, significative differences were found between the WT and Δ*pssA* strains, with *p*= 0.0074 (Figure 5.11A). The median percentage of LPMME found in the WT and Δ*pssA* strains was 32.36 % (95% CI, 31.26 – 36.34) and 26.06 % (95% CI, 23.66 – 29.06).

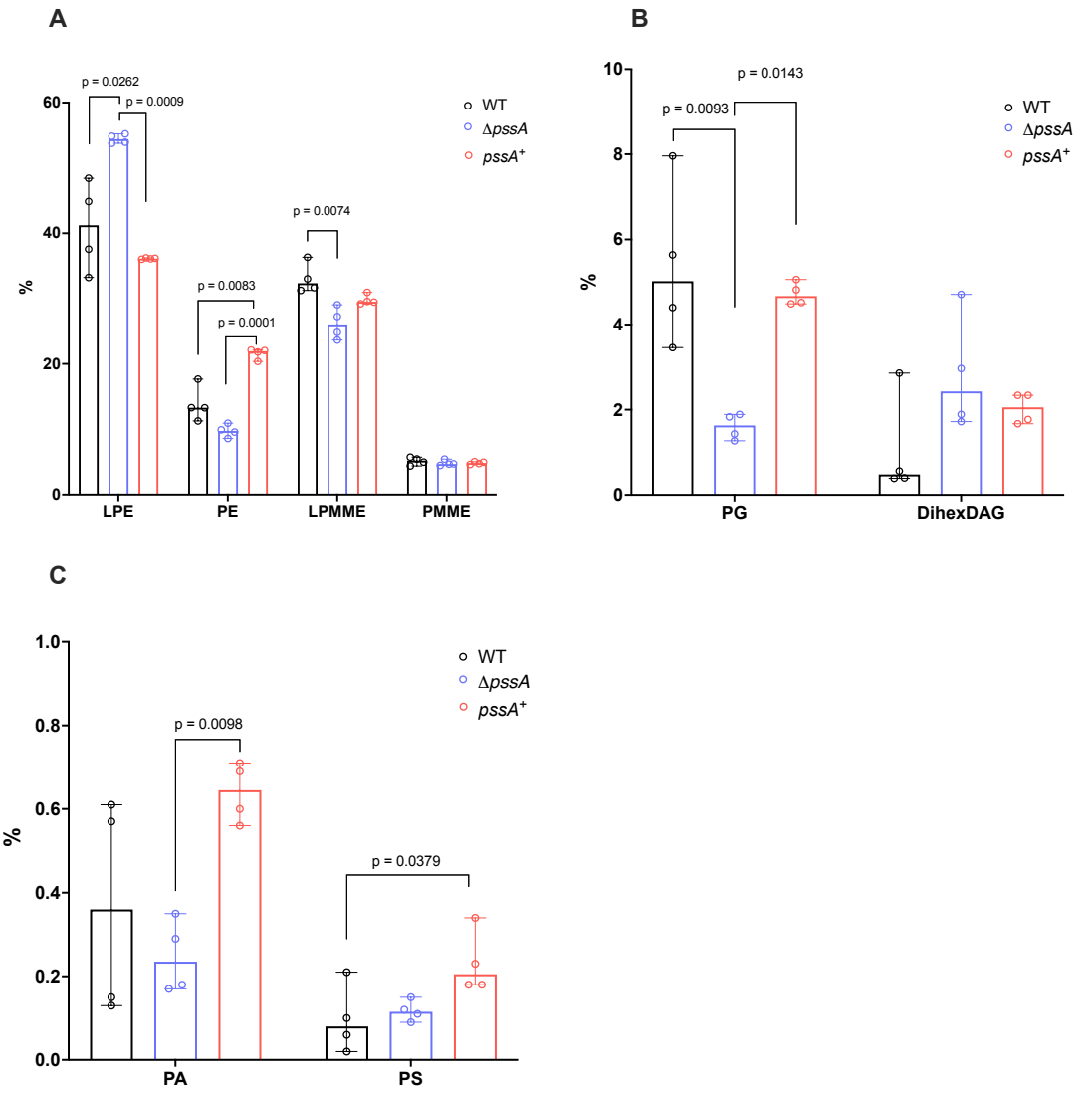

Figure 5.11. Lipid classes distribution in the WT, Δ*pssA* and *pssA*$^+$ strains. Bar charts showing the median and 95% CI of: (A) LPE, PE, LPMME and PMME; (B) PG and DihexDAG; (C) PA and PS. Results were normalised to the total lipids identified in each sample. Samples from four independent biological replicates (*n*=4). Statistical test: non-parametric Kruskall-Wallis and uncorrected Dunn's test for multiple comparisons.

The results obtained for PG (Figure 5.11B) were determined to be statistically significant between WT and Δ*pssA* strains (p= 0.0093) and between *pssA*$^+$ and Δ*pssA* strains (p= 0.0143).

The Δ*pssA* strain produced significantly less PG than the WT with a median of 1.63 % (95% CI, 1.27 – 1.89) and 5.02 % (95% CI, 3.46 – 7.96), respectively. Significantly less PG was also observed for Δ*pssA* strain when comparing to the *pssA*$^{+}$ strain, with a median of 4.67 % (95% CI, 1.27 – 1.89) obtained for the *pssA*$^{+}$ strain. The Δ*pssA* strain contained less than twice the percentage of PG when compared to the WT and *pssA*$^{+}$ strains.

In the case of PA (Figure 5.11B), very low concentrations were quantified among the strains, however, significant more PA was found in the *pssA*$^{+}$ strain, compared to the Δ*pssA*, with p=0.0098. The *pssA*$^{+}$ strain produced 2-fold more PA compared to the Δ*pssA* strain, corresponding to a median of 0.65% (95% CI, 0.56 - 0.71) and 0.24 % (95% CI, 0.17 - 0.35), respectively. In the case of PS (Figure 5.11B), significant more PS was found in the *pssA*$^{+}$ strain, compared to the WT, with p = 0.0379. The percentage of PS in the *pssA*$^{+}$ and WT strains was in median 0.20% (95% CI, 0.18-0.34) and 0.08% (95% CI, 0.002 - 0.210), respectively.

Considering the significant differences observed in the phospholipid classes between strains, the individual LPE, PE, LPMME, PG, PA and PS were characterised in more detail. All the lipid molecules from each class underwent univariate analysis. The forest plots in Figure 5.12 illustrate the fold change in percentage of PE and PG identified between two groups of strains. The forest plots for the LPE, LPMME, PA and PS are shown in Annex 2.

Figure 5.12A shows the fold-change of various PE molecules quantified in the WT and Δ*pssA* strains. More abundant lipids in the Δ*pssA* strain are positioned to the right of the x-axis, while those that are more abundant in the WT strain are located to the left. Lipids situated closer to the central zero point indicate minor changes, whereas those moving away from zero, in either direction, signify more substantial alterations. Results with a $p < 0.05$ are highlighted in black.

The mass spectrometry analysis different PE molecules were identified and quantified, encompassing a range of FA chain lengths from 21 to 38 carbons, different levels of unsaturation, and including a plasmalogen form of PE (PE-O), in both the Δ*pssA* and WT strains (Figure 5.12A) and between the *pssA*$^{+}$ and WT strains (Figure 5.12B). The comparison between the Δ*pssA* and WT strains resulted in 7 PE molecules with significantly higher concentrations in the Δ*pssA* strain ($p < 0.05$). These significant lipids included PE with mid-size and longer FA chains such as: PE (26:1), PE (26:0), PE (28:1), PE (28:0), PE (31:1), PE (37:2) and PE (38:2) (Figure 5.12A). The lipid annotation is stated by the lipid class shorthand abbreviation, the number of carbon atoms:number of double bond equivalents, separate by pair of parentheses.

In the same analysis, 4 PE molecules were found with significantly higher concentrations in the WT strain ($p < 0.05$). These significant lipids included: PE (32:0), PE (34:0), PE (35:1), and PE (Figure 5.12A).

The comparison between the *pssA*$^+$ and WT strains resulted in 5 PE molecules with significantly higher percentage in the *pssA*$^+$ strain ($p < 0.05$, Annex 4). These significant lipids included PE with mid-size and longer FA chains such as: PE (29:0), PE (30:0), PE (31:0), PE (33:0) and PE. No PE lipid molecules were found to have significantly higher percentages in the WT (Figure 5.12B).

For PG phospholipid class, significant differences were found between the Δ*pssA* and WT strains and between the *pssA*$^+$ and Δ*pssA* (Figure 5.12C, D). Within this phospholipid class, 33 different structures were compared, with FA chain lengths ranging from 28 to 38 carbons and different unsaturation level and including a plasmalogen form of PG (PG (32:0-O)) (Figure 5.12C, D). The univariate analysis, as depicted in Figure 5.12C compares the PG molecules between the Δ*pssA* and WT strains. This analysis revealed 4 PG molecules in significantly higher percentage in the WT strain ($p < 0.05$, Annex 3). These lipids corresponded to PG(30:0), PG(32:0), PG(33:1) and PG(35:1). No PG lipid molecules were found to have significantly higher percentages in the Δ*pssA* (Figure 5.12C).

The univariate analysis of LPE between the Δ*pssA* and WT strains identified 6 LPE molecules with statistically higher percentages in the Δ*pssA* strain (Annex 2). The univariate analysis of LPE between the Δ*pssA* and *pssA*$^+$ strains identified 9 LPE molecules with statistically higher percentages in the *pssA*$^+$ strain and only 2 LPE molecules with statistically higher percentages in the Δ*pssA* strain (Annex 2). Relatively to the LPMME, 2 LPMME molecules were found with statistically higher percentages in the WT and 3 LPMME molecules were found with statistically higher percentages in the Δ*pssA* (Annex 2).

The univariate analysis comparing PA and PS between the Δ*pssA* and *pssA*$^+$ strains, as well as between *pssA*$^+$ and WT strains, revealed only 3 lipid species: PA(38:0) and PS(32:0) and PS(30:0), with significantly higher percentages in the *pssA*$^+$ strain. Conversely, only PA(30:0) and PA(32:0) exhibited statistically significant high levels in the Δ*pssA* strain (Annex 3). The forest plots highlighted the substantial discrepancies between pairs of strains, concentrating on the lipid groups where significant distinctions were noted, including PE, PG, LPE, LPMME, PA, and PS.

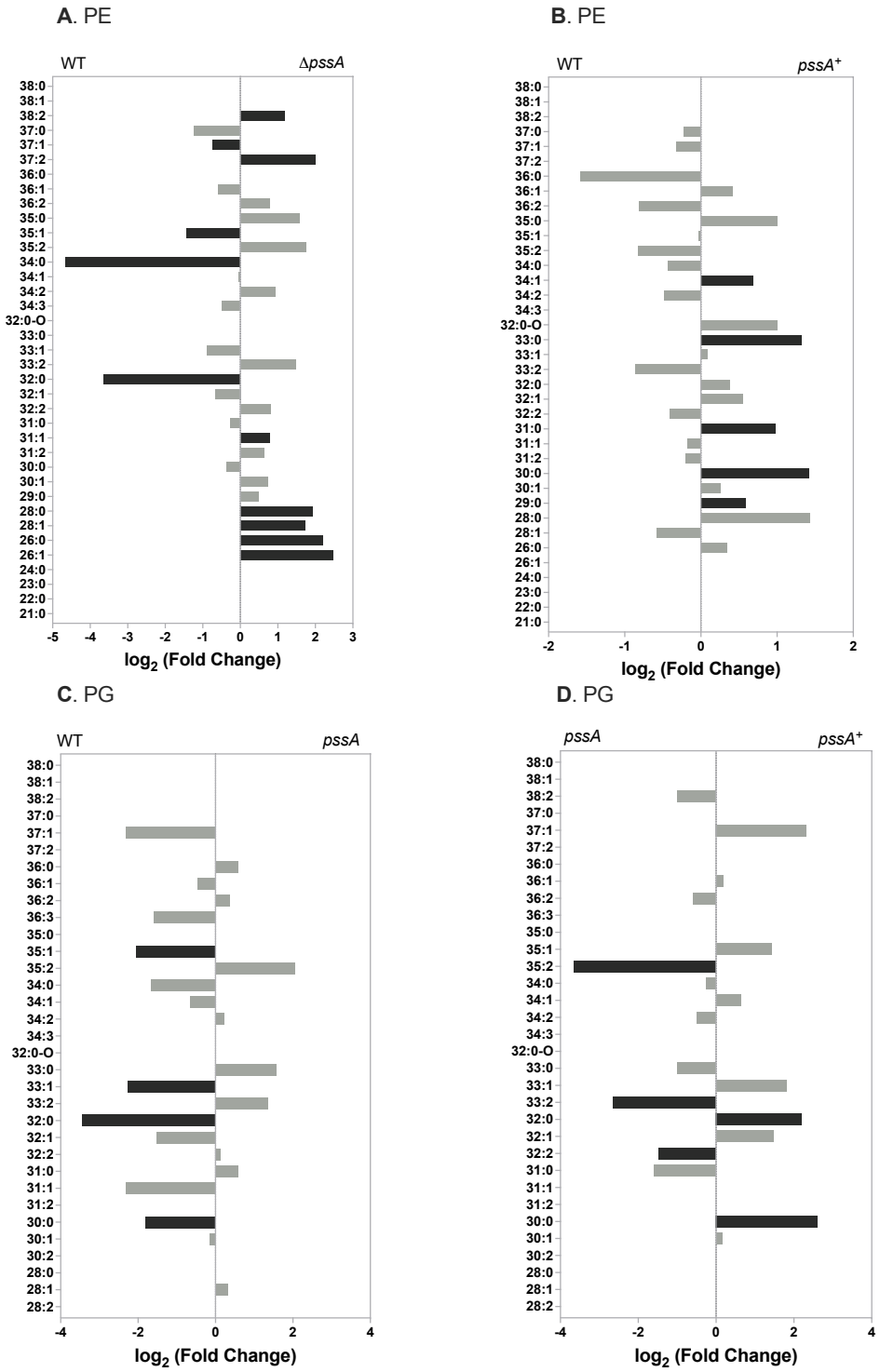

Figure 5.12. Univariant analysis of the PE and PG between the WT, Δ*pssA* and *pssA*$^+$ strains. Comparison of the phospholipid classes: (A) PE, between WT and Δ*pssA* strains; (B) PE, between WT and *pssA*$^+$ strains; (C) PG, between WT and Δ*pssA* strains and (D) PG, between *pssA*$^+$ and Δ*pssA* strains. The x-axis corresponds to the $\log_2$ (fold-change) between a group of 2 strains. Significant results ($p < 0.05$, uncorrected Dunn's test) are highlighted in black. Results from four independent biological repeats (n=4).

To a deeper understanding of the significant shifts within the three strains in the context of individual lipids, a graphical representation known as a "volcano plot," which displays all the individual lipids, was employed (Figure 5.13). This scatter plot is a univariate analysis showing significant changes between two groups. It demonstrates how the *p-values* relate to the fold-change observed among the identified lipids across the four biological replicates of the mutants and WT strains. In this analysis, the log_2 values of the fold changes between the two groups were plotted on the x-axis, while the negative logarithm (base 10) of the p-value results were plotted on the y-axis (Figure 5.13). Lipids with notable and statistically significant differences in production are positioned above the horizontal threshold lines of *p-values* less than 0.01 (orange dots) and 0.05 (blue dots). Lipids positioned closer to the zero point in the x-axis indicate minor changes in expression, whereas those farther away from zero in either direction indicate more significant changes.

The volcano plot from Figure 5.13A shows the significance level ($p < 0.05$) based on the p-value and the fold-change between the *pssA*$^+$ and WT strains. In this graph, statistically different lipids with a fold-change higher than 2.5 between strains were highlighted. This analysis has shown that PS (30:0) and DihexDAG (31:2) production was significantly higher in the *pssA*$^+$ strain. Although with lower fold-changes, lipid molecules from phospholipid groups of PS, PE, PA, PMME, LPE, LPMME and DihexDAG were found with high statistical relevance, being mostly from the PMME and PE phospholipid classes and having increased amounts in the *pssA*$^+$ strain, as comparing to the WT (Annex 4).

Figure 5.13B shows the lipid comparison between the Δ*pssA* and WT strains. The univariate analysis shown 3 statistically relevant lipid species with a fold-change higher than 2.5 in the Δ*pssA*, corresponding to LPMME (21:0), LPE (21:0) and PA (32:2). Conversely, 4 lipid species were significantly increased in the WT strain, having fold changes greater than 2.5 and corresponding to PMME(34:0), PG(32:0), PE (32:0) and PE (34:0). Although with lower fold-changes, lipid molecules from phospholipid groups of PS, PMME, PG, PE, PA, LPMME, LPE and DihexDAG were found with high statistical relevance, being most from the PMME and PE phospholipid classes and having similar distribution between the Δ*pssA* and WT strains (Annex 4).

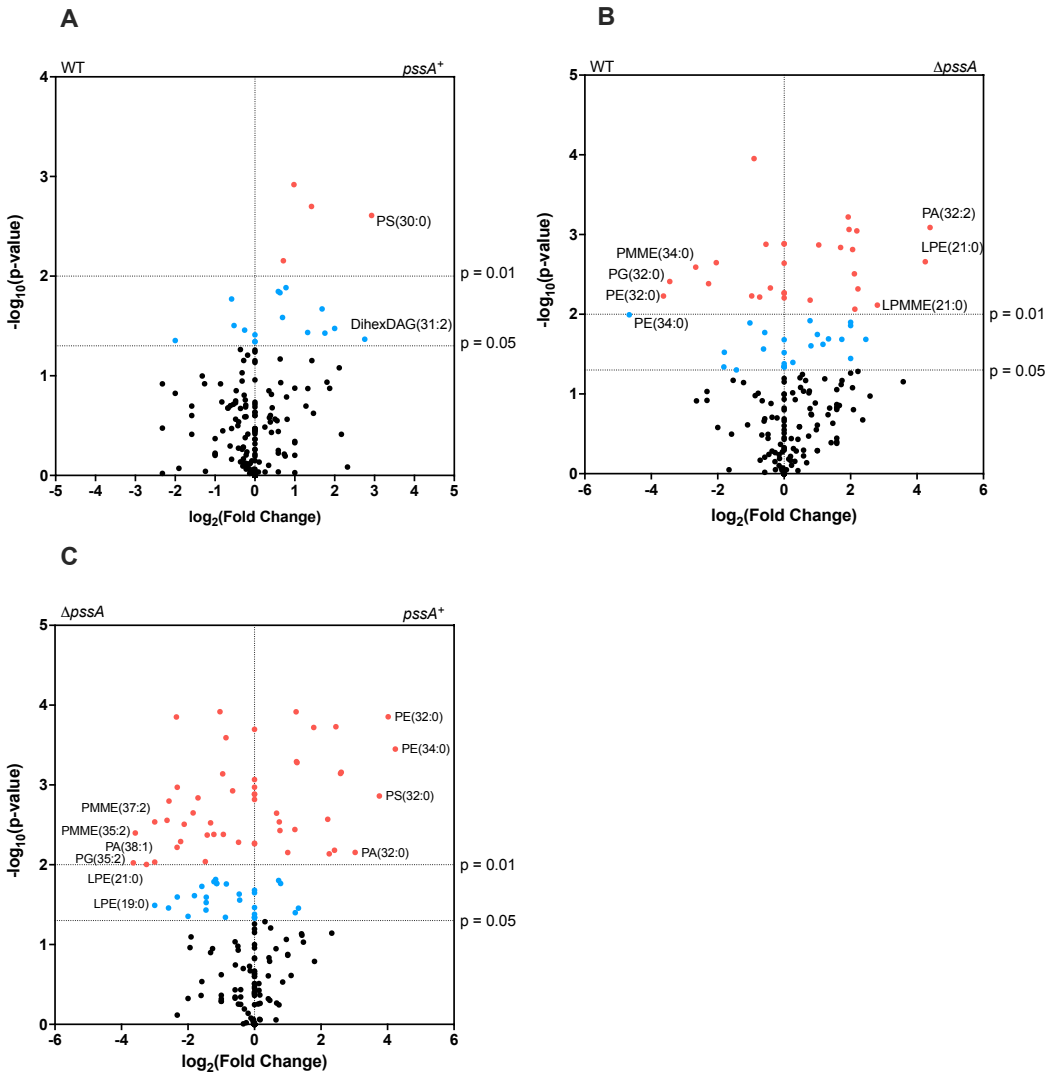

Figure 5.13. Lipid analysis between strains: (A) *pssA*$^+$ and WT; (B) Δ*pssA* and WT and (C) *pssA*$^+$ and Δ*pssA*. The volcano plots summarize both fold-change and p-value criteria for all lipids identified in the mutants and WT strains. Black dots indicate non-significant results ($p \geq 0.05$). Blue dots indicate significant results ($0.05 < p \geq 0.01$). Orange dots indicate highly significant results ($p < 0.01$). Positive values correspond to the lipids more produced in the strains represented on the right side of the plot. Negative values correspond to the lipids more produced in the strains on the left side of the plot. Results from four biological replicates (n=4). The *p-values* were calculated using the uncorrected Dunn's test.

Figure 5.13C shows the lipid comparison between the Δ*pssA* and *pssA*$^+$ strains. The univariate analysis shown 4 statistically relevant lipid species with a fold-change higher than 2.5 in the *pssA*$^+$, corresponding to PE (32:0), PE (34:0), PS (32:0) and PA (32:0). Conversely, 6 lipid species were significantly increased in the Δ*pssA* strain, having fold changes greater than 2.5 and corresponding to PMME(37:2), PMME (35:2), PA (38:1), PG (35:2), LPE (21:0), LPE (19:0).

Although with lower fold-changes, lipid molecules from phospholipid groups of PS, PMME, PG, PE, PE-Cer, PA, LPMME, LPE and DihexDAG were found with high statistical relevance, being most from the PMME and PE phospholipid classes and having similar distribution between the Δ*pssA* and WT strains (Annex 5).

Fatty Acid analysis

To complement the lipidomic characterization of these three strains, the fatty acids (FAs) identified were analysed. The aim was to compare the FA chain length and the number of unsaturations between the mutants and the WT. The FAs were grouped into three categories based on their chain length, specifically containing between 14-22, 23-32, and 33-38 carbons (Figure 5.14). The first group (14-22 carbons) includes the number of carbons identified in all lysolipids and, it also contains short-chain FAs found in some PE and PMME. The second group (23-32 carbons) was designed to represent lipids containing mid-size chain FAs. The last group (33-38 carbons) includes lipids with long chains FAs. This categorisation allows for an understanding of the distribution of FA chain lengths within the lipid classes and how these chain lengths vary across different strains (Figure 5.14A).

In general, all three strains produced more lipids with FA chains ranging from 14 to 22 carbons. Lipids with FAs containing 23 to 32 carbons exhibited greater variability, with significant differences between the WT and *pssA*$^{+}$ strains (p=0.0215). The percentage of FAs (23-32) in *pssA*$^{+}$ strain was in median of 25.30 % (95% CI, 24.17 -25.77) while for the WT it was in median 17.20 % (95% CI, 11.70 – 21.43) (Figure 5.14A).

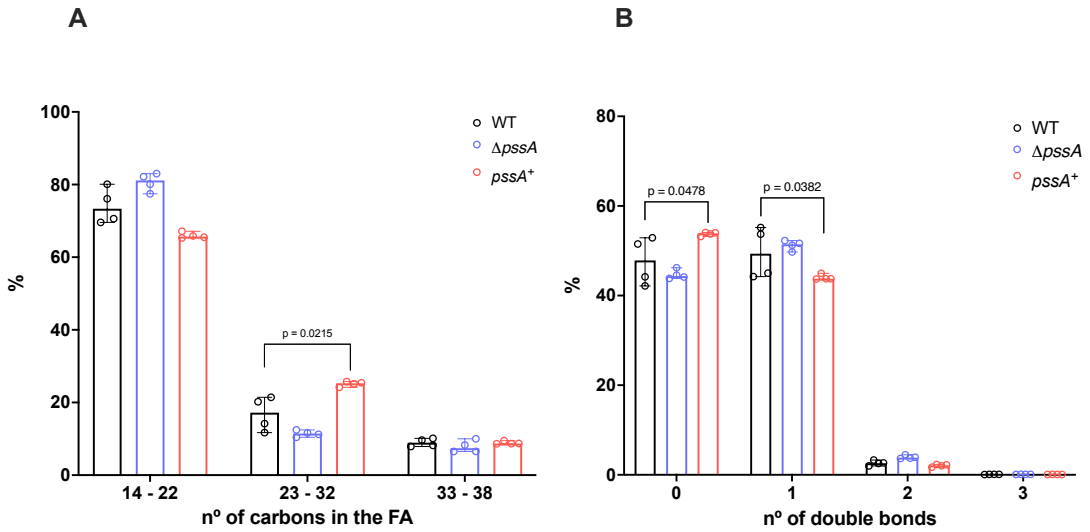

Figure 5.14. Analysis of the FA chains in the WT, Δ*pssA* and *pssA*$^+$ strains. Bar charts showing the median and 95% CI of: (A) FAs containing 14-22, 23-32 and 33-38 carbons; (B) FAs containing 0, 1, 2 and 3 doubles bonds. Results were normalised to the total lipids identified in each sample. Samples from four independent biological replicates (*n*=4). Statistical test: non-parametric Kruskall-Wallis and uncorrected Dunn's test for multiple comparisons.

The results for all the FAs were also aggregated based on the number of unsaturations (Figure 5.14B). According to the graph, most quantified FAs had between 0 and 1 unsaturations, while very few exhibited between 2 and 3 unsaturations. The identification of FAs with between 4 and 6 unsaturations was rare (data not shown). Notably, significant differences were observed in the FAs with 0 and 1 unsaturations between the WT and *pssA*$^+$ strains, with *p-values* of 0.0478 and 0.0382, respectively. The *pssA*$^+$ strain showed higher percentage of FAs without unsaturations compared to the WT, with respective medians of 53.88% (95% CI, 53.18 -54.08) and 47.85% (95% CI, 42.15 – 52.90) (Figure 5.14B). Conversely, the *pssA*$^+$ strain showed a significantly lower percentage of FAs with 1 unsaturation in comparison to the WT, with medians of 43.77% (95% CI, 43.69 -44.98) and 49.35% (95% CI, 44.23 – 55.20) for *pssA*$^+$ and WT, respectively (Figure 5.14B).

The individual FAs were compared by univariance as illustrated in Figure 5.15, significative differences in individual FAs were observed between the strains. In Figure 5.15A significantly higher percentages of FAs with carbon chains ranging from 16 to 28 were identified in the Δ*pssA* strain. In contrast, FAs featuring carbon chains from 30 to 34 were statistically present in higher percentages in the WT strain. Furthermore, FAs with even lengthier chains, from 34:2 to 38:8, were significantly elevated in the Δ*pssA* strain. In Figure 5.15B significantly higher percentages

of FAs with carbon chains with 15:0, 16:0-O, 29, 30 and 31:0, were identified in the *pssA*$^{+}$ strain. In contrast, only 3 FAs featuring carbon chains 14:1, 17:1 and 19:1, were in higher percentages in the WT strain, however with low fold-changes values. In Figure 5.15C significantly higher percentages of FAs with carbon chains ranging from 14 to 15 and from 30 to 34 were identified in the *pssA*$^{+}$ strain. In contrast, FAs featuring carbon chains from 16 to 38 were statistically present in higher percentages in the Δ*pssA* strain.

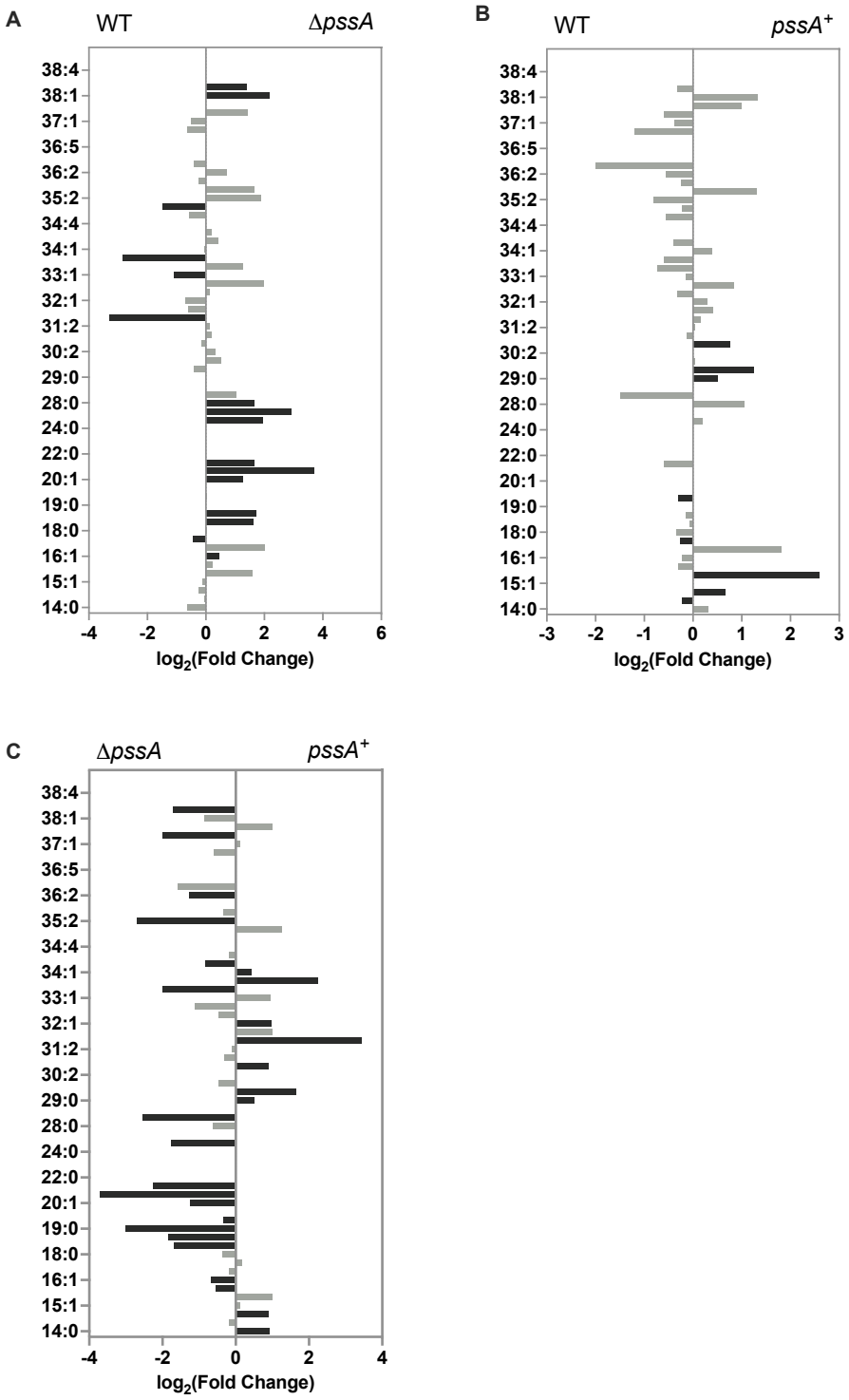

Figure 5.15. Univariant analysis of the Fatty Acid chains between the WT, Δ*pssA* and *pssA*$^+$ strains. Graphs showing the fold-change between: (A) Δ*pssA* and WT; (B) *pssA*$^+$ and WT. (C) *pssA*$^+$ and Δ*pssA*. Positive values represent the FAs found in higher percentages in the strains represented on the right side. Negative values represent the FAs found in higher percentages in the strains represented on the left side. Significant results ($p < 0.05$, uncorrected Dunn's test) are highlighted in black. Results from four biological replicates (n=4).

The volcano plots depicted in Figure 5.16 show the distribution of FA molecules among the WT, *pssA*$^+$, and Δ*pssA* strains, along with their statistical significance. Figure 5.16A compares the *pssA*$^+$ and WT strains, the FA 16:0-O (corresponding to a plasmalogen) stands out as the most significantly increased FA in the *pssA*$^+$ strain (Table 13). The plot from Figure 5.16B comparing the Δ*pssA* and WT strains, reveals that FAs 26:1 and 21:0 were the significantly increased FAs in the Δ*pssA* strain when comparing to WT, while the FAs 32:0 and 34:0 was significantly higher in the WT (Table 13). In Figure 5.16C, which contrasts the FAs composition between *pssA*$^+$ and Δ*pssA* strains, only FA 32:0 emerged as highly significant, with increased production in the *pssA*$^+$ strain. Additionally, FA molecules 28:1, 35:2, 38:2, 21:0, and 19:0 were found to be statistically significantly and more abundant in the Δ*pssA* strain (Table 13).

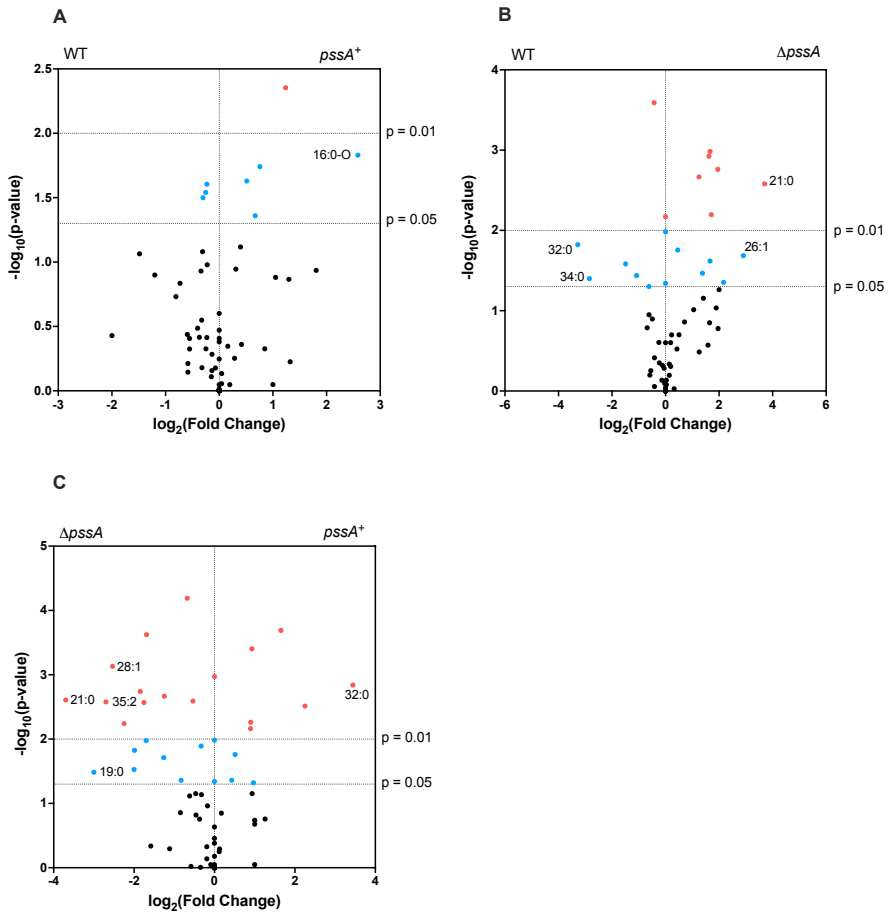

Figure 5.16. Fatty Acids analysis between strains: (A) *pssA*$^+$ and WT; (B) Δ*pssA* and WT and (C) *pssA*$^+$ and Δ*pssA*. The volcano plots summarize both fold-change and p-value criteria (uncorrected Dunn's test) for all lipids identified in the strains. Black dots indicate non-significant results ($p \geq 0.05$). Blue dots indicate significant results ($0.05 < p \geq 0.01$). Orange dots indicate highly significant results ($p < 0.01$). Positive values correspond to the lipids more produced in the strains represented on the right side of the plot. Negative values correspond to the lipids more produced in the strains on the left side of the plot. Results from four biological replicates (n=4).

Table 13. List of FAs analysed by univariance between the strains: (A) *pssA*$^+$ and WT, (B) Δ*pssA* and WT (C) *pssA*$^+$ and Δ*pssA*. Results with $p < 0.05$. FC corresponds to the fold-change. Positive $\log_2$(FC) correspond to higher concentrations of FA found in the strain represented in the numerator and negative $\log_2$(FC) correspond to FA found in higher concentrations in the strain represented in the denominator. Uncorrected Dunn's test was used to calculate the *p-values*.

A

FA	Log_2 (FC)		*p-value*
	WT	*pssA*$^+$	
14:1	-0.229	-	0.025
15:0	-	0.671	0.044
16:0-O	-	2.585	0.015
17:1	-0.252	-	0.029
19:1	-0.304	-	0.032
29:0	-	0.513	0.023
30:0	-	1.238	0.004
31:0	-	0.758	0.018

B

FA	Log_2 (FC)		*p-value*
	WT	Δ*pssA*	
16:1	-	0.455	0.018
17:1	-0.423	-	0.000
18:1	-	1.621	0.001
18:2	-	1.710	0.006
19:0	-	0.000	0.007
20:1	-	1.248	0.002
21:0	-	3.700	0.003
21:1	-	1.663	0.024
22:0	-	0.000	0.010
22:1	-	0.000	0.046
26:0	-	1.953	0.002
26:1	-	2.907	0.021
28:0	-	1.667	0.001
32:0	-3.281	-	0.015
33:1	-1.083	-	0.036
34:0	-2.844	-	0.040
35:1	-1.490	-	0.026
38:1	-	2.170	0.044
38:2	-	1.379	0.034

C

FA	Log_2 (FC)		*p-value*
	pssA$^+$	Δ*pssA*	
14:0	-	0.930	0.000
15:0	-	0.903	0.005
16:0	-0.538	-	0.003
16:1	-0.678	-	0.000
18:1	-1.692	-	0.000
18:2	-1.848	-	0.002
19:0	-3.000	-	0.033
19:1	-0.332	-	0.013
20:1	-1.248	-	0.002
21:0	-3.700	-	0.002
21:1	-2.248	-	0.006
22:0	-	0.000	0.010
22:1	-	0.000	0.046
26:0	-1.757	-	0.003
26:1	-	0.000	0.001
28:1	-2.536	-	0.001
29:0	-	0.513	0.017
30:0	-	1.653	0.000
31:0	-	0.895	0.007
32:0	-	3.441	0.001
32:1	-	0.969	0.048
33:2	-1.988	-	0.015
34:0	-	2.250	0.003
34:1	-	0.429	0.044
34:2	-0.829	-	0.044
35:2	-2.700	-	0.003
36:2	-1.263	-	0.019
37:2	-2.000	-	0.030
38:2	-1.700	-	0.011

Comparison between the FA chain within the phospholipid classes PS, PE and PG

The enzyme PssA (phosphatidylserine transferase) catalyses the incorporation of serine into CDP-diacylglycerol forming phosphatidylserine (PS) (Sohlenkamp and Geiger, 2015). Silencing and overexpressing this gene in *C. saccharoperbutylacetonicum* N 1-4 HMT genome, affected the normal route of the phospholipid biosynthesis, by altering the synthesis of PS and consequently the production of PE and indirectly affect the synthesis of PG (Figure 5.17).

To better understand the effect of the *pssA* mutant strains on the PS, PE and PG composition, further detailed analysis was conducted on the phospholipid classes PS, PE and PG, focusing on the FA chain length and the unsaturation levels. This approach can provide valuable insights into our understanding of membrane thickness and fluidity at the 24h of culture, a period when cells are in transition to the solventogenesis phase (Linney et al., 2023).

Figure 5.17 illustrates the distribution of the FAs chain lengths within three phospholipid classes (PS, PE, and PG). Concerning the subset of phospholipids with acyl chains ranging from 14 to 22 carbons (Figure 5.17C), lipids were only detected from the PE class. The Δ*pssA* strain exhibited significant differences when compared to both the WT (p = 0.0271) and *pssA*$^+$ (p= 0.0048) strains. The median percentages of PE (14-22) identified were 0.007% (95% CI, 0.00 – 0.03), 0.24% (95% CI, 0.17 – 0.35), and 0.0003% (95% CI, 0.00 – 0.002) in the WT, Δ*pssA*, and *pssA*$^+$ strains, respectively. Notably, the Δ*pssA* strain demonstrated a significant more PE comprising 14-22 carbons in the acyl chain relative to the other strains.

In the group of PS with FA ranging from 23 to 32 carbons, *pssA*$^+$ strain exhibited significantly higher percentage when compared to the WT (p =0.0262) and the Δ*pssA* (p=0.0012). Specifically, *pssA*$^+$ strains had a median of 84.76% (95% CI, 83.69 – 86.13) of PS, whereas WT had a median of 67.09 % (95% CI, 42.86 – 90.69) of PS and the Δ*pssA* had a median of 61.55 % (95% CI, 56.61 – 70.75) of PS (Figure 5.17A).

In the group of PG with 23 to 32 carbons (Figure 5.17B), significant differences were observed between the *pssA*$^+$ and Δ*pssA* strains (p = 0.0026), where more PG (23-32) was found in the *pssA*$^+$. The percentage of PG (23-32) in the *pssA*$^+$ strain was 68.74% (95% CI, 67.29 – 70.01) and in the Δ*pssA* strain was 49.62% (95% CI, 47.20 – 60.30).

The increase in PS content in the *pssA*$^+$ strain coincided with an increase in PE with FAs in the 23-32 carbon range (Figure 5.17D). The difference in the PE content was significant between WT and *pssA*$^+$ strains (p=0.0116) and between Δ*pssA* and *pssA*$^+$ strains (p =0.083) (Figure 5.17D). For WT, Δ*pssA* and *pssA*$^+$ strains, medians of 69.20 % (95% CI, 61.75 – 76.70), 70.60% (95% CI, 68.78 – 71.03) and 80.60% (95% CI, 79.33 – 81.06) of PE, were obtained, respectively.

For the group of phospholipids comprising 33 to 38 carbons in the FAs (Figure 5.17A, B, D), noteworthy changes were detected in the phospholipid classes PS, PE and PG. In the *pssA*$^+$ strain significant less PS (33-38) was observed when compared to the WT (p =0.0262) and to the Δ*pssA* (p =0.0012) (Figure 5.17A).

For PG, significantly less PG (33-38) was found in the *pssA*$^+$ strain compared to the Δ*pssA* (p = 0.0026), where in median 31.26% (95% CI, 29.99 – 32.71) and 50.38% (95% CI, 48.08 – 52.80) of PG (33-38) was identified, respectively (Figure 5.17B). The percentage of PE (33-38) found in the *pssA*$^+$ strain was also significantly lower than in the Δ*pssA* strain (p = 0.0083) and comparatively to WT (p =0.0116). In median 30.80% (95% CI, 23.28 – 38.22), 31.26% (95% CI, 29.99 – 32.71) and 50.38% (95% CI, 48.08 – 52.80) of PG (33-38) was identified in the WT, *pssA*$^+$ and Δ*pssA* strains, respectively (Figure 5.17D).

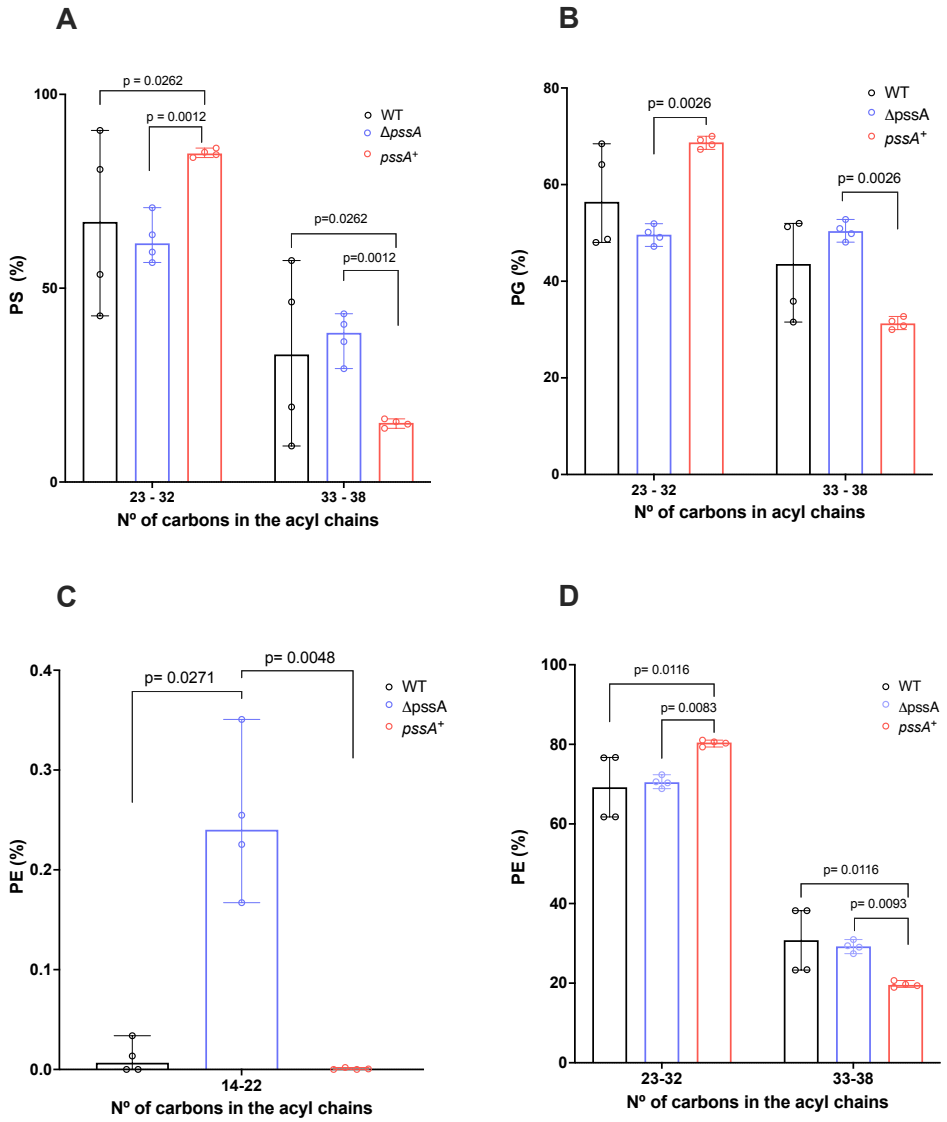

Figure 5.17. Analysis of the FA acyl chains in the phospholipid classes: (A) PS; (B) PG; (C and D) PE; identified in the WT, Δ*pssA* and *pssA*$^{+}$ strains. Bars showing the median and 95% CI of the percentage of FAs containing between 14-22, 23-32 and 33-38 carbons. Samples from four independent biological replicates (*n*=4). Statistical test: non-parametric Kruskall-Wallis and uncorrected Dunn's test for multiple comparisons.

The analysis of unsaturation levels within the acyl chains of phospholipids (PS, PE, and PG) are shown in Figure 5.18. Regarding PS, FAs with between 0 and 6 unsaturations were identified, yet those with 4 to 6 unsaturations were rare present, nearly approximating a percentage of zero, and thus, were not depicted in the graphical data.

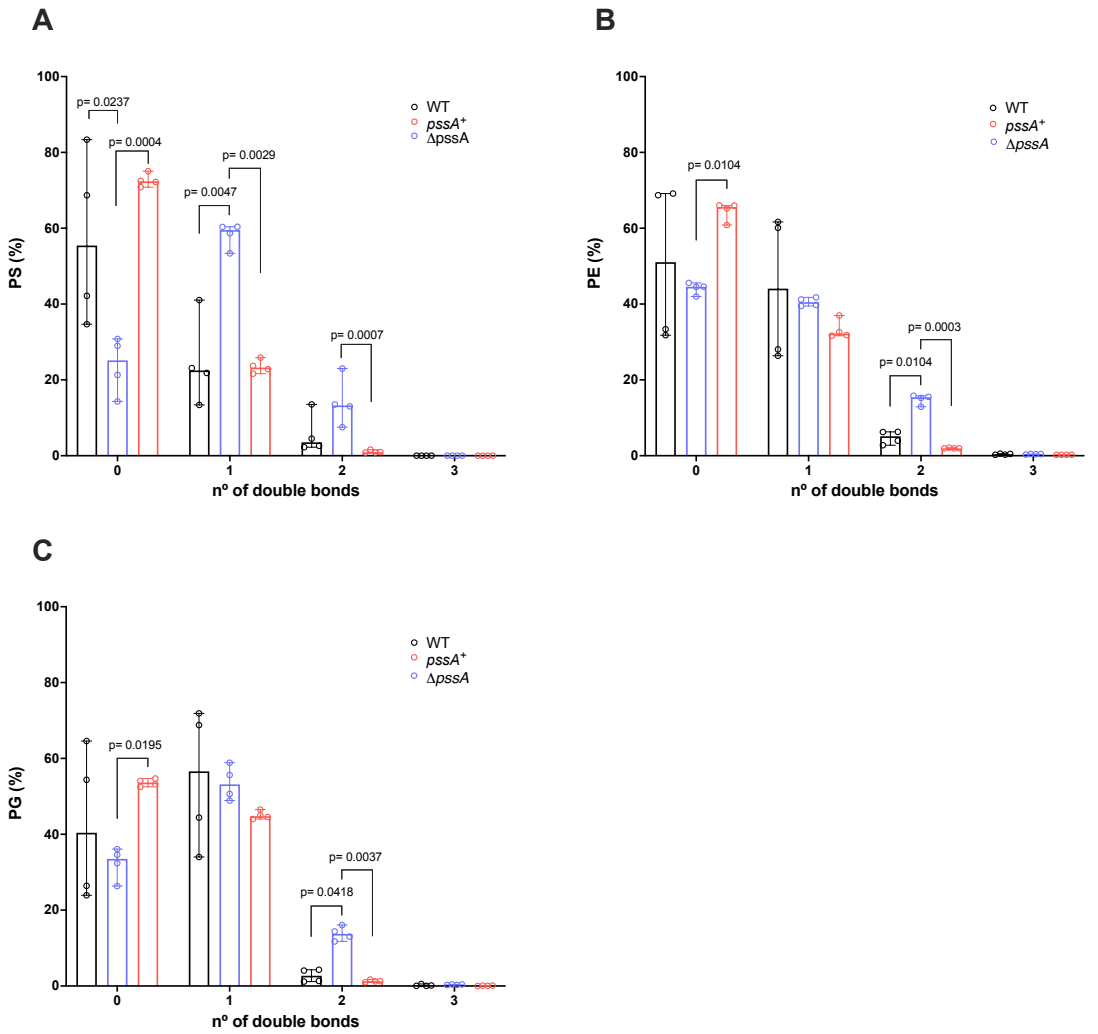

Figure 5.18. Analysis of the number of double bonds in the phospholipid classes: (A, B) PS; (C) PE; (CD) PE; identified in the WT, Δ*pssA* and *pssA*$^+$ strains. Bars showing the median and 95% CI o of the percentage of FAs containing 0 to 3 double bonds. Samples from four independent biological replicates (*n*=4). Statistical test: non-parametric Kruskall-Wallis and uncorrected Dunn's for multiple comparisons.

Notably, the Δ*pssA* strain exhibited significantly lower levels of PS molecules without double bonds when compared to both the WT (p =0.0237) and *pssA*$^+$ (p =0.004) strains (Figure 5.18A). The percentage of PS(0) in the Δ*pssA*, WT and *pssA*$^+$ strains was 25.15% (95% CI, 14.13 – 3.80), 55.44% (95% CI, 34.70 – 83.37) and 72.35% (95% CI, 70.84 – 75.04), respectively (Figure 5.18A).

Furthermore, there were statistical differences observed for PS molecules with 1 double bond, between WT and Δ*pssA* strains (p =0.0047) and between *pssA*$^+$ and Δ*pssA* strains (p =0.0029). Significantly higher percentage of PS(1) was found in the Δ*pssA*, with a median of 59.51% (95%

CI, 53.36 – 60.40), when compared to the WT and *pssA*$^+$, where medians of 22.47% (95% CI, 13.39 – 41.05) and 23.26% (95% CI, 21.63 – 25.86) were obtained, respectively (Figure 5.18A).

PS molecules with 2 double bonds were present in lower concentrations among all strains, but the Δ*pssA* strain produced significantly more PS(2) than the *pssA*$^+$ (p =0.007) strain. For PS(2), the percentage was 13.26% (95% CI, 7.51 – 23.00) and 0.89% (95% CI, 0.82 – 1.61), in Δ*pssA* and *pssA*$^+$, respectively (Figure 5.18A).

For PE, the highest percentage had 0 and 1 double bonds in the FAs (Figure 5.18B). The percentage of PE(0) was significantly higher in the *pssA*$^+$ strain compared to the Δ*pssA* strain (p =0.0104). In the *pssA*$^+$ strain, the median of PE(0) was 65.61% (95% CI, 60.86 – 66.00) whereas for the Δ*pssA* strain was 44.55% (95% CI, 42.00 – 45.57).

Significant differences were also found in the percentage of PE having 2 unsaturations in the FAs, where increased amounts were found in the Δ*pssA* strain compared to the WT strain (p =0.0104) and to the *pssA*$^+$ strain (p =0.003). In median the percentage of PE(2) was 5.11% (95% CI, 2.76 – 6.30), 15.39% (95% CI, 12.92 – 15.81) and 1.92% (95% CI, 1.89 – 2.12), for WT, Δ*pssA* and *pssA*$^+$, respectively. With 1 and 3 unsaturations, the percentage of PE among the three strains did not result in significant differences (Figure 5.18B).

For PG, the predominant percentage of PG molecules contained 0 to 1 double bonds in their FAs, as depicted in Figure 5.18C. Notably, significant differences were observed in the percentage of PE with 0 and 2 unsaturations. Specifically, the percentage of unsaturated PE was significantly distinct between the *pssA*$^+$ strain and the Δ*pssA* strain (p =0.0195). In the *pssA*$^+$ strain, this percentage was significantly higher, with a median of 53.64% (95% CI, 52.51 – 54.71), compared to the Δ*pssA* strain, where it amounted to a median of 33.49% (95% CI, 26.33 – 36.09). With 1 and 3 unsaturations, the percentage of PG among the three strains did not result in significant differences (Figure 5.18C).

Summary

The mass spectrometry analysis revealed notable differences in lipid composition among the WT, Δ*pssA*, and *pssA*$^+$ strains. The manipulation of a gene responsible for the synthesis of PS and PE, which indirectly impacts the availability of plasmalogens of PE and PMME, had a significant effect on the composition of membrane lipids. Table 14 provides an overview of the key distinctions observed among these strains, where overall:

- The Δ*pssA* produced PS and PE.
- The *pssA*$^{+}$ strain showed an increased in PE compared to the Δ*pssA* and WT strains.
- The Δ*pssA* strain exhibited less PG than the WT.
- Significantly more LPE was observed in the Δ*pssA* strain, while significantly less LPMME was observed in the Δ*pssA* strain.
- Higher variations between strains in the lipid groups with FAs (23-32) were observed.
- Analysis of unsaturation levels in PS, PE and PG showed distinct patterns in the Δ*pssA* and *pssA*$^{+}$ strains.

Silencing the *pssA* gene in *C. saccharoperbutylacetonicum* N1-4 HMT neither significantly reduced nor removed the synthesis of PE. This revelation led to further analysis, where a second *pssA* gene was discovered within *the C. saccharoperbutylacetonicum* N1-4 HMT genome as shown in Annex 9 and Annex 10. The lower percentages of PG in the mass spectrometry analysis of *Δpss*A strain, can be a strong indicative of higher percentages of CL.

The significant increase on the PE of *C. saccharoperbutylacetonicum* N1-4 HMT *pssA*$^{+}$ strain is in concordance to what is described in literature. In *E. coli*, *pssA* overexpression by inserting a second copy of the gene in the chromosome shown an increase by 7% in the relative abundance of PE but a decrease by around 50% in the relative abundance of PG (Figure 7.1C) (Tan et al., 2017). However, there was a significant increase on the PG of *C. saccharoperbutylacetonicum* N1-4 HMT *pssA*$^{+}$ strain, which did not match with the literature (Zhang and Rock 2008).

There notable increase in FAs having between 23 and 32 carbons in the *pssA*$^{+}$ strain when compared to the WT contrasts with the findings described in *E. coli* where overexpressing *pssA* resulted in lipids with shorter FAs, only extending up to a maximum of 16 carbons in each tail (Tan et al., 2017). The *pssA*$^{+}$ strain showed FAs with fewer unsaturations in comparison to the WT, which was an opposite finding from the studies in *E. coli* by Tan et al., (2017). These differences might be due to the 2 PssAs from *C. saccharoperbutylacetonicum* N1-4 HMT.

Key questions arise regarding the role of lysolipids in the membrane, potential relationships between reduced PG and increased CL, the significance of glycolipids and plasmalogens, and changes in FA composition as adaptations for membrane stability.

Table 14. Summary of the mass spec analysis of the WT, Δ*pssA* and *pssA*$^{+}$ strains lipidome.

	lipids	Δ*pssA*	*pssA*$^{+}$	notes
Total lipid groups	LPE / LPMME	High concentration in the membrane of both strains		Role of lysolipids in the membrane? Damaged lipids?
	PE	**Similar** to WT	More than WT	Changes in the expression of *pssA*?
	PG	Less than WT	**Similar** to WT	How is Δ*pssA* affecting the PG/CL synthesis?
	PS	**Similar** to WT	More than WT	Overexpression of *pssA*?
Lipid group vs FA chain	FA chain length	More Short FAs (14-22) (very low percentage)	More Mid size FAs (23 -32) than WT	Is the PssA tested preferring mid size FAs?
	PS acyl chain length	**Similar** to WT	**Similar** to WT	Δ*pssA* More unsaturated PE and PG, more fluidity? Longer chain PG to compensate the membrane thickness? *pssA*$^{+}$ Same membrane fluidity as the WT?
	PS acyl chain unsaturations	Less 0 unsaturations than WT More 1 and 2 unsaturations than WT	**Similar** to WT	
	PE acyl chain length	More Shorter FAs (14-22) than WT (very low percentage)	**Similar** to WT	
	PE acyl chain unsaturations	More 2 unsaturations than WT	**Similar** to WT	
	PG acyl chain length	**Similar** to WT	**Similar** to WT	
	PG acyl chain unsaturations	More 2 unsaturations than WT	**Similar** to WT	

5.2.2 Mass Spectrometry data analysis in *pgsA*$^+$ and *cls*$^+$ strains

The *pgsA* and *cls* genes are involved in the synthesis of PG and CL respectively in *Clostridium* (Guan and Goldfine, 2021) (Figure 5.1). Overexpressing these genes from *C. saccharoperbutylacetonicum* N1-4 HMT was shown, via TLC, to cause changes in the lipid composition of these strains when compared to the WT and between these two mutants. The lipidomic characterisation by mass spectrometry resulted in the identification and quantification of 9 different lipid groups, including PA, PG, LPE, PE, LPMME, PMME, PS, Cer-PE, Cer-PMME and DihexDAG. Although the cardiolipins data would be ideal in this section, the lipids are yet to run in the mass spectrometer specific for cardiolipins analysis by Creative Proteomics.

Lipid group analysis

The lipid groups identified and quantified by mass spectrometry varied between the three strains and their relative abundance in the cells is shown in Figure 5.19. On average a total of 5.70, 4.37 and 5.69 nmol of lipid per 10^6 cells were identified in the WT, *pgsA*$^+$ and *cls*$^+$ strains, respectively. According to the charts, LPE, PE and LPMME were the main group of lipids produced by the three strains, corresponding to around 80-90% of all the lipids identified in this analysis. The percentage of PG identified in *cls*$^+$ was lower than the WT and *pgsA*$^+$ strains, corresponding to 3.56 %, 5.57% and 5.13%, respectively. The other lipid groups, including were also found in relatively lower percentages overall.

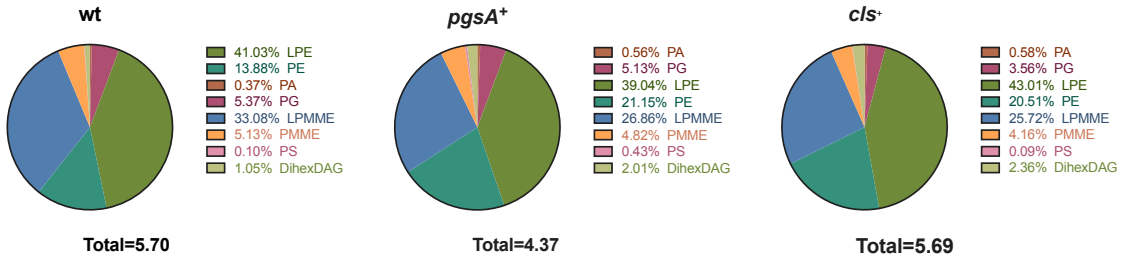

Figure 5.19. Overall lipid distribution in the WT, *pgsA*$^+$ and *cls*$^+$ strains. The charts depict the relative abundance of the lipid classes identified by mass spectrometry. Different colours distinguish different lipid classes. Data from four biological replicates for each strain, expressed in percentage and the total lipids in nmol of lipid per 10^6 cells.

To better comprehend these differences observed in the lipid profiles between strains, the median of the standardized lipid percentage and the 95% confidence interval (median, 95% CI) was plotted for each lipid group (Figure 5.20) and the differences between strains were analyzed for its significance by performing a non-parametric test, Kruskall-Wallis. Significant differences found on the lipid groups were then analysed in more detail by univariant analysis.

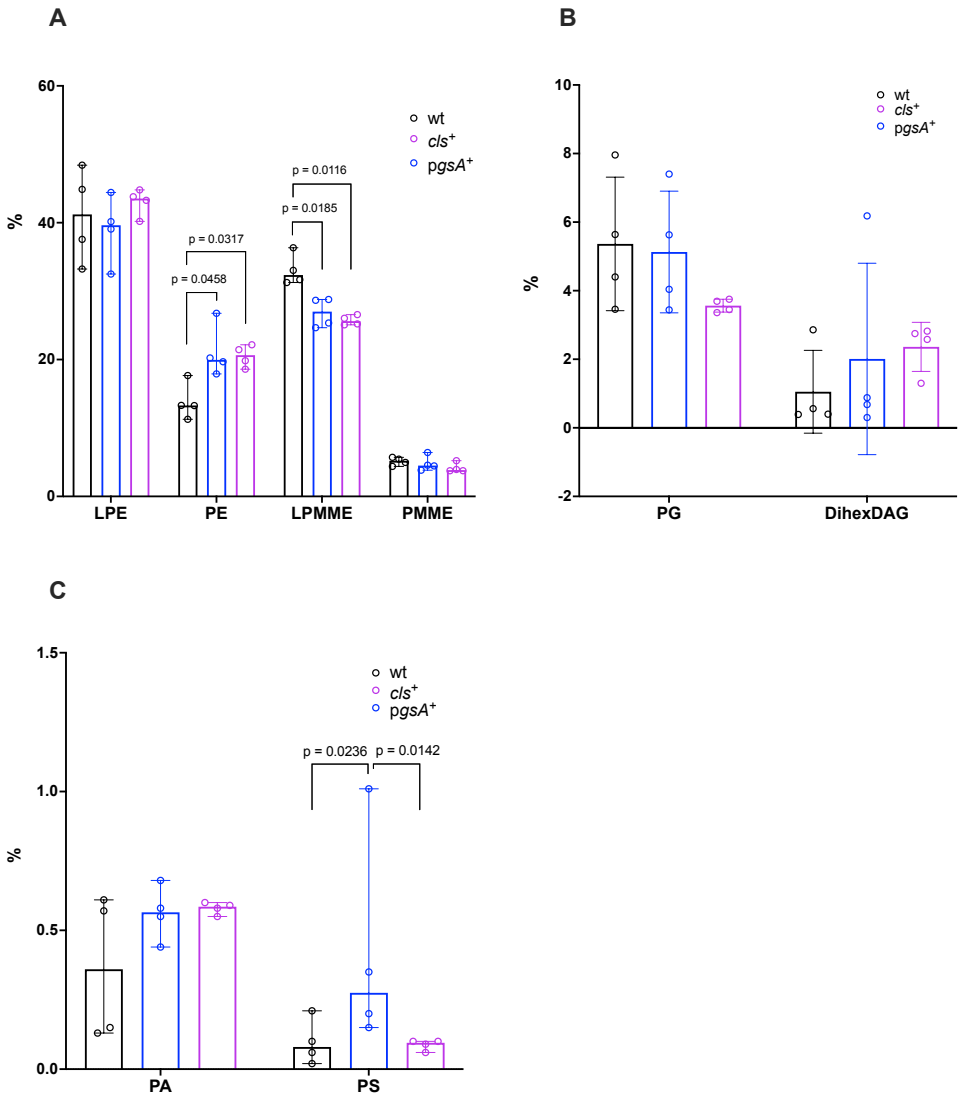

Figure 5.20. Lipid classes distribution in the WT, *pgsA*$^{+}$ and *cls*$^{+}$ strains. Bar charts showing the median and 95% CI of: (A) LPE, PE, LPMME and PMME; (B) PG and DihexDAG; (C) PA and PS. Results were normalised to the total lipids identified in each sample. Samples from four independent biological replicates (*n*=4). Statistical test: non-parametric Kruskall-Wallis and uncorrected Dunn's test for multiple comparisons.

Figure 5.20 presents the comprehensive results for the total LPE, PE, LPMME, PMME, PG, DihexDAG, PA and PS content obtained from the *cls*$^+$ and *pgsA*$^+$ strains. Ethanolamine-containing lipid groups were predominant among the identified lipids (Figure 5.20A). The *pgsA*$^+$ and *cls*$^+$ strains exhibited significantly more PE compared to the WT, with p=0.0458 and p =0.0317, respectively. Specifically, the *pgsA*$^+$ strain shown a median of 19.96% PE (95% CI, 17.91 – 26.76), which was higher than the WT strain median, corresponding to 13.29% (95% CI, 11.27 – 17.67). Additionally, the *cls*$^+$ strain also demonstrated a higher PE median of 20.64% (95% CI, 18.60 – 22.16) compared to the WT strain.

For LPMME, the pattern was the opposite, the WT strain produced significantly more LPMME than the *pgsA*$^+$ and *cls*$^+$ strains, with p =0.0185 and p =0.00116, respectively (Figure 5.20A). The median percentage of LPMME found in the WT, *pgsA*$^+$ and *cls*$^+$ strains was 32.36 % (95% CI, 31.26 – 36.34), 27.01 % (95% CI, 24.66 – 28.78) and 25.62 % (95% CI, 25.07 – 26.57), respectively.

In the case of PS, significant more PS was found in the *pgsA*$^+$ strain, compared to the WT and *cls*$^+$, with p = 0.0236 and p =0.0142, respectively. The percentage of PS in the *pgsA*$^+$, WT and *cls*$^+$ strains was in median 0.28% (95% CI, 0.15-1.01), 0.08% (95% CI, 0.002 - 0.210) and 0.09% (95% CI, 0.06 - 0.10), respectively. More than the double of PS was found in the *pgsA*$^+$ strain.

Considering the significant differences observed in the phospholipid classes between strains, the individual PE, LPMME and PS were characterised in more detail. All the lipid molecules from each class underwent univariate analysis. The forest plots in Figure 5.21 illustrate the fold change in percentage of PE, LPMME and PS identified between WT and *pgsA*$^+$ strains. The forest plots in Figure 5.22 illustrate the fold change in percentage of PE, LPMME and PS identified between WT and *cls*$^+$ strains.

In Figure 5.21A it is shown the fold-change of various PE molecules quantified in the WT and *pgsA*$^+$ strains. More abundant lipids in the *pgsA*$^+$ strain are positioned to the right of the x-axis, while those that are more abundant in the WT strain are located to the left. Lipids situated closer to the central zero point indicate minor changes, whereas those moving away from zero, in either direction, signify more substantial alterations. Results with a $p < 0.05$ are highlighted in black.

The mass spectrometry analysis identified PE molecules, encompassing a range of FA chain lengths from 21 to 38 carbons, different levels of unsaturation, and including a plasmalogen form of PE (PE-O), in both the *pgsA*$^+$ and WT strains. The comparison between the *pgsA*$^+$ and WT strains resulted in 4 PE molecules with significantly higher concentrations in the *pgsA*$^+$ strain

(Figure 5.21A, Annex 6). These significant lipids included PE (26:0), PE (28:0), PE (30:0) and PE (31:0). No lipids with a significant fold-change were noted in the WT.

For LPMME (Figure 5.21B) the comparison between the *pgsA*$^{+}$ and WT strains resulted in 1 LPMME, corresponding to LPMME (15:0), with significantly higher concentrations in the *pgsA*$^{+}$ strain (Figure 5.21B, Annex 6). With significantly higher concentrations in the WT strain, comparing to the *pgsA*$^{+}$ strain, three lipids were identified, corresponding to LPMME(16:0) and LPMME(17:1) (Figure 5.21B, Annex 6).

For PS (Figure 5.21C) the comparison between the *pgsA*$^{+}$ and WT strains resulted in 3 PS lipid molecules, with significantly higher concentrations in the *pgsA*$^{+}$ strain, corresponding to PS (30:0), PS (32:1) and PS (35:1). No lipids with a significant fold-change were noted in the WT. (Figure 5.21C, Annex 6).

In Figure 5.22A it is shown the fold-change of various PE molecules in the WT and *cls*$^{+}$ strains. The comparison between the *cls*$^{+}$ and WT strains resulted in 6 PE molecules with significantly higher concentrations in the *cls*$^{+}$ strain (Figure 5.22A, Annex 6). These significant lipids included PE (26:0), PE (28:0), PE (30:1), PE (32:1), PE (31:1) and PE (34:1). No lipids with a significant fold-change were noted in the WT.

For LPMME (Figure 5.22B) the comparison between the *cls*$^{+}$ and WT strains resulted in 4 LPMME lipid molecules, with significantly higher concentrations in the WT strain. These lipids corresponded to LPMME (15:1), LPMME (16:1), LPMME (16:1) and LPMME (19:1) (Annex 6).

For PS (Figure 5.22C) the comparison between the *pgsA*$^{+}$ and *cls*$^{+}$ strains resulted in 2 PS lipid molecules, with significantly higher concentrations in the *pgsA*$^{+}$ strain, corresponding to PS (30:0) and PS (35:1). No lipids with a significant fold-change were noted in the *cls*$^{+}$ for this comparison. (Figure 5.22C, Annex 6).

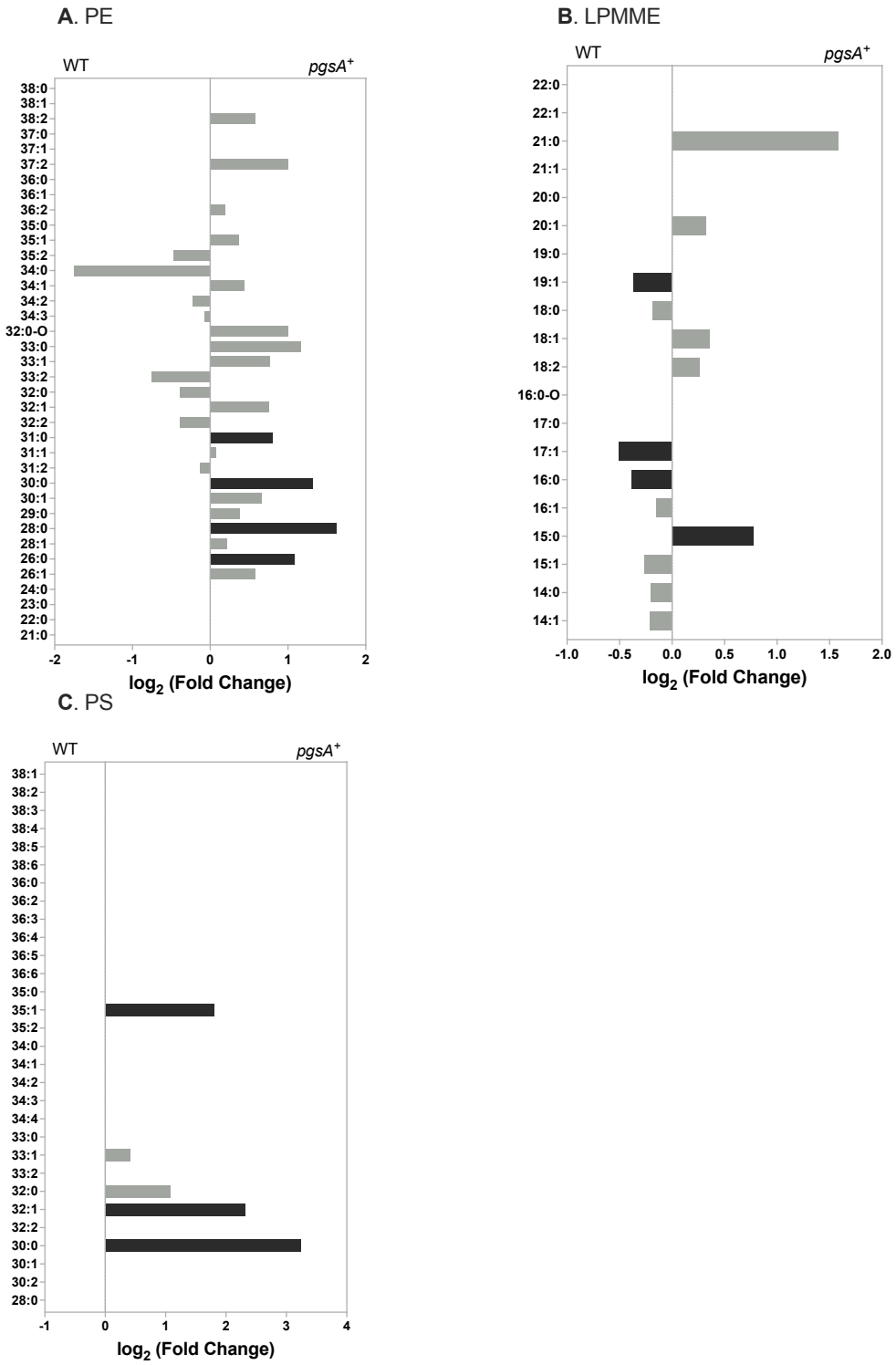

Figure 5.21. Univariant analysis of the PE, LPMME and PS between the WT and *pgsA*$^+$ strains. Comparison of the phospholipid classes: (A) PE; (B) LPMME; (C) PS, between WT and *pgsA*$^+$ strains. The x-axis corresponds to the $\log_2$ (fold-change) between a group of 2 strains. Significant results (p <0.05, uncorrected Dunn's test) are highlighted in black. Results from four independent biological repeats (n=4).

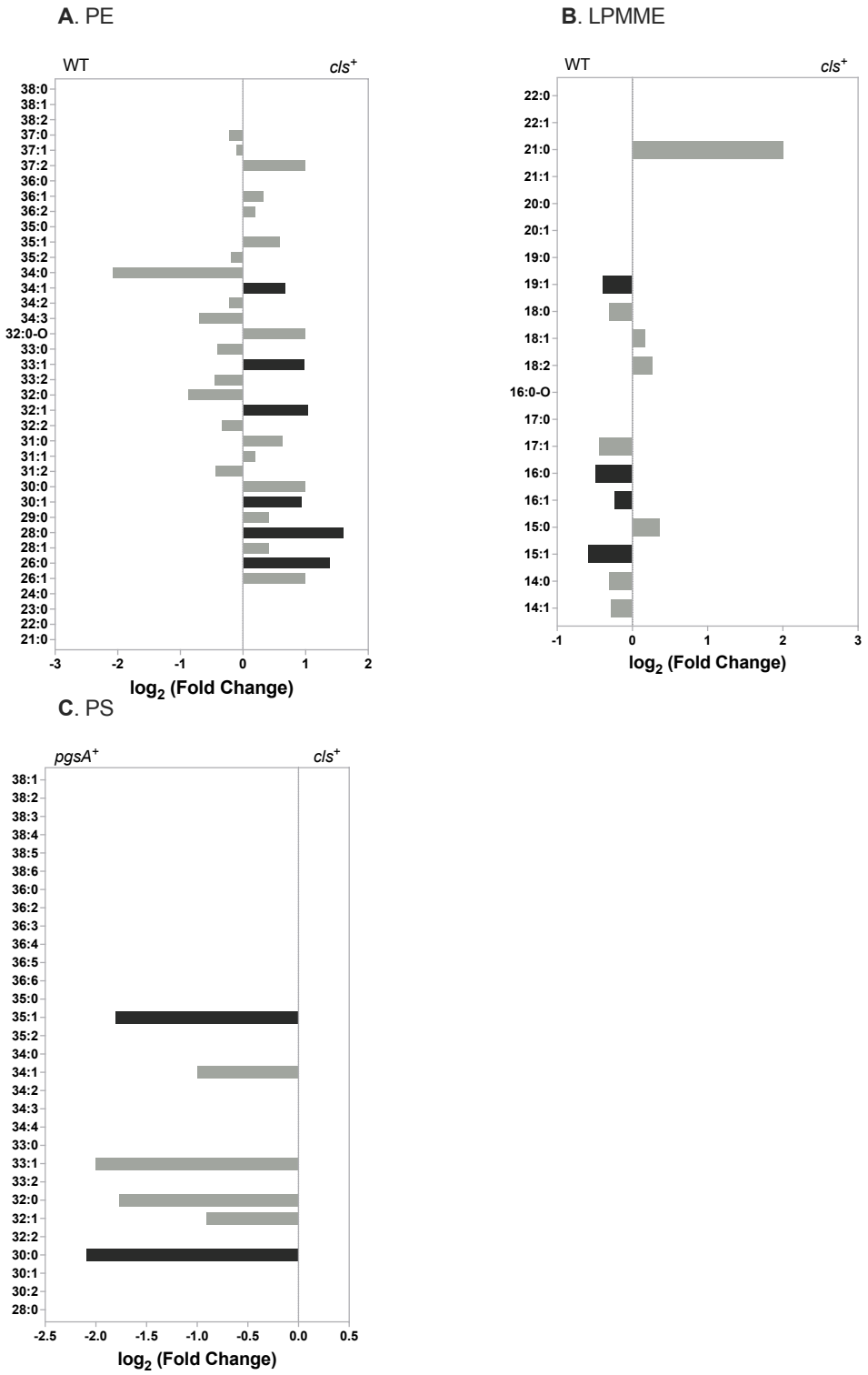

Figure 5.22. Univariant analysis of the PE, LPMME and PS between the WT, *pgsA*$^+$ and *cls*$^+$strains. Comparison of the phospholipid classes: (A) PE between WT and *cls*$^+$ strains; (B) LPMME between WT and *cls*$^+$ strains; (C) PS, between *cls*$^+$ and *pgsA*$^+$ strains. The x-axis corresponds to the $\log_2$ (fold-change) between a group of 2 strains. Significant results ($p < 0.05$, uncorrected Dunn's test) are highlighted in black. Results from four independent biological repeats (n=4).

Individual lipids from all lipid classes identified were plotted in a "volcano plot," as depicted in Figure 5.23. The plot charts the fold-changes of lipids on the x-axis against the significance of those changes on the y-axis. Lipids with significant production differences are highlighted with orange dots ($p < 0.01$) and blue dots ($p < 0.05$), with those closer to the x-axis' zero point indicating minimal changes and those farther indicating substantial changes.

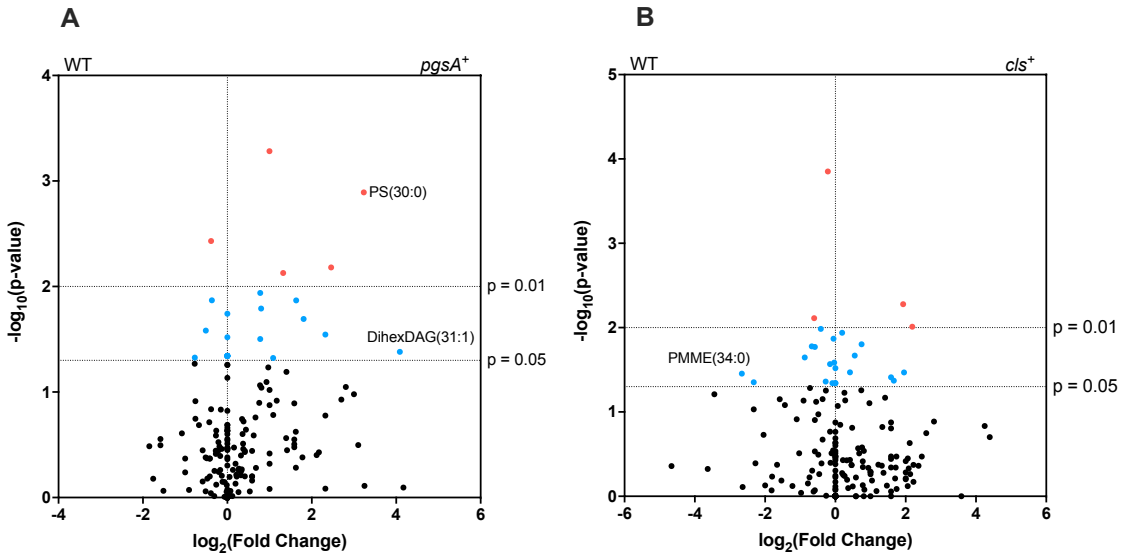

Figure 5.23. Lipid analysis between strains: (A) *pgsA*$^+$ and WT and (B) *cls*$^+$ and WT. The volcano plots summarize both fold-change and p-value criteria for all lipids identified in the mutants and WT strains. Black dots indicate non-significant results ($p \geq 0.05$). Blue dots indicate significant results ($0.05 < p \geq 0.01$). Orange values indicate highly significant results ($p < 0.01$). Positive values correspond to the lipids more produced in the strains represented on the right side of the plot. Negative values correspond to the lipids more produced in the strains on the left side of the plot. Results from four biological replicates (n=4).

The volcano plot from Figure 5.23A shows the significance level ($p < 0.05$) based on the uncorrected Dunn's test and a fold-change between the *pgsA*$^+$ and WT strains. In this graph, lipids that displayed statistically significant differences, with a fold-change exceeding 2.5 between the strains were highlighted. The analysis revealed that, lipids such as PS (30:0) and DihexDAG (31:1) were significantly more abundant in the *pgsA*$^+$ strain, no lipid meeting the criteria was observed in the WT, as detailed in Figure 5.23A. A total of 16 lipids spanning the lipid groups PS, PMME, Cer-PMME, PG, PE, PA, LPMME, LPE and DihexDAG exhibited high

statistical relevance (Annex 6), although with lower fold change values. Most of them were lipids containing ethanolamine in the head group and were prominent in the *pgsA*$^{+}$ strains.

Figure 5.23B shows the lipid comparison between the *cls*$^{+}$ and WT strains. The univariate analysis has shown only PMME(34:0) with statistically relevance and a fold-change higher than 2.5. PMME(34:0) was significantly increased in the WT whereas no lipid meeting that criteria was observed in the *cls*$^{+}$ (Annex 6). A total of 15 lipids spanning the lipid groups PMME, PG, PE, LPMME, LPE and, PMME and DihexDAG exhibited high statistical relevance (Annex 6). Most of them are lipids containing ethanolamine in the head group and were more produced in the *cls*$^{+}$ strain, comparing to the WT.

Fatty Acid analysis

To complement the lipidomic characterization of these three strains, the fatty acids (FAs) identified were analysed. The aim was to compare the FA chain length and the number of unsaturations between the mutants and the WT. The FAs were grouped into three categories based on their chain length, specifically containing between 14-22, 23-32, and 33-38 carbons (Figure 5.14). The first group (14-22 carbons) includes the number of carbons identified in all lysolipids and, it also contains short-chain FAs found in some PE and PMME. The second group (23-32 carbons) was designed to represent lipids containing mid-size chain FAs. The last group (33-38 carbons) includes lipids with long chains FAs. This categorisation allows for an understanding of the distribution of FA chain lengths within the lipid classes and how these chain lengths vary across different strains (Figure 5.24).

In general, all three strains produced more lipids with FA chains ranging from 14 to 22 carbons, that corresponded essentially to the lysolipids LPE and LPMME. Lipids with FAs containing 23 to 32 carbons and 33 to 38 carbons were found in lower percentages, with no significant differences observed between the strains. (Figure 5.24A).

The results for all the FAs were also aggregated based on the number of unsaturations as illustrated in Figure 5.24B. According to the graph, the majority percentage of quantified FAs had between 0 and 1 unsaturations, while very few exhibited between 2 and 3 unsaturations. The identification of FAs with between 4 and 6 unsaturations was rare (data not shown). Significant differences were observed in the FAs with 3 unsaturations between the WT and cls+ strains, with p-value of 0.0387. The *cls*$^{+}$ strain showed lesser percentage of FAs with 3

unsaturations compared to the WT, with respective medians of 0.055% (95% CI, 0.05 -0.07) and 0.10% (95% CI, 0.07 – 0.11) (Figure 5.24B).

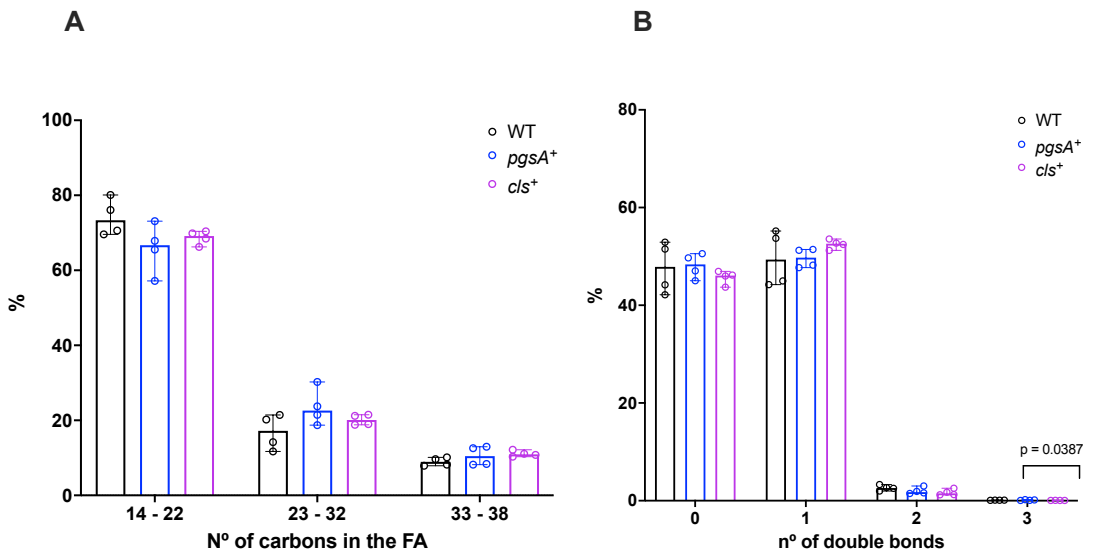

Figure 5.24. Analysis of the FA chains in the WT, *pgsA*$^+$ and *cls*$^+$ strains. Bar charts showing the median and 95% CI of: (A) FAs containing 14-22, 23-32 and 33-38 carbons; (B) FAs containing 0, 1, 2 and 3 doubles bonds. Results were normalised to the total lipids identified in each sample. Samples from four independent biological replicates (*n*=4). Statistical test: non-parametric Kruskall-Wallis and uncorrected Dunn's test for multiple comparisons.

The univariate comparison of individual FAs as depicted in Figure 5.25, revealed discernible differences in individual FAs between the strains. When analysing the differences between the WT and *pgsA*$^+$ strains, overall, very few variations in the fold-change were statistically significant (Figure 5.25A). FAs 17:0, 30:0, and 31:0 were present in significantly higher percentages in the *pgsA*$^+$ strain. Conversely, only 2 FAs, specifically 16:0 and 17:1, exhibited significantly higher percentages in the WT strain.

The univariant analysis between *cls*$^+$ and WT strains resulted in only four FAs with significantly higher percentages in the *cls*$^+$ strain, corresponding to FAs 15:0, 26:0, 28:0 and 36:0. Only FA 32:2 exhibited significantly higher percentages in the WT strain (Figure 5.25B). In this analysis, no discernible pattern related to FA chain length was observed; the FAs sizes were distributed across all strains.

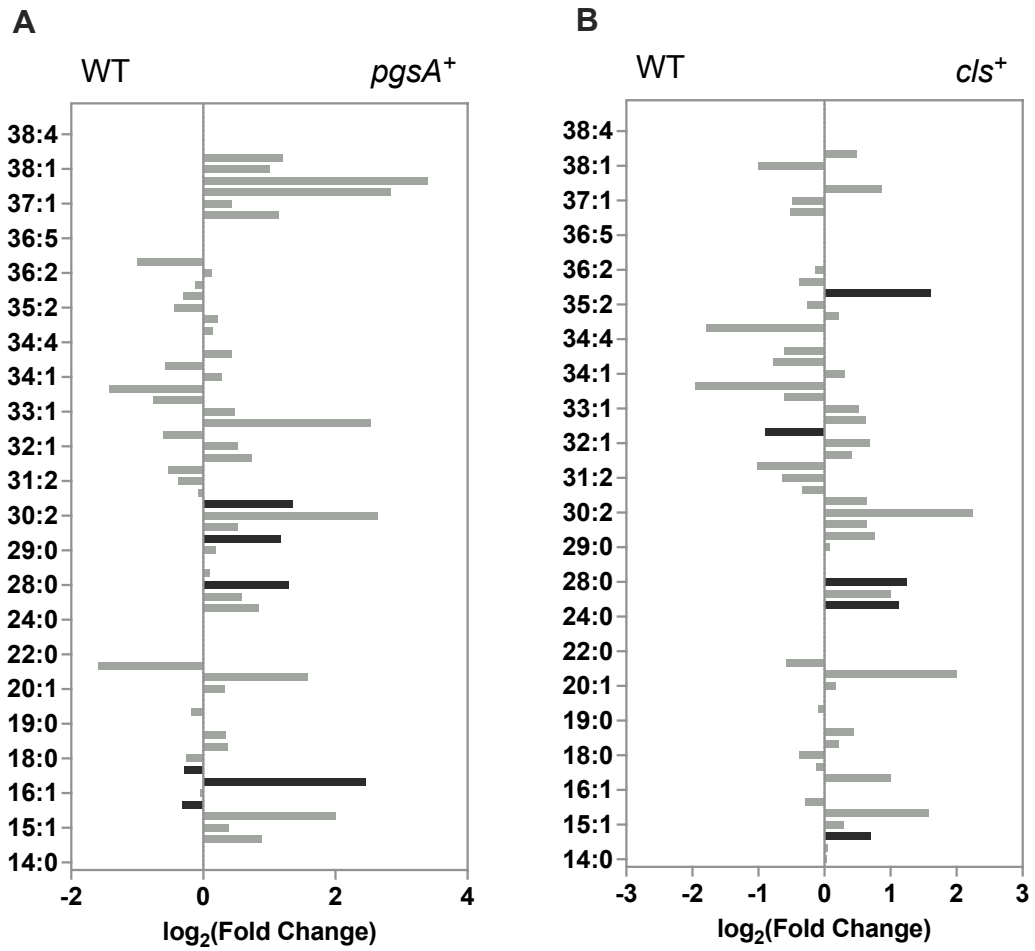

Figure 5.25. Univariant analysis of the Fatty Acid chains between the WT, *pgsA*$^+$ and *cls*$^+$ strains. (A) fold change between *pgsA*$^+$ and the WT; (B) fold change between *cls*$^+$ and the WT. Positive values represent the FAs found in higher concentrations in the strains represented on the right side. Negative values represent the FAs found in higher concentrations in the strains represented on the left side. Significant results (p< 0.05, uncorrected Dunn's test) are highlighted in black. Results from four biological replicates (n=4).

The volcano plots, illustrated in Figure 5.26, display the distribution and statistical significance of FAs among the WT, *pgsA*$^+$, and *cls*$^+$ strains, highlighting lipids that exhibited statistically significant differences and a fold-change exceeding 2 between the strains. In Figure 5.26A, which compares the *cls*$^+$ and WT strains, only one FA (17:0) was found to be statistically significant, with p<0.01 and a fold-change greater than 2. Conversely, the plot in Figure 5.26B, which compares the *pgsA*$^+$ and WT strains, revealed no lipid species with statistically significant differences and a fold-change above 2, suggesting no substantial variations in their production between the *pgsA*$^+$ and WT strains.

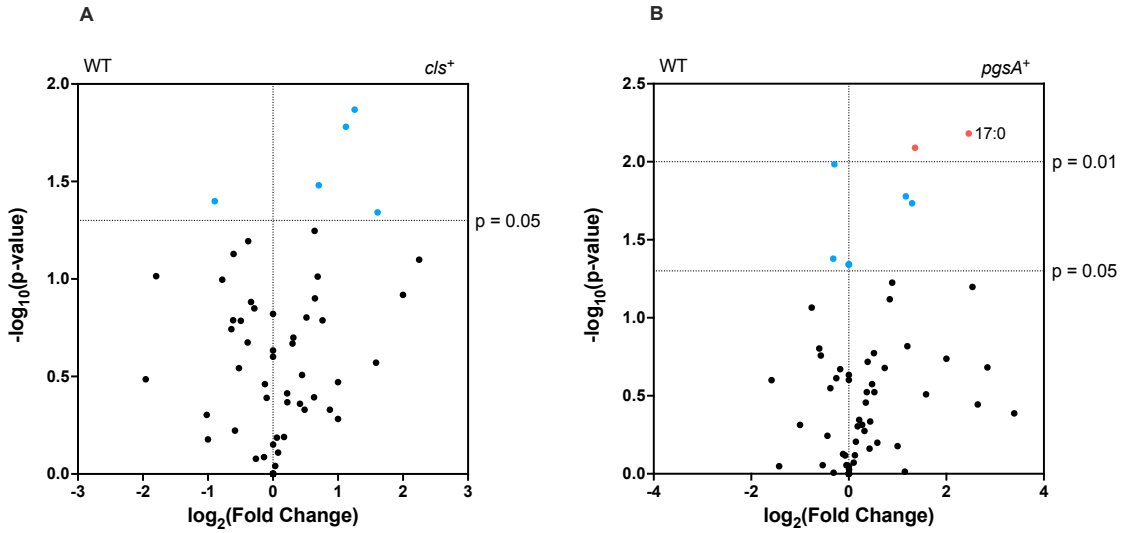

Figure 5.26. Fatty Acids analysis between strains: (A) *cls*$^{+}$ and WT; (B) *pgsA*$^{+}$ and WT. The volcano plots summarize both fold-change and p-value criteria (uncorrected Dunn's test) for all lipids identified in the strains. Black dots indicate non-significant results ($p \geq 0.05$). Blue dots indicate significant results ($0.05 < p \geq 0.01$). Orange values indicate highly significant results ($p < 0.01$). Positive values correspond to the lipids more produced in the strains represented on the right side of the plot. Negative values correspond to the lipids more produced in the strains on the left side of the plot. Results from four biological replicates (n=4).

Comparison between the FA chain within the phospholipid classes PS, PE and PG

The enzyme PgsA plays an important role as an intermediary in the synthesis of PG, while the enzyme Cls is responsible for the condensation of two PG molecules to generate CL (Sohlenkamp and Geiger, 2015). Considering the importance of PG, CL and PE in the membrane composition of *C. saccharoperbutylacetonicum* N 1-4 HMT, as well as the role of PS as an intermediary in PE synthesis, an in-depth analysis of these lipids was conducted. Additionally, recognising that the expression of *pgsA* and *cls* can influence the production of these phospholipid classes was an important factor. The primary focus was on characterizing their FA chain length and unsaturation levels. As a part of the analysis, lipids were categorised within each phospholipid class based on their acyl chain lengths, grouping them into lipids with 14 to 22 carbons, 23 to 32 carbons, and 33 to 38 carbons. For the assessment of unsaturation levels lipids with 0 to 3 unsaturations were also categorised. These values were then standardized and expressed as percentages, facilitating the comparison between different strains, as it is represented in Figure 5.27 and Figure 5.28.

Table 15. List of FAs analysed by univariance between the strains: (A) *pgsA*$^+$ and WT, (B) *cls*$^+$ and WT. Results with $p < 0.05$. FC corresponds to the fold-change. Positive $\log_2$(FC) correspond to higher concentrations of FA found in the strain represented in the numerator and negative $\log_2$(FC) correspond to FA found in higher concentrations in the strain represented in the denominator. Uncorrected Dunn's test was used to calculate the *p-values*.

A

FA	Log_2 (FC)		*p-value*
	WT	*pgsA*$^+$	
16:0	-0,319	-	0,042
17:0	-	2,459	0,007
17:1	-0,297	-	0,010
28:0	-	1,297	0,018
30:0	-	1,170	0,017
31:0	-	1,358	0,008
34:4	-	0,000	0,046
38:4	-	0,000	0,046
38:5	-	0,000	0,046

B

FA	Log_2 (FC)		*p-value*
	WT	*cls*$^+$	
15:0	-	0,705	0,033
26:0	-	1,123	0,017
28:0	-	1,255	0,014
32:2	-0,895	-	0,040
36:0	-	1,609	0,046

Figure 5.27 showcases the distribution of FA acyl chains across three phospholipid classes, specifically PS, PE, and PG. Most of these phospholipids exhibited FAs with chain lengths ranging from 23 to 32 carbons. Phospholipids with longer FA chains (33 to 38 carbons) were present in smaller percentages, and only PE was found with shorter chain lengths of 14 to 22 carbons, although in very minimal percentages. The FA compositions of the PS, PE, and PG lipid classes exhibited notable similarities across the WT, *pgsA*$^+$, and *cls*$^+$ strains.

The analysis of unsaturation levels within the acyl chains of phospholipids (PS, PE, and PG) is shown in Figure 5.28. Regarding PS, FAs with between 0 and 6 unsaturations were identified, yet those with 4 to 6 unsaturations were rare present, nearly approximating a percentage of zero, and thus, were not depicted in the graphical data.

Predominantly, phospholipids with 0 or 1 unsaturations constituted the highest percentage. A considerably lower percentage was noted for phospholipids having 2 double bonds, and an even more diminished percentage was found for those with 3 double bonds. The distribution of phospholipids, categorised by acyl chains with 0 to 3 double bonds, displayed similar patterns across all three strains. Notably, no significant differences were discernible in the composition of PS, PE, and PG within the unsaturation groups amongst the strains.

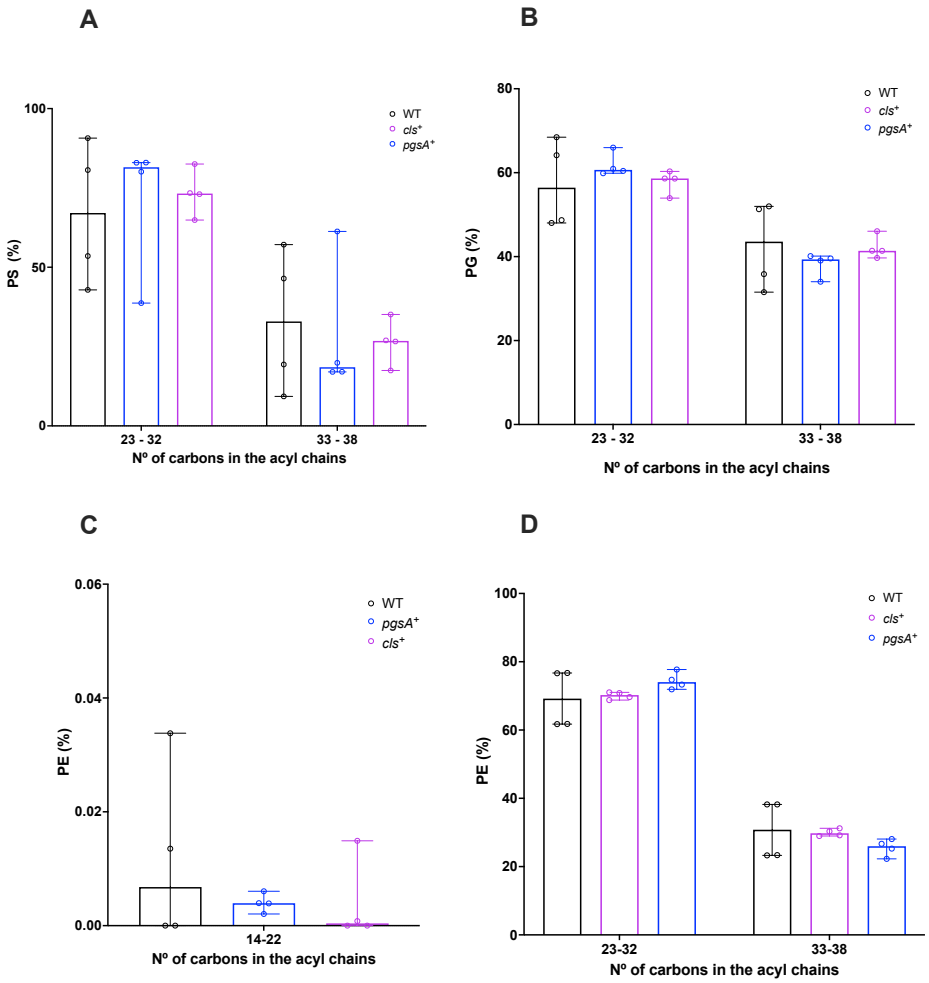

Figure 5.27. Analysis of the FA chain length in the phospholipid classes: (A) PS; (B) PG; (C and D) PE; identified in the WT, *pgsA*$^{+}$ and *cls*$^{+}$ strains. Bars showing the median and 95% CI of the percentage of FAs containing between 14-22, 23-32 and 33-38 carbons. Samples from four independent biological replicates (*n*=4). Statistical test: non-parametric Kruskall-Wallis and uncorrected Dunn's test for multiple comparisons.

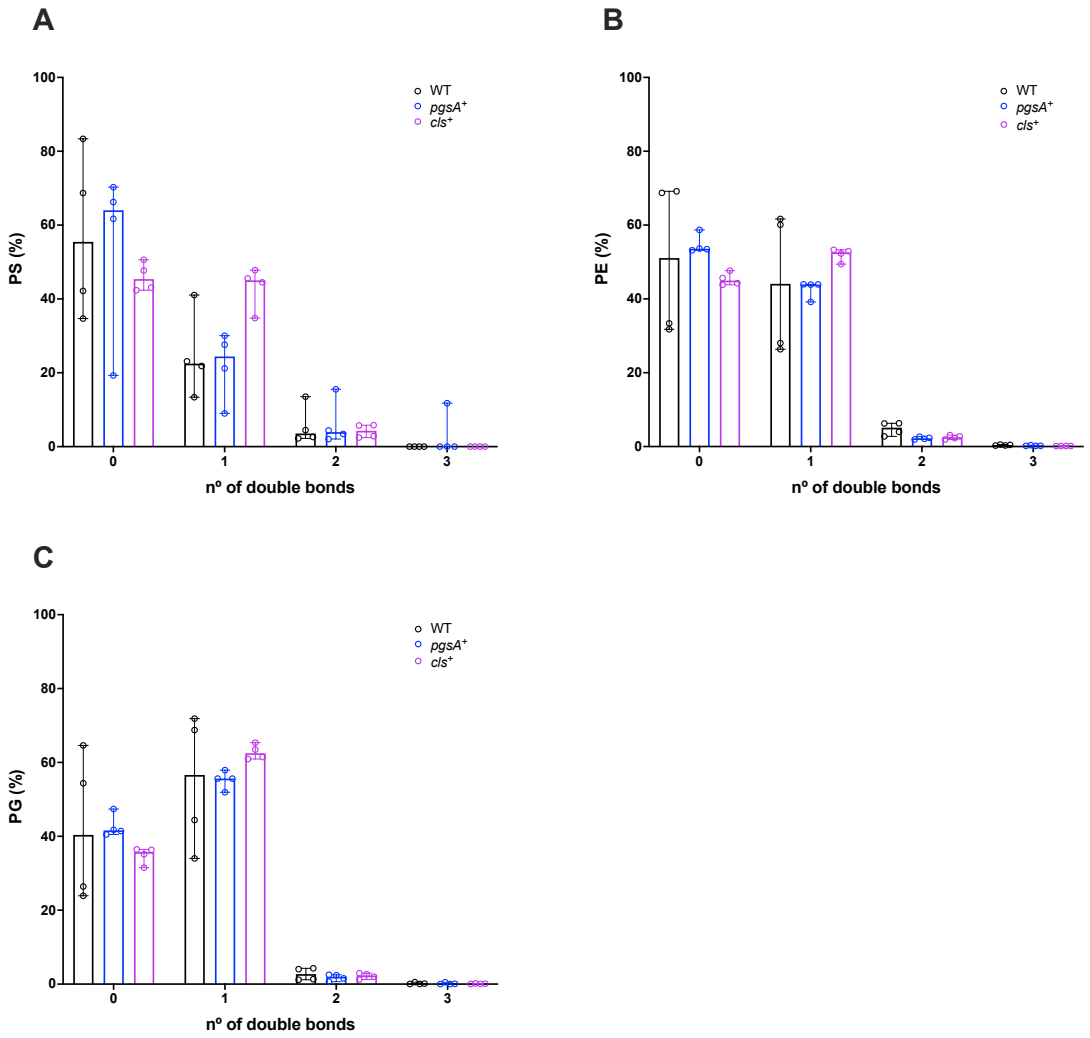

Figure 5.28. Analysis of the number of double bonds in the phospholipid classes: (A) PE; (B) PG; (C) PS; identified in the WT, *pgsA*$^{+}$ and *cls*$^{+}$ strains. Bars showing the median and 95% CI o of the percentage of FAs containing 0 to 3 double bonds. Samples from four independent biological replicates (*n*=4). Statistical test: non-parametric Kruskall-Wallis and uncorrected Dunn's test for multiple comparisons.

Summary

In sum, the mass spectrometry analysis uncovered part of the lipidome of WT, *pgsA*$^{+}$, and *cls*$^{+}$ strains. The manipulation of genes involved in the synthesis of PG and CL had little changes on membrane lipid composition, when compared to the WT, as shown in Table 16. The main differences were on the PE synthesis, where more PE was observed in both *pgsA*$^{+}$, and *cls*$^{+}$ strains. This increase was not due to an increase on the PG levels, as described by the stablished regulation mechanism of phospholipid profile in the membrane of *E. coli* (Zhang and Rock 2008). This result indicates for a possible distinct regulation mechanism in *Clostridium*. Intriguingly,

questions emerge concerning the overexpression of *pgsA* and *cls*, particularly considering their seemingly limited impact on PG and CL content.

Table 16. Summary of the mass spectrometry analysis of the WT, *pgsA*$^{+}$ and *cls*$^{+}$.

	lipids	*pgsA*$^{+}$	*cls*$^{+}$	notes
Total lipid groups	LPE / LPMME	Highest concentration in the membrane of both strains		Role of lysolipids in the membrane? Damaged lipids?
	PE	**More** than the WT	**More** than the WT	*pssA* expression induced?
	LPMME	**Less** than WT	**Less** than WT	Role of lysolipids in the membrane? Damaged lipids?
	PS	**More** than the WT	**Similar** to WT	PS is an intermediate of PE
	PG	**Similar** to WT	**Similar** to WT	
Lipid group vs FA chain	FA chain length	**Similar** to WT	**Similar** to WT	
	PS acyl chain length	**Similar** to WT	**Similar** to WT	Membrane fluidity? Solvent stress? Solvent production? Why no changes in PG? Why is *pgsA* and *cls* affecting PE synthesis?
	PS acyl chain unsaturations	**Similar** to WT	**Similar** to WT	
	PE acyl chain length	**Similar** to WT	**Similar** to WT	
	PE acyl chain unsaturations	**Similar** to WT	**Similar** to WT	
	PG acyl chain length	**Similar** to WT	**Similar** to WT	
	PG acyl chain unsaturations	**Similar** to WT	**Similar** to WT	

5.2.3 Mass Spectrometry data analysis in *mt*1^{+} strain

The heterologous expression of *mt*1 in the C. *saccharoperbutylacetonicum* N 1-4 HMT strain (*mt*1^{+}) was generated as an effort to mitigate cellular stress levels. This initiative aimed to assess the potential impact on this cell factory's suitability for diverse biotechnological processes (Chin et al., 2013). In solventogenic *Clostridium*, the production and accumulation of weak acids and solvents lead to alterations in cellular oxidative conditions and membrane stability, as highlighted in previous studies (Bahl et al., 1995; Linney et al., 2023; Yu et al., 2011). While not fully characterized, it is plausible that changes in oxidative levels and the accumulation of these chemicals within the membrane induce modifications in lipid content to maintain cellular functionality. To a detailed analysis into the lipidome of *mt*1^{+} cells at the 24h growth stage, a mass spectrometry analysis was conducted. This analysis successfully identified and quantified lipid from 9 distinct lipid groups, which included PA, PG, LPE, PE, LPMME, PMME, PS, Cer-PE, Cer-PMME and DihexDAG in the *mt*1^{+} strain.

Lipid group analysis

The percentage of these lipid groups varied between the WT and *mt*1^{+} strains and their relative abundance in the cells is shown in Figure 5.29. On average a total of 5.70 and 2.80 nmol of lipid per 10^6 cells were identified in the WT and *mt*1^{+} strains, respectively. According to Figure 5.29, LPE, PE and LPMME were the main group of lipids produced by the two strains, corresponding to around 80-92% of all the lipids identified in this analysis. The other lipid groups, such as, PMME, PA, PG, PS and DihexDAG were identified in lower percentages.

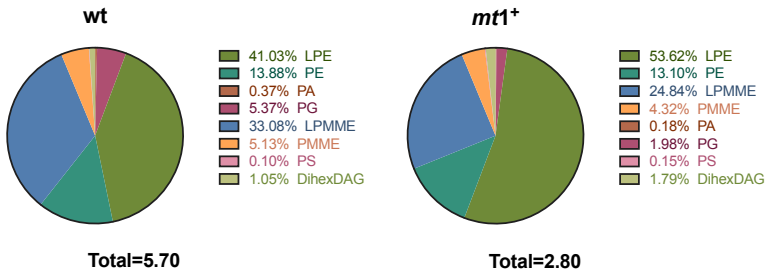

Figure 5.29. Overall lipid distribution in the WT and *mt*1^{+} strains. The charts depict the relative abundance of the lipid classes identified by mass spectrometry. Different colours distinguish different lipid classes. Data from four biological replicates for each strain, expressed in percentage and the total lipids in nmol of lipid per 10^6 cells.

To better comprehend the differences in lipid profiles between strains, the results were normalized to the total lipids identified in each sample and presented as the median of the percentage along with the 95% confidence interval (median, 95% CI) (Figure 5.30). The differences between strains were analyzed for its significance by performing a non-parametric test, Kruskall-Wallis. Significant differences found on the lipid groups were then analysed in more detail by univariant analysis.

Figure 5.30 resents the comprehensive results for the total LPE, PE, LPMME, PMME, PG, DihexDAG, PA and PS content obtained from the two strains. Significant differences were observed for the LPE, LPMME and PG identified between the WT and *mt*1^{+} strains (Figure 5.30A, B).

For LPE (Figure 5.30A) significantly higher percentage was found in the *mt*1^{+} strain relatively to the WT, with a p =0.0262. Specifically, the median percentage of LPE in *mt*1^{+} strain was 54% (95% CI, 50.52 – 55.96), while for the WT strain it was 41.22% (95% CI, 33.24 – 48.28).

For LPMME (Figure 5.30A), significantly lower percentage was found in the *mt*1^{+} strain relatively to the WT, with a p =0.0018. Specifically, the median percentage of LPMME in *mt*1^{+} strain was 24.58% (95% CI, 23.90 – 25.72), while for the WT strain it was 32.36% (95% CI, 31.26 – 36.34).

For PG (Figure 5.30B), significantly lower percentage was found in the *mt*1^{+} strain relatively to the WT, with a p =0.00262. Specifically, the median percentage of PG in *mt*1^{+} strain was 1.95% (95% CI, 1.81 – 2.21), while for the WT strain it was 5.02% (95% CI, 3.46 – 7.96). More than 2-fold less PG was found in the *mt*1^{+}.

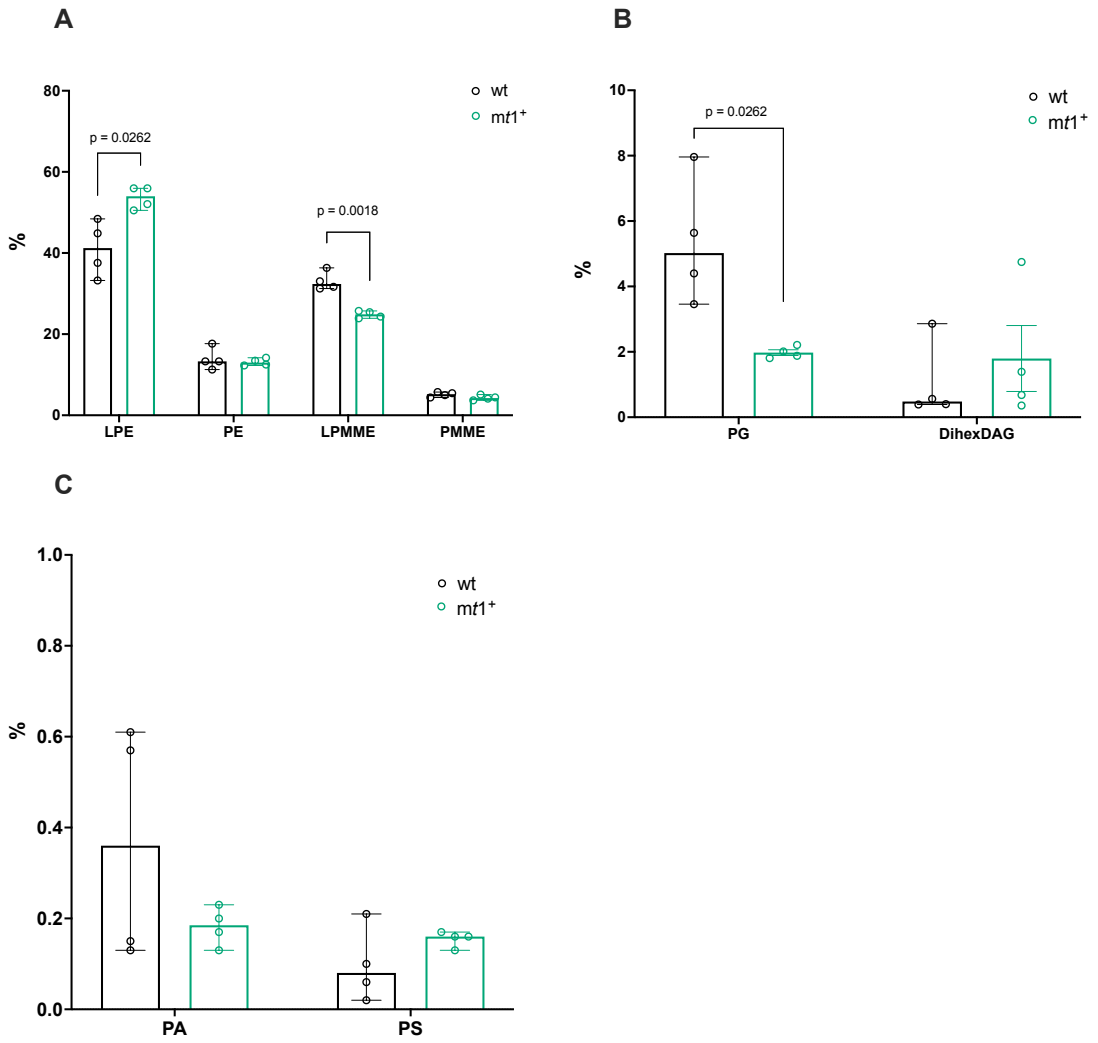

Figure 5.30. Lipid classes distribution in the WT and *mt*1^{+} strains. Bar charts showing the median and 95% CI of: (A) LPE, PE, LPMME and PMME; (B) PG and DihexDAG; (C) PA and PS. Results were normalised to the total lipids identified in each sample. Samples from four independent biological replicates (*n*=4). Statistical test: non-parametric Kruskall-Wallis and uncorrected Dunn's test for multiple comparisons.

Considering the significant differences observed in the phospholipid classes between strains, the individual lipids from LPE, LPMME and PG were characterised in more detail. All these lipids quantified and standardized in the WT and *mt*1^{+} strains underwent univariate analysis (Figure 5.31). The forest plots in Figure 5.31 shown the fold-change of various LPE, LPMME and PG lipid molecules quantified in the *mt*1^{+} and WT strains. More abundant lipids in the *mt*1^{+} strain are positioned to the right of the x-axis, while those that are more abundant in the WT strain are located to the left. Lipids situated closer to the central zero point indicate minor changes, whereas those moving away from zero, in either direction, signify more substantial alterations. Results with a $p < 0.05$ are highlighted in black.

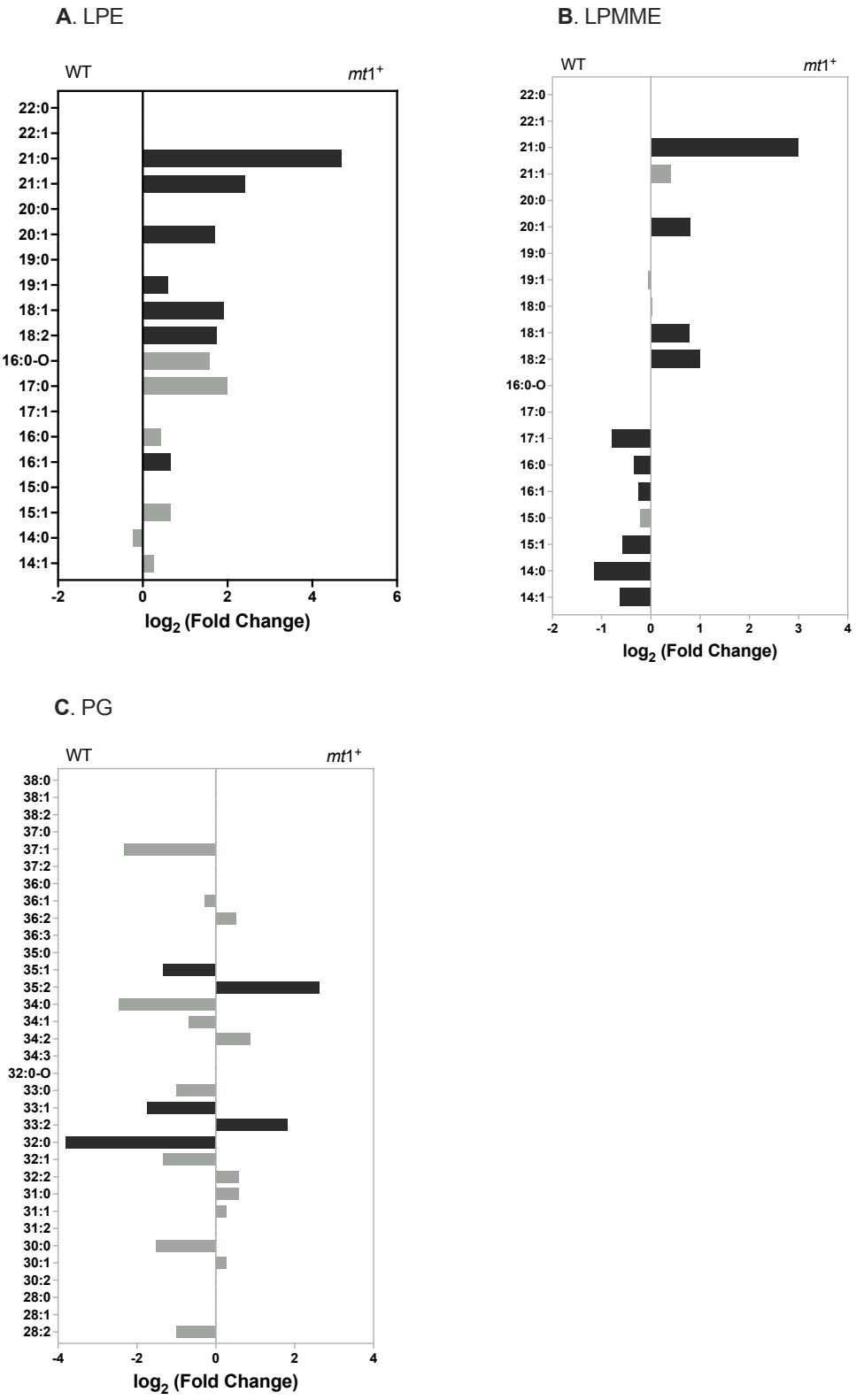

Figure 5.31. Univariant analysis of the LPE, LPMME and PG identified in the WT and *mt*1^{+} strains. Comparison of the phospholipid classes: (A) LPE; (B) LPMME, and (C) PG. The x-axis corresponds to the $\log_2$ (fold-change) between the *mt*1^{+} and WT strains. Significant results ($p < 0.05$, uncorrected Dunn's test) are highlighted in dark. Results from four independent biological repeats (n=4).

For LPE, lipid molecules were compared, with FA chain lengths ranging from14 to 22 carbons and with different unsaturation levels. In Figure 5.31A the fold change between *mt*1^{+} and WT shown 7 LPE lipid molecules yielded significant differences (p < 0.05, Annex 7) and higher percentages on the *mt*1^{+} strain. These lipids corresponded to: LPE (16:1), LPE (18:2), LPE (19:1), LPE (18:1), LPE (21:1), LPE (20:1) and LPE (21:0). No lipids with a significant and increased fold-change in the WT were noted.

For LPMME, lipid molecules were compared, with FA chain lengths ranging from14 to 22 carbons and with different unsaturation levels. In Figure 5.31B the fold change between *mt*1^{+} and WT shown 4 LPMME lipid molecules yielding significant differences (p < 0.05, Annex 7) and higher percentages on the *mt*1^{+} strain. These lipids corresponded to: LPMME (18:2), LPMME (20:1), LPMME (18:1) and LPMME (21:0). In higher concentrations in the WT strain, 6 LPMME lipid molecules were found to be statistically relevant (p < 0.05, Annex 7). These lipids corresponded to: LPMME (14:0), LPMME (14:1), LPMME (15:1), LPMME (16:0), LPMME (16:1) and LPMME (17:1).

Within the phospholipid class PG, lipids with FA chain lengths ranging from 28 to 38 carbons and different unsaturation levels and including a plasmalogen form of PG(32:0-O) were compared between WT and *mt*1^{+} (Figure 5.31C). This analysis shown 2 PG lipid molecules yielding significant differences (p < 0.05, Annex 7, Annex 8) and higher percentages on the *mt*1^{+} strain. These lipids corresponded to: PG (33:2) and PG (35:2). In higher concentrations in the WT strain, 3 PG lipid molecules were found to be statistically relevant (p < 0.05, Annex 7). These lipids corresponded to: PG (32:0), PG (35:1) and PG (33:1).

These results emphasize the significant differences obtained for the total LPE, LPMME and PG quantified in the WT and *mt*1^{+} strains. Non-significant differences were obtained for the other lipid groups identified in the four biological replicates of the two strains. However, to analyse significant changes in each individual lipid within the three strains, a graphical representation known as a "volcano plot" was employed (Figure 5.32).

Individual lipids from all lipid classes identified were plotted in a "volcano plot," as depicted in Figure 5.32. The plot charts the fold-changes of lipids on the x-axis against the significance of those changes on the y-axis. Lipids with significant production differences are highlighted with orange dots (*p-values* < 0.01) and blue dots (*p-values* < 0.05), with those closer to the x-axis' zero point indicating minimal changes and those farther indicating substantial changes.

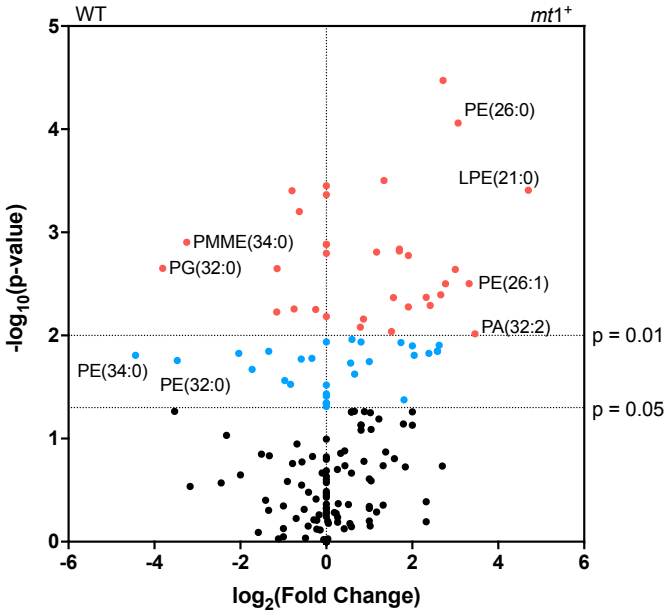

Figure 5.32. Lipid analysis between *mt*1^{+} and WT strains. The volcano plots summarize both fold-change and p-value criteria for all lipids identified in the strains. Black dots indicate non-significant results ($p \geq 0.05$). Blue dots indicate significant results ($0.05 < p \geq 0.01$). Orange dots indicate highly significant results ($p < 0.01$). Positive values correspond to the lipids more produced in the *mt*1^{+} strain. Negative values correspond to the lipids more produced in the WT strain. Results from four biological replicates (n=4). The *p-values* were calculated using the uncorrected Dunn's test.

In Figure 5.32 statistically different lipids, with a fold-change higher than 3 between strains were highlighted. This analysis has shown that PE(26:0), LPE(21:0), PE(26:1) and PA(32:2) were significantly higher in the *mt*1^{+} strain. While PMME(34:0), PG(32:0), PE(34:0) and PE(32:0) were significantly higher in the WT strain. Despite having lower fold-changes, as detailed in Annex 7, a total of 63 lipid molecules exhibited statistical significance (p <0.05) between these two strains. A considerable segment of these lipids was part of the PMME, PE, LPMME, PG, and LPE lipid groups, with noteworthy differences in PE and LPE being especially more abundant in the *mt*1^{+} strain.

Fatty Acid analysis

To complement the lipidomic characterisation of these three strains, the FAs identified were analysed. The aim was to compare the FA chain length and the number of unsaturations between the *mt*1^{+} and the WT strains. The FAs were grouped into three categories based on their chain length, specifically containing between 14-22, 23-32, and 33-38 carbons. The first

group (14-22 carbons) includes the number of carbons identified in all lysolipids. It also contains short-chain FAs found in some PE and PMME. The second group (23-32 carbons) was designed to represent lipids containing mid-size chain FAs. The last group (33-38 carbons) includes lipids with long chain FAs. This categorisation allows for an understanding of the distribution of FA chain lengths within the lipid classes and how these chain lengths vary across different strains (Figure 5.33).

According to Figure 5.33A, in general, both strains produced more lipids with FA chains ranging from 14 to 22 carbons, that corresponded essentially to the lysolipids LPE and LPMME. Lipids with FAs containing 23 to 32 carbons and lipids with FAs containing 33 to 38 carbons shown similar results between both strains. The results for all the FAs were also grouped based on the number of unsaturations. As shown in Figure 5.33B, the highest percentage of FAs had between 0 or 1 unsaturation, while very few had 2 or 3 unsaturations. Notably, the FA size and unsaturation levels exhibited considerable similarity between the *mt*1^{+} and WT strains.

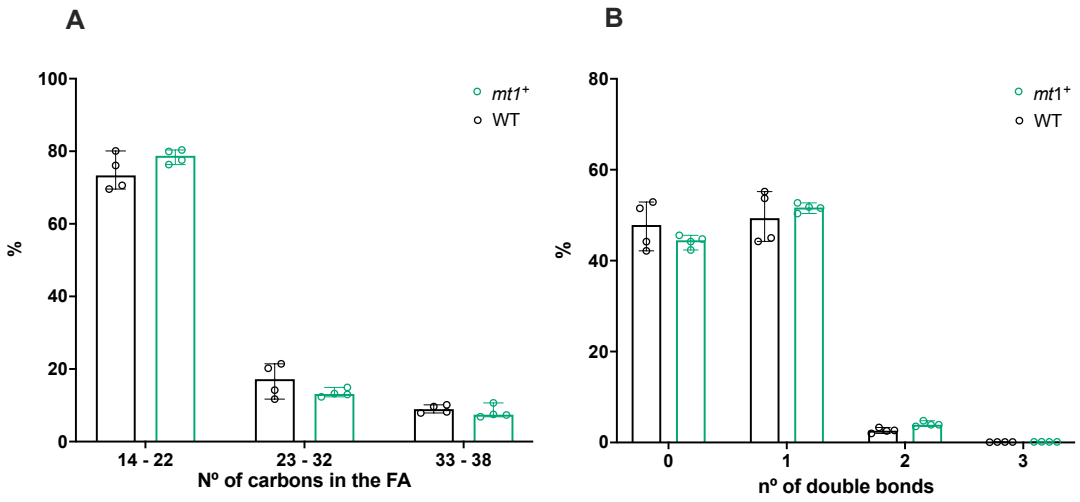

Figure 5.33. FA chains in the WT and *mt*1^{+} strains. Bar charts showing the median and 95% CI of: (A) FAs containing 14-22, 23-32 and 33-38 carbons; (B) FAs containing 0, 1, 2 and 3 doubles bonds. Results were normalised to the total lipids identified in each sample. Samples from four independent biological replicates (*n*=4). Statistical test: non-parametric Kruskall-Wallis and uncorrected Dunn's test for multiple comparisons.

Figure 5.34 presents a univariate comparison of individual FAs between the WT and *mt*1^{+} strains, revealing 17 statistically significant variations in fold-change. Notably, only three FAs—17:1, 32:0, and 34:0—exhibited a fold-change higher in the WT strain. Conversely, the remaining 14

FAs—16:1, 18:1, 18:2, 19:0, 20:1, 21:0, 21:1, 22:0, 26:0, 26:1, 28:0, 28:1, 30:1, 35:2, 37:2, and 38:2—displayed a fold-change higher in the *mt*1^{+} strain, as detailed in Table 17.

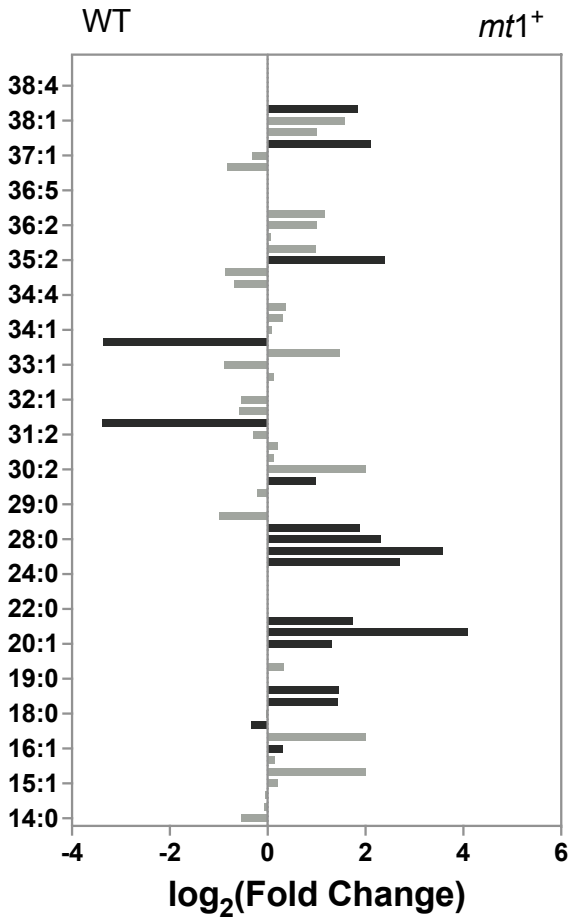

Figure 5.34. Univariant analysis of the Fatty Acid chains between the WT and *mt*1^{+} strains. Positive values represent the FA found in higher concentrations in the *mt*1^{+} strain. Negative values represent the FA found in higher concentrations in the WT strains. Significant results ($p < 0.05$) are highlighted in black. *p-values*: uncorrected Dunn's test. Results from four biological replicates (*n*=4).

Figure 5.35 depicts a volcano plot illustrating the distribution and statistical significance of FAs between the WT and *mt*1^{+} strains, highlighting the lipids that demonstrated statistically significant differences and a fold-change exceeding 2 between the strains. FAs 21:0, 26:1, and 35:2 were identified as statistically significant and exhibited a fold-change greater than 2, being more prevalent in the *mt*1^{+} strain. In contrast, FAs 32:0 and 34:0 were statistically significant and displayed a fold-change greater than 2, being more abundant in the WT strain.

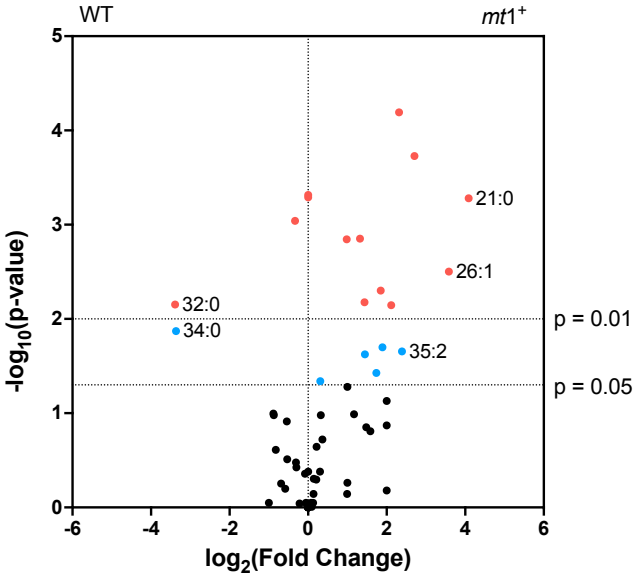

Figure 5.35. Fatty acid analysis between *mt*1^{+} and WT strains. The volcano plots summarize both fold-change and p-value criteria for all FAs identified in the strains. Black dots indicate non-significant results ($p \geq 0.05$). Blue dots indicate significant results ($0.05 < p \geq 0.01$). Orange dots indicate highly significant results ($p < 0.01$). Positive values correspond to the lipids more produced in the *mt*1^{+} strain. Negative values correspond to the lipids more produced in the WT strain. Results from four biological replicates (n=4). The *p-values* were calculated using the uncorrected Dunn's test.

Comparison between the FA chain within the phospholipid classes PS, PE and PG

To investigate whether the overexpression of the *mt*1 gene in the genome of *C. saccharoperbutylacetonicum* N1-4 HMT affected the normal pathways of phospholipid biosynthesis and FA synthesis, a comprehensive analysis of the phospholipid classes PS, PE, and PG was conducted. Specifically, focusing on the FA chain length and unsaturation levels. This approach offers valuable insights into understanding of membrane thickness and fluidity, particularly at the 24-hour culture stage when cells undergo a transition towards the solventogenesis phase (Linney et al., 2023).

Table 17. List of Fatty acids analysed by univariance between the strains *mt*1^{+} and WT. Results with p <0.05 alongside the respective fold-change (FC)). Positive $\log_2$(FC) correspond to higher concentrations of FA found in the strain represented in the numerator and negative $\log_2$(FC) correspond to FA found in

higher concentrations in the strain represented in the denominator. Uncorrected Dunn's test was used to calculate the *p-values*.

Lipid	Log_2 (FC)		*p-value*
	WT	*mt*1$^+$	
16:1	-	0.309	0.046
17:1	-0.333	-	0.001
18:1	-	1.434	0.007
18:2	-	1.447	0.024
19:0	-	0.000	0.000
20:1	-	1.322	0.001
21:0	-	4.087	0.001
21:1	-	1.737	0.037
22:0	-	0.000	0.001
26:0	-	2.708	0.000
26:1	-	3.585	0.003
28:0	-	2.316	0.000
28:1	-	1.893	0.020
30:1	-	0.982	0.001
32:0	-3.388	-	0.007
34:0	-3.365	-	0.013
35:2	-	2.389	0.022
37:2	-	2.115	0.007
38:2	-	1.848	0.005

Figure 5.36 illustrates the distribution of FAs chain lengths within three phospholipid classes (PS, PE, and PG). In the group of phospholipids containing 14 to 22 carbons in the acyl chain (Figure 5.36C), significant differences were observed between the *mt*1$^+$ and WT strains (p= 0.0048). Specifically, the median percentage of PE (14-22) in the WT strain was 0.007% (95% CI, 0.00 – 0.03), while in the *mt*1$^+$ strain, it significantly increased to 0.39% (95% CI, 0.37 – 0.42). This represents a more than 50-fold increase in the *mt*1$^+$ strain compared to the WT.

For the group of lipids with FAs ranging from 23 to 32 carbons and from 33 to 38 carbons, there were no significant differences in the percentage of PE, PG, and PS levels between the *mt*1$^+$ strain and the WT strains. Both strains exhibited similar percentages of FAs within each group, as shown in Figure 5.36A, B, D. Figure 5.37 details the analysis of the unsaturation levels found within the acyl chains of various phospholipids, which include PS, PE, and PG. For PE, the highest percentage had 0 and 1 double bonds in the FAs (Figure 5.37A). However, the percentage of PE molecules with FAs having 0 to 3 double bonds exhibited similar results between both strains. Regarding PG, the predominant percentage of PG molecules contained 0 to 1 double bonds in their FAs, as depicted in Figure 5.36B. Notably, significant differences were observed in the percentage of PG with 2 unsaturations (p=0.0159). In the *mt*1$^+$ strain, the percentage of PG with 2 unsaturations was significantly higher, with a median of 16.01% (95% CI, 13.94 – 17.38),

compared to the WT strain, where it amounted to a median of 2.7% (95% CI, 1.173 – 4.28). With 0, 1 and 3 unsaturations, the percentage of PG among the two strains did not result in significant differences.

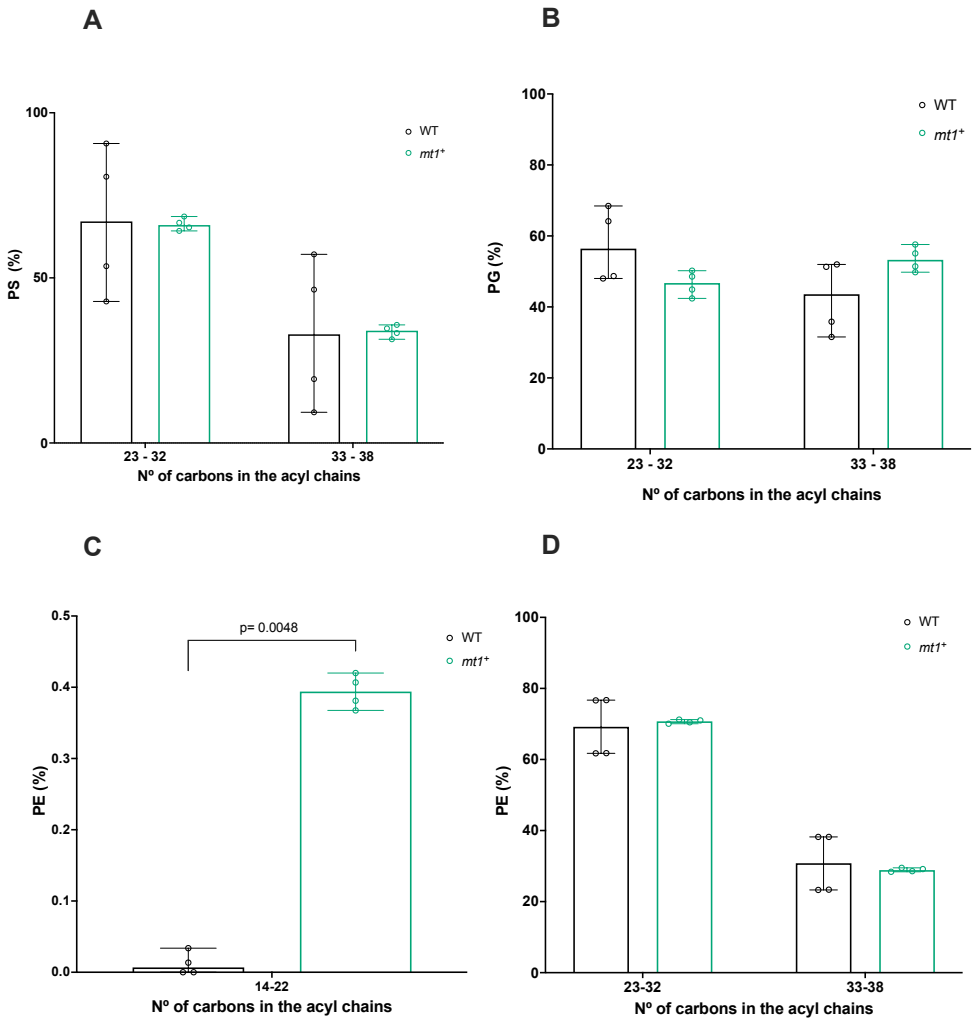

Figure 5.36. Analysis of Fatty Acid chains within various phospholipid classes in WT and *mt*1^{+} strains: (A) PS; (B) PG; (C and D) PE. The bars represent the median and 95% Confidence Interval (CI) of the percentage of FAs, categorized by chain lengths: 14-22, 23-32, and 33-38 carbons. Data derived from four independent biological replicates (*n*=4). Statistical analysis employed the non-parametric Kruskall-Wallis test and an uncorrected Dunn's test for multiple comparisons.

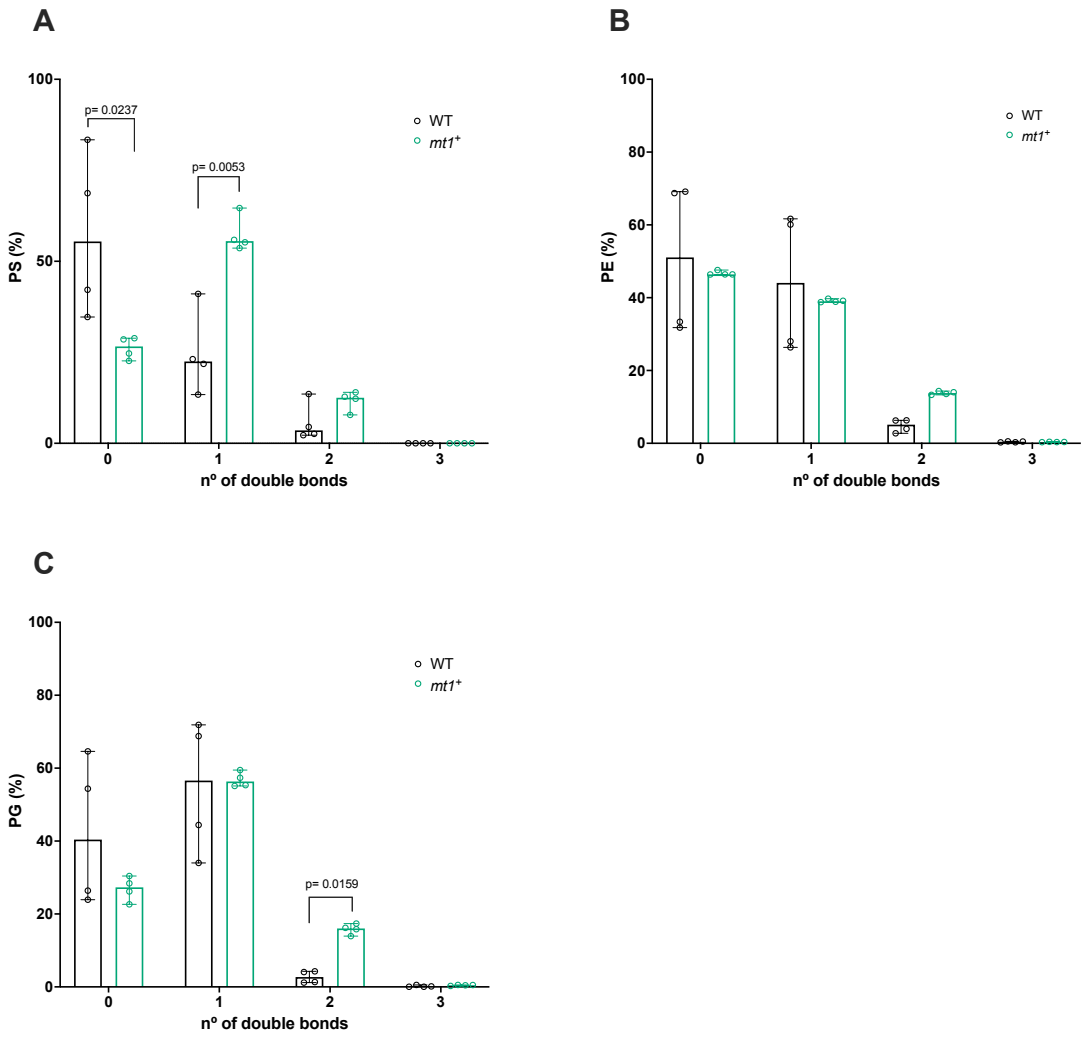

Figure 5.37. Analysis of the number of unsaturations within the phospholipid classes: (A, B) PS; (C) PE; in the WT and *mt*1^{+} strains. Bars represent the median and 95% Confidence Interval (CI) of the percentage of FAs containing 0 to 3 double bonds. Data from four independent biological replicates (*n*=4). Statistical analysis conducted using non-parametric Kruskall-Wallis and uncorrected Dunn's test for multiple comparisons.

Significant differences were obtained for PS with either 0 or 1 double bonds, as indicated in Figure 5.37C. The WT strain demonstrated significantly elevated levels of PS without double bonds, compared to *mt*1^{+}, yielding a *p-value* of 0.0237. Additionally, the median percentage of PS without unsaturations distinctly varied between the strains, specifically, 55.44% (95% CI, 34.7 – 83.37) for the WT and 26.61% (95% CI, 22.63 – 28.88) for the *mt*1^{+} strain.

Conversely, the *mt*1^{+} strain showed significantly higher levels of PS with 1 unsaturation in contrast to the WT strain, registering a *p-value* of 0.0053. The proportion of PS with a single

unsaturation diverged, presenting medians of 22.47% (95% CI, 13.39 – 41.05) for the WT strain and 55.54% (95% CI, 53.63 – 30.03) for the *mt*1^{+} strain. Nevertheless, PS that contained FAs with 2 double bonds showed comparable percentages between the two strains, as visualized in Figure 5.36A.

Summary

The mass spectrometry analysis highlighted significant differences in lipid composition between the WT and *mt*1^{+} strains, across the investigated lipid classes. By cloning a vector to overexpress *mt*1 gene, which is a ROS scavenger in *C. saccharoperbutylacetonicum* N 1-4 HMT strain, a discernible impact on the composition of membrane lipids was obtained as detailed in Table 18. It is important to highlight the decrease in PG, and the lower concentrations of lipids obtained for the *mt*1^{+}strain relatively to the WT. The decrease in PG can potentially be indicative of an increase in CL. Having that information regarding the mass spectrometry will help clarifying this hypothesis in the future, which is in concordance with an increase of *cls* expression under acidic conditions in *S. mutans* (Sohlenkamp, 2017). The differences on the lipid concentration leads to questions as to whether there exist other lipid classes that have not been identified which might counterbalance these findings, or if this is a result of the cells in the *mt*1^{+}strain being smaller than those in the WT, as visualized in Annex 2, Figure 24.1.

Table 18. Summary of the mass spectrometry analysis of the WT and *mt*1^{+}.

	lipids	*mt*1^{+}	notes
Total lipid groups	LPE	More than WT	Role of lysolipids in the membrane? Damaged lipids?
	LPMME	Less than WT	
	PG	Less than WT	-
Lipid group vs FA chain	Total FAs/ unsaturations	**Similar** to WT	Same membrane thickness and fluidity, overall?
	PS acyl chain length	**Similar** to WT	-
	PS acyl chain unsaturations	Less 0 unsaturations than WT More PS(1) and PS(2) than WT	
	PE acyl chain length	More Shorter FAs (14-22) than WT (very low percentage)	-
	PE acyl chain unsaturations	**Similar** to WT	
	PG acyl chain length	**Similar** to WT	Negative charged lipids with more unsaturations.
	PG acyl chain unsaturations	More PG(2) than WT	

5.2.4 Mass Spectrometry data analysis in *BCL* strain

The *BCL* strain is a C. *saccharoperbutylacetonicum* N 1-4 HMT strain mutant generated by the industrial partner Biocleave Ltd. This mutant has been shown to have different membrane morphologies, the TLC results shown small variations on the lipids between *BCL* and WT. To better comprehend this phenotype, the *BCL* culture cells from four biological replicates, sampled at 24h of incubation, were analysed by mass spectrometry. This analysis successfully identified lipids from 9 distinct lipid groups, which included PA, PG, LPE, PE, LPMME, PMME, PS, Cer-PMME and DihexDAG in the *BCL* strain.

Lipid group analysis

The production of the identified lipid groups varied between the WT and *BCL* strains and their relative abundance in the cells is shown in Figure 5.38. On average a total of 5.70 and 5.59 nmol of lipids per 10^6 cells were identified in the WT and *BCL* strains, respectively. According to Figure 5.38, LPE, PE and LPMME remained the main group of lipids identified in the two strains, corresponding to around 80-90% of all the lipids identified in this analysis. The other lipid groups were identified in lower percentages.

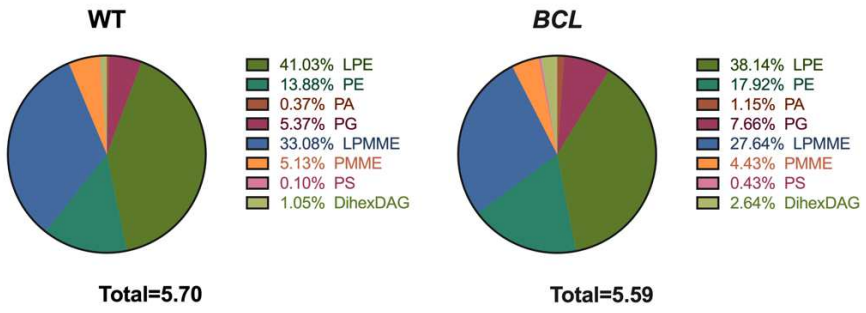

Figure 5.38. Overall lipid distribution in the WT and *BCL* strains. The charts depict the relative abundance of the lipid classes identified by mass spectrometry. Different colours distinguish different lipid classes. Data from four biological replicates for each strain, expressed in percentage and the total lipids in nmol of lipid per 10^6 cells.

To better comprehend the differences in lipid profiles between strains, the results were normalized to the total lipids identified in each sample and presented as the median of the percentage along with the 95% confidence interval (median, 95% CI). The outcomes were

graphically represented for each lipid group and differences between strains were analysed for significance using a non-parametric test, Kruskal-Wallis. Any significant differences identified within the lipid groups were analysed in more detail by univariant analysis.

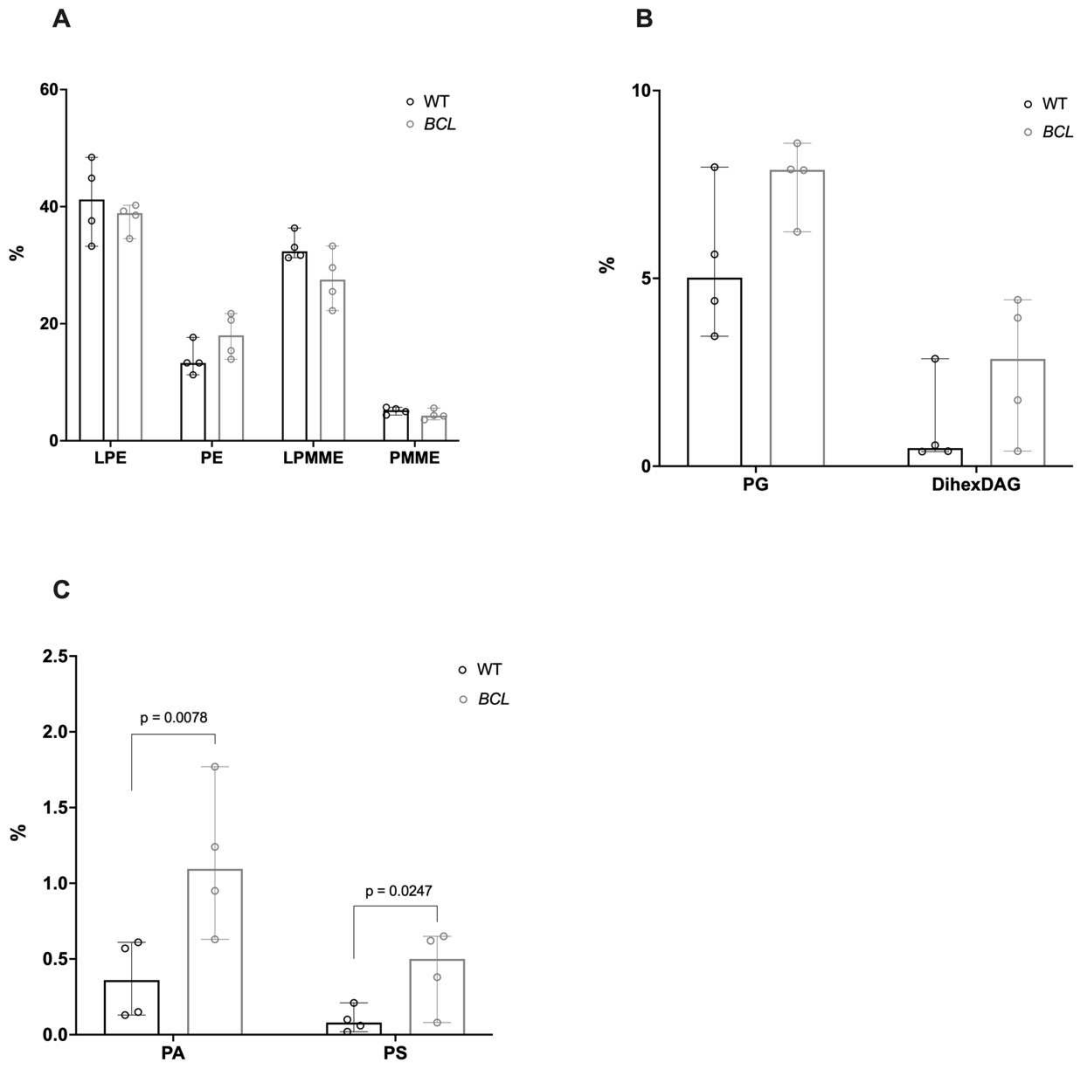

Figure 5.39. Lipid classes distribution in the WT and *BCL* strains. Bar charts showing the median and 95% CI of: (A) LPE, PE, LPMME and PMME; (B) PG and DihexDAG; (C) PA and PS. Results were normalised to the total lipids identified in each sample. Samples from four independent biological replicates (*n*=4). Statistical test: non-parametric Kruskall-Wallis and uncorrected Dunn's test for multiple comparisons.

Figure 5.39 presents results for the total LPE, PE, LPMME, PMME, PG, DihexDAG, PA and PS content obtained from the two strains. The lysolipids LPE and LPMME were consistently the predominant lipids identified across all strains (Figure 5.39A). PE, PMME, PG and DihexDAG were

detected in lesser concentrations. The percentages of the lipid groups containing ethanolamine in the head groups were similar between the *BCL* and WT strains (Figure 5.39A). The percentage of PG and DihexDAG did not shown significant differences between the two strains (Figure 5.39B).

Significant discrepancies were identified in the percentages of PA and PS between the two strains, with *p-values* of 0.0078 and 0.0247, respectively (Figure 5.39C). The *BCL* strain exhibited a higher percentage of PA compared to the WT, with medians of 1.09% (95% CI, 0.63 – 1.77) for *BCL* and 0.36% (95% CI, 0.13 – 0.61) for WT. The *BCL* strain also exhibited significantly higher percentage of PS, with medians of 0.50% (95% CI, 0.08 – 0.65) for *BCL* and 0.08% (95% CI, 0.02 – 0.21) for WT.

Considering the significant differences observed in the phospholipid classes between strains, the individual PA and PS, were characterised in more detail. All the lipid molecules from these two phospholipid classes quantified underwent univariate analysis. The forest plot in Figure 5.40 shown the fold-change of various lipid molecules quantified in the *BCL* and WT strains, where more abundant lipids in the *BCL* strain are positioned to the right of the x-axis.

Relative to PA, lipid molecules were analysed, regarding FA chain lengths that varied from 30 to 38 carbons and with various levels of unsaturation. Figure 5.40A shown certain lipid species identified with a fold change equating to zero, signifying no differences between the strains. The findings also highlighted 2 PA lipid molecules that exhibited significant differences ($p < 0.05$, Annex 8) and were more prevalent in the *BCL* strain. These lipids were identified as PA (30:0) and PA (34:0). No lipids demonstrated a significant and elevated fold-change in the WT strain.

Regarding PS lipid molecules, lipids with FA chain lengths that spanned from 28 to 38 carbons, along with various unsaturation levels were identified. In Figure 5.40B, a notable number of lipid species were identified with a fold change equating to zero, denoting no variations between the strains. The outcomes also displayed 4 PS lipid molecules that produced significant differences and higher percentages in the *BCL* strain ($p < 0.05$, Annex 8). These lipids identified were PS (30:0), PS (32:1), PS (32:0), and PS (35:1). No lipids exhibited a significant and higher fold-change in the WT.

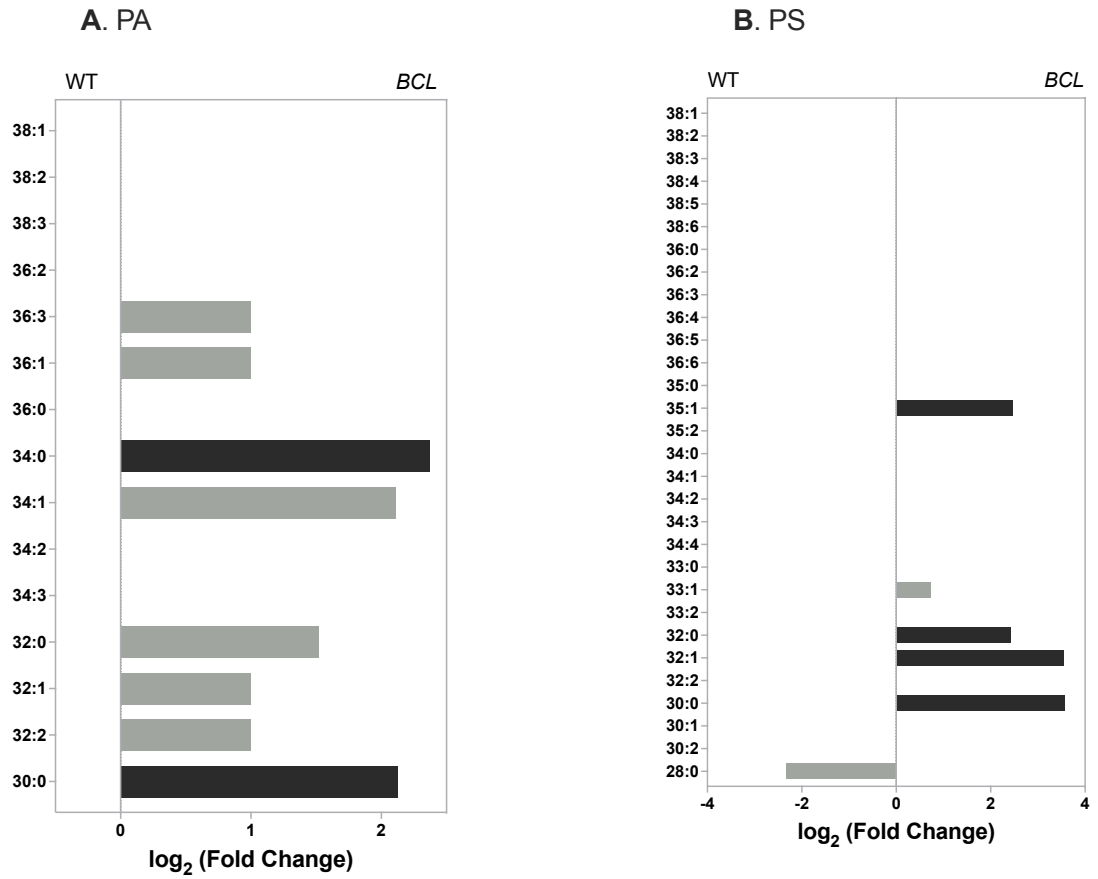

Figure 5.40. Univariant analysis of the PA and PS identified in the WT and *BCL* strains. Comparison of the phospholipid classes: (A) PA; (B) PS. The x-axis corresponds to the $\log_2$ (fold-change) between the *BCL* and WT strains. Significant results ($p < 0.05$, uncorrected Dunn's test) are highlighted in black. Results from four independent biological repeats (n=4).

These results emphasize the significant differences obtained for the total percentage of PA and PS in the WT and *BCL* strains. Non-significant differences were obtained for the other lipid groups identified in the four biological replicates of the two strains. However, to better understand significant changes within the two strains, a graphical representation known as a "volcano plot" with the individual lipids was employed (Figure 5.41). Lipids with significant production differences are highlighted with orange dots ($p < 0.01$) and blue dots ($p < 0.05$), with those closer to the x-axis' zero point indicating minimal changes and those farther indicating substantial changes.

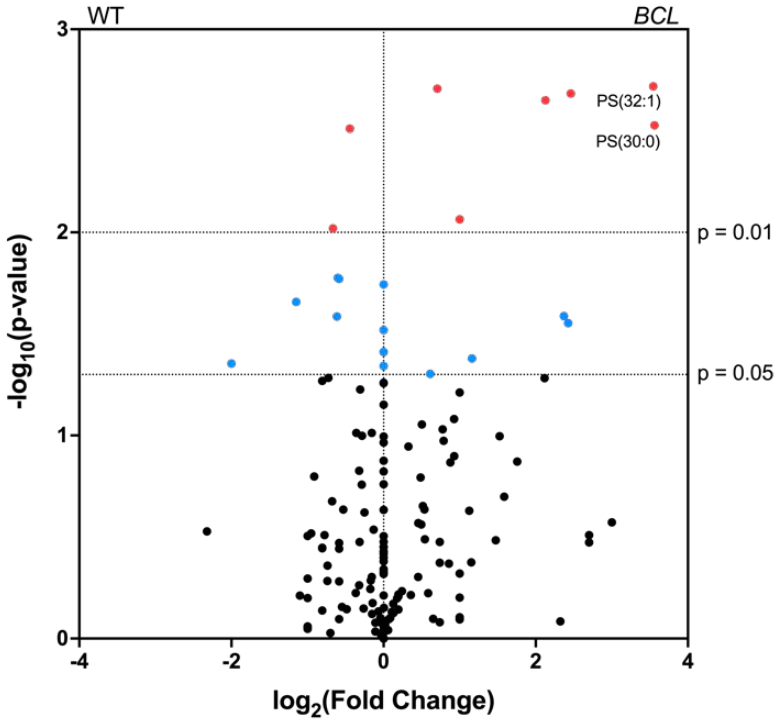

Figure 5.41. Lipid analysis between *BCL* and WT strains. The volcano plots summarize both fold-change and p-value criteria for all lipids identified in the strains. Black dots indicate non-significant results ($p \geq 0.05$). Blue dots indicate significant results ($0.05 < p \geq 0.01$). Orange dots indicate highly significant results ($p < 0.01$). Positive values correspond to the lipids more produced in the *BCL* strain. Negative values correspond to the lipids more produced in the WT strain. Results from four biological replicates (n=4). The *p-values* were calculated using the uncorrected Dunn's test.

In Figure 5.41 statistically different lipids, with a fold-change higher than 2.5 between strains were highlighted. This analysis has shown that PS (32:1) and PS (30:0) were significantly higher in the *BCL* strain, whereas no lipid met the criteria in the WT strain. Despite having lower fold-changes, as depicted in Annex 8, a total of 18 lipid molecules exhibited statistical significance (p<0.05) and a fold-change different than 0, between these two strains. A significant portion of these lipids belonged to the PS, PMME, and PE groups, with the PS group being predominantly in the *BCL* strain.

Fatty Acid analysis

To complement the *BCL* lipidomic characterization, the FAs identified were analysed alongside with the WT. The aim was to compare the FA chain length and the number of unsaturations between the *BCL* and the WT strains. The FAs were grouped into three categories based on their

chain length, specifically containing between 14-22, 23-32, and 33-38 carbons. This categorisation allowed an understanding of the distribution of FA chain lengths within the lipid classes and how these chain lengths varied across different strains.

Based on Figure 5.42A, both the *BCL* and WT strains predominantly produced lipids with FAs chains ranging from 14 to 22 carbons, largely corresponding to the lysolipids LPE and LPMME. Lipids featuring FAs with 23 to 32 carbons and those with 33 to 38 carbons demonstrated similar results across both strains. When the results were categorized based on the number of unsaturations, as depicted in Figure 5.42B, most FAs possessed 0 or 1 unsaturation, while a minimal number had 2 or 3 unsaturations. It was observed that the FA chain length and degree of unsaturation presented similar percentages between the *BCL* and WT strains.

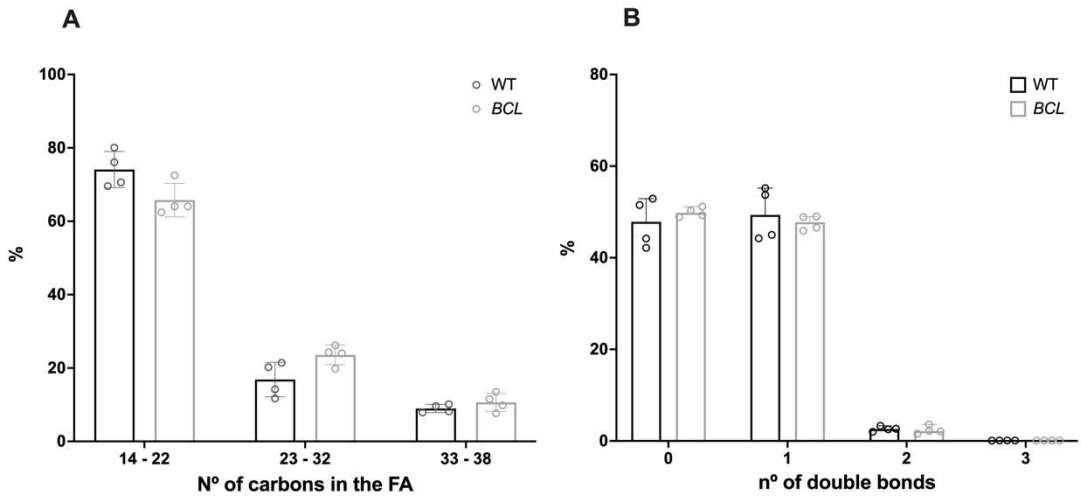

Figure 5.42. Analysis of the FA chains in the WT and *BCL* strains. Bar charts showing the median and 95% CI of: (A) FAs containing 14-22, 23-32 and 33-38 carbons; (B) FAs containing 0, 1, 2 and 3 doubles bonds. Results were normalised to the total lipids identified in each sample. Samples from four independent biological replicates (*n*=4). Statistical test: non-parametric Kruskall-Wallis and uncorrected Dunn's test for multiple comparisons.

Figure 5.43 presents a univariate comparison of individual FAs between the WT and *BCL* strains, revealing only 6 statistically significant variations in fold-change. Notably, only 3 FAs; 29:0, 30:0 and 34:1, exhibited a fold-change higher in the *BCL* strain. The other 3 FAs: 16:0, 18:0 and 33:2, displayed a fold-change higher in the WT strain, as detailed in Table 19. These results were shown in the volcano plot from Figure 5.44, where the 6 FAs with statistical differences were highlighted in the blue dots, however, none of them shown a fold-change higher then 2.

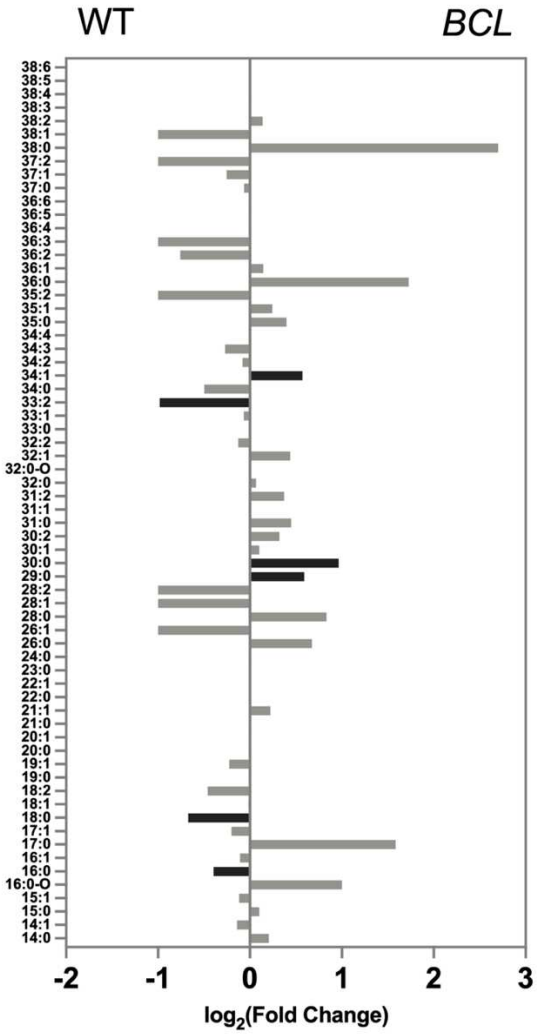

Figure 5.43. Univariant analysis of the Fatty Acid chains between the WT and *BCL* strains. Fold-change between *BCL* and WT. Positive values represent the FA found in higher concentrations in the *BCL* strain. Negative values represent the FA found in higher concentrations in the WT strains. Significant results ($p < 0.05$) are highlighted in black. *p-values*: uncorrected Dunn's test. Results from four biological replicates (n=4).

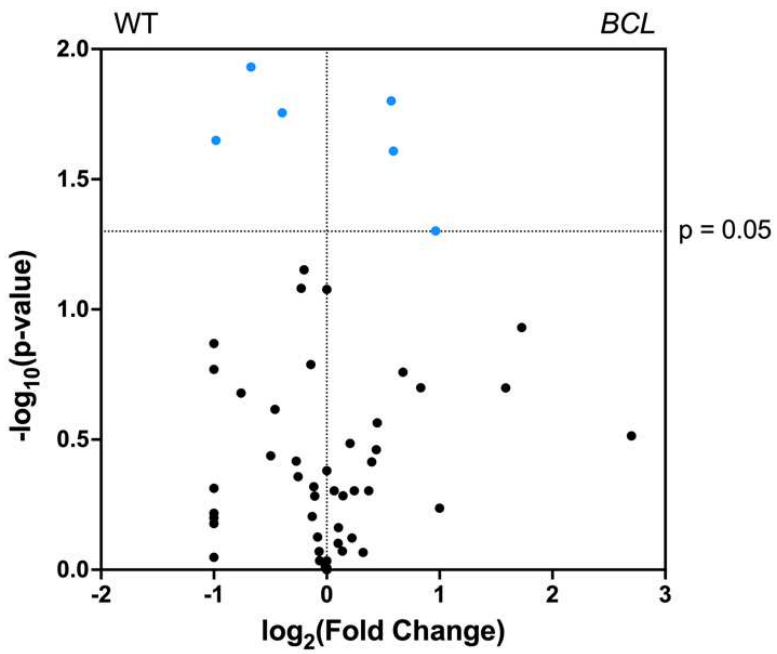

Figure 5.44. Fatty acid analysis between *BCL* and WT strains. The volcano plots summarize both fold-change and p-value criteria for all FAs identified in the strains. Black dots indicate non-significant results ($p \geq 0.05$). Blue dots indicate significant results ($0.05 < p \geq 0.01$). Orange dots indicate highly significant results ($p < 0.01$). Positive values correspond to the lipids more produced in the *BCL* strain. Negative values correspond to the lipids more produced in the WT strain. Results from four biological replicates (n=4). The *p-values* were calculated using the uncorrected Dunn's test.

Table 19. List of FAs analysed by univariance between *BCL* and WT. Results with $p < 0.05$ alongside with the fold-change (FC). Positive $\log_2$(FC) correspond to higher percentages of FA found in the *BCL* and negative $\log_2$(FC) correspond to FA found in higher percentages in the WT strain.

FA	Log_2 (FC)		*p-value*
	WT	*BCL*	
16:0	-0.395	-	0.018
18:0	-0.671	-	0.012
29:0	-	0.590	0.025
30:0	-	0.965	0.050
33:2	-0.982	-	0.022
34:1	-	0.570	0.016

Comparison between the FA chain within the phospholipid classes PS, PE and PG

To investigate whether of *C. saccharoperbutylacetonicum* N 1-4 HMT *BCL* strain provided by the industrial partner affected the normal pathways of phospholipid biosynthesis and FA synthesis, a comprehensive analysis of the phospholipid classes PS, PE, and PG was conducted. Specifically, focusing on the FA chain length and unsaturation levels. This approach offers valuable insights into understanding of membrane thickness and fluidity, particularly at the 24-hour culture stage when cells undergo a transition towards the solventogenesis phase (Linney et al., 2023).

Figure 5.45 illustrates the distribution of FA chain lengths within three phospholipid classes (PS, PE, and PG). Regarding the groups of lipids with FAs ranging from 14 to 22 carbons, from 23 to 32 carbons and from 33 to 38 carbons, there were no significant differences in the percentage of PE, PG, and PS levels between the *BCL* strain and the WT strains. Both strains exhibited similar percentages of FAs within each group.

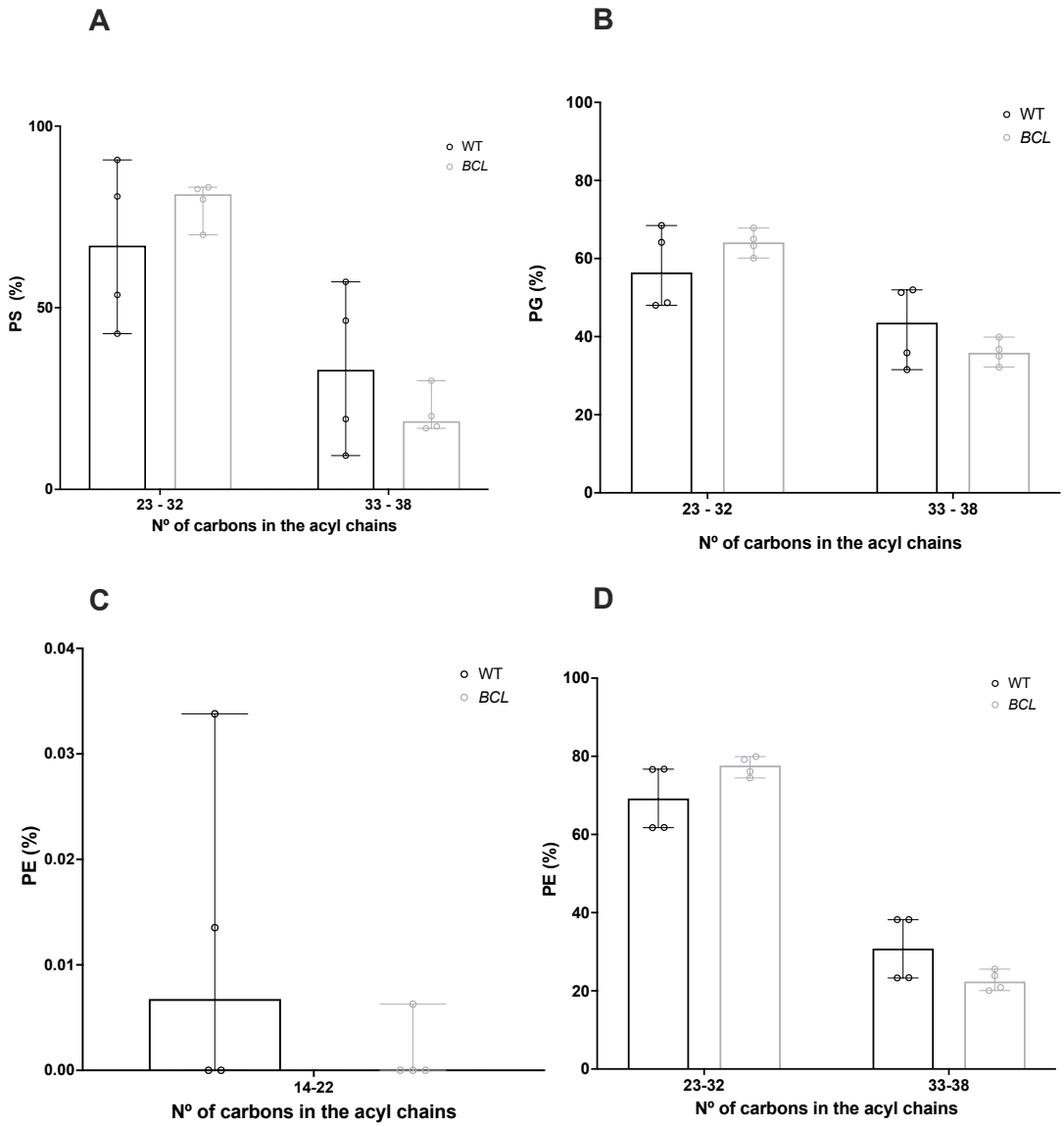

Figure 5.45. Analysis of the acyl chains in the phospholipid classes: (A) PS; (B) PG; (C and D) PE; identified in the WT and *BCL* strains. Bars showing the median and 95% CI of the percentage of FAs containing between 14-22, 23-32 and 33-38 carbons. Samples from four independent biological replicates (*n*=4). Statistical test: non-parametric Kruskall-Wallis and uncorrected Dunn's test for multiple comparisons.

A detailed the analysis of the unsaturation levels found within the acyl chains of the phospholipids PS, PE, and PG is shown in Figure 5.46. No significant differences were obtained for any of the lipid class with either 0, 1, 2 or 3 double bonds. The PS, PE ang PG lipids from BCL displayed a very similar content in the FA chain length and number of unsaturations as the WT strain.

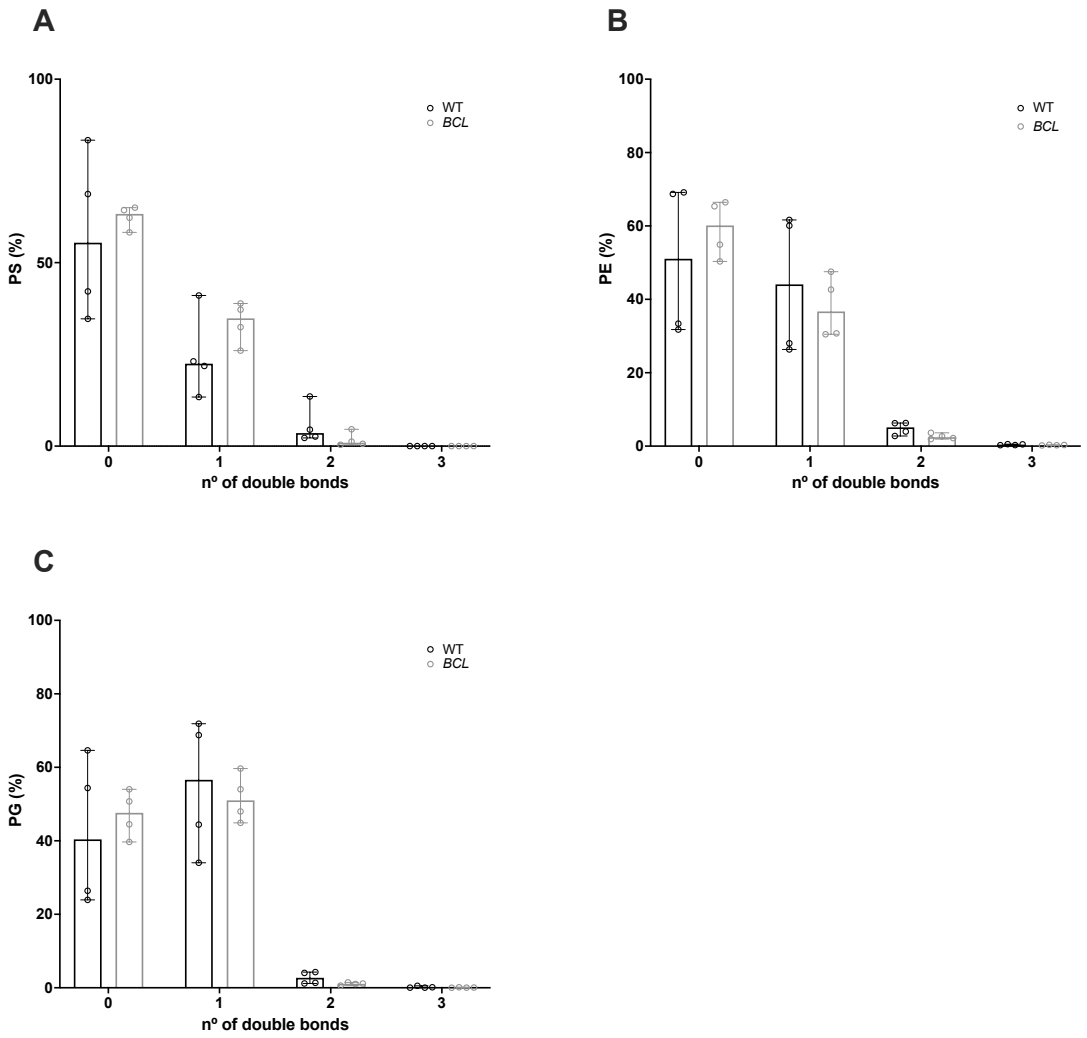

Figure 5.46. Analysis of the number of double bonds in the phospholipid classes: (A) PS; (B) PE and (C) PG; identified in the WT and *BCL* strains. Bars showing the median and 95% CI o of the percentage of FAs containing 0 to 3 double bonds. Samples from four independent biological replicates (*n*=4). Statistical test: non-parametric Kruskall-Wallis and uncorrected Dunn's test for multiple comparisons.

Summary

The mass spectrometry analysis highlighted very similar results between the *BCL* and WT strains. Very few differences were found for the lipid classes analysed, highlighting the PA and PS lipids that were found in higher fold-change in the *BCL* strain, which are intermediate lipids for PE and PG. Notably, even with the increased percentages of these intermediate lipids, there was not a corresponding rise in PE and PG percentages at the 24 h incubation mark.The FA chain length and number of unsaturations were also very similar between the *BCL* and WT strains.

Although the *BCL* strain has been described with a distinct membrane morphology when compared with the WT strain, the targeted mass spectrometry analysis revealed similar lipid profile to the WT. Analysing the lipidome of both strains at different time points during fermentation can provide a better and clear insight on the membrane lipid profile between the strains. Additionally, this targeted analysis was based on the knowledge of the lipid content in *Clostridium* strains from the same cluster as *C. saccharoperbutylacetonicum* N 1-4 HMT (Duerre 2005; Guan and Goldfine, 2021). Advances in lipidomics and a more detailed information on the *Clostridium* lipidome, mainly in *C. saccharoperbutylacetonicum* N 1-4 HMT will help characterising their mutant strain phenotypes. In conclusion, the hypothesis of *BCL* strain having different membrane morphology due to an alteration on the lipid composition need further analysis.

Mass spectrometry summary

Mass spectrometry analysis in the *C. saccharoperbutylacetonicum* N 1-4 HMT mutant and WT strains have highlighted differences in lipid composition:

- The Δ*pssA* and *pssA*$^+$ strains, contrasting lipidic phenotypes were observed. Interestingly the Δ*pssA* strain showed the presence of both PS and PE. Significantly lower percentage of PG was observed relative to the WT and *pssA*$^+$ strains. The *pssA*$^+$ strain indicated a considerably higher percentage of PE, FAs that span between 23-32 carbons and FAs without unsaturations.
- The strains *pgsA*$^+$ and *cls*$^+$ showed higher percentage of PE than the WT. However, no differences were observed for the PG produced by these two mutant strains, relatively to the WT.
- The *mt*1$^+$ strain was found to contain considerably fewer lipids compared to the other strains analysed, based on the lipid classes assessed. Significantly lower percentage of PG was observed relatively to the WT.
- The *BCL* strain revealed similar lipid composition as the WT. An evident distinction was the heightened proportion of PA and PS lipids in the *BCL*, and these lipids serve as precursors for the synthesis of PG and/or PE. Both *BCL* and WT strains manifested analogous FA chain lengths and unsaturation counts.
- Lysolipids were the main lipids observed among all strains however, the variations on the lysoplipdis observed need more analysis. It would be important to account for potential lipid damage during extraction or the mass spectrometry process itself, which

might explain the increased percentages (Criscuolo et al., 2020). Because of that it becomes challenging to distinguish between the percentage of lysolipids existent in the membrane and the percentage of lysolipids resultant from in-source fragmentation.

To sum up, the genetic changes in *C. saccharoperbutylacetonicum* N 1-4 HMT selected for this work had implications on their lipid composition. Moving forward, it is important to characterise the repercussions of these shifts on cell growth, solvents, and organic acids production.

6 Small-scale bottle screening results

The mutant strains Δ*pssA*, *pssA*$^{+}$, *pgsA*$^{+}$, *cls*$^{+}$, *BCL*, and *mt*1^{+} exhibited variations in lipid content compared to the WT in the TLC and mass spectrometry analysis. These mutations potentially affect phospholipid biosynthesis and oxidative stress levels in the cell, resulting in a distinct phenotype in the lipid membrane composition shown in the previous chapters. The key question was whether this altered lipid composition impacts cell growth and the production of acids and solvents during the acidogenesis and solventogenesis phases of ABE fermentation.

To investigate this, a pre-inoculum of these mutant and WT cells was prepared in RCM, and the cultures were grown overnight at 37°C in the anaerobic cabinet. Cells from the overnight culture were transferred to the fermentation culture media TYIR with 50 g.L^{-1} of glucose and 30 mM MES where they grew under anaerobic conditions, at 32°C for 48 h. Each strain was tested in at least five biological replicates.

Samples were collected from the small bottles at different time points (0h, 6h, 24h, and 48h) to assess growth by measuring the culture OD_{600} and pH. The consumption of glucose, and the production of organic acids (lactic acid, acetic acid and butyric acid) and solvents (acetone and butanol) was analysed by HPLC from samples collected at 0h, 6h, 24h, and 48h. However, some samples collected at 6h showed a small peak on the HPLC spectra that merged with the glucose peak at 10 minutes. This indicated glucose production, which did not align with the observed growth pattern, where glucose was being used as substrate and consequently its concentration must be decreasing. Consequently, the HPLC results for the 6h incubation samples were not included in the analysis.

For the HPLC analysis, different concentrations of standards were run in the HPLC column to create a standard curve, which was then used to calculate the concentration of the compounds in the collected samples. These samples from all biological replicates were filtered, diluted four times in HPLC grade water, and run in the HPLC for 50 minutes. Statistical analysis was performed by comparing the selected parameters between strains using the non-parametric test Kruskall-Wallis and the Dunn's test to analyse significant differences and calculate the p-value and for multiple comparisons, respectively. The tests were performed in GraphPad Prism 8.1.

6.1 Small-scale bottle screening of Δ*pssA* and *pssA*$^+$ strains

The Δ*pssA* and the *pssA*$^+$ strains were screened for their growth, acids and solvents production. Δ*pssA* overnight grown cultures exhibited differences comparing to the WT and *pssA*$^+$. In the microscope the Δ*pssA* cells displayed inferior growth compared to both the WT and *pssA*$^+$, characterized by reduced motility and an increased tendency to form aggregates (data not shown). Conversely, the overnight grown *pssA*$^+$ cells showed growth similar to the WT, forming dense cultures with motile and predominantly single cells. These differences observed in the overnight grown cells were consistent with the results obtained from small-scale bottle screening, encompassing growth, acids, and solvent production, as demonstrated across all biological replicates, comprising 7 replicates of the WT, 11 replicates of the Δ*pssA*, and 8 replicates of the *pssA*$^+$ strains (Figure 6.1).

Based on Figure 6.1A, it was observed that the WT, Δ*pssA*, and *pssA*$^+$ strains reached maximum OD_{600} values of 8.72 (95% CI, 7.16 – 10.26), 6.50 (95% CI, 6.93 – 13.15) and 10.98 (95% CI, 7.58 – 13.74) in median, respectively, signifying substantial differences among the strains. At 48h of incubation the *pssA*$^+$ strain exhibited significantly higher growth than the WT (p=0.033), whereas the Δ*pssA* strain demonstrated lower growth. This trend aligned with the results observed for glucose uptake, where the density positively correlated with glucose consumption in both the WT and *pssA*$^+$ strains (Figure 6.1C). Conversely, the Δ*pssA* strain exhibited a decrease in glucose consumption, correlating with a diminished cell growth.

Throughout the 48h of incubation, the pH of the WT and *pssA*$^+$ strains remained relatively stable. However, at the 24h and 48h marks, the pH of the mutant *pssA*$^+$ was higher than that of the WT, with p=0.008 and p=0.009, respectively. In contrast, the Δ*pssA* strain displayed a significant decrease in pH (p=0.015) at the 24h and 48h marks. The lower pH is indicative of the acidogenesis phase and unexpectedly did not exhibit the anticipated increase in pH during solventogenesis. This observation indicated an accumulation of acids in this Δ*pssA* strain, which is further supported by the graphs illustrating lactic acid, acetic acid, and butyric acid production (Figure 6.1B, D, E, F).

The Δ*pssA* strain exhibited a significantly higher production of lactic acid compared to the WT (Figure 6.1D). After 24h of incubation, lactic acid production was 0.16 (95% CI, 0.14 – 0.18) $g.L^{-1}$ for Δ*pssA*, 0.05 (95% CI, 0.025 – 0.13) for WT, and 0.13 (95% CI, 0.12 – 0.15) for the *pssA*$^+$ strain, indicating that both mutants produced more than twice as much lactic acid. However, after 48h of incubation, the *pssA*$^+$ strain likely reassimilated the lactic acid, as no extracellular lactic acid

was quantified, similarly to the WT strain. The Δ*pssA* strain retained the lactic acid concentration after 48h, with a median of 0.16 (95% CI, 0.14 – 0.18) g.L^{-1} and a p=0.062 when compared to the WT strain.

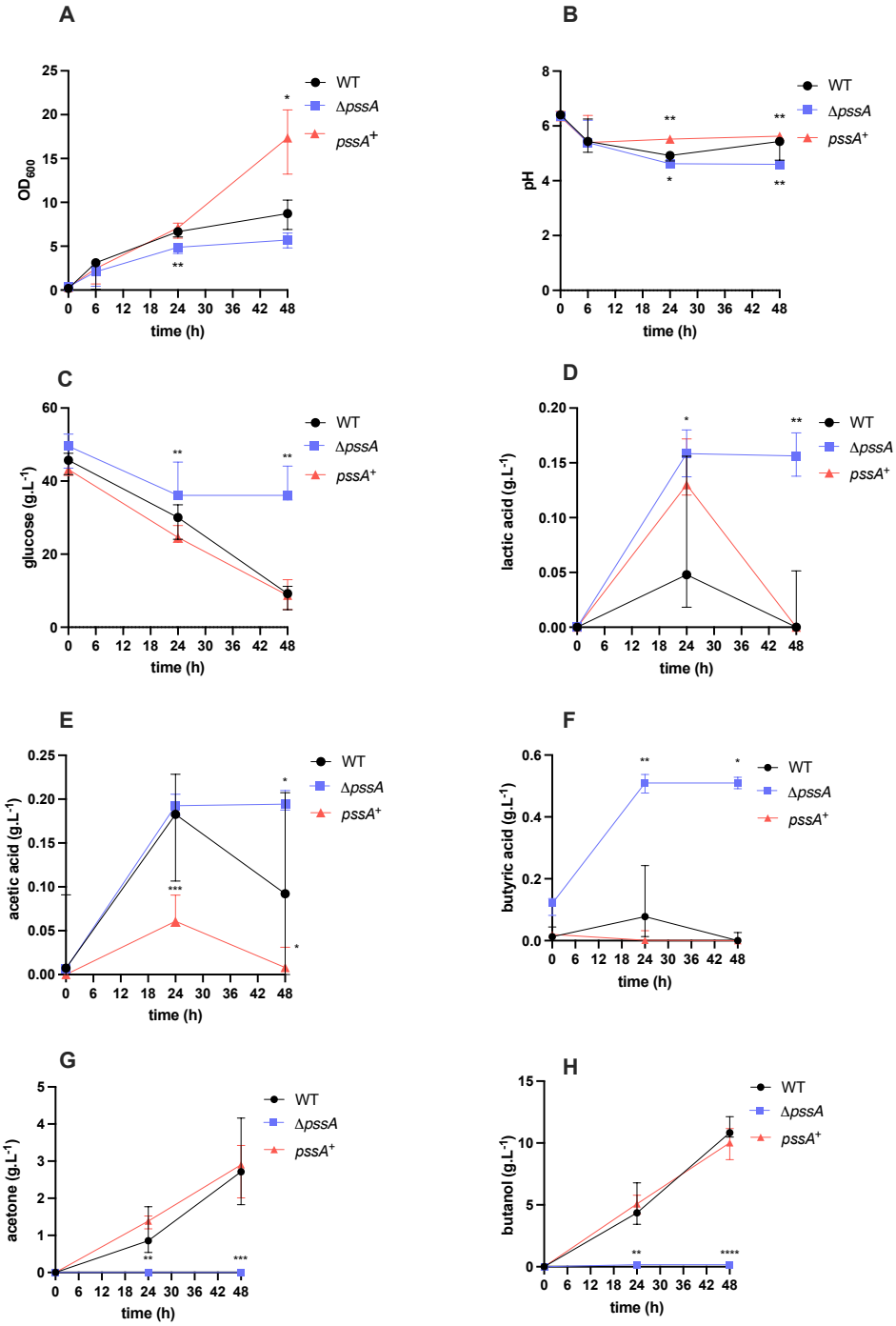

Figure 6.1. Bottle screening of Δ*pssA*, *pssA*$^+$ and WT strains. The graphs depict measurements of OD_{600}, pH, glucose consumption, organic acids and solvents produced. Cultures grown in TYIR with 50 g.L^{-1} of glucose and 30 mM MES, at 32 °C for 48h in anaerobic conditions. Values represented in median and 95% CI. Statistical test: non-parametric Kruskall-Wallis and uncorrected Dunn's test for multiple comparisons. *p <0.05, ** p <0.01; n = 11 (Δ*pssA*), n= 8 (*pssA*$^+$), n= 7 (WT)

In terms of acetic acid production, after 24h of incubation, similar concentrations were found in the WT and Δ*pssA* strains, corresponding to a median of 0.18 (95% CI, 0.14 – 0.20) $g.L^{-1}$ and 0.19 (95% CI, 0.18 – 0.20) $g.L^{-1}$, respectively (Figure 6.1E). In contrast, the *pssA*$^+$ strain only produced 0.06 (95% CI, 0.06 – 0.08) $g.L^{-1}$ of acetic acid in median, less than half of the other strains. However, at 48h, the concentration of acetic acid in WT and *pssA*$^+$ decreased to 0.092 (95% CI, 0.38 – 0.15) $g.L^{-1}$ and 0.008 (95% CI, 0.005 – 0.023) $g.L^{-1}$ in median, respectively. However, the extracellular acetic acid in Δ*pssA* cells was kept to a median of 0.19 (95% CI, 0.18 – 0.21) $g.L^{-1}$. The differences in extracellular acetic acid among the three strains were significant at the 24h and 48h mark of the small-scale fermentation.

Regarding butyric acid, the WT and *pssA*$^+$ strains started and finished the bottle screening with similar concentrations (Figure 6.1F). At 24h, the quantification of butyric acid resulted in 0.08 (95% CI, 0.03 – 0.17) $g.L^{-1}$ in median for WT and 0.001 (95% CI, 0.00 – 0.17) $g.L^{-1}$ in median for *pssA*$^+$, with no statistically significant difference. However, the Δ*pssA* strain exhibited a different pattern, reaching a maximum production of 0.50 (95% CI, 0.48 – 0.53) $g.L^{-1}$ at 24h, which was sustained until the end of the culture. Δ*pssA* strain produced significatively more butyric acid than WT at 24h and 48h mark, with p=0.005 and p=0.015, respectively.

Regarding solvent production, the *pssA*$^+$ strain showed a similar production to the WT strain. For acetone, the *pssA*$^+$ and WT strains reached a maximum of 2.90 (95% CI, 2.34 – 3.29) $g.L^{-1}$ and 2.71 (95% CI, 2.18 – 3.64) $g.L^{-1}$, respectively (Figure 6.1G). For butanol, both *pssA*$^+$ and WT strains followed a similar pattern, reaching a maximum concentration of 10.02 (95% CI, 9.29 – 10.63) $g.L^{-1}$ and 10.84 (95% CI, 10.56 – 11.65) $g.L^{-1}$, respectively (Figure 6.1H). Both strains produced very similar acetone and butanol concentrations. On the other hand, Δ*pssA* cells did not produce any detectable extracellular acetone or butanol, suggesting that the acids produced were being accumulated and not converted into solvents.

The Δ*pssA* and *pssA*$^+$ mutants exhibited opposite phenotypes for the aspects studied in this assay. Growth, acid production, pH results, and solvent production were all contrasting between the two mutants, with *pssA*$^+$ producing similar amounts of solvents as the WT, while Δ*pssA* only accumulated acids.

6.2 Small-scale bottle screening of *pgsA*$^+$ strain

The *pgsA*$^+$ strain, designed to produce more phosphatidylglycerol, was screened for its growth, acid and solvent production compared to the WT strain (Figure 6.2). The overnight grown cultures of the *pgsA*$^+$ strain showed higher density compared to the WT cultures. However, for pH range and motility, the mutant cells were very similar to the WT. The similarities observed in the overnight grown cells were consistent with the results obtained from the small-scale bottle screening, encompassing growth, acids, and solvent production, as demonstrated across all biological replicates, comprising 7 replicates of the WT and 9 replicates of the *pgsA*$^+$ strains (Figure 6.2).

It is important to acknowledge that the results presented for butyric acid and acetone are representative of six biological replicates instead of nine. The HPLC spectra showed the butyric acid peak around 25.9 minutes, and the acetone peak follows closely at around 26.3 minutes. However, in three out of the nine biological replicates, the two peaks were too close, resulting in overlapping, which hindered reliable separation of the peaks. Therefore, the data from these three biological replicates for both butyric acid and acetone were excluded from the analysis to ensure the accuracy and validity of the results.

In terms of growth, *pgsA*$^+$ cell cultures reached a maximum optical density of 14.10 (95% CI, 10.65 – 16.46) g.L^{-1}, which was higher than for the WT, that corresponded to 8.72 (95% CI, 7.16 – 10.26) g.L^{-1}, however the variability among the replicates resulted in non-significative differences (Figure 6.2A). However, the glucose uptake and pH variations were very similar between both strains (Figure 6.2B, C). Both strains exhibited a decrease in pH during the acidogenesis phase, followed by an increase during the solventogenesis phase.

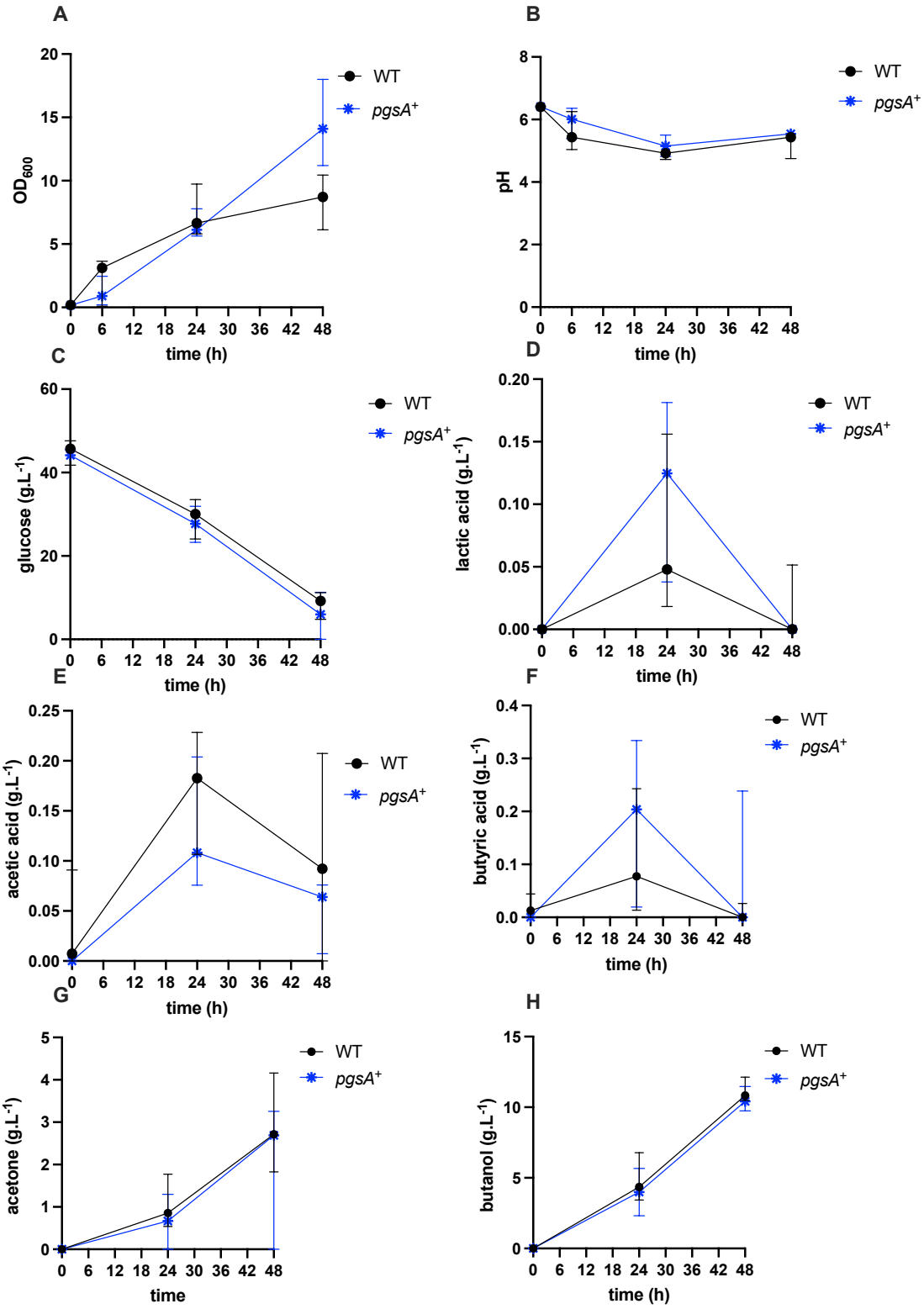

Figure 6.2. Bottle screening of *pgsA*$^+$ and WT strains. The graphs depict measurements of OD_{600}, pH, glucose consumption, organic acids and solvents produced. Cultures grown in TYIR with 50 $g.L^{-1}$ of glucose and 30 mM MES, at 32 °C for 48h in anaerobic conditions. Values represented in median and 95% CI. Statistical test: non-parametric Kruskall-Wallis and uncorrected Dunn's test for multiple comparisons. * p <0.05, ** p <0.01; n = 9 (*pgsA*$^+$), n = 7 (WT).

During the acidogenesis phase and the transition to the solventogenesis phases, there were no significant differences observed in the production and uptake of lactic acid, acetic acid, and butyric acid between the WT and *pgsA*$^+$ strain (Figure 6.2D, E, F). At 24h, marking the lactic acid maximum production, similar concentrations were quantified for the WT and *pgsA*$^+$ strains, corresponding in median to 0.05 (95% CI, 0.03 – 0.13) g.L^{-1} and 0.05 (95% CI, 0.02 – 0.15) g.L^{-1}, respectively. Very similar results between strains were observed for acetic acid and butyric acid at 24h. For acetic acid in WT and *pgsA*$^+$ a median of 0.18 (95% CI, 0.14 – 0.20) g.L^{-1} and 0.12 (95% CI, 0.08 – 0.18) g.L^{-1} was obtained. For butyric acid in WT and *pgsA*$^+$ a median of 0.08 (95% CI, 0.03 – 0.17) g.L^{-1} and 0.20 (95% CI, 0.01 – 0.35) g.L^{-1} was obtained, respectively.

In addition to the similar production and assimilation of organic acids between the WT and the *pgsA*$^+$ strains, there were no significant changes observed in the production of solvents, specifically acetone and butanol, between the two strains. The mutant strain exhibited very similar solvent production to the WT throughout the bottle screening process (Figure 6.2H).

In conclusion, the *pgsA*$^+$ strain exhibited a phenotype that was largely similar to the WT cells in terms of weak acid production, uptake, and solvent production. This is in concordance with the growth pattern, glucose uptake, pH variation, and motility in the microscope that was comparable to the WT strain.

6.3 Small-scale bottle screening of *cls*$^+$ strain

The *cls*$^+$ strain intended to increase cardiolipin levels, was screened for its growth, acids and solvent production and compared to the WT strain (Figure 6.3). The mutant cells were cultivated overnight and exhibited similarities in terms of growth and motility compared to the WT, with the main distinction being a slightly more acidic pH. The overnight cultures pH ranged from pH 4.8 to 5, whereas in the WT strain the pH was always higher than 5.

Figure 6.3 displays the results of 7 biological replicates for both the WT and the *cls*$^+$ strain. In terms of growth, *cls*$^+$ cell cultures reached a maximum optical density of 11.76 (95% CI, 9.29 – 14.18), which was higher than for the WT, that corresponded to 8.72 (95% CI, 7.16 – 10.26), however the variability among the replicates resulted in non-significative differences (Figure 6.3 A). The glucose uptake by both strains was similar. A slight pH variation in the 6h mark of the small-scale bottle screening was observed, and this result was aligned with the longer lag phase, as shown in the optical density curve (Figure 6.3A, B). Both strains exhibited a decrease in pH during the acidogenesis phase, followed by an increase during the solventogenesis phase.

Regarding organic acids production during the acidogenesis phase, no significant differences were observed for the lactic acid (Figure 6.3D). The lactic acid production and uptake by the *cls*$^+$ strain was very similar to the WT throughout the cell culture. For acetic acid production, both WT and *cls*$^+$ strains produced similar concentrations (Figure 6.3E). For butyric acid in WT and *cls*$^+$ a median of 0.08 (95% CI, 0.03 – 0.17) g.L^{-1} and 0.27 (95% CI, 0.21 – 0.37) g.L^{-1} was obtained, respectively (Figure 6.3F). Despite the rise in butyric acid concentration in the *cls*$^+$ strain, substantial variability among replicates resulted in non-significant differences.

For solvent production, at 24 hours of culture, the *cls*$^+$ strain exhibited no detectable acetone on the HPLC, whereas the WT strain yielded a median of 0.86 (95% CI, 0.57 – 1.31) g.L^{-1}. This might be correlated with the longer lag phase observed in the *cls*$^+$ cell growth. However, upon concluding the culture period (48h), the acetone concentrations obtained were analogous between the WT and *cls*$^+$ strains, registering a median of 2.71 (95% CI, 2.18 – 3.64) g.L−1 and 2.49 (95% CI, 2.34 – 3.67) g.L^{-1}, respectively (Figure 6.3).

There were statistically relevant differences for butanol production, with the *cls*$^+$ strain being a less efficient butanol producer (p=0.013). The *cls*$^+$ strain produced in median 8.81 (95% CI, 7.78 – 9.15) g.L^{-1}, where the WT produced in median 10.84 (95% CI, 10.56 – 11.65) g.L^{-1} of butanol (Figure 6.3).

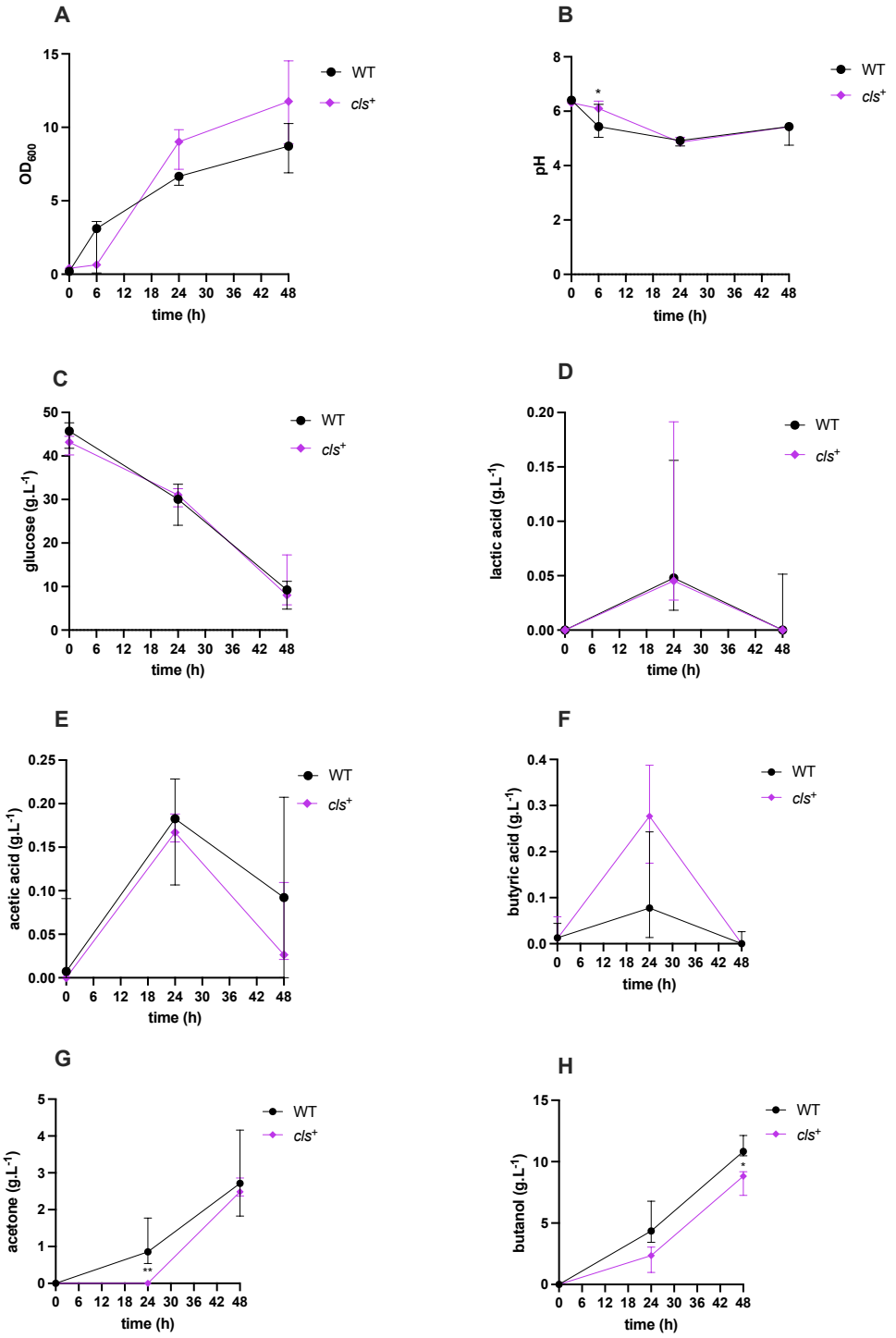

Figure 6.3. Bottle screening of *cls*$^+$ and WT strains. The graphs depict measurements of OD_{600}, pH, glucose consumption, organic acids and solvents produced. Cultures grown in TYIR with 50 $g.L^{-1}$ of glucose and 30 mM MES, at 32 °C for 48h in anaerobic conditions. Values represented in median and 95% CI. Statistical test: non-parametric Kruskall-Wallis and uncorrected Dunn's test for multiple comparisons. *p <0.05, ** p <0.01; n= 7 (*cls*$^+$), n= 7 (WT).

To conclude, even though the *cls*$^{+}$ strain exhibited longer lag phase compared to the WT, the density, pH, and glucose consumption aligned closely after 48h of culture. In the context of weak acids production, no substantial differences were discerned, however the butyric acid production seemed to be higher in the *cls*$^{+}$ than the WT strains. While a significant difference in acetone production was noted at the 24h time point, the outcomes converged to similarity between the strains by the end of the culture. However, a diminished butanol presence was detected in the *cls*$^{+}$ strain.

6.4 Small-scale bottle screening of *mt*1$^+$ strain

The *mt*1$^+$ strain, designed to possibly reduce the oxidative stress level in the cell, was screened for its growth, acids and solvents production and compared to the WT strain (Figure 6.4). Overnight cultures of *mt*1$^+$ strain displayed significant differences, exhibiting lower cell density compared to the WT cultures. In the microscope, the *mt*1$^+$ cells showed reduced motility and an increased tendency to form doubles and multi-chains.

Growth, organic acids, and solvent production were analyzed using the previously described techniques. Figure 6.4 displays the results from seven biological replicates of both the *mt*1$^+$ and WT strains. Regarding growth, the *mt*1$^+$ cell cultures displayed notably reduced growth at both 24h (p=0.0012) and 48h (p=0.026) in comparison to the WT cell cultures. The peak density achieved by the *mt*1$^+$ cell cultures was, in median, 4.5 (95% CI, 4.12 – 5.59), which was nearly half of what was obtained for the WT, corresponding to 8.72 (95% CI, 7.16 – 10.26) (Figure 6.4).

The growth curve aligned with the decrease in glucose uptake by *mt*1$^+$ strain. After 48h of incubation, the *mt*1$^+$ cultures retained 33.28 (95% CI, 32.69 – 34.02) g.L^{-1} of glucose, while in the WT cultures the remained glucose concentration was in median 9.22 (95% CI, 6.46 – 11.16) g.L^{-1} of glucose (Figure 6.4C).

For pH, after the *mt*1$^+$ strain displayed a decrease in pH, indicative of the acidogenesis phase, but it did not exhibit the expected increase in pH for the solventogenesis phase, as observed in the WT strain after 24h and 48h of incubation (Figure 6.4B). This observation suggests an accumulation of acids in this mutant strain, a trend supported by data illustrating lactic acid, acetic acid, and butyric acid quantification, shown in Figure 6.4D, E, F.

The *mt*1$^+$ strain exhibited a significantly higher production of lactic acid in comparison to the WT, with a p=0.0015 at 24h of culture (Figure 6.4D). At the 24h incubation mark, the *mt*1$^+$ cells generated 0.19 (95% CI, 0.17 – 0.21) g.L^{-1} of lactic acid, which is almost four times more than what was produced by the WT, measured at 0.05 (95% CI, 0.03 – 0.13) g.L^{-1}. Additionally, significantly higher concentrations of lactic acid were maintained in the *mt*1$^+$ cell culture even after 48h, amounting to 0.18 (95% CI, 0.17 – 0.20) g.L^{-1} of lactic acid, with a *p-value* of 0.0002.

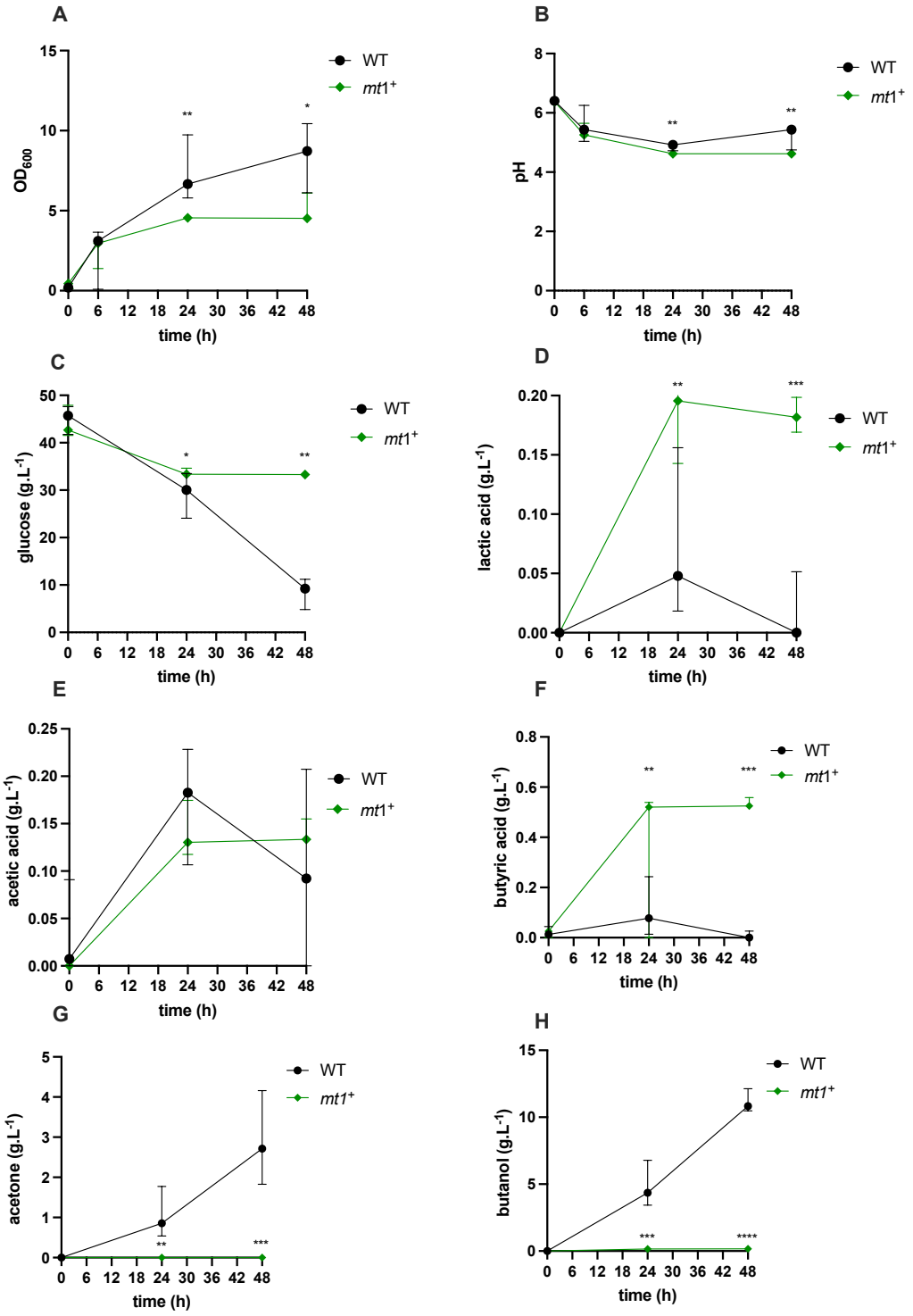

Figure 6.4. Bottle screening of *mt*1^{+} and WT strains. The graphs depict measurements of OD_{600}, pH, glucose consumption, organic acids and solvents produced. Cultures grown in TYIR with 50 g.L^{-1} of glucose and 30 mM MES, at 32 °C for 48h in anaerobic conditions. Values represented in median and 95% CI. Statistical test: non-parametric Kruskall-Wallis and uncorrected Dunn's test for multiple comparisons. *p <0.05, ** p <0.01; n= 7 (*mt*1^{+}), n= 7 (WT).

Regarding the acetic acid production, no significant differences were observed between the WT and *mt*1$^+$ strains. However, a different pattern was obtained for the butyric acid production (Figure 6.4E). The *mt*1$^+$ strain produced significantly higher amounts than the WT. At 24 hours, 0.08 (95% CI, 0.03 – 0.17) g.L^{-1} and 0.52 (95% CI, 0.30 – 0.60) g.L^{-1} of butyric acid were quantified in median in the WT and *mt*1$^+$ strains. This result shown a significant increase in the butyric acid production with high statistical significance (p=0.0064) (Figure 6.4F). The butyric acid production by the *mt*1$^+$ strain remained similar during the 48h incubation period, whereas in the WT, no butyric acid was quantified. Regarding solvent production, no acetone was quantified in any of the *mt*1$^+$ biological replicates, and only 0.16 (95% CI, 0.12 – 0.21) g.L^{-1} of butanol was quantified in the mutant strain cultures (Figure 6.4G,H).

In conclusion, the *mt*1$^+$ cell cultures demonstrated considerably higher concentrations of lactic acid and butyric acid compared to the WT, with an increase of more than 2-fold and 5-fold, respectively. However, this increase in acid production did not result in a corresponding increase in solvent production. The overexpression of *mt*1 is leading to a long acidogenesis phase which can be indicative of low ATP levels and a redox imbalance. Cloning *mt*1 gene into *C. saccharoperbutylacetonicum* N 1-4 (HMT) likely led to changes in the cell membrane composition during ABE fermentation, contributing to the enhanced productions of lactic acid and butyric acid.

6.5 Small-scale bottle screening of *BCL* strain

The *BCL* strain, a mutant strain displaying different membrane morphologies, provided by the industrial partner Biocleave, was screened for its growth, acids and solvents production and compared to the WT strain (Figure 6.5). The *BCL* overnight grown cultures of the showed a very similar growth to the WT cultures. Cells of *BCL* exhibited similar density and motility characteristics as in WT cultures.

Figure 6.5 displays the results from the small-scale fermentation characterisation of five biological replicates of *BCL* and seven biological replicates of WT. It is important to acknowledge that the results presented for butyric acid and acetone at 48 h are representative of three biological replicates instead of five, for *BCL* strain. The HPLC spectra showed the butyric acid peak around 26.0 minutes, and the acetone peak follows closely at around 26.6 minutes. However, in two biological replicates, the two peaks were too close, probably due to band broadening, which hindered reliable separation of the peaks. Therefore, the data from these biological replicates for both butyric acid and acetone at 48h was excluded from the analysis to ensure the accuracy and validity of the results.

In terms of growth, *BCL* cell cultures reached maximum optical densities very similar to the WT cell cultures. The glucose uptake and pH variations were in concordance with the optical density results. Both strains exhibited a decrease in pH during the acidogenesis phase, followed by an increase during the solventogenesis phase. The glucose consumption was similar between strains (Figure 6.5A, C).

During the acidogenesis phase, the main observed difference was for the lactic acid production (Figure 6.5D). The production of lactic acid for the WT cell cultures at 24h was in median 0.05 (95% CI, 0.03 – 0.13) $g.L^{-1}$, whereas for the *BCL* no lactic acid was identified. However, due to the variability among the biological replicates, this difference was not considered significative.

Regarding acetic acid and butyric acid production, there were no significant differences observed between the mutant and WT strains (Figure 6.5E, F). Both strains exhibited very similar production of these acids. The same pattern was observed for solvent production, with both strains showing comparable production of acetone and butanol at 0h, 24h, and 48h of growth.

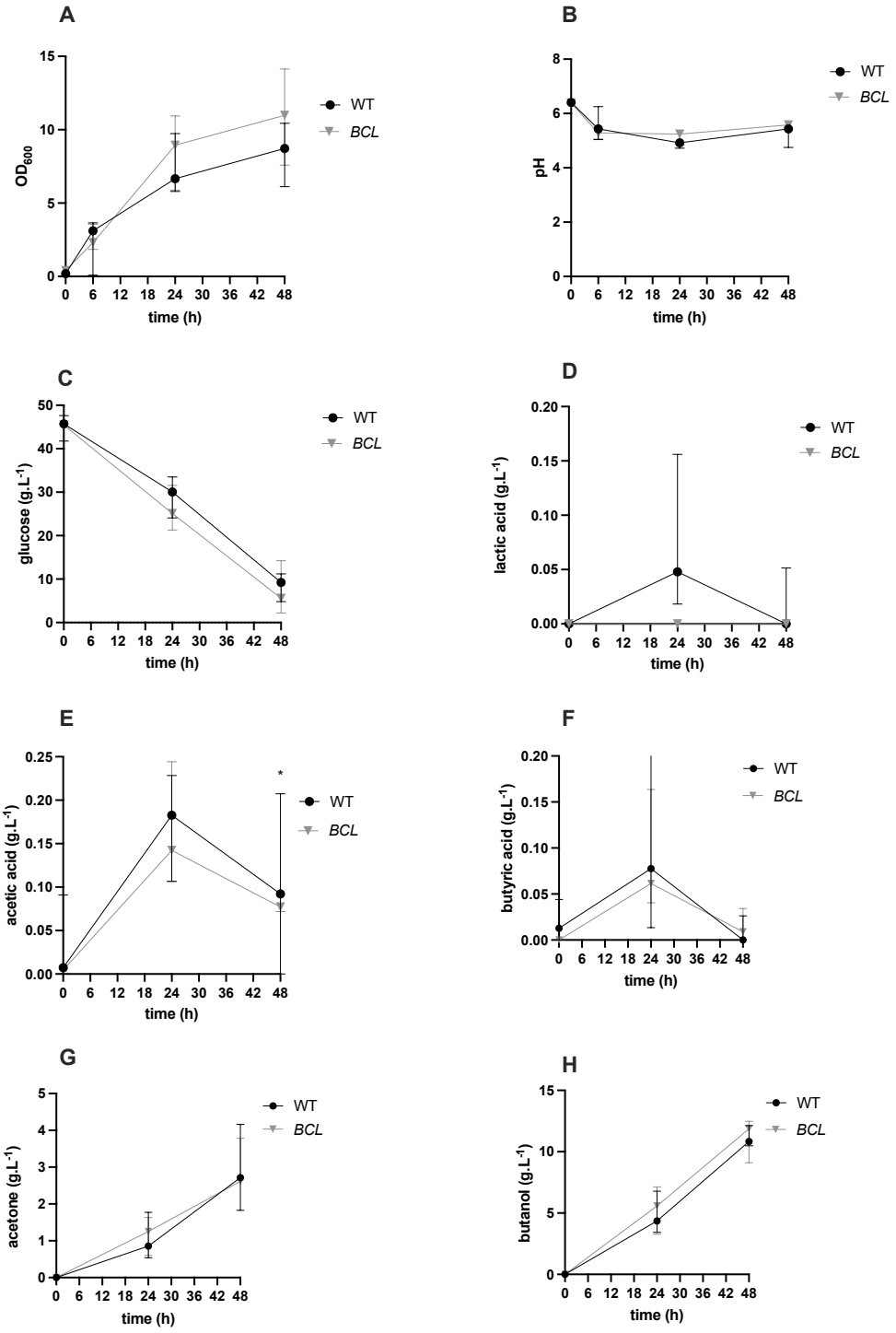

Figure 6.5. Bottle screening of *BCL* and WT strains. The graphs depict measurements of OD_{600}, pH, glucose consumption, organic acids and solvents produced. Cultures grown in TYIR with 50 $g.L^{-1}$ of glucose and 30 mM MES, at 32 °C for 48h in anaerobic conditions. Values represented in median and 95% CI. Statistical test: non-parametric Kruskall-Wallis and uncorrected Dunn's test for multiple comparisons. *p <0.05, ** p <0.01; n= 5 (*BCL*), n= 7 (WT).

In conclusion, *BCL* strain showed a very similar growth compared to the WT strain. Besides the difference on the lactic acid production between strains, the production and uptake of the other acids was very similar, resulting in almost the same concentration of solvents.

Small-scale bottle screening summary:

- The Δ*pssA* and *pssA*$^+$ mutants showed disctinct growth, acid and solvent production, and pH levels. While *pssA*$^+$ had solvent production close to WT, Δ*pssA* primarily accumulated acids.
- The *pgsA*$^+$ strain closely resembled the WT in weak acid production, growth patterns, glucose uptake, pH changes, and microscopic motility.
- The *cls*$^+$ strain had a longer initial lag phase than the WT but showed similar density, pH, and glucose consumption after 48 hours. While its butyric acid production was higher and acetone production differed at 24 hours, the results were similar to WT by the end. However, the *cls*$^+$ strain had reduced butanol levels.
- The *mt*1$^+$ cultures had much higher lactic and butyric acid concentrations than the WT. Despite this, there was not a corresponding rise in solvent production.
- The *BCL* strain growth was largely similar to the WT, with the main difference being lactic acid production. Other acid productions and uptakes were nearly identical, leading to similar solvent concentrations as for the WT.

7 Discussion

Lipids are essential constituents of the cell membrane, not only conferring structural integrity but also play a crucial role in maintaining cellular shape and ensuring internal stability and homeostasis (Parsons and Rock, 2013). The membrane acts as a selective permeable barrier, regulating intracellular conditions via its lipid composition, keeping a vital balance among various lipid classes (Tang, Xia, and Li 2018). In bacteria, the equilibrium is kept among zwitterionic or neutral phospholipids, such as PE, and acidic phospholipids, like PG and CL (Zhang and Rock 2008). It is crucial to note that various aspects, including the FAs chain length, the number of unsaturations in these lipid classes, alterations in other less common lipid classes, and modified versions of these classes (e.g., plasmalogens), dynamically adapt and shift in response to environmental and cellular changes, thus ensuring continuous cellular adaptation and survival (Zhang and Rock 2008).

This study aimed to generate *C. saccharoperbutylacetonicum* N1-4 HMT mutant strains by integrating genes that code for enzymes involved in the biosynthesis of PE, PG, and CL, while concurrently characterizing the expression of an oxidative stress scavenger in the *C. saccharoperbutylacetonicum* N1-4 HMT. Additionally, the *C. saccharoperbutylacetonicum* N1-4 HMT mutant strain, *BCL*, was subjected to testing. The overall reaching goal was to fuse this lipidome knowledge together with information about more tolerant and productive strains, thereby leading to a deeper understanding and potential advancements in microbial cell factory efficacy.

7.1 Why study these genes in *Clostridium*?

In this work, three principal *C. saccharoperbutylacetonicum* N 1-4 HMT mutant strain groups were selected for study, each with the same objective of exploring their influence on membrane stability, cellular viability, and the production of acids and solvents. The first group of strains was designed to target the phospholipid metabolic pathway, encompassing genes such as *pssA*, *pgsA*, and *cls*. The second group concentrated on the higher stress conditions experienced by cells during fermentation and solvent production/accumulation, with a particular focus on the *mt*1 gene. The third was a mutant strain, provided by industrial partner Biocleave Ltd, and was distinguished by its different membrane morphology, being a potential cell factory.

7.1.1 Genes involved in phospholipid biosynthesis.

The lipid membrane of *Clostridium* was the primary focus in this study, primarily due to its significant susceptibility to solvent production and accumulation, with butanol standing out as an important example (Linney et al., 2023). Butanol is known to disrupt the phospholipid packing, thereby destabilizing it, thinning the membrane, and enhancing the lateral diffusion of lipids as well as membrane fluidity (Guo et al., 2020).

The effects of butanol on the membrane have been documented in several *Clostridium* strains, such as *C. acetobutylicum*, where it not only disrupts phospholipids but also induces changes in lipid composition, affecting FA synthesis, phospholipid head groups in the membrane, and the biophysical properties of lipid membrane. These changes affect in turn the lipid turnover of the membrane, an important element in the control of membrane homeostasis (Zhang and Rock 2008). Although a significant number of studies have been reported in aerobic bacteria, a few include certain strains of *Clostridium*. For instance, in *C. acetobutylicum*, a rise in butanol concentration alters the membrane fluidity by increasing the saturated/unsaturated FA ratio (Fayolle 1987). Plasmalogens have emerged as another potential strategy to counteract solvent stress and ensure membrane stability in anaerobic bacteria. Also, in *C. pasteurianum*, where PE, PG, PS, and CL are also identified as the major lipid classes, both diacyl and alkenyl (plasmenyl) acyl chains are present, as well as tetracyl, triacylplasmenil, and diacyl-diplasmenyl subclasses of CLs (Goldfine, 2019; Guan and Goldfine, 2021; Jackson et al., 2021; Kolek et al., 2015).

In *C. saccharoperbutylacetonicum*, changes in the lipidome were observed during fermentation and butanol production (Linney et al., 2023). Specifically, the levels of PG were apparently higher at 15h and 35h of incubation when compared to the initial point of fermentation. Mass spectrometry studies also revealed a slight decline in sugar-containing lipids and CL throughout the 35h of incubation (Linney et al., 2023). It is important to highlight that in *C. saccharoperbutylacetonicum* N1-4 HMT, 15h of fermentation corresponds to the mid-exponential phase, while 35h of incubation signifies the beginning of the death phase.

When *Streptococcus mutans* bacteria accumulate weak acids, *cls* gene expression is increased. Mutants of *S. mutans* lacking CL formation are sensitive to acid environments, which shows how CL is crucial for surviving in these environments (Sohlenkamp 2017). These are a few examples proving that stress conditions cause changes in the lipidome as a protective mechanism to maintain cell viability. Therefore, the phospholipid metabolic pathway of *C. saccharoperbutylacetonicum* was one of the main targets in this study. Given what has been described in Clostridia, the *pssA*, *pgsA*, and *cls* are likely essential genes in phospholipid synthesis. The *pssA* gene encodes an enzyme identified as phosphatidylserine synthase, which catalyses the synthesis of PS, which is an intermediary for the synthesis of PE (Parsons and Rock, 2013). However, on close analysis more than one *pssA* gene was found in *C. saccharoperbutylacetonicum* genome, as discussed in section 7.2.1 .

The *pgsA* gene codes for phosphatidylglycerophosphate synthase, an enzyme that catalyses the synthesis of PG. Subsequently, two PG molecules can be fused to form CL, by the enzyme cardiolipin synthase, expressed though the *cls* gene (Parsons and Rock, 2013). The expression of these enzymes is not necessarily straightforward and does not directly affect the phospholipids of the pathways these genes are involved in. For example, it has been demonstrated that increasing levels of negatively charged phospholipids (PG or CL) induce the expression of *PssA* and its binding into the membrane to increase the synthesis of zwitterionic PE (Zhang and Rock 2008).

In summary, the lipid composition in the membrane is regulated by a variety of factors. Although these are not fully characterized in *Clostridium*, they appear to function in a network to maintain the fluidity and stability of the cell (Guan and Goldfine 2021; Parsons and Rock 2013). Changes in environmental conditions trigger this network to adapt the cell membrane composition. Creating *Clostridium* mutants that target these genes can induce changes in network interaction and lipid synthesis. This thesis will help to increase knowledge of the biosynthetic lipid pathways in *C. saccharoperbutylacetonicum* N1-4 HMT.

7.1.2 Gene expression for solvent stress reduction.

The production of high-value chemicals by *Clostridium* is always associated with an increase in cell stress. For instance, adding butanol to the *C. pasteurianum* culture medium reduced growth rate, potentially due to cellular adaptation to the solvent stress (Kolek et al., 2015). Transcriptomic analysis during the acidogenesis and solventogenesis phases in *C. beijerinckii* and *C. acetobutylicum* revealed an increase in the expression of heat-shock proteins (HSPs) (Bahl et al., 1995; Tomas, Welker, and Papoutsakis 2003). Butanol production and accumulation upregulate the expression of heat-shock genes, mediated by the *groESL* and *dna* operons (Patakova et al., 2019). In *C. acetobutylicum*, the overexpression of the *groESL* operon leads to enhanced solvent tolerance, prolonged and amplified cell growth, and consequently increased solvent production (Tomas, Welker, and Papoutsakis 2003). Other heat shock proteins, such as GrpE and HtpG, were overexpressed in *C. acetobutylicum* and exhibited a slight increase in butanol production (Xue et al., 2017).

The heterologous expression of antioxidant enzymes has also been another strategy to improve other cell factories. For example, expression of metallothionein in *E. coli* cells, has resulted in cells able to tolerate higher levels of butanol (Chin et al., 2013). The improvement in butanol production, obtained by expressing metallothioneins, was then tested in an engineered *E. coli* strain with the Clostridial metabolic pathway for butanol production (Chin et al., 2017). Considering this outcome, and the fact that *C. saccharoperbutylacetonicum* N 1-4 HMT is already a hyper butanol producer and experiences solvent stress, the overexpression of *metallothionein*1 from *Mus musculus* was selected to study its role in cell stress, cell growth, and high-value chemical production.

Understanding the role of the genes involved in the lipid content of *C. saccharoperbutylacetonicum* N 1-4 HMT was one of the main objectives, which can be subsequently used for enhancing this cell factory. Additionally, the selection of the *C. saccharoperbutylacetonicum* N 1-4 HMT mutant strain *BCL*, provided by Biocleave, was driven by the possibility of having a different membrane composition, due to the morphologies observed, and this may potentially indicate better yield and productivity.

7.2 *Clostridium* lipidome

The membrane of *Clostridium* is a self-assembled structure, composed of lipids and proteins, that coexist in a balanced and in a continuous recycling process (Parsons and Rock 2013). Various factors such as acids and solvents production, trigger an adaptation of the lipid composition in the membrane to maintain its fluidity (Goldfine 2019). In the *C. saccharoperbutylacetonicum* N 1-4 HMT wild type strain this process has been shown (Linney et al., 2023). Here, the aim was to rationally engineer the lipid membrane of Clostridia to increase solvent tolerance. In this work *C. saccharoperbutylacetonicum* N 1-4 HMT mutant strains showed different lipid composition during cell growth, acids and solvents production.

7.2.1 Phospholipid headgroup

pssA^{+} and Δ*pssA* lipidome

Changes in the lipidome of WT, Δ*pssA*, and *pssA*$^{+}$ strains were observed. Silencing and overexpressing the *pssA* gene in *C. saccharoperbutylacetonicum* N1-4 HMT, by generating the Δ*pssA*, and *pssA*$^{+}$ strains, respectively, affected the lipidome of the bacteria throughout 48h of small-scale fermentation.

Initial findings were focused on the production of PE by the Δ*pssA* strain. PE was unexpectedly observed in the TLC experiments and subsequently confirmed by mass spectrometry. The overall production of PE by the Δ*pssA* strain was similar to the WT however, the percentage of short chain PE (14-22 carbons) was significantly higher in the Δ*pssA* strain. Interestingly, it was observed that silencing a *pssA* gene in *C. saccharoperbutylacetonicum* N1-4 HMT neither significantly reduced nor removed the synthesis of PE but it has affected the normal growth of the cell, accumulated weak acids and not produced solvents. This revelation led to further analysis, where a second *pssA* gene was discovered within the *C. saccharoperbutylacetonicum* N1-4 HMT genome as shown in Annex 9 and Annex 10.

Knockout *pss* strains from *E. coli*, *Sinorhizobium meliloti*, *Agrobacterium tumefaciens* and *Helicobacter pylori* shown that these cells were able to grow in the absence this gene (Parsons and Rock, 2013). The *pss* knockout in *S. meliloti* resulted in the absence of PE/MMPE and DMPE, as observed on a 2-D TLC silica plate (Vences-Guzmán, Geiger, and Sohlenkamp 2008). These findings were in concordance with studies involving *pss* knockouts of *E. coli* and *A. tumefaciens*, where the strains were unable to produce PE, suggesting that PE synthesis occurs exclusively via

the decarboxylation of PS, assuming only one *pss* gene within the genome (Figure 7.1A) (Parsons and Rock 2013).

Engineered *S. meliloti* and *A. tumefaciens* strains, having the *pss* silenced, created viable strains but only in the presence divalent cations (Ca^{2+}). In these mutant cells, it was described the absence of PE and increased levels of PG and CL (Parsons and Rock, 2013). The CL increase was described as a compensatory mechanism to restore the membrane stability (Karnezis et al., 2002).

Mass spectrometry analysis in the Δ*pssA* strain in the present work revealed a significant reduction in the cellular concentration of PG. This could potentially indicate that lower PG might indicate increased CL concentration (Figure 7.1B) (Goldfine 2019). Following this hypothesis, after 24h of incubation it was possible to observe differences in the lipid spots with similar migration as CL/PG between the Δ*pssA*, and *pssA*$^{+}$ strains. The Δ*pssA* strain displayed a stronger intensity signal of CL/PG. Considering the lower percentages of PG in the mass spectrometry analysis, this can be a strong indicative of higher percentages of CL. Additionally, while no significant differences were found in the PE between the WT and Δ*pssA* strains, there was a slight reduction in the total PE observed in the mutant strain.

C. saccharoperbutylacetonicum N1-4 HMT *pssA*$^{+}$ strain showed changes in the lipidome relatively to the WT and Δ*pssA* strains. There was a significant increase on the PE and PS, when compared to both WT and Δ*pssA* and there was a significant increase on the PG production comparing to the Δ*pssA* strain. This result is in concordance to what is described in *E. coli*, where the *pssA* overexpression by inserting a second copy of the gene in the chromosome shown an increase by 7% in the relative abundance of PE but a decrease by around 50% in the relative abundance of PG (Figure 7.1C) (Tan et al., 2017).

In terms of regulation, it has been described that increased levels of PE decrease the *PssA* membrane association, diminishing the synthesis of this phospholipid (Figure 7.1A) (Zhang and Rock 2008). This hypothesis derives from studies involving the heterologous expression of a modified PssA enzyme from *B. subtilis* in *E. coli pssA* mutant strains. Unlike the native PssA from *E. coli*, which is a transiently membrane-associated enzyme, the *B. subtilis* PssA is an integral membrane protein. Notably, heterologous expression of *B. subtilis* PssA in *E. coli* enhanced both relative and absolute PE concentrations, yet impaired cell growth (Saha, Furukawa, et al., 1996). Therefore, it is hypothesized that, within native *E. coli*, the equilibrium between zwitterionic and acidic phospholipids is intrinsically tied to the synthesis and availability of PG and is subject to a regulation of PE synthesis through the PssA/Psd pathway (Figure 1.14A) (Saha et al., 1996).

However, the 2 PssAs from *C. saccharoperbutylacetonicum* N1-4 HM, with GenBanK codes AGF55550.1 and AGF58887.1 have 4 and 5 transmembrane domains, respectively, according to TMHMM 2.0. This result indicates that both PssAs are highly likely to be membrane proteins.

Similar percentages of PS were observed between the Δ*pssA* and WT strains, however, more PS was observed in the *pssA*$^{+}$, along with higher percentages of PE and PG, which is in concordance with the regulation mechanisms to maintain the balance in the membrane. For that, the proportion of phospholipid polar head groups in the membrane is tightly controlled to balance the composition of zwitterionic or neutral phospholipids such as PE and glucosyldiacylglycerol and acidic phospholipids such as, PG and CL (Parsons and Rock 2013).

Glyceroglycolipids are present in higher percentages during increasing stressful conditions. For example, higher percentages of DihexDAG were found in *C. acetobutylicum* cultures with added octanol (surrogate of acetone and butanol) (Guan and Goldfine, 2021). Studies in *A. laidlawii* shown an increase in DihexDAG, upon adding solvents that perturbed the bilayer arrangement, to stabilise it (Guan and Goldfine, 2021). In this work, only two molecules of DihexDAG showed significantly higher percentages in the Δ*pssA*, when compared to the WT. However, it is important to note that specific alterations in lipid profiles, such as the increase in DihexDAG *in Clostridium spp*. and *A. laidlawii* might be synchronized with solvent concentrations (Guan and Goldfine, 2021).

In the *pssA*$^{+}$ strain it was observed a significant increase on the plasmalogens PE (32:0-O) compared to the WT. These findings add another layer to understanding the membrane adaptations in response to butanol production stress. Plasmalogen variants of CL, PE and of glycolipids are described having an important role on the cellular homeoviscous adaptation during solvent induced stress (Goldfine, 2022; Johnston and Goldfine, 1983; Kogat and Goldfine, 1984; Kolek et al., 2015). Alterations in CL within the cellular membrane during solvent stress seem to be an important part of a complex cellular response (Kolek et al., 2015). More information regarding the role of CL lipid class and its plasmalogens forms in Δ*pssA* and *pssA*$^{+}$ cells is still in progress. This can signify the potential adaptive strategies employed by these microbes to manage the membrane dynamics under solventogenic conditions (Goldfine 2019, 2022).

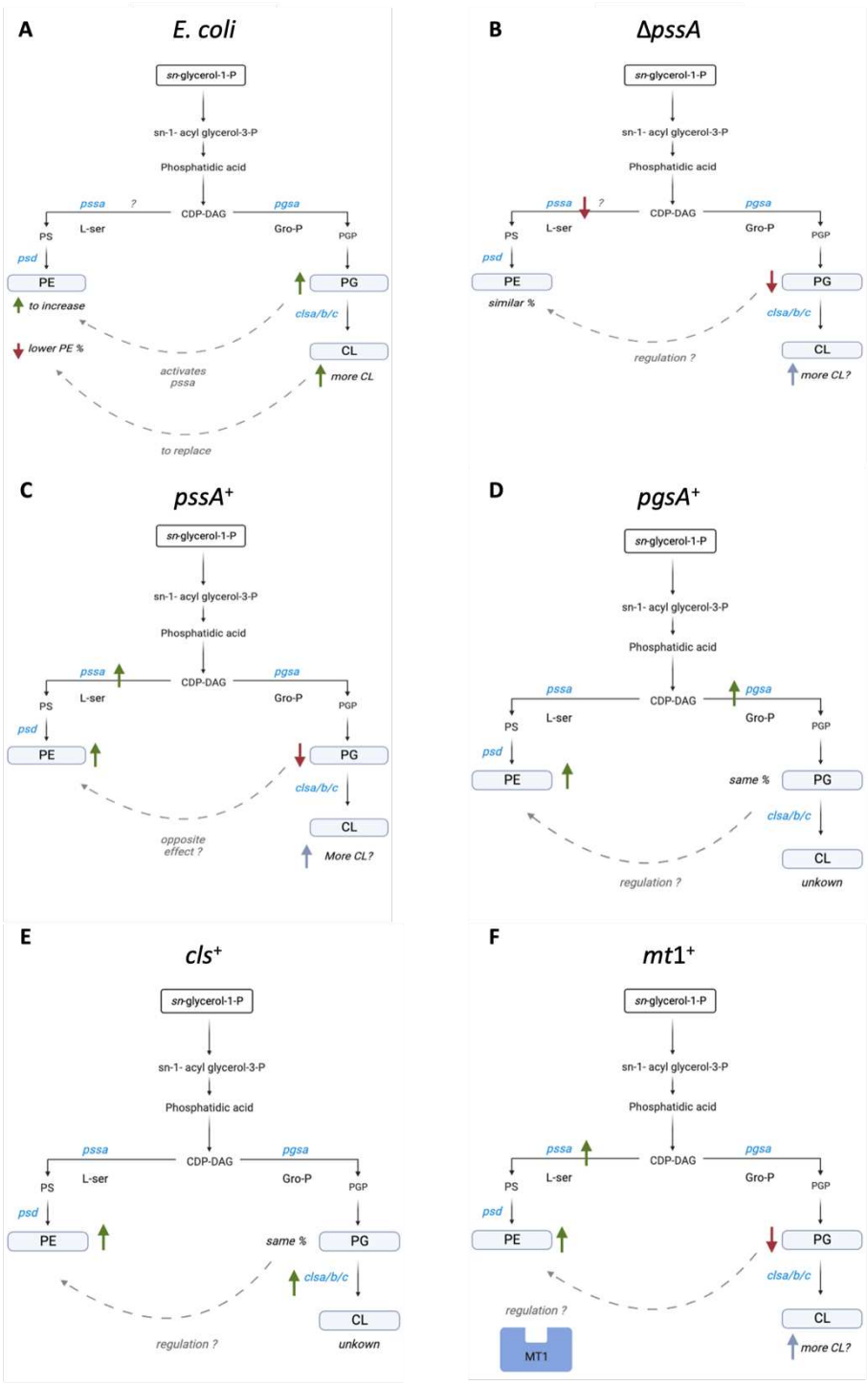

Figure 7.1. Possible regulation mechanisms for the phospholipid synthesis. Based on the theory described in literature (A) and on a combination of the mass spectrometry analysis from this work for the strains: (B) Δ*pssA*, (C) *pssA*$^{+}$, (D) *pgsA*$^{+}$ and (E) *cls*$^{+}$ strains. Information from samples collected at 24h of incubation (Zhang and Rock, 2008).

pgsA^{+} and *cls*$^{+}$ lipidome

PG in *E. coli* has been described as an essential lipid for cell viability, initiation of DNA replication and to processes related to translocation of proteins across the membrane (Suzuki, Hara, and Matsumoto 2002). In *E. coli* cells that are *pgsA* deficient, had altered synthesis of the major outer membrane lipoproteins and led to cell lysis (Suzuki, Hara, and Matsumoto 2002). In another study, an attempt to generate *E. coli* cells *pgsA* knockout was unsuccessful. However, in the same study, this gene was overexpressed, and PG increased by 38% in cells growing in a culture media containing octanoic acid (Tan et al., 2017). The overexpression of *pgsA* in *E. coli* caused a slight decrease in the percentage of PE, that was 87.8% in the WT and 84.7% in the overexpressing strain. No effect was observed in the CL percentage between strains (Tan et al., 2017). The increase in PG did not lead to an increase of PE, as the possible mechanism for the regulation of phospholipid profile in the membrane (Zhang and Rock, 2008).

In *C. saccharoperbutylacetonicum* N1-4 HMT *pgsA*$^{+}$ cells, the PG percentage in the four samples collected at 24h of culture was very similar to the WT, based on the mass spectrometry data. The TLC data showed a similar result for the 24h samples but the intensity of the PG/CL spots was smaller in *pgsA*$^{+}$ than in WT at 0h, 6h and 48h. Unfortunately, it was not possible to discern between these two lipids in the TLC data.

The enzyme cardiolipin synthase catalyses the condensation of two PG molecules to produce CL. In *E. coli*, the membrane content of this lipid is typically minimal, constituting below 5% of the total lipids. In the membranes of certain *Clostridium* species, higher percentages of CL were observed, ranging from 15 to 26%. For instance, in *C. innocuum,* CL represents 26% of total lipids, while PG makes up 1% (Duerre, 2005; Parsons and Rock, 2013). Overexpressing *cls* in *E. coli* has increased the CL content in 12% relatively to the control strain (Tan et al., 2017).

In *C. saccharoperbutylacetonicum* N1-4 HMT *cls*$^{+}$ cells, the CL content has not been analysed using mass spectrometry, yet. Nevertheless, the proportion of PG was not notably less than that of the WT, which might suggest CL levels are comparable to the WT. The mass spectrometry data on *pgsA*$^{+}$ and *cls*$^{+}$ strains has shown significative more PE on these mutants than the WT and less LPMME than the WT (Figure 7.1D, E). This result could mean that more PgsA and Cls could not directly be connected with increasing amounts of PG and CL, because their activity is dependent on the availability of other lipids. For example, PGP and availability of CDP-DAG, that is believed to have a direct competition with the PssA enzyme for the synthesis of PS and consequently PE (Parsons and Rock 2013). Another possible reason is the fact these enzymes are not being correctly overexpressed but further analysis is needed to confirm this hypothesis.

Differences on the TLC plates stained with ninhydrin were observed for both *pgsA*$^{+}$ and *cls*$^{+}$ strains, at 0h, 6h and 48h of incubation. These differences could indicate the presence of lipids containing amino groups. Although the spots do not have the same pattern as the standard PE, it can be indicative of the presence of PMME and LPME. Also, the migration pattern in the TLC silica plate it is very similar to the separation of PE, PMME and PDME in TLC silica plate from a study about phospholipid N-methyltransferases in phosphatidylethanolamine derivatives from thermophilic bacteria (Kleetz et al., 2021). However, it is important to consider that the mobile phase used both studies was different.

Two DihexDAG lipid molecules were highlighted as being significantly more produced in the *cls*$^{+}$ strain. Glycolipids are important to stabilize the membrane under stressful conditions (Guan and Goldfine, 2021).

*mt*1^{+} lipidome

The heterologous expression of a metallothionein (MT) from tilapia fish (*O. mossambicus*) has been shown to improve butanol tolerance in *E. coli* and butanol production in engineered *E. coli* with a butanol pathway from Clostridia (Chin et al., 2013, 2017). Fluorescence microscopy showed that *E. coli* expressing tilapia MT in fusion with the outer membrane protein (OmpC) had less cell membrane damage the control strain (Chin et al., 2017). The heterologous expression of *mt*1 from *M. musculus* in *C. saccharoperbutylacetonicum* N1-4 HMT led to changes in the lipid membrane composition. There was an increase in the percentage of the LPE and a decrease in LPMME and PG, relatively to the WT.

The decrease in PG can potentially by indicative of an increase in CL (Figure 7.1F). Having that information regarding the mass spectrometry will help clarifying this hypothesis in the future, which is in concordance with an increase of *cls* expression under acidic conditions in *S. mutans* (Sohlenkamp 2017). The TLC data for the *mt*1^{+} strain revealed notable differences compared to the WT at the 6h, 24h, and 48h incubation marks. These variances aligned with spots present in the WT but absent in the *mt*1^{+} strain. These differences suggest the presence of lipids with amino groups. Analysis of the 24h samples by mass spectrometry showed that the LPMME lipid production was considerably higher in the WT strain, suggesting these lipids as the ones from mentioned spot.

The *BCL* strain is a mutant of *C. saccharoperbutylacetonicum* N1-4 HMT, with distinct membrane morphology when compared with the WT strain. The industrial collaborator, Biocleave Ltd,

supplied this strain for characterization. Upon lipidomic analysis, the lipid profile closely was similar to the WT. The prominent differences were observed in the higher percentages of PA and PS in the *BCL* strain. Notably, even with the increased percentages of these intermediate lipids, there was not a corresponding rise in PE or PG percentages at the 24 h incubation mark.

Lysolipids were the main lipids identified by mass spectrometry.

Lysolipids were the main lipids observed among the analysed strains being statistically significant in some of the mutant strains, relatively to the WT. In gram-negative bacteria lysolipids are a small fraction of the membrane, corresponding to approximately 1% (Zheng et al., 2017). Two possible reactions for their synthesis have been described, it can be from *de novo* synthesis, which is the reaction of glycerol 3-phosphate with a fatty acyl-CoA, or it can be through conversion of phospholipids to lysophospholipids by an enzymatic reaction catalised by A1 or A2 phospholipases (Kern et al., 2001).

The role of lysophospholipids in bacterial systems is not yet fully understood (Zheng et al., 2017). These lipids might be important for the adaptability and flexibility of bacterial membranes to environmental changes, particularly in maintaining a balance between bilayer and non-bilayer lipid formations (Zheng et al., 2017). When *E. coli* experienced a temperature rise from 30 °C to 42°C, there was a significant 4-fold increase in LPE levels. Moreover, LPE has been shown to help protein refolding after being denatured by urea (Kern et al., 2001). Certain lysophospholipids play a protective role having chaperone-like properties, preventing membrane enzymes from heat-induced denaturation (Kern et al., 2001).

In pituitary cells, the combination of unsaturated cone-shaped PE with PG results in an elastic curvature strain within the bilayer. The inverted cone-like configuration of LPE acts to counteract this curvature stress (Ben-Zeev, Telias, and Nussinovitch 2010). Evidence from *E. coli* cells shows that the accumulation of LPE frequently corresponds with a rise in CL levels. It is suggested that LPE might be located at the cell division region to alleviate the bilayer tension caused by non-bilayer CL or to ensure the membrane retains its ideal curvature (Sutterlin et al., 2016). This hypothesis gains weight from the observed activity of the PldA enzyme during cell division, which breaks down lipids (Sutterlin et al., 2016).

Information regarding CL may provide clearer information on the percentages of LPE observed in the cells within this study. For instance, there was a notable increase in LPE percentages in the Δ*pssA* strain, accompanied with a significant reduction in PG synthesis. This suggests a

potential rise in CL percentages, suggesting at a mechanism oriented towards stabilising the membrane curvature. A similar pattern was observed in the *mt*1^{+} strain, with a significant increase in LPE percentage compared to the WT strain, while there was a corresponding decrease in PG percentage compared to WT. In contrast, the other mutant strains demonstrated LPE percentages similar to the WT, as did their PG percentages.

While evaluating the higher percentages of lysophospholipids across samples, it would be important to account for potential lipid damage during extraction or the mass spectrometry process itself, which might explain the increased percentages. The quality of the lipid identification is a major analytical problem related to mass spectrometry. The collision of neutral gas with accelerated ions between the electrospray ionization source and the analyser in the mass spectrometer can cause in source fragmentation. The in-source fragmentation can lead to false-positive lipid identification, which can be the case of lysolipids (Criscuolo, Zeller, and Fedorova 2020). The degree of fragmentation can be influenced by the design of the source and the type of the analyte, as certain biomolecules are more prone to fragmentation than others (Criscuolo, Zeller, and Fedorova 2020). Because of that is becomes challenging to distinguish between the percentage of lysolipids existent in the membrane and the percentage of lysolipids resultant from in-source fragmentation.

Nonetheless, prior research indicates that lysolipids could play a pivotal role in the membrane structure of Gram-negative bacteria (Zheng et al., 2017). Characterising this mechanism in Gram-positive bacteria, such as *C. saccharoperbutylacetonicum* N1-4 HMT would be important for a complete and detailed characterisation of its lipidome and mechanisms for homeostasis.

7.2.2 FAs and membrane fluidity

Modifications in the FAS are important in controlling membrane fluidity (Willdigg and Helmann, 2021). Such modifications include the balance between saturated and unsaturated FAs, shifting between cis and trans configurations of unsaturated FAs, cyclic FAs and adjusting the acyl chain length (Mrozik and Łabużek, 2004). Furthermore, the physical properties of membranes are significantly influenced by factors such as temperature, pressure, ions, and chemicals (Mrozik and Łabużek, 2004).

The overexpression of the *pssA* gene in *E. coli* cells led to noticeable changes in both the length of the FA chain and its levels of unsaturation (Tan et al., 2017). In particular, the strain overexpressing *pssA* exhibited longer FA acyl chains with a higher degree of unsaturation

compared to the standard *E. coli* WT strain (Tan et al., 2017). These findings revealed a decrease in the FAs 16:1, alongside an increase in FAs 18:1. Additionally, there was a noted decrease in the abundance of the cyclic ring (cyclic FAs), with a specific focus on C17cyc (Tan et al., 2017). Furthermore, the study demonstrated that the *E. coli* strains with overexpressed *pssA* had an enhanced tolerance to octanoic acid. Not only that, but these strains also produced the solvent in greater amounts (Tan et al., 2017).

In this study focusing on *C. saccharoperbutylacetonicum* N1-4 HMT *pssA*$^{+}$ strain, there was a notable increase in FAs having between 23 and 32 carbons when compared to the WT. Interestingly, this observation contrasts with the findings from the research previously described in *E. coli* where the FAs were shorter, only extending up to a maximum of 16 carbons in each tail (Tan et al., 2017). The *pssA*$^{+}$ strain showed FAs with fewer unsaturations in comparison to the WT, which was an opposite finding from the studies in *E. coli* by Tan et al., (2017) These differences might be due to the 2 PssAs from *C. saccharoperbutylacetonicum* N1-4 HMT.

In the *pssA*$^{+}$ strain there was notable increase in the FAs 16:0-O, indicative of plasmalogens LPE and LPMME. Plasmalogens are part of the *Clostridium* membrane and are distinguished by the presence of an sn-1-vinyl ether bond (Goldfine 2022). Membranes with a high concentration of the plasmalogen form of PE can impede the phase transition within the membrane, which is vital for ensuring the membrane functions appropriately (Goldfine 2017). Additionally, molecular dynamics simulations provided insights into the structural behavior of plasmalogens in lipid bilayers. Compared to PC, plasmalogens lead to the formation of lipid bilayers that are both more compact and thicker (Rog and Koivuniemi, 2016). The vinyl-ether linkage in plasmalogens promotes a higher order in both the sn-1 chain and the sn-2 acyl chains when observed in PCs and PEs (Rog and Koivuniemi, 2016). However, lysolipids of plasmalogens have not been described in *Clostridium* and for that reason it is also important to acknowledge the in-source fragmentation that occurs when the samples are running the mass spectrophotometer (Criscuolo et al., 2020; Guan and Goldfine, 2021).

The FAs composition within cells can vary based on the pH conditions they experience. Certain adaptations have been observed in cells when they are exposed to acidic environments (Fozo and Quivey, 2004; Sohlenkamp, 2017). When *E. coli* cells are in a stationary phase and subjected to acidic conditions, there is a shift in their FA profile. Specifically, there is a conversion of unsaturated fatty acids to cyclopropane fatty acids (CFAs) (Chang and Cronan 1999). The formation of CFAs from unsaturated fatty acids is facilitated by the enzyme named cyclopropane fatty acid synthase (CFA). An interesting observation was made with *E. coli* cells that had

mutations in the *cfa* gene, they did not produce CFAs, and they exhibited a higher sensitivity to acid shock (Chang and Cronan, 1999). In *S. melliloti* cells with a *cfa2* mutation, these cells showed minimal CFAs presence (less than 0.1%) when grown under acidic conditions (Basconcillo et al., 2009). On the contrary, the wild type *S. melliloti* demonstrated an increase in CFA percentages, ranging between 10 to 15%, under conditions of acid stress. This underscores the importance and adaptability of CFAs in response to changing environmental conditions.

The FA composition of Lactic Acid bacteria (LAB) membranes is affected in acidic conditions (Fonseca et al., 2019). A predominant portion of the FA composition in LAB membranes comprises FAs with 16 and 18 carbon atoms. This composition confers the physical properties of the membrane, especially in determining its phase transition temperature (Fonseca et al., 2019). The nature of the FA chains, specifically their length and degree of saturation, influences this transition temperature. Essentially, longer, and more saturated FA chains result in a higher phase transition temperature (Fonseca et al., 2019). Additionally, LAB in acidic conditions increases the content of CFAs as the culture time progresses. This increase correlates with a decrease in the unsaturated fatty acid (UFA) to saturated fatty acid (SFA) ratio (Fonseca et al., 2019). From a biophysical point of view, CFAs possess properties similar to unsaturated FAs. However, they seem to have an added advantage exhibiting greater stability against environmental challenges like acid stress (A. Fonseca, Spencer-Martins, and Van Uden 1991).

In the present study, while CFAs were not the focal point of analysis, it is intriguing to consider their presence in a future analysis, especially given the nature of *C. saccharoperbutylacetonicum* N1-4 HMT, which produces weak acids. The strains Δ*pssA* and *mt*1^{+} showed acid accumulation and had significatively higher percentages of unsaturations in some lipid species relatively to the WT. The Δ*pssA* had significatively higher percentages of PS with 1 unsaturation, PE and PG with 2 unsaturations, all relatively to the WT. The *mt*1^{+} strain had significatively higher percentages of PS with 1 unsaturation and PG with 2 unsaturations relatively to the WT. This result matched with the mechanism of adaptation in acidic conditions (Sohlenkamp 2017).

Short-chain FAs have also been highlighted for their role in increasing membrane fluidity (Sohlenkamp, 2017; Sohlenkamp and Geiger, 2015). The reason behind this is their lower melting points compared to their long-chain FAs. While longer acyl chains can traverse the entire width of the lipid bilayer, resulting in a more packed and gel-like consistency, the shorter chains face challenges in achieving this span (Russell 1984). This limited reach across the bilayer makes it difficult for short-chain FAs to establish hydrophobic interactions with adjacent lipids and proteins, as they might with longer chains (Russell 1984). Consequently, the motion of the

unbound ends of these acyl chains intensifies, amplifying the fluidity and instability of the membrane (Russell 1984).

The mass spectrometry data indicates that the Δ*pssA* and *mt*1^{+} strains, from the present work, despite having a lower overall percentage, exhibited a notably higher percentage of short-chain PE ranging from 14 to 22 carbons, relatively to the WT and the other mutants. This adaptation can be interpreted as a possible response to specific environmental or metabolic demands that these strains might be experiencing, and it aligns with the established knowledge of the role of short-chain FAs in adapting to conditions that require increased membrane fluidity (Russell 1984; Sohlenkamp 2017).

Environmental shifts, namely the production of solvents like butanol, cause notable alterations in the FAs profile of microorganisms. A study on *C. pasteurianum* revealed that adding butanol into the culture led to a decrease in the ratio of saturated to unsaturated FAs (Kolek et al., 2015). It is intriguing to note that the change in the saturated/unsaturated FAs ratio is dependent upon the source of butanol, whether it is produced internally (endogenous) or externally introduced to the culture. The data suggests a distinct FA profile alteration when the butanol is generated by the organism itself (Kolek et al., 2015).

In the present work, mass spectrometry analyses were performed on samples collected 24 hours of growth. At this time point, the WT cells exhibited a butanol concentration of about 5 g.L^{-1}. In this setting, with such a concentration of butanol and the presence of weak acids, the observed ratio between saturated and unsaturated FAs was approximately 1:1. A subsequent analysis after 48 hours of incubation could yield more insightful data. Given that the WT cells at 48h would potentially have a diminished presence of weak acids and double the concentration of butanol, this might provide important insights into the adaptive strategies employed by the cell membrane under such stress conditions. The composition of the membrane plays a crucial role in ensuring cell viability, especially when exposed to potentially toxic solvents. Thus, understanding these adaptive shifts in *C. saccharoperbutylacetonicum* N1-4 HMT could be crucial for optimizing industrial processes or biotechnological applications involving butanol-producing microorganisms.

The structural conformation of UFAs help determining membrane fluidity. Cis UFAs are characterized by their bent steric structures, which prevent them from packing together as tightly, leading to increased membrane fluidity (Sohlenkamp 2017). This bent conformation is due to the specific orientation of the double bond in the FA chain, resulting in the molecule having a kinked shape (Fonseca et al., 2019). In contrast, trans UFAs possess long linear

structures, resembling the characteristics of saturated FAs. Their straight-chain configuration allows them to align closely, similar to how saturated FAs pack, leading to a more ordered and less fluid membrane (Denich et al., 2003). Furthermore, the tight packing of saturated FAs, which have straight acyl chains, means that membranes rich in these FAs have higher melting points. They optimize their van der Waals interactions (Denich et al., 2003).

The assays in current research did not focus into these details cis and trans unsaturated FAs. However, this data will be important to understand the membrane fluidity of the different mutant strains. Especially when examining how *C. saccharoperbutylacetonicum* N1-4 HMT membrane adapt and respond to various external factors or stress conditions.

7.2.3 Weak acids and solvents production

Altering the phospholipid head distribution increases tolerance to octanoic acid and potentially butanol (Linney et al., 2023). Overexpressing the native *pssA*, *pgsA* and *cls* genes from *E. coli* by duplicating their gene in the chromosome led to increases in the percentages of PE, PG and CL, respectively (Tan et al., 2017). The increased production of CL did not affect the cell growth. An *E. coli* mutant strain with increased production of PG had its growth compromised in the presence of octanoic acid. Finally, the overexpression of *pssA* in *E. coli*, led to improvements in the growth of the cells in the presence of octanoic acid, the growth rate increase by 29% when compared to the control strain (Tan et al., 2017).

E. coli cells overexpressing *pssA* and consequently producing more PE were associated with altered membrane properties, namely an increase in the membrane integrity (Tan et al., 2017). The membrane integrity was studied in the presence of 10mM of octanoic acid. In these conditions *E. coli* cells overexpressing *pssA* had a 78% increase on the membrane integrity and a decrease of ion leakage by 25%, relative to the control strain (Tan et al., 2017). The increase in PE and decrease in PG/CL were also possible explanations for the decrease on the surface negative potential, due to these lipid charges. In the presence of 10mM octanoic acid, the membrane of *E. coli* overexpressing *pssA* kept its fluidity. Overall, the increase of PE is thought to improve the tolerance to organic solvents (Tan et al., 2017). In the present work, *C. saccharoperbutylacetonicum* N1-4 HMT *pssA*$^{+}$ strain shown an increase in PE but no effect was observed in the percentage of PG. The solvent production of *C. saccharoperbutylacetonicum* N1-4 HMT *pssA*$^{+}$ was similar to the WT.

Fluidity and membrane integrity assays conducted on liposomes with varying PE:PG ratios (1:1, 2:1 and 3:1), as well as liposomes composed solely of PC, revealed reduced fluidity and enhanced membrane integrity with increasing PE:PG ratios, indicating higher butanol tolerance (Linney et al., 2023). Molecular dynamic simulations, comparing PE:PG and POPC bilayers, also shown that the combination of PE:PG enhances the resistance to butanol integration within the phospholipid bilayer. Interestingly, the PE:PG combination registered a 34% increase in hydrogen bonds formed by PE, offering superior stability at the interface (Murzyn, Róg, and Pasenkiewicz-Gierula 2005). The proximity between PE-PG lipids and the broader distance between PC-PC lipids indicate that intramolecular water bridges are more probable than their intermolecular counterparts (Murzyn, Róg, and Pasenkiewicz-Gierula 2005).

If the membrane thickness of *C. saccharoperbutylacetonicum* N1-4 HMT *pssA*$^{+}$ strain was augmented by an increase in PE, it might retain more butanol. It is important to note that the solvent analysis by HPLC was performed only in the extracellular component. In terms of acids production, significant less acetic acid was quantified in the extracellular component of the *pssA*$^{+}$ cultures. In the *pssA*$^{+}$ strain, the pH of the cells culture did not decrease as much as in the WT between the 6h and 48h of incubation. These factors can be indicators of a decrease in the movement of acids and solvents though the membrane, similarly to what was tested in *E. coli* (Tan et al., 2017). This is an hypothesis warranting future exploration.

Previous studies have shown a rise in PG levels in *C. saccharoperbutylacetonicum* N1-4 HMT during fermentation (Linney et al., 2023). It has been suggested that rising PG percentage over fermentation could be an evolutionary response to escalating butanol concentrations (Linney et al., 2023). Nevertheless, efforts to increase PG lipid synthesis in this study did not yield higher PG outputs in percentage, and butanol yields remained similar with the WT. Growth, extracellular pH, acid, and solvent production echoed the patterns seen in the WT strain.

The present work also focused on a *C. saccharoperbutylacetonicum* N1-4 HMT strain genetically modified to overexpress *cls*, thus expecting it to lead to augmented CL production. While comprehensive results on CL remain pending, preliminary data did not show a significant decrease in PG presence. However, the four biological samples indicated diminished PG percentages, verging on the lower part of the 95% CI from the WT and *pgsA*$^{+}$ strains. More replicates might provide more clarity in this analysis. A dip in PG might suggest heightened CL production. Still, deducing that this genetically modified strain did not yield more CL would be premature. *Clostridium spp.* literature associates CL plasmalogens to an increased solvent and cellular stress levels (Kolek et al., 2015) reinforcing this theory. Other bacterial species, like *P.*

putida, have shown elevated CL levels, especially in the presence of contaminants like toluene. This strain show changes in fatty acid profiles when exposed to toluene (Rühl, Schmid, and Blank 2009; Weber, Lsken, and De Bont 1994).

Transcriptomic analysis of *C. beijerinckii* in cultures with added butanol revealed alterations in gene expression related to lipid synthesis (Patakova et al., 2019). Genes linked to CL and lyso-PG synthesis, were overexpressed after butanol shock, while those associated with LPA, PA, PS, and PC decreased in expression (Patakova et al., 2019). These insights emphasize the needed of verifying the overexpression of *pgsA* and *cls* genes in the mutant strains and deliberating on potential optimisation strategies.

Organic acids such as butyric or octanoic acid, can cross the cell membrane freely by diffusion at high concentrations (Tran and Zhao, 2022). When in their dissociated form (anionic) is present in the cytoplasm an accumulation of protons is observed, which leads to a decrease of the intracellular pH (Hirshfield et al., 2003; Tran and Zhao, 2022). In *E .coli* cells overexpressing *pssA* the pH did not decrease as much as the control strain confirming that this mutant strain has blocked the passage of octanoic acid to the inside of the cell (Tan et al., 2017). Further simulations suggested that increased PE content in the membrane increases membrane thickness and decreases cell penetration of these acids (Tan et al., 2017). The *pssA*$^{+}$ strain did not lower its pH as much as the WT, it had higher PE levels with longer FA tails, relatively to the *E. coli* strain overexpressing *pssA*. This is a strong suggestion of an increase of the membrane thickness in the *pssA*$^{+}$ strain.

C. saccharoperbutylacetonicum N1-4 HMT Δ*pssA* and *mt*1^{+} strains showed accumulation of weak acids and no production of solvents. In the case of Δ*pssA* significantly more lactic acid and butyric acid was detected by HPLC, relatively to the WT, corresponding to 0.16 (95% CI, 0.14 – 0.18) g.L^{-1} and 0.50 (95% CI, 0.48 – 0.53) g.L^{-1}, respectively. Similarly, for *mt*1^{+} strain, significantly more lactic acid and butyric acids was detected by HPLC compared to WT, corresponding to 0.19 (95% CI, 0.17 – 0.21) g.L^{-1} and 0.52 (95% CI, 0.30 – 0.60) g.L^{-1}, respectively. These acids are of biotechnological interest due to their application in products needed in our daily life (Sauer et al., 2008).

In terms of butyric acid production, other cell factories of interest are native butyric acid producers like *C. beijerinckii*, *C. acetobutylicum*, *C. thermobutyricum*, *C.butyricum*, and *C. tyrobutyricum.*. Many studies have been performed to optimise *C. tyrobutyricum* as a cell factory for butyric acid production (Linger et al., 2020). For instance, in a study from Suo et al., (2017) it was observed that *the* overexpression of heat shock proteins, namely groESL and htpG

significantly improved *C. tyrobutyricum* tolerance to butyric acid. The batch fermentation led to butyrate concentrations of 34.3 $g.L^{-1}$ and 44.1 $g.L^{-1}$ for the WT and engineered *C. tyrobutyricum* strains, respectively. In terms of rate and yield, the results were 0.39 $g.L^{-1}.h$ and 0.34 $g.g^{-1}$ for the mutant strain, which very similar to the WT (Suo et al., 2017). Relatively to lactic acid there are other competitive lactic acid producing bacteria in the market. *Rhizopus oryzae*, for instance, has been utilized for lactic acid production, achieving a high titer of 231 $g.L^{-1}$ of lactic acid. This yield and productivity reached 0.92 $g.g^{-1}$ glucose and 1.83 $g.L^{-1}.h$, respectively, when *R. oryzae* was immobilized in a fed-batch culture (Yamane and Tanaka, 2013).

The levels of butyric acid and lactic acids documented from *C. tyrobutyricum* and *R. oryzae* were significantly higher than those observed in the Δ*pssA* and *mt*1^{+} strains. However, drawing a direct comparison between these experiments is challenging due to different scales of production. Future evaluating of yields and productivities in Δ*pssA* and *mt*1^{+} strains would be important to analyse their potential uses.

7.2.4 Stress adaptations

During fermentation there is an increase in the stress conditions in *Clostridium spp* cells, that in turn increase the expression levels of heat shock proteins and of genes involved in the phospholipid synthesis (Patakova et al., 2019). Phospholipids have been shown to adapt under stress conditions and cellular functions in *E. coli* (Rowlett et al., 2017). *E. coli pssA* mutant strain and. *E. coli* with the three *cls* genes deleted were studied for their lipid adaptation (Rowlett et al., 2017). These two strains were absent in PE and CL, respectively and did not result in the appearance of other lipid species. These strains had lower growth rates which was particularly drastic for cells without CL (Rowlett et al., 2017). *E. coli* strains lacking PE and CL, shown an increase in oxidative stress, highlighting the PE mutant strain having a stronger effect on energy metabolism (Rowlett et al., 2017). However, previous studies in yeast shown that the lipid adaptation in stress conditions is difficult to predict. Research on how *Saccharomyces* hybrid yeast adapts to ethanol for wine making found that understanding their lipid makeup is complex (Lairón-Peris et al., 2021). Even the mutant yeast strains more tolerant to ethanol shown that all under high ethanol concentrations, the lipid composition was similar to the other strains tested (Lairón-Peris et al., 2021).

In *C. acetobutylicum* the oxidative stress is thought to be modulated by the redox-responsive repressor Rex (Zhang Lei et al., 2014). Rex is a transcriptional repressor responsible for regulating the expression of NADH dehydrogenase in the respiratory chain (Figure 1.3). However, the role of Rex in *C. acetobutylicum*, especially in conditions where there is a shift in the cellular redox balance due to factors like heightened NAD(P)H levels or oxidative stress, remains unexplored. Based on (Zhang Lei et al., 2014) studies in *C. acetobutylicum*, Rex appears to monitor the NADH/NAD^+ ratio in vivo, influencing gene expression, fermentation, product formation, and the oxidative stress response.

In a study from (Monaghan et al., 2022) glyceraldehyde-3-phosphate dehydrogenase (*gapN*) was deleted from *C. saccharoperbutylacetonicum* N1-4 HMT genome, to characterise the NADH and ATP availability and its effect in the solvent production. GapN is an enzyme involved in the glucose metabolism and has been identified with absolute specification for NADPH. Its activity is likely to diminishes NADH and ATP production (Monaghan et al., 2022). *C. saccharoperbutylacetonicum* N1-4 HMT knockout *gapN* strain increased the ATP production and the ratio of NADH:NAD+ and it was able to diminish acid production, which allowed for an earlier shift into solventogenesis (Monaghan et al., 2022). ATP production, variation of pH generated by acid production and reducing conditions within the cell are important factors in the shift to solventogenesis (Wang et al., 2012; Wietzke and Bahl, 2012; Liu et al., 2018). It has been shown that in cultures with lower ATP levels acidogenesis phase is longer, it is a major route for energy generation, whereas cultures with elevated ATP levels produce more solvents (Meyer and Papoutsakis, 1989).

In *C. saccharoperbutylacetonicum* N1-4 HMT Δ*pssA* and *mt*1^+ strains there was an acid accumulation without a shift to the solventogenesis phases. These cells did not grow as much as the WT strain and shown much less motility. All these features can indicate for a possible energetic imbalance due to stress responses. Silencing one the *pssA* genes from *Clostridium* did not affect the PE synthesis possibly due to a second *pssA* in the genome but impaired growth. Overexpressing *mt*1 in *C. saccharoperbutylacetonicum* N1-4 HMT also affected the cell growth. MT1 has a MT-Zinc cluster that in oxidizing conditions the thiolate cluster from Zinc-MT bound is oxidized releasing this bound, the resultant MT-Disulfide is degraded (Ruttkay-nedecky et al., 2013). When there is an increase in glutathione (GSH)/glutathione disulfide (GSSG), the environment becomes more reduced (NADH/NADPH) and MTs are again reduced to MT-thiols, in the presence of Zinc in a process enhanced by the catalyst selenium. The free -SH (thiolate) moieties of MT can help on the reactive species scavenging (Ruttkay-nedecky et al., 2013). Mt1 can possibly lead to a redox imbalance in *C. saccharoperbutylacetonicum* N1-4 HMT, considering

that this enzyme constantly needs NADH for become active. However, this is just a speculation that needs further study and characterisation. A future analysis of the membrane integrity and measuring the NADH and ATP available in these cells will help understanding the regulation of these mechanisms. The combination of all factors such as, lipid composition, oxidative stress of the cell, energy requirements and acidogenesis/solventogenesis phase can potentially be interconnected even though hard to predict.

7.2.5 Engineering *C. saccharoperbutylacetonicum* N1-4 HMT

Knocking out the *pgsA* and *cls* genes, necessary in synthesizing PG and CL respectively, in *C. saccharoperbutylacetonicum* N1-4 HMT was one of the goals of this project that turned out to be a challenge. Possible explanations might be either due to technical problems during the experiments or because the bacteria will not be able to survive without these genes. In past studies, trying to turn off a *pssA* in other bacteria like *A. tumefaciens* made them grow poorly, showing that this task can sometimes be tricky because the genes are important for the viability of the bacteria (Karnezis et al., 2002). Previous efforts to silence *pssA* gene in *E. coli* were unsuccessful, demonstrating its vital role under the conditions used in that work (Tan et al., 2017). Consequently, it is important to acknowledge that the procedure of gene knockout can be complicated and occasionally affected by the fact that the genes are indispensable.

The methodology used to modify *C. saccharoperbutylacetonicum* N1-4(HMT) genome using the CLEAVE™ method requires two vectors. The first vector was specific for homologous recombination of chromosomal DNA in the *pgsA* and *cls* regions. However, trying to clone the step1 vector for *pgsA* was very challenging, preventing the use of CLEAVE™ method to deplete this gene. Despite numerous attempts, cloning this vector remained unsuccessful.

The vector for homologous recombination and the killing vector were cloned to create the Δ*cls* mutant strain. *C. saccharoperbutylacetonicum* N1-4(HMT) was transformed with these vectors. The first colony PCR to confirm the deletion of the *cls* gene in *C. saccharoperbutylacetonicum* N1-4(HMT) showed DNA bands matching the expected size. However, subsequent testing of the same colonies showed results patterns to the WT. This suggested the potential for cells to reverse the recombination. Following this recombination event, the DNA associated with the complete gene was swapped to the homologous recombination vector. While the killing vector demonstrated effectiveness, its efficacy was not 100%, as shown in Figure 4.11, from the cloning

results section. If the killing vector did not kill all cells, surviving cells possessing the correct knockout, containing the vector with the full *cls* gene sequence, could have reverted to the genome.

Some are the limitations regarding the recombination events. In bacteria the recombination efficiency in bacteria depends on the chromosomal segregation during cell division, requiring two replication cycles to completely segregate the introduced alteration to a daughter cell (Pines et al., 2015). This was the reason why several subcultures of transformed *C. saccharoperbutylacetonicum* N1-4(HMT) cells were performed.

Exponentially growing bacteria can have up to 8 chromosome copies decreasing homologous recombination efficiency. It has been described that while 5% of input cells undergo transformation, only 3-6% achieve the desired modification, resulting in a peak recombination efficiency of about 0.15-0.3% (Pines et al., 2015). To mitigate this, co-transformation with diverse drug resistance markers is an alternative. Using counter selection to eliminate non edited cells via CRISPR-cas9 cleavage enhances the efficiency t 65% (Pines et al., 2015), which was the case of the present work.

Another limitation of the CRISPR-Cas9 system for gene editing is the incomplete targeting of non-edited WT cells, allowing non-edited cells on growth plates. In *E. coli*, it has been described their ability to survive to certain Cas9 target cleavages by activating an SOS response, which facilitates DNA repair through homologous recombination with a sister chromosome (Cui and Bikard, 2016). Additionally, non-edited cells might occur due to spontaneous mutations in components like crRNA, PAM, or protospacer sequences, making them resistant to the specific CRISPR-Cas9 nuclease targeting sequences ,(Cui and Bikard. 2016). Other challenge with CRISPR-Cas9 genome editing by homologous recombination is the Cas9-induced cytotoxicity (Vento, Crook, and Beisel 2019).

7.2.6 Exploring the membrane of microbial cell factories

Understanding the plasma membrane is important to stablish the biological functions or for exploiting cellular systems in microbial-based processes (Ferraz et al., 2021). Integrating data deriving from different research technologies to describe the plasma membrane can describe the whole system. In this work, cloning technologies allowed to generate *C. saccharoperbutylacetonicum* N1-4 HMT mutant strains focused on the phospholipid

biosynthesis and the solvent stress during ABE fermentation. These strains were analysed for their membrane composition using technologies for lipid analysis, such as TLC and mass spectrometry.

TLC enabled a preliminary, cost-effective analysis of the lipidomes of WT and mutant strains (Deranieh, Joshi, and Greenberg 2013), revealing the presence of lipids PE, PG, and CL across all strains. However, this technique remains challenging in many aspects. The consistency in results presented challenges due to variable factors like plate and sample preparation, and chromatogram development conditions (Di Prima, Librizzi, and Carrotta 2020). Another limitation is the lipid quantification, due to the lack of sensitivity to PG based phospholipids (Charles and Stewart, 1980; Di Prima et al., 2020). Notably, in *C. saccharoperbutylacetonicum* N1-4(HMT), PG and CL represent two of the three main lipid classes known in the membrane (Guan and Goldfine, 2021). Although the TLC limitations this technique gave an important overview of the lipids in the *C. saccharoperbutylacetonicum* N1-4(HMT) at different growth stages and shown variations between the strains. It showed the adaptions of the membrane by modifying these dynamic molecules to support variations in physiological and environmental conditions (Linney et al., 2023).

To the identification and quantification of lipids in detail, mass spectrometry was employed. Mass spectrometry based lipidomics aimed the analysis and quantification of lipid species in the cells (Köfeler et al., 2012). This study identified the lipids of a cellular phenotype at a particular time point (24h) and therefore allowed to correlate a specific membrane lipid composition with specific conditions. environments and growth stages. However, the connection between the cellular mechanism which led to this specific membrane composition remains missing.

8 Conclusion and future perspectives

In conclusion, there is a complex relationship between the lipid membrane composition, cell homeostasis and ABE fermentation. Understanding the lipid membrane composition in the stress adaptation can provide important strategy to optimise *C. saccharoperbutylacetonicum* N 1–4 (HMT) as a cell factory. These findings can go beyond this strain and the principle can be applied in other cell factories.

To complement this work, it is urgent to have the lipidomic information regarding the CL in *C. saccharoperbutylacetonicum* N1-4(HMT) WT and mutant strains. This will provide an insight clearer about the membrane composition and understanding the mechanisms of lipid regulation. Confirming if lower percentages of PG are indicative of CL and less percentages of PE are also accompanied by an increase of CL, as it has been proposed to happen in bacteria membrane, to compensate the bilayer arrangement (Zhang and Rock 2008). Plasmalogen forms of CL have been described in the presence of stress conditions in *Clostridium* (Kolek et al., 2015). Additionally, CL has been described as an essential lipid in acidic environments, that were observed in Δ*pssA* and *mt*1^{+} strains.

The lipidomic analysis of the *C. saccharoperbutylacetonicum* N1-4(HMT) mutant strains from this study at different growth and fermentation stages, such as at 0h, 6h, 24h and 48h, will confer important information to connect possible networks between cell growth, acids accumulations, solvents accumulation and the stress adaptations. A detailed analysis of the FAs, namely on the cyclic ring and cis- and trans- isomerization, will help characterising the membrane arrangement keeping the cell fluidity.

Testing the membrane fluidity and membrane stress responses of the strains would be the following steps. Assays to analyse the membrane fluidity will provide an important output to characterise the effects of the lipidome changes in the mutant strains, when compared to the WT strain. This in turn can confer information about the interactions between the chemicals produced (butanol and weak acids) with the lipid bilayer. The laurdan assay is one possible methodology to test the fluidity of the membrane. *In vitro* laurdan assays have been used by our research group to characterise the effect of butanol in liposomes with different lipid composition (Linney et al., 2023).

Liposome models of membrane fluidity and membrane integrity confer very valuable insights into the interactions of lipids with different compounds. To complement them, bioinformatics

tolls can be an important resource to predict the structure and dynamics of the plasma membrane in different conditions (Ferraz et al., 2021; Linney et al., 2023). The detailed information in the lipid composition of the different mutant strains of *C. saccharoperbutylacetonicum* N1-4(HMT) at 24h of growth and knowing the acids and solvents concentrations at that time point, can contribute to make a MD prediction more accurate. This can in turn provide strategies for optimising these cell factories.

Atomic force microscopy is another method to complement the information regarding the weak acids and solvents interaction with the membrane. This technique was used by Linney et al., (2023) to study the butanol effects in the physical and mechanical properties of the membrane. This study showed that butanol induced pore formation however, the study was performed in a PC monolayer and not in living cells (Linney et al., 2023). Howeve, this technique has the advantage of allowing working with living cells under physiological conditions (Linney et al., 2023).

Genome-Scale Metabolic Models (GEMs) can be an instrument to optimise cell factories. Serving as a comprehensive network, GEMs compile the metabolic data of a biological system, enabling phenotype predictions grounded on genetic modifications (Ferraz et al., 2021). However, the reliability of these model-based forecasts is contingent on the accuracy of GEMs, presenting a possible limitation for *C. saccharoperbutylacetonicum* N1-4(HMT).

These are a group of possible and important assays to complement this study on the impact of metabolic engineered *C. saccharoperbutylacetonicum* N1-4(HMT) for the phospholipid synthesis and oxidative stress. The assays will provide more information regarding this phospholipid synthesis regulation that is still poorly understood. They can be important to understand the interaction of weak acids and solvents with the membrane. They can give better insights on strategies to modulate the solvent stress and loss of membrane integrity. Continued research in this direction could pave the way for optimized microbial strains with enhanced productivity or resilience, offering advantages in industrial applications.

In conclusion, the lipid membrane engineering has shown to be an important target for modulating weak acids and solvents production in *C. saccharoperbutylacetonicum* N1-4(HMT). Nevertheless, this work findings show a connection between membrane composition, cellular stress and ABE fermentation, revealing future routes for membrane engineering. By understanding how the lipid membrane adapts during production and when exposed to organic acids and solvents, it is possible to unlock the key to refining various biotechnological processes.

9 Annex

Annex 1. Table representing the lipid migration in the four solvent systems selected in this work. Rf values represent relative migration only, whereas absolute values depend on various environmental parameters (e.g. temperature, humidity) which may vary depending on location. (Adapted from Avanti polar lipids).

Lipids	Solvent System (Rf)			
	i	ii	iii	iv
Phosphatidylethanolamine	0.79	0.55		0.43
Phosphatidyl (Monomethylethanolamine)	0.71	0.41		0.33
Cardiolipin	0.67	0.56	0.38	
Phosphatidylglycerol	0.60	0.50	0.31	0.36
Phosphatidyl (Dimethylethanolamine)	0.58	0.56		0.27
Phosphatidic Acid	0.55	0.05	0.58	
Phosphatidylinositol	0.39	0.10		
Phosphatidylcholine	0.34	0.30		0.17
Phosphatidylserine	0.33	0.12		
Cerebrosides	0.94	0.55		
Sphingosine	0.28	0.75		
Sphingomyelin	0.28	0.13		
Synthetic Cardiolipin	0.29	0.20		
Lyso-Phosphatidylglycerol	0.54	0.20		
Lyso-Phosphatidylethanolamine	0.45	0.20		
Monolysocardiolipin	0.45	0.34		
Lyso-Phosphatidic Acid	0.40	0.01		

Annex 2. Univariant analysis of the LPE and LPMME between the WT, Δ*pssA* and *pssA*$^{+}$ strains obtained by mass spectrometry. Comparison of the phospholipid classes: (A) LPE, between WT and Δ*pssA* strains; (B) LPE, between Δ*pssA* and *pssA*$^{+}$ strains; (C) LPMME, between WT and Δ*pssA* strains and (D) The x-axis corresponds to the $\log_2$ (fold-change) between a group of 2 strains. Significant results ($p < 0.05$, uncorrected Dunn's test) are highlighted in black. Results from four independent biological repeats (n=4).

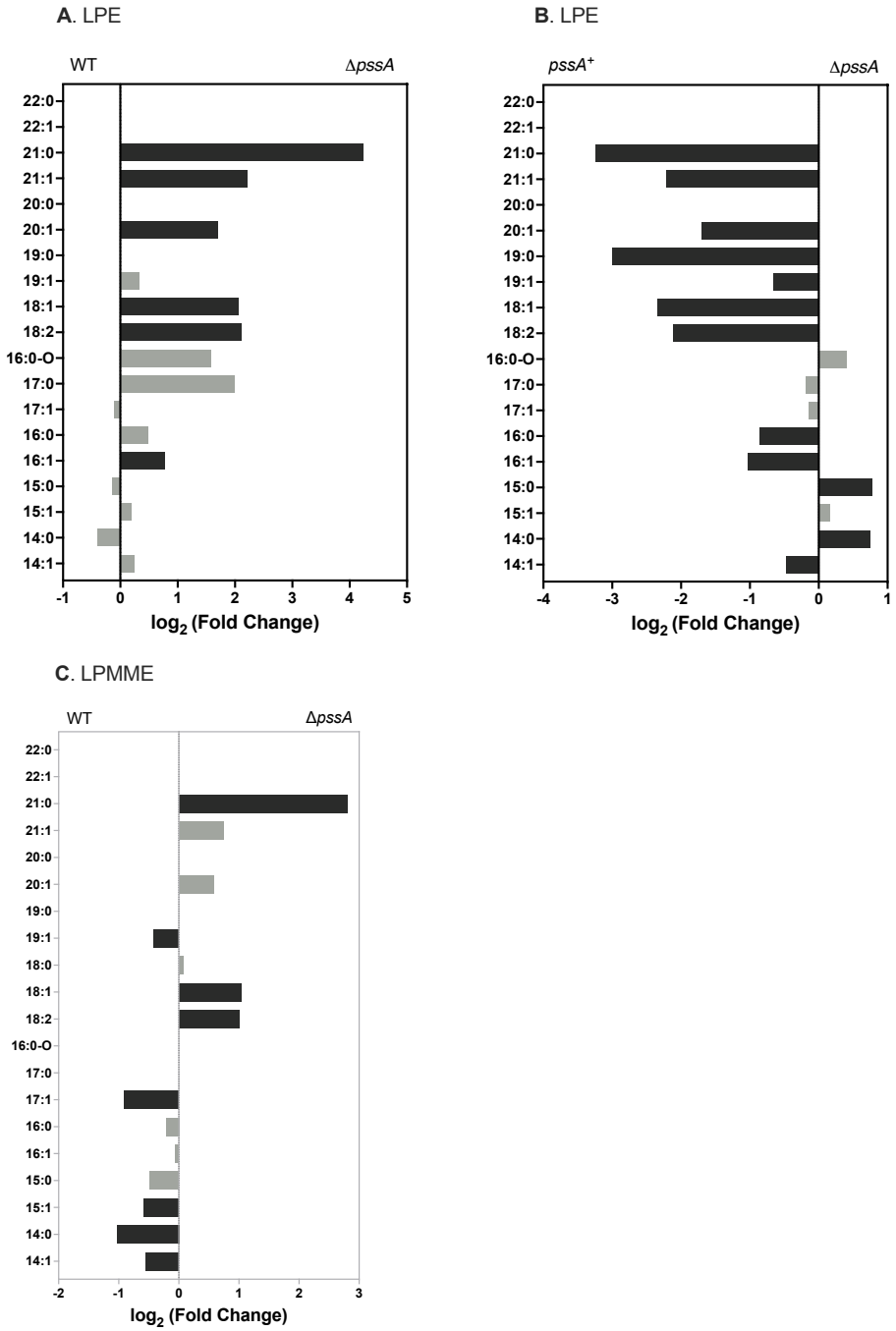

Annex 3. Univariant analysis of PA and PS between the WT, Δ*pssA* and *pssA*$^{+}$ strains obtained by mass spectrometry. Comparison of the phospholipid classes: (A) PA, between Δ*pssA* and *pssA*$^{+}$ strains strains; (B) PS, between *pssA*$^{+}$ and WT strains. Significant results ($p < 0.05$, uncorrected Dunn's test) are highlighted in black. Results from four independent biological repeats (n=4).

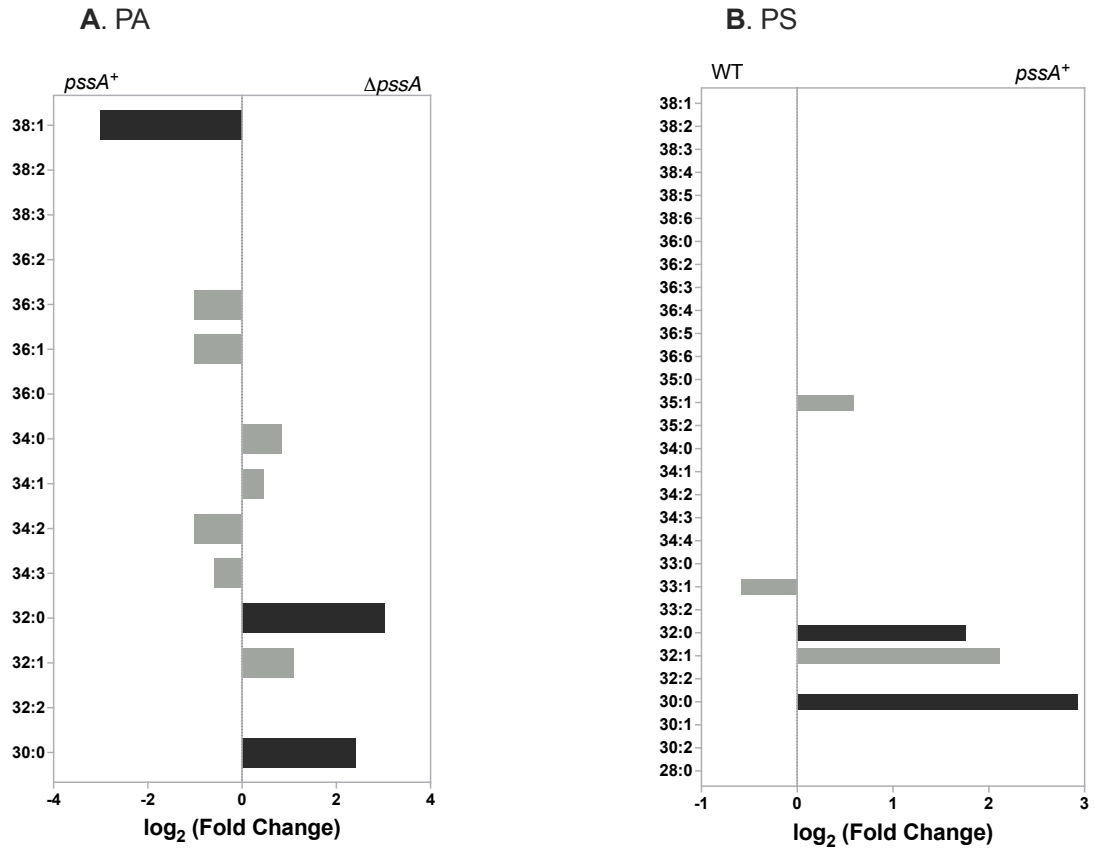

Annex 4. List of lipids analysed by univariate analysis between strains: (A) Δ*pssA* / WT and (B) *pssA*$^+$ / WT; with *p-values* < 0.05 and along with their fold-change (FC) values. Positive log_2(FC) indicates higher concentrations of lipids found in the strain represented in the numerator, while a negative log_2(FC) indicates lipids found in higher concentrations in the strain represented in the denominator. The *p-values* were calculated using the uncorrected Dunn's test.

A

Lipid	Log_2 (FC)		*p-value*
	WT	Δ*pssA*	
PS(32:2)	-	0.000	0.005
PMME(28:0)	-	1.954	0.001
PMME(22:0)	-	0.000	0.001
PMME(26:1)	-	0.000	0.001
PMME(34:0)	-2.663	-	0.003
PMME(33:1)	-0.976	-	0.006
PMME(37:2)	-	2.000	0.013
PMME(26:0)	-	1.336	0.020
PMME(38:2)	-	0.807	0.025
PMME(32:1)	-0.621	-	0.027
PMME(32:0)	-1.801	-	0.030
PMME-Cer(18:0)	-	0.000	0.046
PMME(32:0-O)	-	0.000	0.046
PG(35:1)	-2.043	-	0.002
PG(32:0)	-3.445	-	0.004
PG(33:1)	-2.274	-	0.004
PG(30:0)	-1.815	-	0.046
PE(28:0)	-	1.929	0.001
PE(26:0)	-	2.189	0.001
PE(22:0)	-	0.000	0.005
PE(32:0)	-3.634	-	0.006
PE(37:1)	-0.737	-	0.006
PE(34:0)	-4.663	-	0.010
PE(31:1)	-	0.779	0.012
PE(37:2)	-	2.000	0.014
PE(26:1)	-	2.459	0.021
PE(28:1)	-	1.737	0.021
PE(38:2)	-	1.170	0.024
PE(36:0)	-	0.000	0.030
PE-Cer(18:0)	-	0.000	0.046
PE(35:1)	-1.438	-	0.050
PA(32:2)	-	4.392	0.001
PA(38:1)	-	2.000	0.036
PA(38:2)	-	0.000	0.042
LPMME(17:1)	-0.907	-	0.000
LPMME(14:1)	-0.548	-	0.001
LPMME(18:1)	-	1.042	0.001
LPMME(19:1)	-0.414	-	0.005
LPMME(21:0)	-	2.807	0.008
LPMME(14:0)	-1.031	-	0.013
LPMME(15:1)	-0.585	-	0.017
LPMME(18:2)	-	1.000	0.018
LPE(20:1)	-	1.700	0.001
LPE(18:1)	-	2.062	0.002
LPE(21:0)	-	4.248	0.002
LPE(18:2)	-	2.115	0.003
LPE(21:1)	-	2.222	0.005
LPE(19:0)	-	0.000	0.006
LPE(16:1)	-	0.781	0.007
LPE(22:1)	-	0.000	0.046
DihexDAG(30:0)	-	0.000	0.002
DihexDAG(32:1)	-	2.129	0.009
DihexDAG(30:1)	-	0.000	0.021
DihexDAG(34:2)	-	0.263	0.040

B

Lipid	Log_2 (FC)		*p-value*
	WT	*pssA*$^+$	
PS(30:0)	-	2.926	0.002
PS(32:0)	-	1.755	0.037
PMME(30:0)	-	0.712	0.007
PMME(31:0)	-	0.628	0.015
PMME(30:1)	-0.524	-	0.031
PMME(28:1)	-2.000	-	0.044
PMME-Cer(18:0)	-	0.000	0.046
PMME(32:0-O)	-	0.000	0.046
PE(31:0)	-	0.979	0.001
PE(30:0)	-	1.419	0.002
PE(29:0)	-	0.585	0.014
PE(34:1)	-	0.691	0.026
PE(33:0)	-	1.322	0.037
PA(30:0)	-	1.684	0.021
LPMME(15:0)	-	0.778	0.013
LPMME(15:1)	-0.585	-	0.017
LPE(16:0-O)	-	2.000	0.034
LPE(17:1)	-0.259	-	0.035
DihexDAG(33:2)	-	0.000	0.039
DihexDAG(31:2)	-	2.755	0.043

Annex 5. List of lipids analysed by univariate analysis between strains: *pssA*$^+$ / Δ*pssA*; with *p-values* < 0.05 along with their fold-change (FC) values. Positive log_2(FC) indicates higher concentrations of lipids found in the strain represented in the numerator, while a negative log_2(FC) indicates lipids found in higher concentrations in the strain represented in the denominator. The *p-values* were calculated using the uncorrected Dunn's test.

Lipid	Log_2 (FC)		*p-value*
	pssA$^+$	Δ*pssA*	
PS(32:0)	-	3.755	0.001
PS(32:2)	-	0.000	0.005
PS(30:0)	-	2.248	0.007
PS(33:1)	-1.807	-	0.024
PMME(32:0)	-	2.447	0.000
PMME(34:0)	-	2.585	0.001
PMME(22:0)	-	0.000	0.001
PMME(26:1)	-	0.000	0.001
PMME(37:2)	-3.000	-	0.003
PMME(29:0)	-	1.214	0.004
PMME(31:0)	-	0.766	0.004
PMME(35:2)	-3.585	-	0.004
PMME(38:2)	-1.222	-	0.004
PMME(26:0)	-1.480	-	0.009
PMME(35:1)	-1.138	-	0.017
PMME(36:2)	-1.138	-	0.017
PMME(30:1)	-0.459	-	0.023
PMME(28:0)	-1.452	-	0.026
PMME(34:1)	-0.446	-	0.028
PMME(33:2)	-1.454	-	0.030
PMME(28:1)	-2.000	-	0.044
PMME(34:3)	-0.874	-	0.046
PG(30:0)	-	2.608	0.001
PG(32:0)	-	2.202	0.003
PG(33:2)	-2.632	-	0.003
PG(35:2)	-3.644	-	0.009
PG(28:1)	-	0.000	0.022
PG(32:2)	-1.459	-	0.037
PG(36:0)	-	0.000	0.047

Lipid	Log_2 (FC)		*p-value*
	pssA$^+$	Δ*pssA*	
PE(31:0)	-	1.251	0.000
PE(32:0)	-	4.019	0.000
PE(30:0)	-	1.782	0.000
PE(34:0)	-	4.235	0.000
PE(31:1)	-0.956	-	0.001
PE(37:2)	-	0.000	0.001
PE(26:1)	-	0.000	0.001
PE(28:1)	-2.322	-	0.001
PE(35:2)	-2.572	-	0.002
PE(26:0)	-1.846	-	0.002
PE(34:2)	-1.422	-	0.004
PE(22:0)	-	0.000	0.005
PE(33:2)	-2.329	-	0.006
PE(36:1)	-	1.000	0.007
PE(38:2)	-1.170	-	0.015
PE(34:1)	-	0.725	0.016
PE(32:2)	-1.219	-	0.016
PE(31:2)	-0.848	-	0.017
PE(36:2)	-1.585	-	0.019
PE(33:0)	-	1.322	0.035
PE(32:1)	-	1.226	0.040
PE-Cer(18:0)	-	0.000	0.046
PA(32:2)	-	0.000	0.000
PA(30:0)	-	2.406	0.007
PA(32:0)	-	3.027	0.007
PA(38:1)	-3.000	-	0.009
PA(38:2)	-	0.000	0.042

Lipid	Log_2 (FC)		*p-value*
	pssA$^+$	Δ*pssA*	
LPMME(15:0)	-	1.263	0.001
LPMME(14:0)	-	1.280	0.001
LPMME(21:0)	-	0.000	0.002
LPMME(17:1)	-	0.663	0.002
LPMME(18:2)	-1.322	-	0.003
LPMME(18:1)	-0.937	-	0.004
LPMME(21:1)	-2.322	-	0.025
LPE(16:1)	-1.038	-	0.000
LPE(18:1)	-2.350	-	0.000
LPE(16:0)	-0.858	-	0.000
LPE(19:1)	-0.657	-	0.001
LPE(20:1)	-1.700	-	0.001
LPE(14:0)	-	0.746	0.003
LPE(18:2)	-2.115	-	0.003
LPE(21:1)	-2.222	-	0.005
LPE(14:1)	-0.479	-	0.005
LPE(21:0)	-3.248	-	0.010
LPE(15:0)	-	0.784	0.017
LPE(19:0)	-3.000	-	0.032
LPE(22:1)	-	0.000	0.046
DihexDAG(30:1)	-	0.000	0.021
DihexDAG(37:1)	-	0.000	0.034
DihexDAG(34:2)	-2.585	-	0.035

Annex 6. List of lipids analysed by univariate analysis between strains: (A) *pgsA*$^+$ / WT and (B) *cls*$^+$ / WT; with *p-values* < 0.05 along with their fold-change (FC) values. Positive $\log_2$(FC) indicates higher concentrations of lipids found in the strain represented in the numerator, while a negative $\log_2$(FC) indicates lipids found in higher concentrations in the strain represented in the denominator. The *p-values* were calculated using the uncorrected Dunn's test.

A

Lipid	$\log_2$ (FC)		*p-value*
	WT	*pgsA*$^+$	
PS(30:0)	-	3.233	0.001
PS(35:1)	-	1.807	0.020
PS(32:1)	-	2.322	0.029
PS(30:2)	-	0.000	0.046
PS(34:4)	-	0.000	0.046
PS(34:3)	-	0.000	0.046
PS(38:5)	-	0.000	0.046
PS(38:4)	-	0.000	0.046
PMME(30:0)	-	0.997	0.001
PMME-Cer(18:0)	-	0.000	0.046
PMME(32:0-O)	-	0.000	0.046
PMME(33:2)	-0.772	-	0.047
PG(38:2)	-	0.000	0.018
PE(30:0)	-	1.323	0.007
PE(28:0)	-	1.630	0.014
PE(31:0)	-	0.801	0.016
PE(36:0)	-	0.000	0.030
PE(26:0)	-	1.085	0.048
PA(36:2)	-	0.000	0.046
LPMME(16:0)	-0.386	-	0.004
LPMME(19:1)	-0.366	-	0.014
LPMME(17:1)	-0.510	-	0.026
LPMME(15:0)	-	0.778	0.031
LPE(17:0)	-	2.459	0.007
LPE(15:1)	-	0.778	0.012
DihexDAG(31:1)	-	4.087	0.042

B

Lipid	$\log_2$ (FC)		*p-value*
	WT	*cls*$^+$	
PMME(31:1)	-1.060	-	0.008
PMME(30:0)	-	0.623	0.021
PMME(28:0)	-	1.030	0.034
PMME(34:0)	-1.663	-	0.035
PMME(32:2)	-1.124	-	0.044
PMME-Cer(18:0)	-	0.000	0.046
PMME(32:0-O)	-	0.000	0.046
PMME(31:2)	-0.879	-	0.046
PG(31:1)	-	0.000	0.044
PE(28:0)	-	1.605	0.005
PE(26:0)	-	1.384	0.010
PE(30:1)	-	0.940	0.016
PE(32:1)	-	1.034	0.017
PE(33:1)	-	0.982	0.023
PE(34:1)	-	0.671	0.026
PE(36:0)	-	0.000	0.030
LPMME(16:0)	-0.485	-	0.000
LPMME(19:1)	-0.389	-	0.010
LPMME(16:1)	-0.230	-	0.014
LPMME(15:1)	-0.585	-	0.017
LPE(15:1)	-	0.778	0.012
LPE(15:0)	-	0.807	0.027
DihexDAG(30:2)	-	2.663	0.034
DihexDAG(33:2)	-	0.000	0.039
DihexDAG(36:0)	-	1.634	0.043

Annex 7. List of lipids analysed by univariate analysis between *mt*1⁺ and WT strains, with *p-values* < 0.05 along with their fold-change (FC) values. Positive log_2(FC) indicates higher concentrations of lipids found in the strain represented in the numerator, while a negative log_2(FC) indicates lipids found in higher concentrations in the strain represented in the denominator. The *p-values* were calculated using the uncorrected Dunn's test.

A

Lipid	Log₂ (FC)		*p-value*
	WT	*mt*1⁺	
PS(33:2)	-	0.000	0.002
PS(32:1)	-	2.663	0.004
PS(30:1)	-	0.000	0.007
PS(32:2)	-	0.000	0.037
PMME(34:0)	-3.248	-	0.001
PMME(22:0)	-	0.000	0.001
PMME(26:1)	-	0.000	0.001
PMME(38:2)	-	1.170	0.002
PMME(28:0)	-	1.907	0.002
PMME(33:1)	-1.146	-	0.002
PMME(26:0)	-	1.562	0.004
PMME(32:1)	-0.752	-	0.006
PMME(37:2)	-	2.000	0.013
PMME(32:0)	-2.038	-	0.015
PMME(29:0)	-0.967	-	0.027
PMME(31:1)	-0.834	-	0.030
PMME-Cer(18:0)	-	0.000	0.046
PMME(32:0-O)	-	0.000	0.046
PG(32:0)	-3.807	-	0.002
PG(37:2)	-	0.000	0.012
PG(35:2)	-	2.624	0.012
PG(35:1)	-1.341	-	0.014
PG(33:1)	-1.729	-	0.021
PG(33:2)	-	1.807	0.042
PG(31:2)	-	0.000	0.045
PG(38:0)	-	0.000	0.049

B

Lipid	Log₂ (FC)		*p-value*
	WT	*mt*1⁺	
PE(28:0)	-	2.715	0.000
PE(26:0)	-	3.065	0.000
PE(30:1)	-	1.342	0.000
PE(22:0)	-	-	0.000
PE(38:2)	-	1.700	0.002
PE(26:1)	-	3.322	0.003
PE(28:1)	-	2.773	0.003
PE(37:2)	-	2.322	0.004
PE(31:1)	-	0.865	0.007
PE(36:2)	-	1.515	0.009
PE(35:2)	-	2.384	0.015
PE(34:0)	-4.441	-	0.016
PE(32:0)	-3.468	-	0.018
PE(29:0)	-	0.564	0.019
PE(36:0)	-	-	0.030
PA(32:2)	-	3.459	0.010
PA(36:1)	-	2.585	0.014
PA(36:3)	-	2.585	0.014
LPMME(17:1)	-0.800	-	0.000
LPMME(14:1)	-0.630	-	0.001
LPMME(21:0)	-	3.000	0.002
LPMME(16:1)	-0.248	-	0.006
LPMME(14:0)	-1.154	-	0.006
LPMME(18:1)	-	0.791	0.008
LPMME(20:1)	-	0.807	0.012
LPMME(16:0)	-0.336	-	0.017
LPMME(15:1)	-0.585	-	0.017
LPMME(18:2)	-	1.000	0.018
LPE(21:0)	-	4.700	0.000
LPE(19:0)	-	-	0.000
LPE(20:1)	-	1.700	0.001
LPE(21:1)	-	2.415	0.005
LPE(18:1)	-	1.909	0.005
LPE(19:1)	-	0.596	0.011
LPE(18:2)	-	1.737	0.012
LPE(16:1)	-	0.657	0.024
DihexDAG(32:1)	-	2.044	0.016
DihexDAG(33:2)	-	0.000	0.039

Annex 8. List of lipids analysed by univariate analysis between *BCL* and WT strains, with *p-values* < 0.05 along with their fold-change (FC) values. Positive log_2(FC) indicates higher concentrations of lipids found in the strain represented in the numerator, while a negative log_2(FC) indicates lipids found in higher concentrations in the strain represented in the denominator. The *p-values* were calculated using the uncorrected Dunn's test.

Lipid	**Log_2 (FC)**		***p-value***
	WT	*BCL*	
PS(32:1)	-	3.544	0.002
PS(35:1)	-	2.459	0.002
PS(30:0)	-	3.561	0.003
PS(34:1)	-	0.000	0.018
PS(32:0)	-	2.426	0.028
PMME(37:0)	-	1.000	0.009
PMME(30:1)	-0.666	-	0.010
PMME(32:1)	-0.613	-	0.026
PMME(28:1)	-2.000	-	0.044
PMME-Cer(18:0)	-	0.000	0.046
PMME(32:0-O)	-	0.000	0.046
PG(30:0)	-	1.162	0.042
PE(29:0)	-	0.705	0.002
PE(33:2)	-1.150	-	0.022
PE(36:0)	-	0.000	0.030
PE(34:1)	-	0.612	0.050
PA(30:0)	-	2.126	0.002
PA(34:0)	-	2.369	0.026
LPMME(16:0)	-0.444	-	0.003
LPMME(18:0)	-0.603	-	0.017
LPMME(15:1)	-0.585	-	0.017
DihexDAG(33:2)	-	0.000	0.039

Annex 9. Agarose gel electrophoresis of the colony PCR results to confirm the deletion of the *pssA* gene within *C. saccharoperbutylacetoncium* N1-4 HMT genome. (A) strategy 1: primers that bind to the homologous regions upstream the gene and the middle of the gene. (B) strategy 2: primers that bind to the homologous regions upstream the gene and downstream of the gene. No band in Δ*pssA* strain (A) and a band with lower sizer in Δ*pssA* strain (B) indicate the correct knockout *pssA* strain. The *pssA*$^{+}$ and WT strains were used as positive controls. (-) was used as negative control without DNA. Molecular Weight ladder: generuler 1kb plus DNA ladder (ThermoFisher, UK).

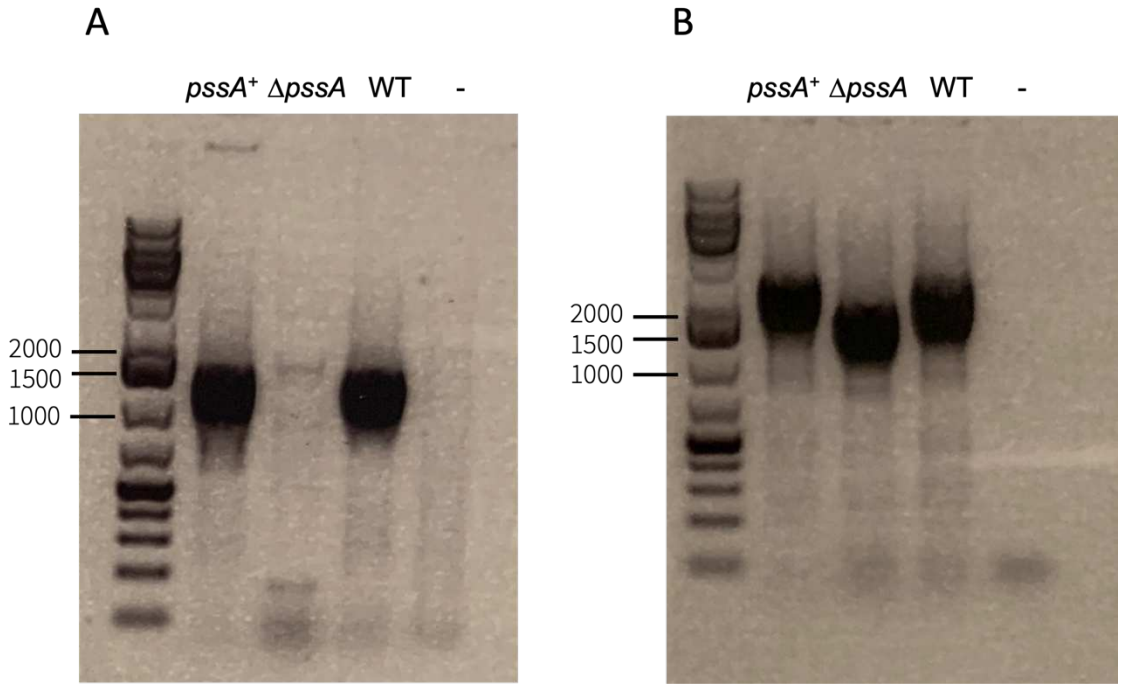

Annex 10. Information regarding the two *pssA* genes from *C. saccharoperbutylacetoncium* N1-4 HMT genome. The genes have different locus, different DNA sequence but code for the exact same protein sequence. (A) Corresponds to the gene tested in this work in both Δ*pssA* and *pssA*$^{+}$ strains. (B) Corresponds to the *pssA* gene that remained in the genome of both mutant and WT strains. (C) Alignment between the two PssA enzymes (NCBI Bastp).

A. *pssA* selected in this study

GenBank - CP004121.1:1970881-1971402

Gene locus – Cspa_c17800

Product - CDP-diacylglycerol--serine O-phosphatidyltransferase (PssA)

5'- ATGTTAAAAAAATATATACCAAATATATTAACATTTATGAATTTATCGTTTGGAATTCTTTCAATAATTG
AAGTTTTTAATAAAAATTTTAGTAGAGGAGCTTTATTTATAATTGCTGCTGCGTTAATAGATAGATATGA
TGGCAGAATTGCAAGATATTTTAAGGTATCCAGTGAAATAGGAAAAGAACTAGATTCTTTAGCAGATTTA
ATTTCCTTTGGAGTTGCACCGGCTATATTAATATTTTCTAAATATATTTTTGGTTTTCAGGCGTTTGGCG
TGATTGGAATTATTTCAGCACAAGCTTATATTATATGTGGTTGTTACAGATTAGCAAAATATAATGTTAG
TGAATTTAATGGAACTTTCACAGGAATTCCAATAACTATTGCAGGTTTAATTCTAGCATTATTTTCGTTA
TTTGTACCTAAAAATAACGTATTTGTAATAATACTATCAGTTATTTTAATGAGCGTTCTTGCTTATCTTA
TGATAGCAAAATTTAAGTTGAAAAAGATTTGA – 3'

B. Second *pssA* found in the genome

GenBank - CP004121.1:5680455-5680976

Gene locus – Cspa_c51360

Product - CDP-diacylglycerol--serine O-phosphatidyltransferase

5'- ATGAGGAAAAGTTGTATTCCTAATGTATTTACCTTTATTAATTTGTCTTGCGGAATTATATCTATATTAT
CAGCAATGAATGATAACTATCCATTAGCAGGTGCTTTTATCTTATTAGCTGGATTAGTTGATAGATATGA
TGGAAGAATAGCTCGTTTTTTAGATGTATCTAGTGATTTGGGAAAAGAATTGGATTCATTGGCTGACTTG
GTTTCTTTTGGTGTAGCACCATCTATATTAGTATATATATTATTTAATCTTAATACCTTTGGTCCTAATG
GATTATTAGGTTATATAGTTTTACTATTATTCCCAATCTGTGGTGCATATAGGTTGGCAAGATTTAATAC
TACTGATTTTGATGGTTCTTTTACAGGCGTTCCTATAACAATTGTAGGGTGTTTTATGGCACTTTTTTCA
TTACTTAACTTAAATACAAAAGCACCAGTTTATCTTGTTGTAATTTTAATGTTAATAGGTTCGTATTTAA
TGGTATCTAAACTTAAATTGAAGAAATTCTAA– 3'

C. Protein alignment: two PssA protein sequences from *C. saccharoperbutylacetonicum* N1-4 HMT

Score	Expect	Method	Identities	Positives	Gaps
174 bits(440)	6e-61	Compositional matrix adjust.	92/175(53%)	124/175(70%)	6/175(3%)

```
Query  1    MLKKYIPNILTFMNLSFGILSIIEVFNKNFSRGALFIIAAALIDRYDGRIARYFKVSSEI  60
            M K  IPN+ TF+NLS GI+SI+   N N+     FI+ A L+DRYDGRIAR+  VSS++
Sbjct  1    MRKSCIPNVFTFINLSCGIISILSAMNDNYPLAGAFILLAGLVDRYDGRIARFLDVSSDL  60

Query  61   GKELDSLADLISFGVAPAILIFSKYIFGFQAF---GVIGIISAQAYIICGCYRLAKYNVS  117
            GKELDSLADL+SFGVAP+IL++   +F    F   G++G I    + ICG YRLA++N +
Sbjct  61   GKELDSLADLVSFGVAPSILVY--ILFNLNTFGPNGLLGYIVLLLFPICGAYRLARFNTT  118

Query  118  EFNGTFTGIPITIAGLILALFSLFVPKNNVFVIILSVILMSVLAYLMIAKFKLKK  172
            +F+G+FTG+PITI G  +ALFSL +  N    + L VILM + +YLM++K KLKK
Sbjct  119  DFDGSFTGVPITIVGCFMALFSL-LNLNTKAPVYLVVILMLIGSYLMVSKLKLKK  172
```

Annex 11. Growth analysis by microscopy of WT and *mt*1^{+}. Cells were incubated in TYIR media with 50 g.L^{-1} of glucose and 30 mM MES where they grew under anaerobic conditions, at 32°C for 24 hours. The *mt*1^{+} culture media was supplemented with 75µg.ml^{-1} of Thiamphenicol. Images were captured at 0h, 6h, and 24h, revealing noticeable distinctions in the cellular physiology of each strain. Notably, *mt*1^{+} cells appear to be smaller in size and exhibit significantly reduced motility compared to the WT cells.

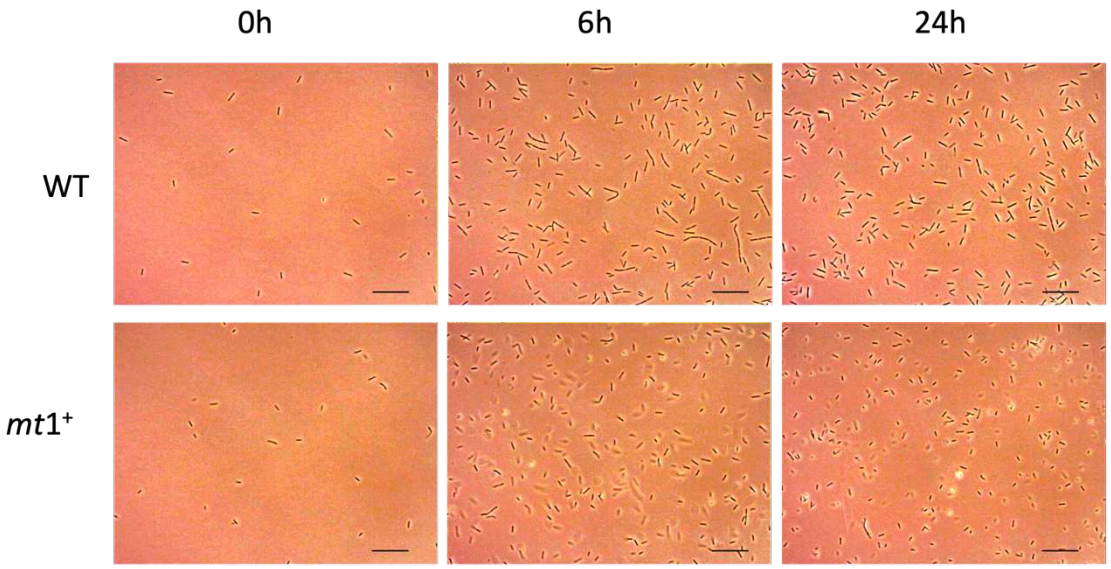

10 Bibliography

Aktas, Meriyem, and Franz Narberhaus. 2009. “In Vitro Characterization of the Enzyme Properties of the Phospholipid N-Methyltransferase PmtA from Agrobacterium Tumefaciens.” *Journal of Bacteriology* 191(7): 2033–41. doi:10.1128/JB.01591-08.

Alsaker, Keith V, Carlos Paredes, and Eleftherios T Papoutsakis. 2010. “Metabolite Stress and Tolerance in the Production of Biofuels and Chemicals: Gene-Expression-Based Systems Analysis of Butanol, Butyrate, and Acetate Stresses in the Anaerobe Clostridium Acetobutylicum.” *Biotechnology and Bioengineering* 105(6): 1132–47. doi:10.1002/bit.22628.

Amoah, Jerome, Prihardi Kahar, Chiaki Ogino, and Akihiko Kondo. 2019. “Bioenergy and Biorefinery: Feedstock, Biotechnological Conversion, and Products.” *Biotechnology Journal* 14(6). doi:10.1002/biot.201800494.

Atmadjaja, Aretha N., Verity Holby, Amanda J. Harding, Preben Krabben, Holly K. Smith, and Elizabeth R. Jenkinson. 2019. “CRISPR-Cas, a Highly Effective Tool for Genome Editing in Clostridium Saccharoperbutylacetonicum N1-4(HMT).” *FEMS Microbiology Letters* 366(6): 1–10. doi:10.1093/femsle/fnz059.

Bahl, Hubert, Harald Miiller, Susanne Behrens, Heinke Joseph, Franz Narberhaus, Institut Mikrobiologie, and D- Gi. 1995. “Expression of Heat Shock Genes in Clostridium Acetobutylicum.” *FEMS Microbiology Reviews* 17: 341–48.

Basconcillo, Libia Saborido, Rahat Zaheer, Turlough M. Finan, and Brian E. McCarry. 2009. “Cyclopropane Fatty Acyl Synthase in Sinorhizobium Meliloti.” *Microbiology* 155(2): 373–85. doi:10.1099/mic.0.022608-0.

Belin, Brittany J., Nicolas Busset, Eric Giraud, Antonio Molinaro, Alba Silipo, and DIanne K. Newman. 2018. “Hopanoid Lipids: From Membranes to Plant-Bacteria Interactions.” *Nature Reviews Microbiology* 16(5): 304–15. doi:10.1038/nrmicro.2017.173.

Ben-Zeev, Galia, Michael Telias, and Itzhak Nussinovitch. 2010. “Lysophospholipids Modulate Voltage-Gated Calcium Channel Currents in Pituitary Cells; Effects of Lipid Stress.” *Cell Calcium* 47(6): 514–24. doi:10.1016/j.ceca.2010.04.006.

Bessa, Daniela, Filipa Pereira, Roxana Moreira, Björn Johansson, and Odília Queirós. 2012. "Improved Gap Repair Cloning in Yeast: Treatment of the Gapped Vector with Taq DNA Polymerase Avoids Vector Self-Ligation." *Yeast* 29(10): 419–23. doi:10.1002/yea.2919.

Blanco, Antonio, and Gustavo Blanco. 2017. "Lipids." In Medical Biochemistry, 99–119. doi:10.1016/B978-0-12-803550-4/00005-7.

Bligh, E. G., and W. J. Dyer. 1959. "A RAPID METHOD OF TOTAL LIPID EXTRACTION AND PURIFICATION." *Canadian Journal of Biochemistry and Physiology* 37(8): 911–17.

Blindauer, Claudia A. 2011. "Bacterial Metallothioneins: Past, Present, and Questions for the Future." *JBIC Journal of Biological Inorganic Chemistry* 16(7): 1011–24. doi:10.1007/s00775-011-0790-y.

Cajka, Tomas, and Oliver Fiehn. 2017. "LC–MS-Based Lipidomics and Automated Identification of Lipids Using the LipidBlast in-Silico MS/MS Library." *Methods in Molecular Biology* 1609: 149–70. doi:10.1007/978-1-4939-6996-8_14.

Chang, Ying Ying, and John E. Cronan. 1999. "Membrane Cyclopropane Fatty Acid Content Is a Major Factor in Acid Resistance of Escherichia Coli." *Molecular Microbiology* 33(2): 249–59. doi:10.1046/j.1365-2958.1999.01456.x.

Charles, John, and Marshali Stewart. 1980. "Colorimetric Determination of Phospholipids with Ammonium Ferrothiocyanate." *Analytical Biochemistry* 104: 10–14.

Charubin, Kamil, R. Kyle Bennett, Alan G. Fast, and Eleftherios T. Papoutsakis. 2018. "Engineering Clostridium Organisms as Microbial Cell-Factories: Challenges & Opportunities." *Metabolic Engineering* 50(June): 173–91. doi:10.1016/j.ymben.2018.07.012.

Chen, Yun, and Jens Nielsen. 2016. "Biobased Organic Acids Production by Metabolically Engineered Microorganisms." *Current Opinion in Biotechnology* 37: 165–72. doi:10.1016/j.copbio.2015.11.004.

Cheng, Sy Chyi, Min Zong Huang, and Jentaie Shiea. 2011. "Thin Layer Chromatography/Mass Spectrometry." *Journal of Chromatography A* 1218(19): 2700–2711. doi:10.1016/j.chroma.2011.01.077.

Cherubini, F., G. Jungmeier, M. Wellisch, T. Willke, I. Skiadas, R. Van Ree, and E. de Jong. 2009. "Toward a Common Classification Approach for Biorefinery Systems." *Biofuels, Bioproducts and Biorefining* 3(5): 534–46. doi:10.1002/bbb.172.

Chin, Wei Chih, Kuo Hsing Lin, Jui Jen Chang, and Chieh Chen Huang. 2013. “Improvement of N-Butanol Tolerance in Escherichia Coli by Membrane-Targeted Tilapia Metallothionein.” *Biotechnology for Biofuels* 6(1): 1–9. doi:10.1186/1754-6834-6-130.

Chin, Wei Chih, Kuo Hsing Lin, Chun Chi Liu, Kenji Tsuge, and Chieh Chen Huang. 2017. “Improved N-Butanol Production via Co-Expression of Membrane-Targeted Tilapia Metallothionein and the Clostridial Metabolic Pathway in Escherichia Coli.” *BMC Biotechnology* 17(1): 1–14. doi:10.1186/s12896-017-0356-3.

Chino, Ayako, Kenji Watanabe, and Hisao Moriya. 2010. “Plasmid Construction Using Recombination Activity in the Fission Yeast Schizosaccharomyces Pombe” ed. Jürg Bähler. *PLoS ONE* 5(3): e9652. doi:10.1371/journal.pone.0009652.

Cho, Jae Sung, Gi Bae Kim, Hyunmin Eun, Cheon Woo Moon, and Sang Yup Lee. 2022. “Designing Microbial Cell Factories for the Production of Chemicals.” *JACS Au* 2(8): 1781–99. doi:10.1021/jacsau.2c00344.

Costantini, David. 2019. “Understanding Diversity in Oxidative Status and Oxidative Stress : The Opportunities and Challenges Ahead.” doi:10.1242/jeb.194688.

Criscuolo, Angela, Martin Zeller, and Maria Fedorova. 2020. “Evaluation of Lipid In-Source Fragmentation on Different Orbitrap-Based Mass Spectrometers.” *Journal of the American Society for Mass Spectrometry* 31(2): 463–66. doi:10.1021/jasms.9b00061.

Cui, Lun, and David Bikard. 2016. “Consequences of Cas9 Cleavage in the Chromosome of Escherichia Coli.” *Nucleic Acids Research* 44(9): 4243–51. doi:10.1093/nar/gkw223.

Dahman, Yaser, Kashif Syed, Sarkar Begum, Pallavi Roy, and Banafsheh Mohtasebi. 2019. “Biofuels: Their Characteristics and Analysis.” In *Biomass, Biopolymer-Based Materials, and Bioenergy: Construction, Biomedical, and Other Industrial Applications*, Elsevier, 277–325. doi:10.1016/B978-0-08-102426-3.00014-X.

Denich, T J, L A Beaudette, H Lee, and J T Trevors. 2003. *Effect of Selected Environmental and Physico-Chemical Factors on Bacterial Cytoplasmic Membranes*. www.elsevier.com/locate/jmicmeth.

Deranieh, Rania M., Amit S. Joshi, and Miriam L. Greenberg. 2013. “Thin-Layer Chromatography of Phospholipids.Pdf.” *Membrane Biogenesis: Methods and Protocols* 1033: 21–27. doi:10.1007/978-1-62703-487-6_2.

Dörr, Tobias, Patrick J Moynihan, and Christoph Mayer. 2019. "Editorial: Bacterial Cell Wall Structure and Dynamics." *Frontiers in Microbiology* 10: 4–7. doi:10.3389/fmicb.2019.02051.

Du, Yinming, Wenyan Jiang, Mingrui Yu, I. Ching Tang, and Shang Tian Yang. 2015. "Metabolic Process Engineering of Clostridium Tyrobutyricum Δack-AdhE2 for Enhanced n-Butanol Production from Glucose: Effects of Methyl Viologen on NADH Availability, Flux Distribution, and Fermentation Kinetics." *Biotechnology and Bioengineering* 112(4): 705–15. doi:10.1002/bit.25489.

Duerre, Peter. 2005. Taylor & Francis Group *Handbook on Clostridia*.

Eggers, Lars F., and Dominik Schwudke. 2016. "Lipid Extraction: Basics of the Methyl-Tert-Butyl Ether Extraction." In *Encyclopedia of Lipidomics*, Springer Netherlands, 1–3. doi:10.1007/978-94-007-7864-1_96-1.

Evans, R I, P J Mcclure, G W Gould, and N J Russell. 1998. 40 International Journal of Food Microbiology *The Effect of Growth Temperature on the Phospholipid and Fatty Acyl Compositions of Non-Proteolytic Clostridium Botulinum*.

Ezraty, Benjamin, Alexandra Gennaris, Frédéric Barras, and Jean François Collet. 2017. "Oxidative Stress, Protein Damage and Repair in Bacteria." *Nature Reviews Microbiology* 15(7): 385–96. doi:10.1038/nrmicro.2017.26.

Fahy, Eoin, Dawn Cotter, Manish Sud, and Shankar Subramaniam. 2011. "Lipid Classification, Structures and Tools." *Biochimica et Biophysica Acta - Molecular and Cell Biology of Lipids* 1811(11): 637–47. doi:10.1016/j.bbalip.2011.06.009.

Fayolle, F. 1987. 133 Journal of General Microbiology *Changes in Membrane Lipid Composition of Clostvidium Acetobutylicum during Acetone-Butanol Fermentation: Effects of Solvents, Growth Temperature and PH*.

Fels, Ursula, Kris Gevaert, and Petra Van Damme. 2020. "Bacterial Genetic Engineering by Means of Recombineering for Reverse Genetics." *Frontiers in Microbiology* 11. doi:10.3389/fmicb.2020.548410.

Ferraz, Luís, Michael Sauer, Maria João Sousa, and Paola Branduardi. 2021. "The Plasma Membrane at the Cornerstone Between Flexibility and Adaptability: Implications for Saccharomyces Cerevisiae as a Cell Factory." *Frontiers in Microbiology* 12. doi:10.3389/fmicb.2021.715891.

Fischer, Curt R., Daniel Klein-Marcuschamer, and Gregory Stephanopoulos. 2008. “Selection and Optimization of Microbial Hosts for Biofuels Production.” *Metabolic Engineering* 10(6): 295–304. doi:10.1016/j.ymben.2008.06.009.

Fonseca, A., I. Spencer-Martins, and N. Van Uden. 1991. “Transport of Lactic Acid InKluyveromyces Marxianus: Evidence for a Monocarboxylate Uniport.” *Yeast* 7(8): 775–80. doi:10.1002/yea.320070803.

Fonseca, Fernanda, Caroline Pénicaud, E. Elizabeth Tymczyszyn, Andrea Gómez-Zavaglia, and Stéphanie Passot. 2019. “Factors Influencing the Membrane Fluidity and the Impact on Production of Lactic Acid Bacteria Starters.” *Applied Microbiology and Biotechnology* 103(17): 6867–83. doi:10.1007/s00253-019-10002-1.

Fozo, Elizabeth M., and Robert G. Quivey. 2004. “Shifts in the Membrane Fatty Acid Profile of Streptococcus Mutans Enhance Survival in Acidic Environments.” *Applied and Environmental Microbiology* 70(2): 929–36. doi:10.1128/AEM.70.2.929-936.2004.

Gavrilescu, Maria. 2009. *Environmental Biotechnology: Achievements, Opportunities and Challenges*. Iasi.

Geiger, Otto, Christian Sohlenkamp, and Isabel M. López-Lara. 2019. “Formation of Bacterial Glycerol-Based Membrane Lipids: Pathways, Enzymes, and Reactions.” In *Biogenesis of Fatty Acids, Lipids and Membranes*, Springer International Publishing, 87–107. doi:10.1007/978-3-319-50430-8_8.

Goel, Anisha, Meike Tessa Wortel, Douwe Molenaar, and Bas Teusink. 2012. “Metabolic Shifts: A Fitness Perspective for Microbial Cell Factories.” *Biotechnology Letters* 34(12): 2147–60. doi:10.1007/s10529-012-1038-9.

Goldfine, Howard. 2010. “The Appearance, Disappearance and Reappearance of Plasmalogens in Evolution.” *Progress in Lipid Research* 49(4): 493–98. doi:10.1016/j.plipres.2010.07.003.

Goldfine, Howard. 2017. “The Anaerobic Biosynthesis of Plasmalogens.” *FEBS Letters* 591(18): 2714–19. doi:10.1002/1873-3468.12714.

Goldfine, Howard. 2019. “Membrane Lipid Biogenesis.” In *Biogenesis of Fatty Acids, Lipids and Membranes*, ed. O Geiger. Cham: Springer International Publishing, 525–38. doi:10.1007/978-3-319-50430-8_34.

Goldfine, Howard. 2022. “Plasmalogens in Bacteria, Sixty Years On.” *Frontiers in Molecular Biosciences* 9. doi:10.3389/fmolb.2022.962757.

Gong, Guiping, Bo Wu, Linpei Liu, Jianting Li, Qili Zhu, Mingxiong He, and Guoquan Hu. 2022. "Metabolic Engineering Using Acetate as a Promising Building Block for the Production of Bio-based Chemicals." *Engineering Microbiology* 2(4). doi:10.1016/j.engmic.2022.100036.

Green, Michael R., and Joseph Sambrook. 2012. "Molecular Cloning." In *Molecular Cloning : A Laboratorial Manual*, ed. Michael R. Green; Joseph Sambrook. COLD SPRING HARBOR LABORATORY PRES, 158–258. http://www.cshlpress.com/pdf/sample/2013/MC4/MC4FM.pdf (April 19, 2017).

Gu, Yanyan, Jun Feng, Zhong-Tian Zhang, Liang Guo, Yifen Wang, and Yi Wang. 2018. *Curing the Endogenous Megaplasmid in Clostridium Saccharoperbutylacetonicum N1-4 (HMT) Using CRISPR-Cas9 and Preliminary Investigation of the Role of the 2 Plasmid for the Strain Metabolism*.

Guan, Ziqiang, and Goldfine. 2021. "Lipid Diversity in Clostridia." *Biochimica et Biophysica Acta (BBA) - Molecular and Cell Biology of Lipids* 1866(9): 158966. doi:10.1016/j.bbalip.2021.158966.

Guo, Liang, Zixuan Pang, Cong Gao, Xiulai Chen, and Liming Liu. 2020. "Engineering Microbial Cell Morphology and Membrane Homeostasis toward Industrial Applications." *Current Opinion in Biotechnology* 66: 18–26. doi:10.1016/j.copbio.2020.05.004.

Gustavsson, Martin, and Sang Yup Lee. 2016. "Prospects of Microbial Cell Factories Developed through Systems Metabolic Engineering." *Microbial Biotechnology* 9(5): 610–17. doi:10.1111/1751-7915.12385.

Gutiérrez, Juan-Carlos, Patricia de Francisco, Francisco Amaro, Silvia Díaz, and Ana Martín-González. 2019. "Structural and Functional Diversity of Microbial Metallothionein Genes." In *Microbial Diversity in the Genomic Era*, Elsevier, 387–407. doi:10.1016/B978-0-12-814849-5.00022-8.

Heap, John T., Muhammad Ehsaan, Clare M. Cooksley, Yen Kuan Ng, Stephen T. Cartman, Klaus Winzer, and Nigel P. Minton. 2012. "Integration of DNA into Bacterial Chromosomes from Plasmids without a Counter-Selection Marker." *Nucleic Acids Research* 40(8). doi:10.1093/nar/gkr1321.

Hebecker, Stefanie, Joern Krausze, Tatjana Hasenkampf, Julia Schneider, Maike Groenewold, Joachim Reichelt, Dieter Jahn, Dirk W. Heinz, and Jürgen Moser. 2015. "Structures of Two Bacterial Resistance Factors Mediating TRNA-Dependent Aminoacylation of

Phosphatidylglycerol with Lysine or Alanine." *Proceedings of the National Academy of Sciences of the United States of America* 112(34): 10691–96. doi:10.1073/pnas.1511167112.

Hines, Kelly M., and Libin Xu. 2019. "Lipidomic Consequences of Phospholipid Synthesis Defects in Escherichia Coli Revealed by HILIC-Ion Mobility-Mass Spectrometry." *Chemistry and Physics of Lipids* 219: 15–22. doi:10.1016/j.chemphyslip.2019.01.007.

Hirshfield, Irvin N, Stephanie Terzulli, and Conor O'Byrne. 2003. "Weak Organic Acids: A Panoply of Effects on Bacteria." *Science progress* 86(Pt 4): 245–69. http://www.ncbi.nlm.nih.gov/pubmed/15508892 (May 5, 2017).

Huffer, Sarah, Melinda E. Clark, Jonathan C Ning, Harvey W. Blanch, and Douglas S. Clark. 2011. "Role of Alcohols in Growth, Lipid Composition, and MembraneFluidity of Yeasts, Bacteria, and Archaea." *Applied and Enviromental Microbiology* 77: 6400–6408.

Imlay, James A. 2002. 46 Advances in Microbial Physiology *How Oxygen Damages Microbes: Oxygen Tolerance and Obligate Anaerobiosis*. doi:10.1016/S0065-2911(02)46003-1.

Imlay, James A. 2020. "Where in the World Do Bacteria Experience Oxidative Stress?" *Environ Microbiol. Author manuscript* 21(2): 521–30. doi:10.1111/1462-2920.14445.Where.

Jackson, B. J., J. M. Gennity, and E. P. Kennedy. 1986. "Regulation of the Balanced Synthesis of Membrane Phospholipids. Experimental Test of Models for Regulation in Escherichia Coli." *Journal of Biological Chemistry* 261(29): 13464–68. doi:10.1016/s0021-9258(18)67041-3.

Jackson, David R., Chelsi D. Cassilly, Damian R. Plichta, Hera Vlamakis, Hualan Liu, Stephen B. Melville, Ramnik J. Xavier, and Jon Clardy. 2021. "Plasmalogen Biosynthesis by Anaerobic Bacteria: Identification of a Two-Gene Operon Responsible for Plasmalogen Production in Clostridium Perfringens." *ACS Chemical Biology* 16(1): 6–13. doi:10.1021/acschembio.0c00673.

Johnson, E A. 2009. "Clostridia." *Elsevier Inc.*: 87–93.

Johnston, Norah C., and Goldfine. 1983. 129 Journal of General Microbiology *Lipid Composition in the Classification of the Butyric Acid-Producing Clostridia*. doi:0022-1287/83/0001-070.

de Jong, Ed, and Gerfried Jungmeier. 2015. "Biorefinery Concepts in Comparison to Petrochemical Refineries." In *Industrial Biorefineries and White Biotechnology*, Elsevier, 3–33. doi:10.1016/B978-0-444-63453-5.00001-X.

Karnezis, Tara, Helen C. Fisher, Gregory M. Neumann, Bruce A. Stone, and Vilma A. Stanisich. 2002. "Cloning and Characterization of the Phosphatidylserine Synthase Gene of Agrobacterium Sp. Strain ATCC 31749 and Effect of Its Inactivation on Production of High-Molecular-Mass (1→3)-β-D-Glucan (Curdlan)." *Journal of Bacteriology* 184(15): 4114–23. doi:10.1128/JB.184.15.4114-4123.2002.

Karstens, Katja, Sergej Trippel, and Peter Götz. 2021. "Process Engineering of the Acetone-Ethanol-Butanol (ABE) Fermentation in a Linear and Feedback Loop Cascade of Continuous Stirred Tank Reactors: Experiments, Modeling and Optimization." *Fuels* 2(2): 108–29. doi:10.3390/fuels2020007.

Kell, Douglas B., Neil Swainston, Pinar Pir, and Stephen G. Oliver. 2015. "Membrane Transporter Engineering in Industrial Biotechnology and Whole Cell Biocatalysis." *Trends in Biotechnology* 33(4): 237–46. doi:10.1016/j.tibtech.2015.02.001.

Kern, Renée, Danièle Joseleau-Petit, Madhab K. Chattopadhyay, and Gilbert Richarme. 2001. "Chaperone-like Properties of Lysophospholipids." *Biochemical and Biophysical Research Communications* 289(5): 1268–74. doi:10.1006/bbrc.2001.6093.

Köfeler, Harald C., Alexander Fauland, Gerald N. Rechberger, and Martin Trötzmüller. 2012. "Mass Spectrometry Based Lipidomics: An Overview of Technological Platforms." *Metabolites* 2(1): 19–38. doi:10.3390/metabo2010019.

Kogat, Yosuke, and Goldfine. 1984. 159 JOURNAL OF BACTERIOLOGY *Biosynthesis of Phospholipids in Clostridium Butyricum: Kinetics of Synthesis of Plasmalogens and the Glycerol Acetal of Ethanolamine Plasmalogen*. https://journals.asm.org/journal/jb.

Kolek, Jan, Petra Patáková, Karel Melzoch, Karel Sigler, and Tomáš Řezanka. 2015. "Changes in Membrane Plasmalogens of Clostridium Pasteurianum during Butanol Fermentation as Determined by Lipidomic Analysis" ed. Ing-Feng Chang. *PLOS ONE* 10(3): e0122058. doi:10.1371/journal.pone.0122058.

Kordi, Masoumeh, Robab Salami, Parisa Bolouri, Nasser Delangiz, Behnam Asgari Lajayer, and Eric D. van Hullebusch. 2022. "White Biotechnology and the Production of Bio-Products." *Systems Microbiology and Biomanufacturing* 2(3): 413–29. doi:10.1007/s43393-022-00078-8.

Kranenburg, Marieke, and Berend Smit. 2005. "Phase Behavior of Model Lipid Bilayers." *Journal of Physical Chemistry B* 109(14): 6553–63. doi:10.1021/jp0457646.

Kumar, Raman, Anil Kumar Sharma, and Sarabjeet Singh Ahluwalia. 2017. Advances in Environmental Biotechnology *Advances in Environmental Biotechnology*. Springer Singapore. doi:10.1007/978-981-10-4041-2.

Lairón-Peris, M., S. J. Routledge, J. A. Linney, J. Alonso-del-Real, C. M. Spickett, A. R. Pitt, J. M. Guillamón, et al., 2021. "Lipid Composition Analysis Reveals Mechanisms of Ethanol Tolerance in the Model Yeast Saccharomyces Cerevisiae." *Applied and Environmental Microbiology* 87(12): 1–22. doi:10.1128/AEM.00440-21.

Li, Shubo, Li Huang, Chengzhu Ke, Zongwen Pang, and Liming Liu. 2020. "Pathway Dissection, Regulation, Engineering and Application: Lessons Learned from Biobutanol Production by Solventogenic Clostridia." *Biotechnology for Biofuels* 13(1): 1–25. doi:10.1186/s13068-020-01674-3.

Liao, Chen, Seung Oh Seo, Venhar Celik, Huaiwei Liu, Wentao Kong, Yi Wang, Hans Blaschek, Yong Su Jin, and Ting Lu. 2015. "Integrated, Systems Metabolic Picture of Acetone-Butanol-Ethanol Fermentation by Clostridium Acetobutylicum." *Proceedings of the National Academy of Sciences of the United States of America* 112(27): 8505–10. doi:10.1073/pnas.1423143112.

Liew, Fungmin Eric, Robert Nogle, Tanus Abdalla, Blake J. Rasor, Christina Canter, Rasmus O. Jensen, Lan Wang, et al., 2022. "Carbon-Negative Production of Acetone and Isopropanol by Gas Fermentation at Industrial Pilot Scale." *Nature Biotechnology* 40(3): 335–44. doi:10.1038/s41587-021-01195-w.

Linger, Jeffrey G., Leah R. Ford, Kavita Ramnath, and Michael T. Guarnieri. 2020. "Development of Clostridium Tyrobutyricum as a Microbial Cell Factory for the Production of Fuel and Chemical Intermediates From Lignocellulosic Feedstocks." *Frontiers in Energy Research* 8. doi:10.3389/fenrg.2020.00183.

Linney. 2021. "Engineering Bacteria for the Enhanced Production of High-Value Chemicals." Aston University.

Linney, John A., Sarah J. Routledge, Simon D. Connell, Tony R. Larson, Andrew R. Pitt, Elizabeth R. Jenkinson, and Alan D. Goddard. 2023. "Identification of Membrane Engineering Targets for Increased Butanol Tolerance in Clostridium Saccharoperbutylacetonicum." *Biochimica et Biophysica Acta - Biomembranes* 1865(8). doi:10.1016/j.bbamem.2023.184217.

Louie, Kathryn, Yang-Chang Chen, and William Dowhan. 1986. 165 JOURNAL OF BACTERIOLOGY *Substrate-Induced Membrane Association of Phosphatidylserine Synthase from Escherichia Coli*.

Luo, Lian Hua, Pil Soo Seo, Jeong Woo Seo, Sun Yeon Heo, Dae Hyuk Kim, and Chul Ho Kim. 2009. "Improved Ethanol Tolerance in Escherichia Coli by Changing the Cellular Fatty Acids Composition through Genetic Manipulation." *Biotechnology Letters* 31(12): 1867–71. doi:10.1007/s10529-009-0092-4.

Matsumoto, Kouji, Masahiro Okada, Yuko Horikoshi, ‡ Hiroshi Matsuzaki, Tsutomu Kishi, Mitsuhiro Itaya, and Isao Shibuya. 1998. 180 JOURNAL OF BACTERIOLOGY *Cloning, Sequencing, and Disruption of the Bacillus Subtilis Psd Gene Coding for Phosphatidylserine Decarboxylase*. https://journals.asm.org/journal/jb.

Mattanovich, Diethard, Michael Sauer, and Brigitte Gasser. 2014. "Yeast Biotechnology: Teaching the Old Dog New Tricks." *Microbial cell factories* 13(1): 34. doi:10.1186/1475-2859-13-34.

Mazzoli, Roberto. 2012. "Development of Microorganisms for Cellulose-Biofuel Consolidated Bioprocessings: Metabolic Engineers' Tricks." *Computational and Structural Biotechnology Journal* 3(4): e201210007. doi:10.5936/csbj.201210007.

Monaghan, Taylor I., Joseph A. Baker, Preben Krabben, E. Timothy Davies, Elizabeth R. Jenkinson, Ian B. Goodhead, Gary K. Robinson, and Mark Shepherd. 2022. "Deletion of Glyceraldehyde-3-Phosphate Dehydrogenase (GapN) in Clostridium Saccharoperbutylacetonicum N1-4(HMT) Using CLEAVE^{TM} Increases the ATP Pool and Accelerates Solvent Production." *Microbial Biotechnology* 15(5): 1574–85. doi:10.1111/1751-7915.13990.

Moon, Hyeon Gi, Yu Sin Jang, Changhee Cho, Joungmin Lee, Robert Binkley, and Sang Yup Lee. 2016. "One Hundred Years of Clostridial Butanol Fermentation." *FEMS microbiology letters* 363(3). doi:10.1093/femsle/fnw001.

Mrozik, A, and S Łabużek. 2004. "Cytoplasmatic Bacterial Membrane Responses to Environmental Perturbations." *Polish Journal of Environmental Studies* 13(5): 487–94.

Murzyn, Krzysztof, Tomasz Róg, and Marta Pasenkiewicz-Gierula. 2005. "Phosphatidylethanolamine-Phosphatidylglycerol Bilayer as a Model of the Inner Bacterial Membrane." *Biophysical Journal* 88(2): 1091–1103. doi:10.1529/biophysj.104.048835.

Nanda, Sonil, Rachita Rana, Prakash K. Sarangi, Ajay K. Dalai, and Janusz A. Kozinski. 2018. "A Broad Introduction to First-, Second-, and Third-Generation Biofuels." *Recent Advancements in Biofuels and Bioenergy Utilization*: 1–25. doi:10.1007/978-981-13-1307-3_1.

Ohta, Akinori, Karen Waggoner, Anna Radominska-Pyrek, and William Dowhan. 1981. 147 JOURNAL OF BACTERIOLOGY *Cloning of Genes Involved in Membrane Lipid Synthesis: Effects of Amplification of Phosphatidylglycerophosphate Synthase in Escherichia Coli*.

Pajerski, Wojciech, Dorota Ochonska, Monika Brzychczy-Wloch, Paulina Indyka, Magdalena Jarosz, Monika Golda-Cepa, Zbigniew Sojka, and Kotarba Andrzej. 2019. "Attachment Efficiency of Gold Nanoparticles by Gram-Positive and Gram-Negative Bacterial Strains Governed by Surface Charges." *J Nanopart Res* 21: 21–186. doi:10.1007/s11051-019-4617-z.

Panevska, Anastasija, Matej Skočaj, Igor Križaj, Peter Maček, and Kristina Sepčić. 2019. "Ceramide Phosphoethanolamine, an Enigmatic Cellular Membrane Sphingolipid." *Biochimica et Biophysica Acta - Biomembranes* 1861(7): 1284–92. doi:10.1016/j.bbamem.2019.05.001.

Parsons, Joshua B., and Charles O. Rock. 2013. "Bacterial Lipids: Metabolism and Membrane Homeostasis." *Progress in Lipid Research* 52(3): 249–76. doi:10.1016/j.plipres.2013.02.002.

Patakova, Petra, Barbora Branska, Karel Sedlar, Maryna Vasylkivska, Katerina Jureckova, Jan Kolek, Pavlina Koscova, and Ivo Provaznik. 2019a. "Acidogenesis, Solventogenesis, Metabolic Stress Response and Life Cycle Changes in Clostridium Beijerinckii NRRL B-598 at the Transcriptomic Level." *Scientific Reports* 9(1371): 1–21. doi:10.1038/s41598-018-37679-0.

Patakova, Petra, Barbora Branska, Karel Sedlar, Maryna Vasylkivska, Katerina Jureckova, Jan Kolek, Pavlina Koscova, and Ivo Provaznik. 2019b. "Acidogenesis, Solventogenesis, Metabolic Stress Response and Life Cycle Changes in Clostridium Beijerinckii NRRL B-598 at the Transcriptomic Level." *Scientific Reports* 9(1371): 1–21. doi:10.1038/s41598-018-37679-0.

Patakova, Petra, Michaela Linhova, Mojmir Rychtera, Leona Paulova, and Karel Melzoch. 2013. "Novel and Neglected Issues of Acetone–Butanol–Ethanol (ABE) Fermentation by

Clostridia_ Clostridium Metabolic Diversity, Tools for Process Mapping and Continuous Fermentation Systems." *Biotechnology Advances* 31: 58–67.

Pines, Gur, Emily F. Freed, James D. Winkler, and Ryan T. Gill. 2015. "Bacterial Recombineering: Genome Engineering via Phage-Based Homologous Recombination." *ACS Synthetic Biology* 4(11): 1176–85. doi:10.1021/acssynbio.5b00009.

Di Prima, Giulia, Fabio Librizzi, and Rita Carrotta. 2020. "Light Scattering as an Easy Tool to Measure Vesicles Weight Concentration." *Membranes* 10(9): 1–14. doi:10.3390/membranes10090222.

Rangel, Albert E T. 2020. "Added Compounds : The Design of Efficient Microbial Cell Factories By." *Biofuels, Bioproducts and Biorefining* 14(6): 1228–38. doi:10.1002/bbb.2127.

Riebe, Oliver, Ralf Jorg Fischer, David A. Wampler, Donald M. Kurtz, and Hubert Bahl. 2009. "Pathway for H2O2 and O2 Detoxification in Clostridium Acetobutylicum." *Microbiology* 155(1): 16–24. doi:10.1099/mic.0.022756-0.

Robinson, Nigel J., Simon K. Whitehall, and Jennifer S. Cavet. 2001. "Microbial Metallothioneins." *Advances in Microbial Physiology* 44: 183–213.

Rog, Tomasz, and Artturi Koivuniemi. 2016. "The Biophysical Properties of Ethanolamine Plasmalogens Revealed by Atomistic Molecular Dynamics Simulations." *Biochimica et Biophysica Acta - Biomembranes* 1858(1): 97–103. doi:10.1016/j.bbamem.2015.10.023.

Rowlett, Veronica W, Venkata K P S Mallampalli, Anja Karlstaedt, William Dowhan, Heinrich Taegtmeyer, William Margolin, and Heidi Vitrac. 2017. "Impact of Membrane Phospholipid Alterations in Escherichia Coli on Cellular Function and Bacterial Stress Adaptation." doi:10.1128/JB.

Roy, Hervé. 2009. "Tuning the Properties of the Bacterial Membrane with Aminoacylated Phosphatidylglycerol." *IUBMB Life* 61(10): 940–53. doi:10.1002/iub.240.

Rühl, Jana, Andreas Schmid, and Lars Mathias Blank. 2009. "Selected Pseudomonas Putida Strains Able To Grow in the Presence of High Butanol Concentrations." *Applied and Environmental Microbiology* 75(13): 4653–56. doi:10.1128/AEM.00225-09.

Russell, Nicholas J. 1984. "Mechanisms of Thermal Adaptation in Bacteria: Blueprints for Survival." *Elsevier Science Publishers B.V*: 108–12.

Ruttkay-nedecky, Branislav, Lukas Nejdl, Jaromir Gumulec, Ondrej Zitka, and Rene Kizek. 2013. "The Role of Metallothionein in Oxidative Stress." *International Journal of Molecular Sciences* 14: 6044–66. doi:10.3390/ijms14036044.

Saha, Soumitra Kumar, Yutaka Furukawa, Hiroshi Matsuzaki, Isao Shibuya, and Kouji Matsumoto. 1996. "Directed Mutagenesis, Ser-56 to Pro, of Bacillus Subtilis Phosphatidylserine Synthase Drastically Lowers Enzymatic Activity and Relieves Amplification Toxicity in Escherichia Coli." *Bioscience, Biotechnology and Biochemistry* 60(4): 630–33. doi:10.1271/bbb.60.630.

Saha, Soumitra Kumar, Satomi Nishijima, Hiroshi Matsuzaki, Isao Shibuya, and Kouji Matsumoto. 1996. "A Regulatory Mechanism for the Balanced Synthesis of Membrane Phospholipid Species in Escherichia Coli." *Biosci Biotechnol Biochem* 60(1): 111–16. doi:10.1271/bbb.60.111.

Sahoo, Rajesh Kumar, Aradhana Das, Mahendra Gaur, Suchanda Dey, Saubhagini Sahoo, and Enketeswara Subudhi. 2019. "Bacteria for Butanol Production: Bottlenecks, Achievements and Prospects." *Journal of Pure and Applied Microbiology* 13(3): 1429–40. doi:10.22207/JPAM.13.3.13.

Sandberg, Troy E., Michael J. Salazar, Liam L. Weng, Bernhard O. Palsson, and Adam M. Feist. 2019. "The Emergence of Adaptive Laboratory Evolution as an Efficient Tool for Biological Discovery and Industrial Biotechnology." *Metabolic Engineering* 56: 1–16. doi:10.1016/j.ymben.2019.08.004.

Sanders, Johan, Elinor Scott, Ruud Weusthuis, and Hans Mooibroek. 2007. "Bio-Refinery as the Bio-Inspired Process to Bulk Chemicals." *Macromolecular Bioscience* 7(2): 105–17. doi:10.1002/mabi.200600223.

Sauer, Michael. 2016. "Industrial Production of Acetone and Butanol by Fermentation-100 Years Later." *FEMS Microbiology Letters* 363(13). doi:10.1093/femsle/fnw134.

Sauer, Michael, and Diethard Mattanovich. 2012. "Construction of Microbial Cell Factories for Industrial Bioprocesses." *Journal of Chemical Technology and Biotechnology* 87(4): 445–50. doi:10.1002/jctb.3711.

Sauer, Michael, Danilo Porro, Diethard Mattanovich, and Paola Branduardi. 2008. "Microbial Production of Organic Acids: Expanding the Markets." *Trends in Biotechnology* 26(2): 100–108. doi:10.1016/j.tibtech.2007.11.006.

Sauer, Uwe. 2001. “Evolutionary Engineering of Industrially Important Microbial Phenotypes.” *Advances in biochemical engineering/biotechnology* 73: 129–69. doi:10.1007/3-540-45300-8_7.

Schujman, Gustavo E., and Diego de Mendoza. 2008. “Regulation of Type II Fatty Acid Synthase in Gram-Positive Bacteria.” *Current Opinion in Microbiology* 11(2): 148–52. doi:10.1016/j.mib.2008.02.002.

Shabb, J.B., W.W. Muhonen, and A.A. Mehus. 2017. “Quantitation of Human Metallothionein Isoforms in Cells, Tissues, and Cerebrospinal Fluid by Mass Spectrometry.” In *Methods in Enzymology*, , 413–31. doi:10.1016/bs.mie.2016.11.004.

Sies, Helmut, Carsten Berndt, and Dean P Jones. 2017. “Oxidative Stress.” *Annual review of biochemistry* (86): 715–48.

Silhavy, Thomas J., Daniel Kahne, and Suzanne Walker. 2010. “The Bacterial Cell Envelope.” *Cold Spring Harbor Laboratory Press*: 1–17. doi:10.1101/cshperspect.a000414.

Sohlenkamp, Christian. 2017. “Membrane Homeostasis in Bacteria upon PH Challenge.” In *Biogenesis of Fatty Acids, Lipids and Membranes*, Springer International Publishing, 1–13. doi:10.1007/978-3-319-43676-0_57-1.

Sohlenkamp, Christian, and Otto Geiger. 2015. “Bacterial Membrane Lipids: Diversity in Structures and Pathways.” *FEMS Microbiology Reviews* 40(1): 133–59. doi:10.1093/femsre/fuv008.

Sohlenkamp, Christian, and Otto Geiger. 2016. “Bacterial Membrane Lipids: Diversity in Structures and Pathways” ed. Franz Narberhaus. *FEMS Microbiology Reviews* 40(1): 133–59. doi:10.1093/femsre/fuv008.

Spickett, Corinne M., Ana Reis, and Andrew R. Pitt. 2011. “Identification of Oxidized Phospholipids by Electrospray Ionization Mass Spectrometry and LC–MS Using a QQLIT Instrument.” *Free Radical Biology and Medicine* 51: 2133–49. doi:10.1016/j.freerdbiomed.2011.09.003.

Startek, Justyna B., Brett Boonen, Karel Talavera, and Victor Meseguer. 2019. “TRP Channels as Sensors of Chemically-Induced Changes in Cell Membrane Mechanical Properties.” *International Journal of Molecular Sciences* 20(2). doi:10.3390/ijms20020371.

Strahl, Henrik, and Jeff Errington. 2017. “Bacterial Membranes: Structure, Domains, and Function.” *Annual Rev. Microbiol.* 71: 519–38. doi:10.1146/annurev-micro-102215-095630.

Suo, Yukai, Sheng Luo, Yanan Zhang, Zhengping Liao, and Jufang Wang. 2017. “Enhanced Butyric Acid Tolerance and Production by Class I Heat Shock Protein-Overproducing Clostridium Tyrobutyricum ATCC 25755.” *Journal of Industrial Microbiology and Biotechnology* 44(8): 1145–56. doi:10.1007/s10295-017-1939-7.

Sutterlin, Holly A., Handuo Shi, Kerrie L. May, Amanda Miguel, Somya Khare, Kerwyn Casey Huang, and Thomas J. Silhavy. 2016. “Disruption of Lipid Homeostasis in the Gram-Negative Cell Envelope Activates a Novel Cell Death Pathway.” *Proceedings of the National Academy of Sciences of the United States of America* 113(11): E1565–74. doi:10.1073/pnas.1601375113.

Suzuki, Motoo, Hiroshi Hara, and Kouji Matsumoto. 2002. “Envelope Disorder of Escherichia Coli Cells Lacking Phosphatidylglycerol.” *Journal of Bacteriology* 184(19): 5418–25. doi:10.1128/JB.184.19.5418-5425.2002.

Tan, Zaigao, Pouyan Khakbaz, Yingxi Chen, Jeremy Lombardo, Jong Moon Yoon, Jacqueline V. Shanks, Jeffery B. Klauda, and Laura R. Jarboe. 2017a. “Engineering Escherichia Coli Membrane Phospholipid Head Distribution Improves Tolerance and Production of Biorenewables.” *Metabolic Engineering* 44: 1–12. doi:10.1016/j.ymben.2017.08.006.

Tan, Zaigao, Pouyan Khakbaz, Yingxi Chen, Jeremy Lombardo, Jong Moon Yoon, Jacqueline V. Shanks, Jeffery B. Klauda, and Laura R. Jarboe. 2017b. “Engineering Escherichia Coli Membrane Phospholipid Head Distribution Improves Tolerance and Production of Biorenewables.” *Metabolic Engineering* 44: 1–12. doi:10.1016/j.ymben.2017.08.006.

Tan, Zaigao, Jong Moon Yoon, David R. Nielsen, Jacqueline V. Shanks, and Laura R. Jarboe. 2016. “Membrane Engineering via Trans Unsaturated Fatty Acids Production Improves Coli Robustness and Production of Biorenewables.” *Metabolic Engineering, Elsevier* 35: 105–13.

Tang, Yannan, Hao Xia, and Dianfan Li. 2018. “Membrane Phospholipid Biosynthesis in Bacteria.” In *Advances in Membrane Proteins: Part I: Mass Processing and Transportation*, Springer Singapore, 77–119. doi:10.1007/978-981-13-0532-0_4.

Tian, Bing, Ziqiang Guan, and Goldfine. 2013. “An Ethanolamine-Phosphate Modified Glycolipid in Clostridium Acetobutylicum That Responds to Membrane Stress.” *Biochimica et Biophysica Acta - Molecular and Cell Biology of Lipids* 1831(6): 1185–90. doi:10.1016/j.bbalip.2013.03.005.

Tomas, Christopher A., Neil E. Welker, and Eleftherios T. Papoutsakis. 2003. “Overexpression of GroESL in Clostridium Acetobutylicum Results in Increased Solvent Production and Tolerance, Prolonged Metabolism, and Changes in the Cell’s Transcriptional Program.” *Applied and Environmental Microbiology* 69(8): 4951–65. doi:10.1128/AEM.69.8.4951-4965.2003.

Tran, Vinh G., and Huimin Zhao. 2022. “Engineering Robust Microorganisms for Organic Acid Production.” *Journal of Industrial Microbiology and Biotechnology* 49(2). doi:10.1093/jimb/kuab067.

Tuzimski, Tomasz, and Joseph Sherma. 2016. “Thin-Layer Chromatography and Mass Spectrometry for the Analysis of Lipids.” In *Encyclopedia of Lipidomics*, Springer Netherlands, 1–20. doi:10.1007/978-94-007-7864-1_62-1.

Usmani, Zeba, Minaxi Sharma, Abhishek Kumar Awasthi, Tiit Lukk, Maria G. Tuohy, Liang Gong, Phuong Nguyen-Tri, et al., 2021. “Lignocellulosic Biorefineries: The Current State of Challenges and Strategies for Efficient Commercialization.” *Renewable and Sustainable Energy Reviews* 148. doi:10.1016/j.rser.2021.111258.

Vasylkivska, Maryna, and Petra Patakova. 2020. “Role of Efflux in Enhancing Butanol Tolerance of Bacteria.” *Journal of Biotechnology* (320): 17–27.

Vences-Guzmán, Miguel Angel, Otto Geiger, and Christian Sohlenkamp. 2008. “Sinorhizobium Meliloti Mutants Deficient in Phosphatidylserine Decarboxylase Accumulate Phosphatidylserine and Are Strongly Affected during Symbiosis with Alfalfa.” *Journal of Bacteriology* 190(20): 6846–56. doi:10.1128/JB.00610-08.

Vento, Justin M., Nathan Crook, and Chase L. Beisel. 2019. “Barriers to Genome Editing with CRISPR in Bacteria.” *Journal of Industrial Microbiology and Biotechnology* 46(9–10): 1327–41. doi:10.1007/s10295-019-02195-1.

Wang, Pixiang, Jun Feng, Liang Guo, Oladiran Fasina, and Yi Wang. 2019. “Engineering Clostridium Saccharoperbutylacetonicum for High Level Isopropanol-Butanol-Ethanol (IBE) Production from Acetic Acid Pretreated Switchgrass Using the CRISPR-Cas9 System.” *ACS*

Sustainable Chemistry and Engineering 7(21): 18153–64. doi:10.1021/acssuschemeng.9b05336.

Weber, Frans J, and Jan A M De Bont. 1996. 1286 Biophysica Acta *Adaptation Mechanisms of Microorganisms to the Toxic Effects of Organic Solvents on Membranes*.

Weber, Frans J, Sonja Lsken, and Jan A M De Bont. 1994. 140 *Cisltrans Isomerization of Fatty Acids as a Defence Mechanism of Pseudomonas Putida Strains to Toxic Concentrations of Toluene*.

Wiegel, Juergen, Ralph Tanner, and Fred A. Rainey. 2006. "An Introduction to the Family Clostridiaceae." In *The Prokaryotes*, Springer US, 654–78. doi:10.1007/0-387-30744-3_20.

Willdigg, Jessica R., and John D. Helmann. 2021. "Mini Review: Bacterial Membrane Composition and Its Modulation in Response to Stress." *Frontiers in Molecular Biosciences* 8. doi:10.3389/fmolb.2021.634438.

Wittmann, Christoph, and James C Liao. 2017. *Industrial Biotechnology*. 12th ed. eds. Christoph Wittmann and James C Liao. Weinheim: Wiley-VCH.

Wu, Chongde, Juan Zhang, Miao Wang, Guocheng Du, and Jian Chen. 2012. "Lactobacillus Casei Combats Acid Stress by Maintaining Cell Membrane Functionality." *Journal of Industrial Microbiology and Biotechnology* 39(7): 1031–39. doi:10.1007/s10295-012-1104-2.

Xu, Z., and L. Jiang. 2011. "Butyric Acid." In *Comprehensive Biotechnology, Second Edition*, Elsevier Inc., 207–15. doi:10.1016/B978-0-08-088504-9.00181-1.

Xue, Chuang, and Chi Cheng. 2019. 4 Advances in Bioenergy *Butanol Production by Clostridium*. 1st ed. Elsevier Inc. doi:10.1016/bs.aibe.2018.12.001.

Xue, Chuang, Jingbo Zhao, Lijie Chen, Shang-tian Yang, and Fengwu Bai. 2017. "Recent Advances and State-of-the-Art Strategies in Strain and Process Engineering for Biobutanol Production by Clostridium Acetobutylicum." *Biotechnology Advances* 35(2): 310–22. doi:10.1016/j.biotechadv.2017.01.007.

Yamane, Tsuneo, and Ryohsuke Tanaka. 2013. "Highly Accumulative Production of l(+)-Lactate from Glucose by Crystallization Fermentation with Immobilized Rhizopus Oryzae." *Journal of Bioscience and Bioengineering* 115(1): 90–95. doi:10.1016/j.jbiosc.2012.08.005.

Yu, Mingrui, Yali Zhang, I-Ching Tang, and Shang-Tian Yang. 2011. “Metabolic Engineering of Clostridium Tyrobutyricum for N-Butanol Production.” *Metabolic Engineering* (13): 373–82.

Zeng, Weizhu, Likun Guo, Sha Xu, Jian Chen, and Jingwen Zhou. 2020. “High-Throughput Screening Technology in Industrial Biotechnology.” *Trends in Biotechnology* 38(8): 888–906. doi:10.1016/j.tibtech.2020.01.001.

Zhang Lei, Nie Xiaoqun, Ravcheev Dmitry A., Rodionov Dmitry A., Sheng Jia, Gu Yang, Yang Sheng, Jiang Weihong, and Yang Chen. 2014. “Redox-Responsive Repressor Rex Modulates Alcohol Production and Oxidative Stress Tolerance in Clostridium Acetobutylicum.” *Journal of Bacteriology* 196(22): 3949–63. doi:10.1128/JB.02037-14.

Zhang Yong Mei, and Rock Charles O. 2008. “Membrane Lipid Homeostasis in Bacteria.” *Nature Reviews Microbiology* 6(3): 222–33. doi:10.1038/nrmicro1839.

Zheng, Lei, Yibin Lin, Shuo Lu, Jiazhe Zhang, and Mikhail Bogdanov. 2017. “Biogenesis, Transport and Remodeling of Lysophospholipids in Gram-Negative Bacteria.” *Biochimica et Biophysica Acta - Molecular and Cell Biology of Lipids* 1862(11): 1404–13. doi:10.1016/j.bbalip.2016.11.015.

Zhu, Ying, and Shang Tian Yang. 2003. “Adaptation of Clostridium Tyrobutyricum for Enhanced Tolerance to Butyric Acid in a Fibrous-Bed Bioreactor.” *Biotechnology Progress* 19(2): 365–72. doi:10.1021/bp025647x.